

DISSERTATION

MODELING POOL SEDIMENT DYNAMICS

IN A MOUNTAIN RIVER

Submitted by

Sara L. Rathburn

Department of Earth Resources

In partial fulfillment of the requirements

for the Degree of Doctor of Philosophy

Colorado State University

Fort Collins, Colorado

Fall 2001

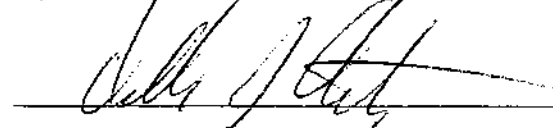
COLORADO STATE UNIVERSITY

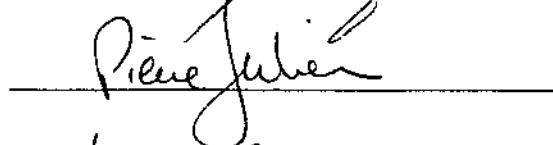
August 31, 2001

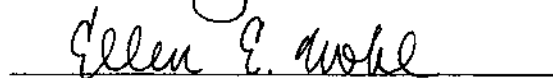
WE HEREBY RECOMMEND THAT THE DISSERTATION PREPARED UNDER
OUR SUPERVISION BY SARA L. RATHBURN ENTITLED MODELING POOL
SEDIMENT DYNAMICS IN A MOUNTAIN RIVER BE ACCEPTED AS
FULFILLING IN PART REQUIREMENTS FOR THE DEGREE OF DOCTOR OF
PHILOSOPHY.

Committee on Graduate Work

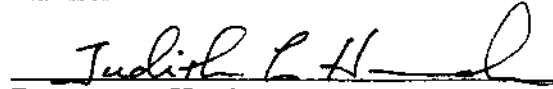








Adviser



Department Head

COLORADO STATE UNIVERSITY

August 31, 2001

WE HEREBY RECOMMEND THAT THE DISSERTATION PREPARED UNDER
OUR SUPERVISION BY SARA L. RATHBURN ENTITLED MODELING POOL
SEDIMENT DYNAMICS IN A MOUNTAIN RIVER BE ACCEPTED AS
FULFILLING IN PART REQUIREMENTS FOR THE DEGREE OF DOCTOR OF
PHILOSOPHY.

Committee on Graduate Work

[REDACTED]

[REDACTED]

[REDACTED]

[REDACTED]

[REDACTED]

Adviser

[REDACTED]

Department Head

ABSTRACT OF DISSERTATION

MODELING POOL SEDIMENT DYNAMICS

IN A MOUNTAIN RIVER

An increasingly important source of sediment into river systems is sediment that accumulates within reservoirs and is subsequently released into the downstream ecosystem. In Colorado alone, five large-scale sediment releases from reservoirs within the last decade have resulted in a host of environmental hazards, particularly the loss of aquatic biota and their habitat. The most recent example occurred in September 1996 when approximately 7,000 m³ of clay- to gravel-sized sediment were released from Halligan Dam into the North Fork Cache la Poudre River in northern Colorado. The sediment caused extensive aggradation of the original cobble-boulder bed, primarily in pools, and complete fish mortality for 12 km downstream from the dam. Because of the thriving, pre-release wild trout fishery downstream from Halligan Reservoir, flushing of sediment from pools to recreate overwinter fish habitat was of prime concern.

The purpose of this investigation was to evaluate the applicability of various hydraulic and sediment transport models as predictors of pool recovery along the steep-gradient, bedrock-controlled North Fork River. Two modeling scenarios representing a low and high flushing discharge were modeled using one- and semi-two dimensional sediment transport models, HEC-6 and GSTARS2.0, respectively. The models were calibrated against quantitative measurements of pool bed elevation obtained during field

surveys. HEC-6 results indicate that long-term, robust simulations yield the closest agreement between predicted and measured pool bed elevation change. Greater than 50 percent of the actual scour and deposition within three pools was modeled using HEC-6. Modeling accuracy using GSTARS2.0 was considerably more variable, and no pool-wide trends were obtained.

A two-dimensional, finite element hydraulic model, RMA2, improved delineation of flow hydraulics in areas of flow separation and recirculation within a compound pool. RMA2 results of depth-averaged velocity magnitude and vectors broadly agree with timed photographs of surface flow patterns, and correspond with velocity measurements for low-velocity areas such as eddy pools. Patterns of boundary shear stress and a particle stability index accurately predict gross areas of scour and deposition, but fail to represent the simultaneous aggradation and degradation measured in pools. Estimates of bedload transport capacity from the two-dimensional modeling results are one order of magnitude greater than measured transport rates, and indicate that supply-limited conditions existed along the North Fork following a clear-water flushing release. Further correlations between observed and modeled sedimentation patterns are hindered by the disparity in resolution between the field data and modeled results; field-based cross sectional information is quickly outstripped by the finite element model RMA2.

Finally, a conceptual model of pool sediment dynamics was developed for water resource specialists as an alternative to the time-intensive effort and expertise required of the numerical modeling. Predictable sites of channel aggradation and degradation resulting from a sediment pulse are identified on a reach-scale hierarchy. Processes of sediment delivery, storage, and transfer into and out of eddies that influence fish occur on

the width scale, however. Sedimentation within laterally confined pools is dependent on pool geometry, distance downstream from the dam (a surrogate of sediment supply), and the duration and magnitude of flows following the release. At low flows, sediment deposition is restricted to small areas of recirculating flow. As discharge increases, migration of the separation point and development of a strong shear zone limits the transfer of sediment between the eddy and the main flow. The sediment release from Halligan induced persistent, long-term storage of fine sediment because of an elevated channel bed and loss of channel capacity. Recognition of the hazards associated with a large influx of sediment into a riverine ecosystem is critical for a greater understanding of the effects of sediment releases, and future management of sediment within reservoirs.

Sara L. Rathburn
Department of Earth Resources
Colorado State University
Fort Collins, CO 80523
Fall 2001

ACKNOWLEDGEMENTS

Many people have contributed in a myriad of ways to the completion of this document. It was in no way singly undertaken, and I offer a modification to an existing saying; *'It takes a village to complete a Ph.D.'* First, I want to thank my advisor Dr. Ellen Wohl for agreeing to take on a part-time, highly non-traditional student. These past four years have been stimulating, challenging, and exceedingly enjoyable. I have relished our hours in the field, in the office, and elsewhere, discussing my project, geomorphology in general, and mountain rivers in particular. Ellen's clarity and insight always kept me focused and ensured thoroughness and perseverance in spite of my struggles with the model-of-the-day. I look forward to more scientific interactions with her.

Thank you to my other committee members Drs. Deborah Anthony, Pierre Julien, and Stanley Schumm. Deb offered substantive input and encouragement, provided key insight into sediment transport processes and evaluation of the modeling results, and allowed me to sit in on an excellent class on fluvial and eolian transport. Pierre taught two semesters of courses on erosion and sedimentation and river mechanics, and his courses, along with Deb's, were the best classes I took during my graduate tenure. I refer to those notes and the texts more than any other. Stan kindly offered to fill in as a third department committee member, as a favor, after I lost one committee member to a job change. Thank you to Dr. Robert Ward for substituting during my orals, and for his overall interest in my research. Dr. Brian Cluer provided encouragement and initial assistance during early phases of my research.

Initial phases of this research were supported by funding from the Colorado Water Conservation Board, U.S. Bureau of Reclamation, and Trout Unlimited. Major support was provided by National Science Foundation Grant CMS-9727061 to Dr. Ellen Wohl. Additionally, I received a Career Development Grant from the American Association of University Women, the American Water Resources Association Rich Herbert Scholarship, a Rocky Mountain Association of Geologist Foundation Grant, and the Ned

and Barbara Dils Scholarship. All of this monetary support was crucial to the completion of my degree.

Heather Knight, John Stokes, and various interns working at The Nature Conservancy's Phantom Canyon Preserve have been enthusiastic and helpful, providing logistical support throughout the duration of this research. North Poudre Irrigation Co. provided access to Halligan Dam and to upstream reaches of the study site. I appreciate the opportunity to explore sediment dynamics in such a lovely, fascinating setting.

Numerous graduate students assisted me throughout various phases of my research. I thank Dan Cenderelli, Janet Curran, Jasper Hardison, and Ron Zelt, Doug Thompson, and John O'Brien for assisting in the data collection prior to my beginning school. Dan Cenderelli's effort was critical to the overall high quality of data collected along the North Fork, and I appreciate discussions with him and field companionship. Greg Springer provided Adobe Illustrator guidance, and was open to an exchange of ideas about eddy system hydraulics. Greg Stewart offered important, patient insight into a fickle two-dimensional model, and served as a main-stay in my support system. I have missed our daily discussions tremendously.

Additional individuals to whom I am grateful include Jason Alexander and Allison Thorton, summer assistants through the REU program sponsored by NSF. Karla Schmidt, work study, helped with a poster presentation. Francisco Simoes, U.S. Bureau of Reclamation, graciously reviewed my GSTARS2.0 data files, and provided insight into model particulars that would have been missed. Lyle Zevenbergen, Ayres Associates, kindly offered his time and expertise with RMA2 and SMS when I felt really stuck.

To my parents, Buz and Katie Rathburn, I am tremendously grateful for their emotional support, help with childcare, and understanding the multifaceted roles in my life. Thank you to my mother, who in a mother-daughter phone conversation encouraged me to pursue a Ph.D. in the first place, and offered immense support in all ways. To my father, who worked on a doctorate for seven years while maintaining a full-time job and helping to raise three young children, thank you for instilling in me a love of the outdoors, for taking an interest in my research, and enjoying the shared thrill of working on rivers like the Colorado River through Grand Canyon. This dissertation is dedicated to you both.

My friends Sheri Quesnel and Jan Harrison have helped in ways that are the offerings of true friendship. Thank you for the emergency childcare, the meals, the patience, the birthday breakfasts, and most of all for being there, always. I also thank Lisa Gimlett for support, encouragement, and exercising outlets.

A special thanks to my patient and generous husband Jim Finley for his endless understanding and support. Jim offered a steadiness and strength to my life that kept the struggles of graduate school in perspective. He offered help in practical, time-consuming ways that cleared a route for me to pursue good work on an equal basis with his own. Much of his help involved tenderly caring for our two children, and constantly adjusting his busy work schedule to supplement my hours at the university. It has been a tremendous gift having Jim in my life, and I am thankful that we crossed paths in these very halls of CSU some 18 years ago.

Finally, the vitality of our two children Canace and Sawyer, now 7 and 5, buoyed me throughout the process by requiring that I dig, swing, sing, read, and imagine with them during my days at home. Their presence is a constant reminder of the pulse of life outside of school, and I thank them for the symmetry and balance they provide me. May they enjoy the same satisfaction from their academic endeavors that I have received from mine.

Thank you all.

TABLE OF CONTENTS

| | |
|---|-----|
| Abstract..... | iii |
| Acknowledgements..... | vi |
| Chapter 1 Introduction..... | 1 |
| 1.1 Mountain River Sedimentation | 3 |
| 1.2 Pools and Riffles | 6 |
| 1.2.1 Flow Separation and Recirculation in Pools..... | 8 |
| 1.2.2 Sedimentation within Eddies | 10 |
| 1.3 Pools and Fish Habitat..... | 11 |
| 1.4 Study Site | 12 |
| 1.4.1 Channel Characteristics | 13 |
| 1.4.2 Effects of the Sediment Release | 16 |
| 1.4.2.1 Sediment Transport | 22 |
| 1.4.2.1.1 Experimental Release..... | 22 |
| 1.4.2.1.2 Snowmelt Discharge..... | 25 |
| 1.5 Numerical Models as Predictors of Channel Recovery | 26 |
| 1.6 Study Objectives | 27 |
| 1.7 Summary | 29 |
| Chapter 2 One- and Semi Two-Dimensional Sediment Transport Modeling | 30 |
| 2.1 Introduction | 30 |
| 2.2 Model Characteristics..... | 31 |
| 2.2.1 HEC-6 | 32 |
| 2.2.2 GSTARS 2.0 | 33 |
| 2.3 Sediment Transport Model Applications | 35 |
| 2.4 Methodology | 36 |
| 2.4.1 Calibration Data Set..... | 36 |
| 2.4.2 Sediment Transport Modeling | 40 |
| 2.4.3 Step Backwater Computations..... | 44 |

| | | |
|-----------|---|----|
| 2.4.4 | Sediment Transport Capacity..... | 44 |
| 2.4.5 | Scour and Fill..... | 51 |
| 2.5 | Modeling Results..... | 51 |
| 2.5.1 | HEC-6 Experimental Discharge | 51 |
| 2.5.1.1 | Default Simulations..... | 51 |
| 2.5.1.2 | Robust Simulations | 53 |
| 2.5.2 | HEC-6 Snowmelt Runoff..... | 54 |
| 2.5.2.1 | Default Simulations..... | 54 |
| 2.5.2.2 | Robust Simulations | 54 |
| 2.6 | Model Validation..... | 59 |
| 2.7 | Sensitivity Analysis..... | 60 |
| 2.8 | GSTARS 2.0 Results..... | 61 |
| 2.8.1 | Experimental Discharge..... | 61 |
| 2.8.1.1 | Robust Simulations | 61 |
| 2.8.2 | Snowmelt Runoff..... | 63 |
| 2.8.2.1 | Robust Simulations | 63 |
| 2.9 | Discussion | 63 |
| 2.10 | Summary | 66 |
| Chapter 3 | Two-Dimensional Hydraulic Modeling..... | 70 |
| 3.1 | Introduction | 70 |
| 3.2 | Model Characteristics..... | 71 |
| 3.3 | Applications of Two-Dimensional Hydraulic Models..... | 73 |
| 3.4 | Methods..... | 75 |
| 3.4.1 | Field Data Collection | 75 |
| 3.4.2 | Data Reduction..... | 77 |
| 3.4.3 | Mesh Construction and Parameterization | 77 |
| 3.4.3.1 | Roughness | 78 |
| 3.4.3.2 | Turbulent Exchange Coefficients..... | 80 |
| 3.4.3.3 | Wetting and Drying..... | 82 |
| 3.4.4 | Model Simulations Using RMA2 | 82 |
| 3.4.5 | Bed Shear Stress and Particle Stability..... | 84 |

| | | |
|-----------|--|-----|
| 3.4.6 | Sediment Transport..... | 87 |
| 3.5 | Results | 87 |
| 3.5.1 | HEC-RAS | 87 |
| 3.5.2 | Finite Element Mesh and Parameterization | 89 |
| 3.5.3 | Experimental Discharge – RMA2..... | 91 |
| 3.5.3.1 | Model Calibration and Validation..... | 100 |
| 3.5.3.1.1 | Sensitivity Analyses | 103 |
| 3.5.4 | Snowmelt Runoff – RMA2..... | 106 |
| 3.5.4.1 | Model Calibration and Validation..... | 112 |
| 3.5.5 | Hydraulic Properties and Sediment Deposition..... | 113 |
| 3.5.6 | Bed Shear Stress and Incipient Motion..... | 117 |
| 3.5.7 | Sediment Transport Calculations..... | 124 |
| 3.6 | Discussion | 130 |
| 3.7 | Summary | 133 |
| Chapter 4 | Conceptual Model of Pool Sedimentation Patterns | 136 |
| 4.1 | Introduction | 136 |
| 4.2 | Sediment Supply to Mountain Rivers | 139 |
| 4.2.1 | Previous Research on Sediment Influxes to Mountain Rivers..... | 139 |
| 4.2.2 | Reach Scale Response to a Sediment Pulse – A Review..... | 142 |
| 4.2.3 | Width-Scale Response to a Sediment Pulse – A Review | 147 |
| 4.3 | Conceptual Model of Pool Sedimentation for the North Fork..... | 150 |
| 4.4 | Channel Recovery | 157 |
| 4.5 | Recommended Sediment Monitoring Background Data | 158 |
| 4.6 | Sediment Release Recommendations..... | 160 |
| 4.7 | Summary | 162 |
| Chapter 5 | Conclusions..... | 165 |
| 5.1 | Introduction | 165 |
| 5.2 | One- and Semi-Two-Dimensional Numerical Modeling..... | 165 |
| 5.3 | Two-Dimensional Hydraulic Modeling | 167 |
| 5.4 | Conceptual Model for Laterally-Confined Pools..... | 168 |
| 5.5 | Recommendations for Future Work..... | 170 |

| | |
|--|-----|
| Appendix A Sediment Transport Equations..... | 183 |
| Appendix B HEC-RAS Sensitivity Analysis..... | 186 |
| Appendix C HEC-6 Sensitivity Analysis..... | 188 |

CHAPTER 1 INTRODUCTION

It has long been recognized that river regulation through the use of dams causes major alteration in sediment dynamics and channel morphology in downstream reaches of the river (Williams and Wolman, 1984; Collier et al., 1996). Upstream from the dam, sediment accumulation within the reservoir will eventually threaten the storage capacity of the reservoir and the operating efficiency and expected life of a dam. In the semi-arid western U.S., where sediment fluxes from hillslopes may be greater than under any other climate (Schumm, 1965), the hundreds of small reservoirs constructed in the last century are undergoing siltation, forcing state and federal agencies, irrigation companies, and often municipalities to address sediment management issues. The estimate of world-wide reservoir storage capacity loss resulting from siltation alone is approximately $4.9\text{E}^{10}\text{ m}^3$, or the equivalent of \$6 billion in replacement costs every year (Fan and Springer, 1990).

Sediment management practices within reservoirs may include flushing or sluicing reservoir sediments, sometimes voluminously and catastrophically, into the downstream channel. In Colorado alone, five large-scale sediment releases from reservoirs within the last decade have resulted in massive fish kills (Wohl, 1999; Table 1.1). Sediment released into the downstream channel can be highly detrimental to the aquatic biota and their habitat, can significantly alter the channel morphology, and can impair diversion and irrigation structures, water quality, and recreational opportunities downstream (American Rivers, 1999; Wohl, 1999). The sediment infilling may also

affect the capacity of the channel to convey water and sediment, especially during floods. In some cases, the flushing of reservoir sediment has had less detrimental, short-term effects on benthic populations (Gray and Ward, 1982), while in other cases the sediment release resulted in a shift in macroinvertebrate feeding guilds with an overall decrease in species diversity and evenness (Zuellig, et al., in press). Depending on the timing of the sediment release and the channel configuration, the residence time of sediment in the downstream channel may be months to years.

Table 1.1. Reservoir sediment releases in Colorado with associated sediment hazards (modified from Wohl, 1999).

| Reservoir/River | Channel Morphology | Sediment Hazard |
|---|---|---|
| Halligan Reservoir/North Fork Cache la Poudre River, South Platte River basin | Bedrock controlled mountain channel with pool-riffle sequence | Reservoir sediment release in fall 1996, filled pools within downstream channel and killed approximately 4,000 fish |
| DeWeese Reservoir/Grape Creek, Arkansas River basin | Confined bedrock canyon with pool-riffle sequence | Reservoir sediment release in 1992, filled pools and killed approximately 2,000 trout |
| Strontia Springs/Buffalo Creek; South Platte River basin | Bedrock controlled mountain channel with pool-riffle sequence | Increased sediment loads from Buffalo Creek fires filled channel with coarse-grained sediment |
| Paonia Reservoir/North Fork Gunnison River | Cobble bed river with pool-riffle sequence | Details not available |
| Kenney Reservoir/White River | Cobble bed river with pool-riffle sequence | Details not available |

Although flushing sediment into the downstream channel is an effective, low-cost method of managing sediment build-up in reservoirs, current regulatory, environmental and recreational interests in rivers downstream from dams regard indiscriminate releases of large volumes of sediment as unacceptable. If sediment releases are desirable to manage the recognized problem of sediment accumulation in reservoirs, then methods for

assessing the degree of channel change and channel recovery time are required to understand the potential downstream impacts of sediment releases.

The most recently documented large-scale sediment release in Colorado occurred in September 1996 when approximately 7,000 m³ of fine-grained sediment were released from Halligan Reservoir into the North Fork Cache la Poudre River (North Fork) in north central Colorado (Figure 1.1). Sediment from the release filled pools to varying degrees for more than 8 km downstream, completely destroying resident fish populations and benthic macroinvertebrates. This research investigates pool recovery following the sediment release on the North Fork downstream from Halligan Dam through the application and assessment of widely used hydraulic and sediment transport models. The primary objective of the research is to test the ability of the various models to simulate field-measured erosion and deposition in pools following the sediment release within this steep-gradient mountain river. In addition, recommendations for reservoir operation are presented to identify sediment management practices that minimize the deleterious effects to the downstream channel, especially pools, which provide critical overwinter habitat for fish.

1.1 Mountain River Sedimentation

Mountain channels in the western U.S., such as the North Fork, are increasingly subject to sedimentation hazards including those imposed by reservoir releases because of increased urban pressures, and recently, years of drought which have resulted in increased numbers of forest fires. Although mountain channels have had a long history of the standard extractive industries such as mining, logging, and grazing (Wohl, 2000), continued expansion of these activities into pristine watersheds also contributes sediment

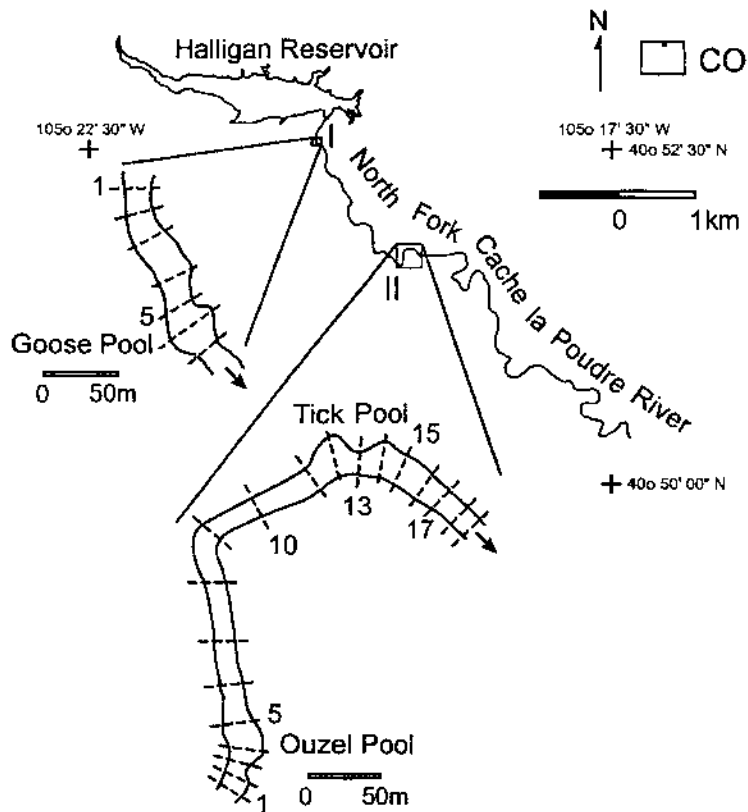


Figure 1.1. Location map of the North Fork study site and modeling reaches. Roman numerals indicate modeling reaches with cross section locations shown as dashed lines perpendicular to the channel. Certain cross sections are numbered and are referred to in the text.

into mountain rivers and streams. At the same time, various agencies are deciding to decommission aging dams subject to re-licensing. Issues of sediment management during dam removal are particularly germane given the large number of dams slated for removal, many of which exist along mountain rivers. The main factor inhibiting dam removal is sedimentation issues and the associated hazards to the downstream ecosystem.

Typically, mountain valleys are bedrock-dominated and rivers within these systems commonly exhibit abrupt variations in gradient, valley width, channel pattern, and grain sizes of bed material and sediment load (Wohl, 2000). Sedimentation within bedrock-controlled rivers may in fact pose more of a hazard than within their alluvial counterparts, especially if sensitive ecosystems or habitats are involved. Typically, mountain rivers are sediment-supply-limited systems, with aquatic species adapted to low sediment loads, clear water, and cold temperatures. A large influx of sediment may have lasting biological consequences (Farnworth et al., 1979; Milhous, 1982), such as impacting fisheries by burying spawning gravel, degrading juvenile rearing areas, decreasing overwinter habitat, and impairing populations of algae and benthic macroinvertebrates.

Sedimentation hazards within mountain channels are in part driven by the channel morphology and associated hydraulic conditions within the fluvial system. Channel morphology within mountain rivers typically consists of alternating pools and riffles or a step-pool sequencing. The hydraulic conditions of mountain rivers are strongly influenced by the steep gradients, and the large grain and form roughness which characterize such systems, and which contribute to their non-logarithmic velocity profiles, localized critical and supercritical flow, and turbulent, three-dimensional flow.

1.2 Pools and Riffles

The development of alternating deeps (pools) and shallows (riffles) is characteristic of both straight and meandering channels with heterogeneous bed material in the size range of 2-256mm (Knighton, 1998). Pools are topographically low areas of the channel bed produced by scour at high flow, and fill at low flow when water-surface gradients are very low. Riffles are topographically high areas of the channel bed which tend to fill at high flow and scour at low flow, and which have relatively high water-surface gradients at low flow. Pools are especially associated with meander bends, and often have a lateral bar, giving the cross section a distinctly asymmetric shape.

Pool and riffle sequences are found in both alluvial and bedrock rivers, and have been described as meandering in the vertical dimension (Keller and Melhorn, 1978). Several studies of pools have documented regular pool spacing, which has been related to channel width (Keller and Melhorn, 1978) and channel gradient (Wohl et al., 1993) among other factors. A velocity-reversal hypothesis was proposed first by Gilbert (1914) and then by Keller (1971), as a way by which pool-riffle spacing and sequences are maintained. These studies proposed that as discharge increases, velocity in pools increases more rapidly than in adjacent riffles, thus explaining the observation that pools scour at high flow and fill at low flow, with the converse occurring in riffles. Thompson et al. (1996) emphasize the importance of pool geometry at high flow, and show that recirculating eddies constrict the downstream flow in pools, allowing higher velocities in pools versus riffles. As a result, pools have higher stream competence than riffle areas (Keller, 1971; Thompson, 1994). The centers of each pool represent an area of maximum stream competence, with decreasing stream competence along the pool exit-slope and lateral

areas of flow recirculation. The regularity of pool spacing has led to studies that interpret the undulating bed topography of pools and riffles as a way of regulating flow energy dissipation (Wohl, 2000).

Pool-riffle sequences in most mountain rivers are initiated by the generation of turbulent flow structures upstream and downstream from a major flow obstacle (Clifford, 1993), such as bank protrusions of bedrock, tree roots, accumulations of vegetative debris, or debris fans from tributary inflow. Lisle (1986) found that the flow obstructions must affect a certain critical percentage of the approaching flow to form large scour holes that extend across the entire channel. The converging flow at the pool head develops a scour hole downstream from the constriction, and is analogous to a flow jet impinging on the channel bed (Lisle and Hilton, 1992), encouraging channel-bed scour and maintaining pool volumes. A jet of high velocity flow occurs when fluid is ejected from an orifice or constriction (Tritton, 1988). At certain locations, the constriction leads to an upstream pool created by the damming effect of the hydraulic control, and a downstream pool from the converging streamlines, with recirculating flow in both eddies. This is similar to the fan-eddy complexes of the Grand Canyon (Schmidt and Rubin, 1995). If the flow obstacle persists long enough, it fixes the local flow pattern and causes modification of the channel form which is maintained by pool-riffle processes such as velocity reversals (Keller, 1971) or bed shear stress reversals (Lisle, 1979) at high flows.

Pools are characterized by an entrance slope and reverse gradient exit-slope at the downstream end. Pool exit slopes are areas of strong turbulent energy dissipation and increased sediment deposition, and also control the size of material leaving pool areas (Thompson et al., 1996). Pool/riffle morphology is ultimately the consequence of the

interactions among flow, sediment transport, and bed morphology integrated over the range of sediment-transporting discharges present in the flow hydrograph (Thompson et al., 1998).

1.2.1 Flow Separation and Recirculation in Pools

The phenomenon of flow separation occurs when flow along a physical boundary develops an adverse pressure gradient, becomes unstable and detaches from the wall, and begins to flow upstream adjacent to the physical boundary (Tritton, 1988). As such, the two necessary factors which cause flow separation are an adverse pressure gradient (increasing pressure gradient in the streamwise direction) and viscosity (Chang, 1970). At high Reynolds numbers, this flow separation process is responsible for the formation of wakes and recirculating eddy systems (Tritton, 1988). Because fluid inertia can be important, flow separation is more common at high Reynolds numbers (Tritton, 1988).

Flow separation begins near the separation point, which describes the point on the channel boundary where the boundary layer detaches from the physical boundary, (Middleton and Southard, 1984). A boundary layer is the zone of flow in the immediate vicinity of a solid surface or boundary in which the motion of a fluid is affected by the frictional resistance exerted by the boundary (Middleton and Southard, 1984). At a point downstream of separation, because of the existing adverse pressure gradient there, reverse flow occurs. Owing to this reverse flow, the boundary layer thickens considerably (Chang, 1970). The reattachment point indicates the location where flow is again parallel to the banks.

Boundary layer separation can create small-scale, periodic, whirlpool-like turbulent features called vortices (Middleton and Southard, 1984). Lateral separation eddies in rivers shed vortices off the eddy fence, which then stretch and dissipate downstream toward the reattachment point. This vortex stretching and associated Reynolds stresses transfer energy from the larger to the small scale eddies such that small eddies become dissipated by viscous stresses in the fluid (Tritton, 1988). Because of the deviation of potential flow stream lines as a result of separation and formation of vortices, the flow separation causes loss of energy. The turbulent flow provides a mixing mechanism through eddy motions and bulk movement of the fluid. The effect of mixing is often expressed as a turbulent shear stress $\tau = \epsilon(du/dy)$, where viscosity ϵ is called eddy viscosity (Chang, 1970).

Flow separation, recirculation, and reattachment occur in virtually all fluvial channels, wherever the bed or bank bends too abruptly for the flow to follow. The separated boundary layer functions as a zone of high shear, and is referred to by various names including an eddy fence, a flow-separation zone, a free shear layer, or a mixing layer (Schlichting, 1979; Middleton and Southard, 1984; Tritton, 1988). The eddy fence is a vertically oriented plane separating the recirculating current from the main downstream flow. The eddy fence appears continuous and unbroken at the water surface at steady discharge (Schmidt, 1990). The eddy fence follows movement of the separation and reattachment points, and can form a substantial hydraulic barrier to the exchange of sediment between the eddy cell and the main channel (Schmidt, 1990).

Flow separation and jet flow at obstructions usually create an area of upstream flowing water termed a recirculating eddy (Tritton, 1988; Schmidt et al., 1993).

Recirculating currents within eddies show a remarkably consistent pattern of flow, and are organized into one primary eddy, and possibly a smaller secondary eddy, both with a vertical axis of rotation (Schmidt, 1990). In the Grand Canyon, recirculating eddies occupy one-third to one-half of the channel width (Schmidt et al., 1993). Rubin and McDonald (1995) have documented irregularly pulsating flow in these recirculating eddies of the Grand Canyon and within flume experiments. Their work derives from field observations of oscillation ripples that are formed by reversing flow in recirculating zones (Rubin and McDonald, 1995). In all cases, eddies derive their energy from the main flow, and can transform large quantities of kinetic energy to latent heat through viscous dissipation (Tritton, 1988). Recirculating flow in lateral separation eddies is typically weaker than main stem flow and provides an effective environment for trapping sediment (Rubin and McDonald, 1995). Recirculating eddy velocities have been measured at greater than 20 percent of free-stream velocities (Schmidt et al., 1993).

Debris within the recirculation zone does not typically float across the eddy fence into the main current. After a sudden increase in discharge, Schmidt (1990) observed boils rising to the surface within the recirculation zone and migrating across the eddy fence. The migrating boils appeared to have higher suspended sediment concentrations, and may be important processes by which fine sediment is moved out of eddy pools.

1.2.2 Sedimentation within Eddies

Eddies are characteristically areas of low velocity, and hence sites of deposition. In the Grand Canyon, deposition of bars occurs in areas where velocity is least, near the separation and reattachment points, and at the center of the eddy (Schmidt, 1990). Carling (1995) observed deposition within recirculating eddies during high flow and

predicted an 87 percent drop in sediment transport efficiency within a recirculating eddy relative to the main flow. Lateral separation zones forming eddies are typically efficient traps for the fraction of diffused suspended sand that is advected across the boundary between the primary and separated flow (Nelson et al., 1994). Sand particles transported into flow separation zones quickly deposit because of prolonged retention of water in the eddy, relative to the settling velocity of sand particles (Schmidt et al., 1993). Work in the Grand Canyon has shown that the size distribution of measured sediment loads and eddy sand deposits are similar (Howard and Dolan, 1981; Schmidt et al., 1993).

1.3 Pools and Fish Habitat

In addition to their geomorphological significance, pool-riffle sequences provide the habitats needed for the maintenance of viable populations of several fish species and a range of invertebrate fauna (Sullivan et al., 1987). Fish move continuously to find and exploit zones of preferred depth, velocity, shear stress and turbulence (Statzner et al., 1988), and recirculating eddy systems in pools are of particular importance as a low-velocity refuge for fish (Shields et al., 1994). Low-velocity areas, such as pools, are also the preferred habitat for newly emerged fish (Sullivan et al., 1987). The best feeding sites for fish are low-velocity zones adjacent to higher-velocity flows or eddies, which provide a concentrated source of food (Sullivan et al., 1987). Fish desire more nonuniform flow, with more of the channel occupied by eddies and regions of reduced velocity. For example, in-channel debris has an effect of creating a varied pattern of velocity distribution (Gipple, 1995) that contributes to physical heterogeneity and enhanced habitat quality. One measure of pool dimension that represents low flow conditions important as summer rearing habitats for fish is the concept of residual depth

(Lisle and Hilton, 1992). Residual depth is a flow-independent measure of pool volume, where residual pools are defined as stream areas that contain water at zero discharge because of the damming effect of the downstream riffle crest. Thus, residual depths represent extreme low flow conditions, which can limit the capacity of a stream to support fish populations (Lisle and Hilton, 1992).

1.4 Study Site

The North Fork Cache la Poudre River is incised into granite of the Silver Plume Formation (Tweto, 1979), and flows within a broad gorge 160 m deep within the South Platte River drainage basin, approximately 60 km northwest of Fort Collins, CO (Figure 1.1). Total drainage area above Halligan Reservoir is 904 km², and the reservoir has a maximum storage capacity of 7.90x10⁶ m³ (6,400 acre-ft). Halligan Dam was built in 1910-1911, constructed of concrete with two outlet valves at the base of the dam which release water to a maximum capacity of approximately 3.5-4.0 m³/s. The head gates are operated by hydraulic controls located above and on the east side of the dam, and because of antiquated technology, fine control of water releases is not possible. During normal reservoir operations, minimal sediment is released from Halligan Dam, and bed material of the North Fork is largely immobile. Sediment accumulation in the Halligan Reservoir continues to affect the storage capacity of the reservoir (Steve Smith, pers. comm., 2001).

Even with the presence of Halligan Dam, the flow regime along the North Fork is strongly snowmelt driven, with minimal flow throughout the winter. Once Halligan reservoir fills in spring, spilling over the dam produces a marked peak in the hydrograph, usually lasting from May through July. The range of mean annual discharge for the period of record (1997 to present) is 0.1 to 30 m³/s.

1.4.1 Channel Characteristics

The channel of the North Fork is bedrock-controlled, with a well developed pool-riffle sequence along a strongly armored cobble and boulder bed. Bed slope, on the reach scale, ranges from 0.011 to 0.02 m/m, with local slopes as high as 0.04 m/m in some riffle areas. Locations of pools along the North Fork are controlled in part by a vertical bedrock wall along at least one side of the channel and the lateral constriction created by the bedrock outcrop. The abundant outcrops of resistant bedrock effectively constitute non-erodible boundaries at the timescale of any given flow, and hence pools are formed where eddies created by these rock masses scour the channel bed.

Pools along the North Fork are consistently spaced approximately 12 times the mean channel width (Wohl and Cenderelli, 2000), a wider spacing than the spacing established by Keller and Melhorn (1978) as characteristic of pool-riffle sequences for alluvial and bedrock rivers. Pool dimensions along the North Fork average 52 m long and 19 m wide, and may be up to 3.5 m deep. Prior to the sediment release from Halligan Reservoir, pools were covered with a thin veneer of coarse sand to pebbles, with cobbles, boulders, and intact bedrock underneath.

Coarse materials in the cobble to boulder size class make up the bed of riffles within the North Fork system. No tributaries enter the main stem of the North Fork, and hence tributary inflow does not control the location of riffles as in other bedrock channels.

One important characteristic of many pools along the North Fork is that they exhibit two areas of flow recirculation, one upstream and one downstream from the lateral constriction (Figure 1.2). Pools of this type are henceforth referred to as

compound or two-part pools, with two topographically deep areas, one upstream of the constriction, and a main scour hole downstream of the constriction. One of the two-part pools may be larger in size (laterally), and contain a more extensive recirculation zone with a larger eddy cell. In most of the compound pools, the upstream eddy derives from backwater resulting from the constriction, and may form in areas where one or both banks are comprised of alluvium. Thompson et al. (1998) found that the backwater resulting from lateral-constrictions serves an important hydraulic role by elevating the water surface, and driving a high-velocity jet of water through the thalweg.

All three pools in Figure 1.1, referred to informally as the Goose, Ouzel, and Tick Pools, are compound pools, with the Tick Pool showing the most pronounced two-part eddy system (Figure 1.2). Much of the numerical modeling completed in this investigation focused on study reaches that included the Tick Pool. From here on, reference to the ‘upstream eddy’ in the Tick Pool refers to the largest area of recirculation upstream from the bedrock outcrop, and reference to the ‘downstream eddy’ indicates the area in the lee of the bedrock outcrop, just downstream from the area of greatest width constriction.

The local hydraulics within the Tick Pool are created by the strong lateral constriction on the left bank (Figure 1.2). The constriction decreases the pressure in the direction of flow as velocity increases because of a decreasing cross sectional area of the channel. Hence, the pressure gradient is negative at the constriction, and flow adheres completely to the walls. However, because of the wall divergence, the pressure increases behind the constriction creating an adverse pressure gradient where the boundary layer separates from the wall and vortices and flow recirculation are formed.

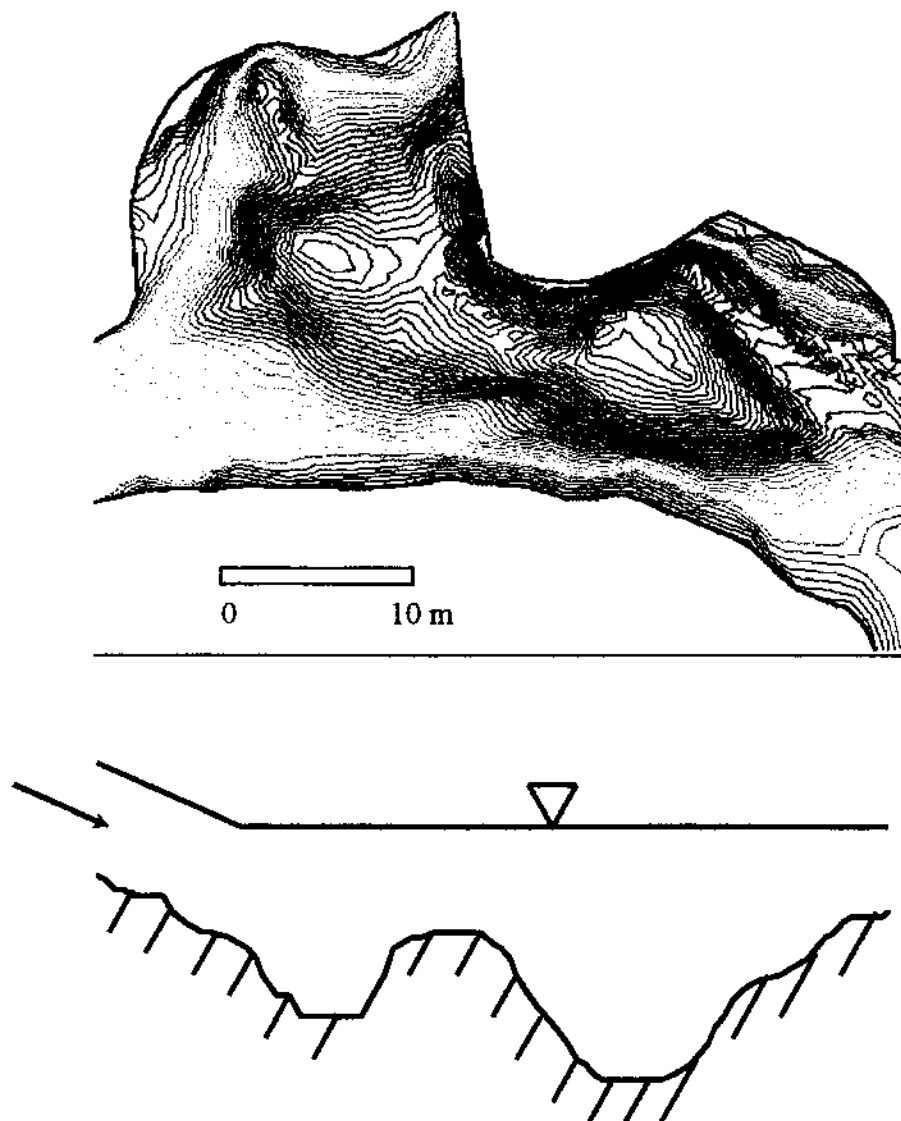


Figure 1.2. Topographic map and schematic longitudinal profile through the Tick Pool, a compound pool along the North Fork Cache la Poudre River. Blue and green (cool colors) indicate topographically deep areas, and orange and red (warm colors) indicate topographically high areas of the channel bed.

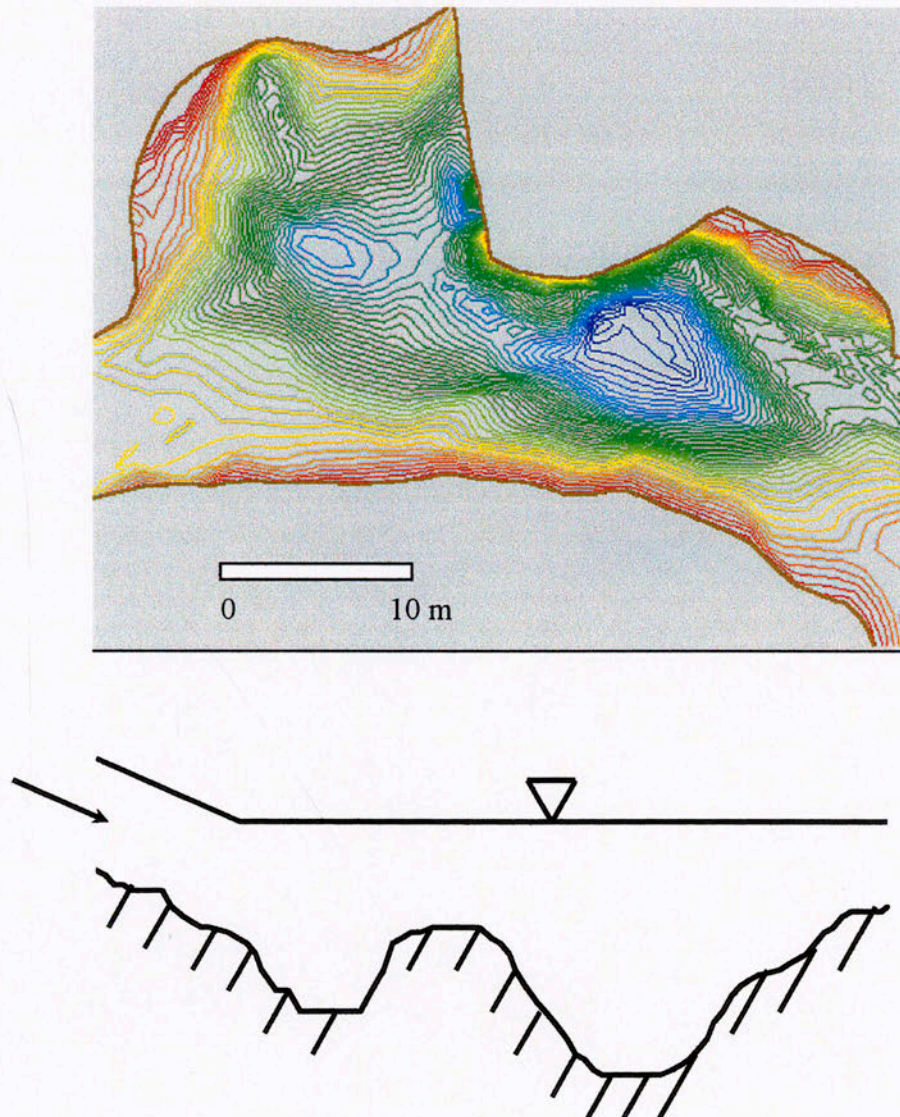


Figure 1.2. Topographic map and schematic longitudinal profile through the Tick Pool, a compound pool along the North Fork Cache la Poudre River. Blue and green (cool colors) indicate topographically deep areas, and orange and red (warm colors) indicate topographically high areas of the channel bed.

1.4.2 Effects of the Sediment Release

The article by Wohl and Cenderelli (2000) describes the sediment deposition and transport patterns and following the release, and much of that information is summarized within the following two sections. The main by-product of the 1996 release was the infilling of pools to varying degrees for more than 8 km downstream, forming a thick veneer of fine-grained sediment over the original cobble/boulder substrate (Figure 1.3), the thickness of which decreased with distance downstream from the dam. At 0.5 km downstream from the dam, pools were completely filled, up to 3.5 m deep, with a uniform layer of gravel- to clay-sized sediment, forming essentially a plane bed within the channel. At 3.2 km downstream from the dam, pools were filled 50% (Figure 1.4) with primarily sand, silt and clay. The sedimentation patterns within the North Fork River are consistent with expected aggradation and degradation, given the general hydraulic conditions of mountain rivers. Thick deposits of sediment were noted in pools, particularly where flow separation was strong, around the periphery of pools, behind large boulders, and as marginal bars. Deposits were commonly absent under the thalweg where velocity is high.

Grab samples of marginal pool deposits at 3.2 km downstream from the reservoir, collected in early October following the sediment release, contained approximately 8% sand, 82% silt, and 10% clay. Within the entire 8 km, deposition within riffles was minimal and nonuniform, occurring as bars along the margins of the channel, and in the lee of large clasts within the channel bed. Fine sediment also infiltrated the interstices of the coarse-grained riffle substrate to a depth of approximately 6 cm.



Figure 1.3. Sediment infilling of the North Fork Cache la Poudre River after the reservoir sediment release from Halligan Reservoir, September 1996. Downstream from the bedrock outcrop on the left bank is a pool, 3.5 m deep, that was filled almost completely with fine-grained sediment. Arrow shows direction of flow.



Figure 1.3. Sediment infilling of the North Fork Cache la Poudre River after the reservoir sediment release from Halligan Reservoir, September 1996. Downstream from the bedrock outcrop on the left bank is a pool, 3.5 m deep, that was filled almost completely with fine-grained sediment. Arrow shows direction of flow.

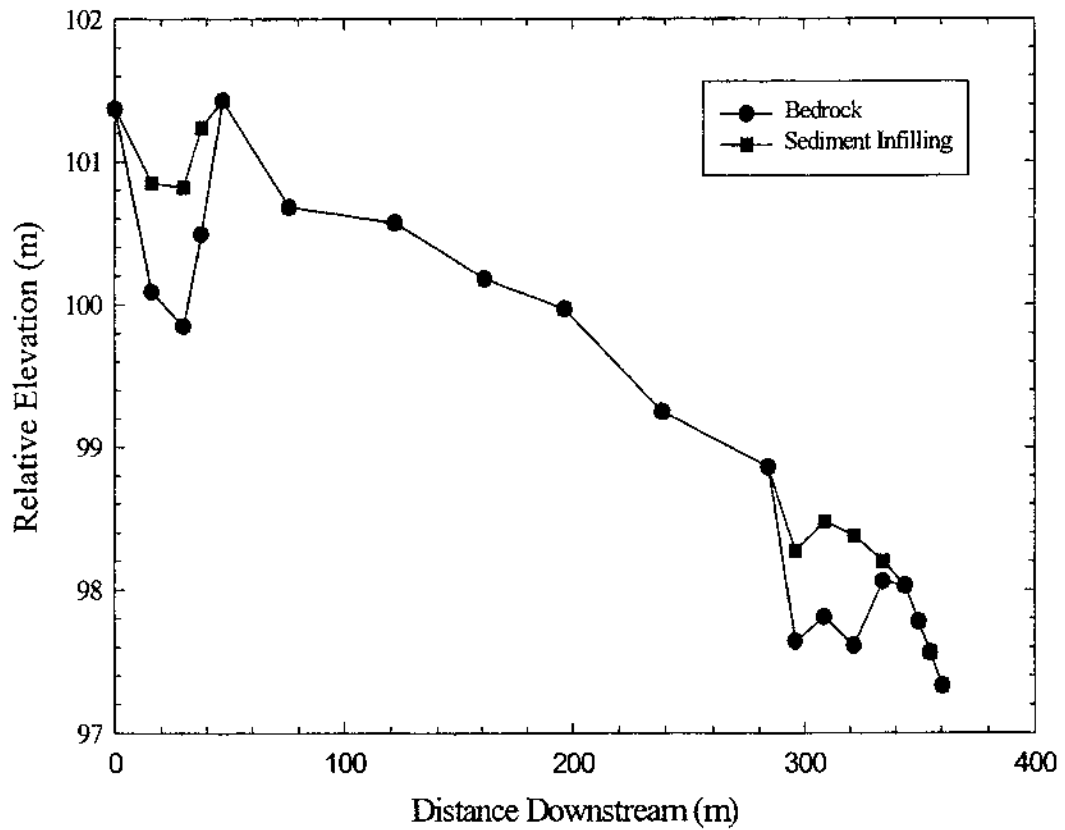


Figure 1.4. Longitudinal profile through the Ouzel and Tick Pools. Sediment infilling of the pools occurred as a result of a sediment release from Halligan Reservoir during the fall of 1996. Vertically exaggerated.

An estimated 4,000 fish, mostly rainbow trout (*Salmo gairdneri*), brown trout (*Salmo trutta*), and white suckers (*Catostomus commersoni*) were killed by the sediment release. The fish loss was significant because of the noted wild trout fishery within The Nature Conservancy's Phantom Canyon Preserve that occupies approximately 10 km along the river corridor downstream from the dam. In an attempt to flush sediment downstream and clear pools critical to fish, a stepped-experimental discharge was released from Halligan Reservoir for one month, from late February to late March 1997, with a peak of $3.4 \text{ m}^3/\text{s}$ (Figure 1.5). In the spring of 1997, flow increased naturally with the onset of snowmelt in the headwaters of the North Fork, and peaked on June 3 at $10.1 \text{ m}^3/\text{s}$. The three distinct peaks of discharge during the maximum snowmelt runoff period reflect either rain-on-snow events at higher elevations or heavy rainfall at lower elevations that increased inflow into the reservoir and subsequent outflow from the reservoir. Discharge at the time of the release was unknown, but high water marks from the sediment release flow correspond to a maximum discharge of $3.9 \text{ m}^3/\text{s}$. Reported capacity of the outlet valve at the base of Halligan Dam is $3.5 \text{ m}^3/\text{s}$, however, measurements in the field indicate the releases from the outlet valve varied from $3.4\text{-}4.0 \text{ m}^3/\text{s}$. This range of flows represents the low flow, flushing discharge used in simulations of all the numerical models tested.

Two study reaches were established for modeling purposes after the sediment release to monitor sediment movement through the river over time. Reach I, located 0.5 km downstream from Halligan Dam, is 120 m long and includes seven surveyed cross sections through one riffle and one pool (Table 1.2; Figure 1.1). Reach II, 3.2 km

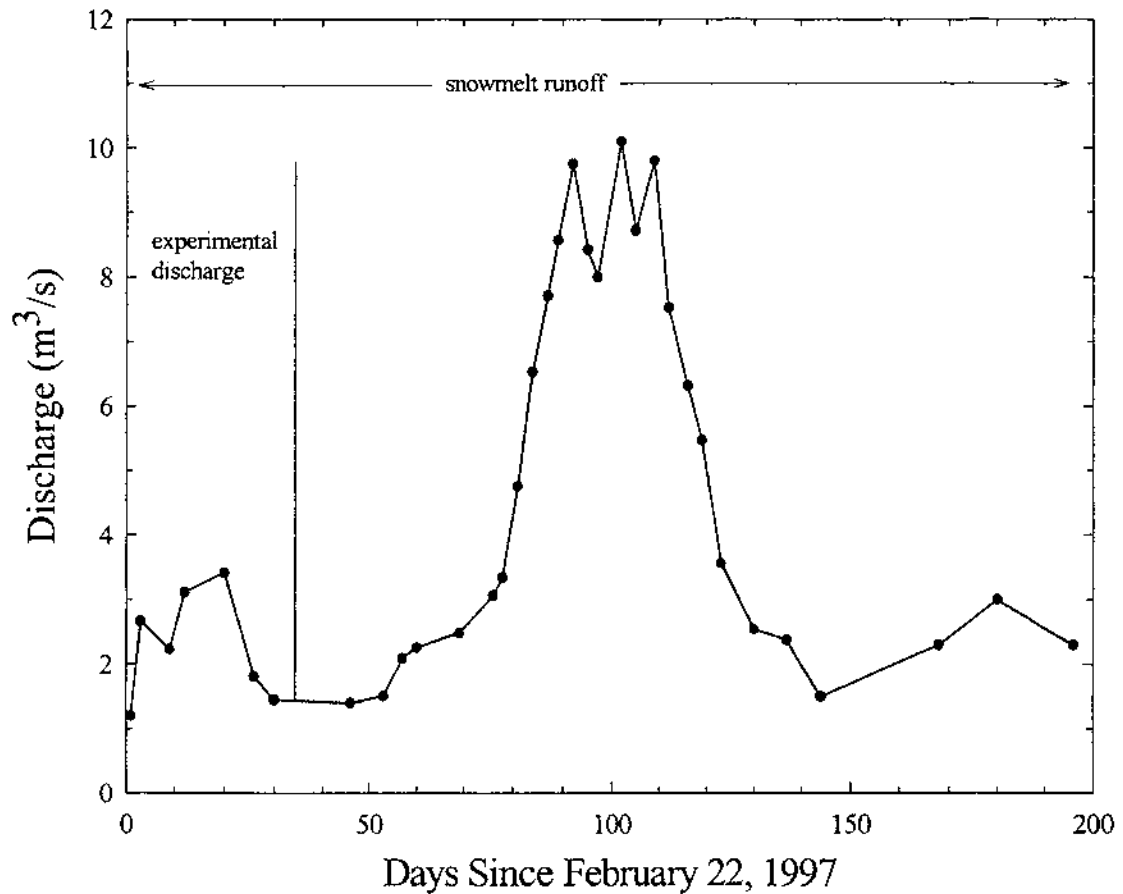


Figure 1.5. Hydrograph for the North Fork beginning on 22 February, the day flow began to rise from winter base flow and a one-month experimental discharge was released from Halligan Reservoir with the intent of flushing sediment from the downstream channel. Two modeling scenarios were conducted which correspond to the delineations shown on the hydrograph: an experimental discharge simulation and a snowmelt runoff simulation.

Table 1.2. Summary of field data collection for the North Fork Cache la Poudre River following the Halligan Reservoir sediment release.

| Dates | Surveyed Cross Sections, Reach I (Fig. 1.1) | Surveyed Cross Sections, Reach II (Fig. 1.1) | Velocity Measurements* | Staff Plate Readings | Sediment Transport * | Grab Samples and/or Pebble Counts | Timed Photos, Tick Pool only |
|----------------|---|--|---------------------------|--------------------------------|----------------------|-----------------------------------|------------------------------|
| Oct.-Nov. 1996 | 1-7 | 1-19 | no | no | no | yes | no |
| March 1997 | 4-7 | 1-4 and 11-15 | yes | yes, at Cross Sec. 1 and 17 | yes | yes | no |
| Aug. 1997 | 4-7 | 1-4 and 11-15 | yes | yes, at Cross Section 1 and 17 | yes | yes | no |
| Snowmelt 1998 | no | no | no | yes | no | no | yes |
| Sept. 1998 | no | entire Tick Pool | yes, within the Tick Pool | yes, within the Tick Pool | no | no | no |

Note: Columns with * indicate that flow velocity, staff gage readings and sediment transport were measured continuously on either a weekly or biweekly basis throughout the snowmelt season of 1997.

downstream from the dam, is 400 m long, with 19 surveyed cross sections, including two pools and two riffles. An additional study reach was established 4.9 km downstream from Halligan Dam, consisting of one pool, and included in the investigation by Wohl and Cenderelli (2000). The downstream-most study reach was not used in this analysis because of the lesser amounts of sediment accumulation in pools at this distance from the dam, and because of its distance from riffles in which field measurements were made to establish boundary conditions for the models. Many of the patterns of erosion and deposition noted in pools in the other two study reaches were also present in the third reach.

1.4.2.1 Sediment Transport

Sediment transport within the North Fork (Figure 1.6) consisted of an initial flush of suspended sediment within a few days of the rising limb of the experimental release hydrograph. Another minor suspended sediment peak occurred during the onset of the snowmelt runoff. Maximum bedload discharge occurred in the Tick Pool when water discharge was highest during the snowmelt period, occurring earlier for pools closer to Halligan Dam. Bedload transport rates are strongly linked to the supply of sediment from upstream pools that were filled by the fall 1996 reservoir release. Sediment storage in pools and the transfer of sediment between pools was the key control on sediment volume stored within the channel, and the major factor in determining habitat availability for fish within the North Fork.

1.4.2.1.1 Experimental Release

During the pre-snowmelt, stepped-experimental discharge, scour along the thalweg of each pool within the study reaches and additional deposition on the channel margins created a narrow, deep cross section, with an accompanying lateral shift in the thalweg. Within the Tick Pool, the experimental release reworked sediment within the thalweg, scouring down to the original bed elevation at Cross Section 12 and 13, the upper pool and the constriction (Figure 1.7). As much as 0.5 m of deposition occurred along the thalweg at Cross Section 14 at the pool exit slope. Transport of sediment from the Tick Pool to the next downstream pool was interrupted, because boundary shear stress was not sufficient to transport sediment out of the Tick Pool to the downstream riffle. Lisle and Hilton (1992) found similar patterns of sediment movement between pools and riffles on eight gravel bed streams that are tributaries of the Trinity River in northwestern CA.

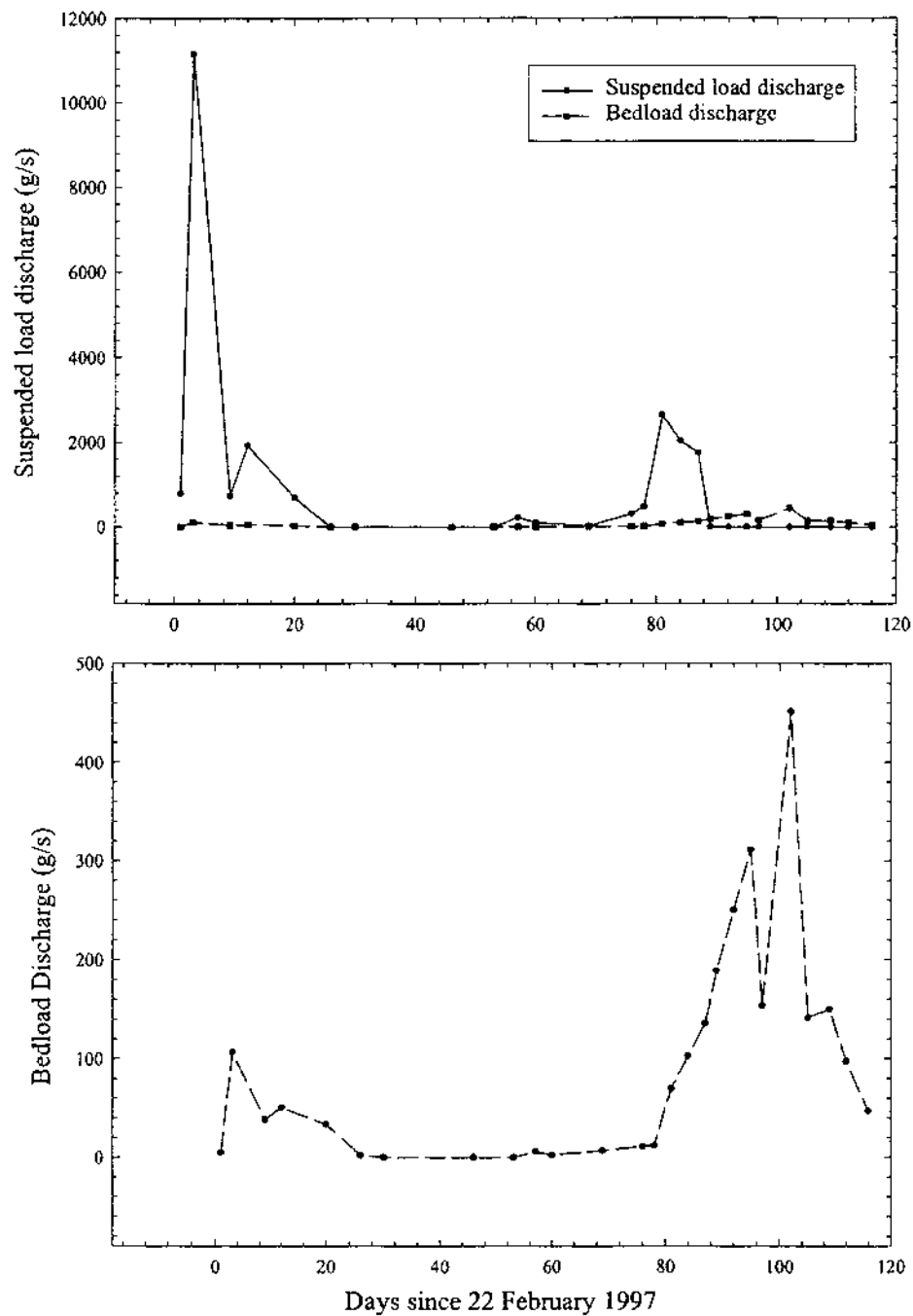


Figure 1.6. Suspended and bedload discharge collected at Cross Section 13 beginning on 22 February, the day flow began to rise from winter base flow and a one-month experimental discharge was released from Halligan Reservoir. Modified from Wohl and Cenderelli (2000).

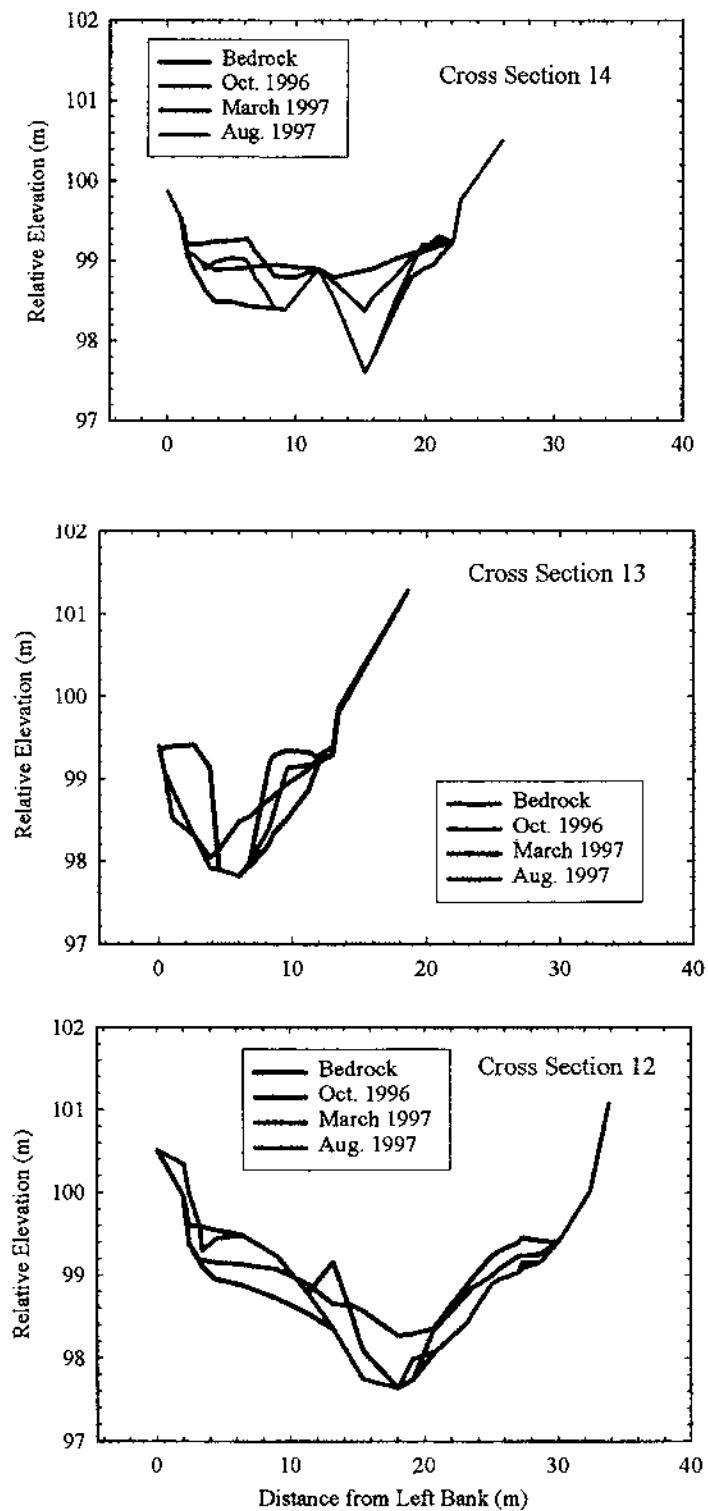


Figure 1.7. Cross sections through the Tick Pool, North Fork Poudre River following field surveys of bed changes due to scour and deposition of reservoir-released sediment. Cross Section 12 is upstream, Cross Section 14 is downstream.

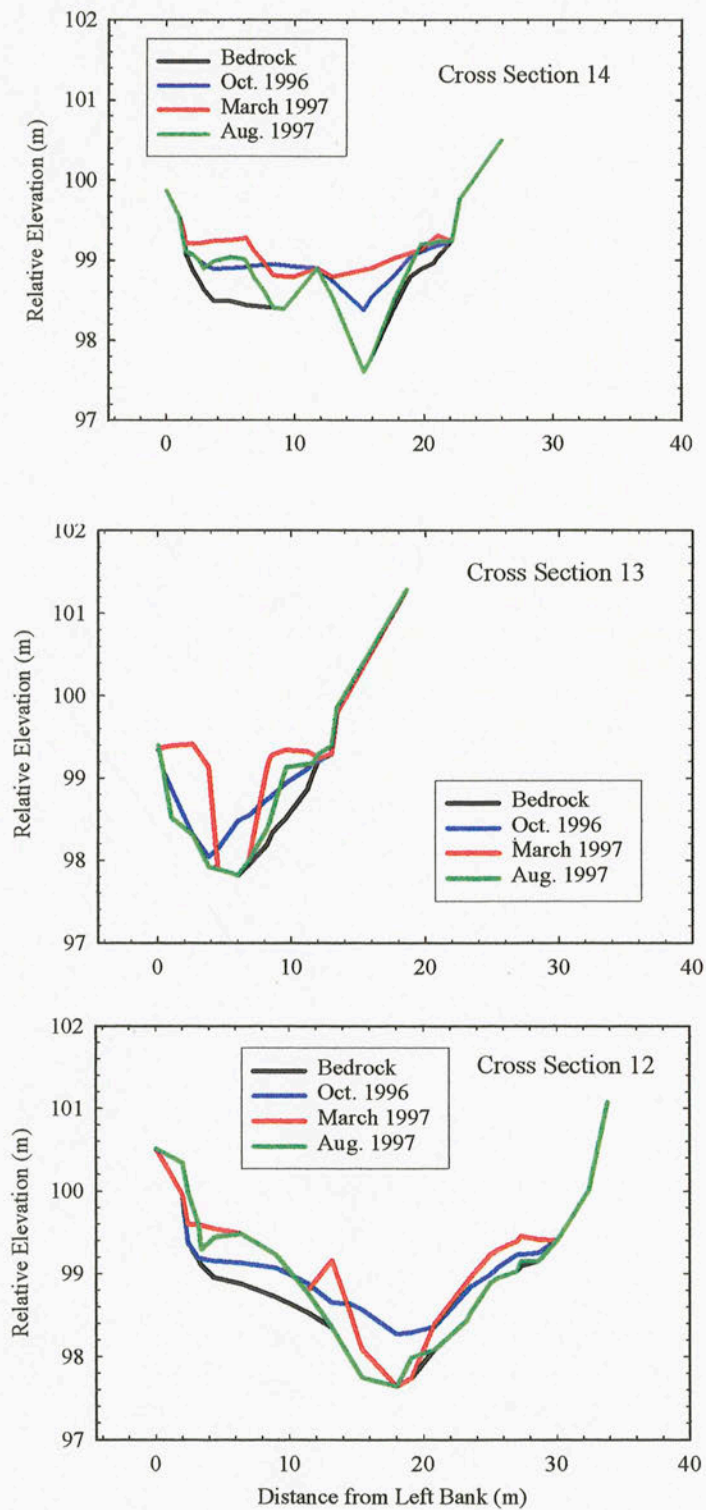


Figure 1.7. Cross sections through the Tick Pool, North Fork Poudre River following field surveys of bed changes due to scour and deposition of reservoir-released sediment. Cross Section 12 is upstream, Cross Section 14 is downstream.

When local transport capacity in the pools became insufficient to transport sediment onto riffles, the pools aggraded with fine sediment.

At all cross sections within the Tick Pool, aggradation occurred adjacent to the left and right banks on top of the October bed surface as a result of the experimental release (Figure 1.7). This occurred because the sediment that filled the pools reduced pool volume and elevated pool bottom surfaces, causing sediment transport to higher levels in lateral pool areas.

1.4.2.1.2 Snowmelt Discharge

After the snowmelt runoff, lateral scour within the pools increased channel widths in nearly all pools in the study reaches, resulting in an overall pool volume recovery of approximately 80% of the pre-release volume. As an example, the plot of channel Cross Sections 12-14 through the Tick Pool (Figure 1.7), shows that between March 1997 and August 1997, the most effective sediment clearing occurred at Cross Section 14, which bisects the downstream eddy. Conversely, Cross Section 13 through the constriction indicates no additional scour and removal of sediment between March 1997 and August 1997, except for a small area near the left-most bank. Marginal deposits within Cross Sections 12 and 14 were largely unaltered by the snowmelt discharge, and these deposits within the Tick Pool have become the most persistent sediment storage sites following the reservoir release. In fact, vegetation became established on many of the lateral aggradation bars as water levels dropped following the snowmelt runoff and the saturated deposits of fine sediment became exposed.

1.5 Numerical Models as Predictors of Channel Recovery

Large influxes of sediment into downstream ecosystems are recognized as hazards to the aquatic community, recreation, water quality, and engineered structures. As a result, investigations that are focused on the prediction of channel recovery, and that incorporate hypothetical scenarios of flushing flows, may be the only way to develop and test potential flushing regimes. Where restrictions on water releases exist, such as the semi-arid west, numerical models are especially useful. Unfortunately, there are no commercially available flow models that are uniquely designed for use in bedrock channels, nor are there particular solution techniques devised specifically for bedrock channels (Miller and Cluer, 1998). Flow patterns in bedrock rivers are complex and flow fields are often difficult to measure directly, especially at high flows when conditions are hazardous and accessibility is limited. Thus, flow models become more important in efforts to understand mountain river behavior, even as the availability of data for model verification lags behind.

The number of published modeling studies treating bedrock-controlled systems is still quite small by comparison with the volume of literature on flow modeling in alluvial channels. Among the studies that do treat bedrock systems, the majority have focused on the application of one type of model, the one-dimensional step-backwater model for computation of water-surface profiles (Baker, 1984; Wohl, 1992; O'Connor, 1993; Rathburn, 1993). One-dimensional step-backwater models have been more frequently applied to bedrock systems than any other type of model, with most of the research directed at reconstructing paleoflood discharges. Bedrock canyons and their tributaries

are particularly opportune locations for the preservation of paleostage indicators such as fine-grained slackwater deposits (Patton et al., 1979).

In situations where numerical models are applied to recent discharges along mountain rivers, adequate calibration and validation data may become more available through technological advances in hydraulic field data acquisition. In these instances, application of numerical models can be more appropriately constrained by field data and observational experience. In the end, numerical models have the potential to provide predictive insight into certain channel responses to changes in water and sediment discharge. The application of such models to mountain rivers requires recognition of model limitations within the context of the study objectives.

1.6 Study Objectives

Large volumes of sediment introduced to mountain rivers pose serious hazards to the ecological community, and change the channel morphology in ways that can diminish the functioning of the fluvial system. Using the North Fork Poudre River as a case study, sediment transport and hydraulic models were applied to flow scenarios to predict pool volume recovery for the reestablishment of fish habitat. Following an approach presented by Lane et al. (1999), the assessment of the models includes the distinction between predictive ability, or the extent to which a model provides adequate representation of an independently acquired data set, and prediction utility, or the extent to which the model provides information appropriate to the study objectives.

The primary objective of this study is to evaluate the ability of various numerical models to simulate field-measured erosion and deposition and hydraulic conditions following the sediment release for purposes of sediment management within pools along

the North Fork from the perspective of a water resource specialist. Because of the thriving, pre-release wild trout fishery downstream from Halligan Reservoir, flushing of pools along the North Fork to re-create overwinter fish habitat was of prime concern. To date, most flushing flow research has been directed at identifying discharges that effectively flush fine sediments from spawning gravel within riffles and runs (Kondolf and Matthews, 1993; Wilcock et al., 1996). In the case of the North Fork, minimal amounts of sediment from the reservoir release accumulated in riffles, whereas sedimentation of pools was substantial.

Chapter 2 presents the methods and results of one- and semi-two-dimensional sediment transport modeling that was directed at pool flushing to enhance overwinter pool volumes for fish. The modeling was designed to test the following research hypothesis:

Hypothesis 2.1: One and semi two-dimensional sediment transport models are useful predictors of pool recovery. The models are evaluated against field-measured pool bed change.

Two-dimensional hydraulic modeling of flow recirculation within the Tick Pool is presented in Chapter 3, and designed to test the following hypothesis:

Hypothesis 3.1: A two-dimensional hydraulic model provides improved representation of eddy pool hydraulics, the results from which can be used to infer sediment transport characteristics. The model is tested against field measurements of flow velocity and pool depth, and quantified patterns of pool scour and deposition.

To supplement the numerical modeling, a qualitative model of sediment movement and storage in pools is presented in Chapter 4. Additionally,

recommendations for reservoir operation are provided to identify minimum discharge requirements to flush sediments from critical habitat reaches. The final hypothesis tested is as follows:

Hypothesis 4.1: A conceptual model may be the most useful for predicting channel response to sediment releases in situations where numerical models are infeasible. The conceptual model is compared to observations of sediment transport and storage in pools at different distances from Halligan Dam.

1.7 Summary

Excess sediment delivered to fluvial systems poses a threat to the proper physical and biological functioning of the channel. Excess sediment preferentially fills pools, especially where lateral flow separation and recirculation comprise a significant portion of the pool area. Pools are important low-velocity rearing sites for fish, and the best feeding sites include low-velocity zones adjacent to higher-velocity flows, which provide a constant source of food.

A recent reservoir sediment release in northern Colorado resulted in pool infilling along approximately 12 km of the steep-gradient, bedrock-controlled North Fork Cache la Poudre River. Compound pools within the North Fork system provide important overwinter habitat for several species of wild trout. Channel recovery was measured through repeat surveys of sediment erosion and deposition at study reaches at various distances downstream from the dam. This document tests numerical and conceptual models against measured pool recovery via three research hypotheses.

CHAPTER 2 ONE- AND SEMI TWO-DIMENSIONAL SEDIMENT TRANSPORT MODELING

2.1 Introduction

Following the 1996 sediment release from Halligan Reservoir, questions of channel recovery, especially pool recovery, began to emerge from water resource specialists who realized the need to reestablish critical overwinter habitat for fish. Numerical models are recognized as useful instruments in prediction, and can aid in decision-making about the outcomes of alternative courses of action, in this case flushing flows for the removal of sediment within pools.

One-dimensional sediment transport models have become increasingly useful predictive tools to assess aggradation and degradation within channels, particularly in and around hydraulic structures. In addition, where long-term predictions are required, numerical models are the only way to simulate aggradation and degradation of the channel bed. It is hypothesized (*Hypothesis 2.1*) that one-dimensional sediment transport models are useful tools to estimate channel recovery times and flushing flow needs after a reservoir sediment release. Particularly in situations of limited water availability, where any discharge release is expensive and undesirable, models may be useful in designing a minimum flow regime necessary to flush sediment and restore the aquatic habitat. Much of the information in this chapter draws upon and expands the results of Rathburn and Wohl (2001).

2.2 Model Characteristics

The two, one-dimensional models selected for application to the North Fork were HEC-6, developed by the U.S. Army Corps of Engineers, Hydrologic Engineering Center (U.S. Army Corps of Engineers, 1998a), and GSTARS version 2.0, created by the U.S. Bureau of Reclamation (Yang et al., 1998a). The models were selected because they are economical, widely accessible, and likely to be used as predictive tools by water resource managers faced with channel infilling associated with released reservoir sediment. It should be noted that neither model is well suited for a steep gradient mountain channel with an immobile bed. The question of whether or not moderately user-friendly, one-dimensional numerical models can be used in such environments is a major component of this research, and one that was tested by applying the models to the North Fork sediment release.

The primary criterion used to evaluate HEC-6 and GSTARS was the ability of the model to reproduce pool scour and fill measured in repeat field surveys under varied discharges. Models that reproduce measured scour and fill could then be used to identify the appropriate flushing flows which would minimize or eliminate the hazards of pool infilling from reservoir sediment releases. An additional aspect of the model evaluation was the time investment and level of expertise required to obtain meaningful simulation results. A truly useful reservoir management tool would not require extensive training in hydraulics and sediment transport; would have data requirements that are not too labor or cost intensive; and could be developed and run in a timely manner, yielding useful raw model output. However, the state of numerical models suggests that this will not be the situation for the foreseeable future. Therefore, existing models were applied to the

problem of pool infilling along the North Fork, and the reasonableness of the output was interpreted in the context of existing model limitations and study objectives.

2.2.1 HEC-6

The HEC-6 model is a one-dimensional model that predicts scour and deposition within rivers and reservoirs (U.S. Army Corps of Engineers, 1998a). In river applications, HEC-6 simulates uniform changes in river bed elevation over the entire width of the channel caused by erosion and deposition over time under subcritical flow. The model has no provisions for simulating lateral channel changes such as meander migration or lateral changes in bed slope. The governing equations in HEC-6 include the energy equation, and conservation of mass for water and sediment. The momentum equation is not included in HEC-6, so environments with rapid fluctuations between subcritical and supercritical flow are inappropriate for modeling. In addition, HEC-6 assumes that sediment supply and demand are satisfied within each reach at each time step, and the model takes into account the effects of sediment gradation. HEC-6 is one of the most widely used and economical, commercially available sediment transport models. The most recent version of HEC-6 can be downloaded from the web at <http://www.wrc-hec.usace.army.mil/>.

Three model components comprise HEC-6 and require specification by the user. These include a geometric component consisting of surveyed channel cross sections; a hydrologic component of discharge at the upstream boundary, represented as a series of steady, uniform flows; and a sediment component including inflowing sediment load, sediment rating curve, and the gradation of bed material. Several default options allow the user to select recommended input settings should some of the input data be

unavailable or should the user be unsure of which option to choose. In other cases, input settings offer several choices, such as selecting one of 14 sediment transport equations. The output of interest in this application of HEC-6 is the average or uniform bed change at a given channel cross section (Figure 2.1).

2.2.2 GSTARS 2.0

In contrast to HEC-6, GSTARS is a quasi-two dimensional model that utilizes a stream tube approach to accommodate differential scour and deposition over the width of a cross section (Yang et al., 1998a). Stream tubes are conceptual tube-like surfaces whose walls are defined by streamlines, imaginary lines which show the direction and magnitude of velocity as the tangent at every point along the line, at each instant in time. In GSTARS, hydraulic parameters and sediment routing computations are made for each stream tube, allowing the position and width of each stream tube to change. In this way, vertical and lateral variations in cross sectional elevation can be simulated (Figure 2.1). The governing equations are largely similar between HEC-6 and GSTARS, except that GSTARS incorporates the momentum equation in backwater computations when the flow regime changes from subcritical to supercritical or vice versa. GSTARS was selected for testing along the North Fork to evaluate the applicability of another comparable sediment transport model, to overcome suspected limitations of the purely one-dimensional HEC-6 model, and to potentially improve the accuracy of the output without substantially increasing input effort.

Input for GSTARS is similar to HEC-6, but offers a broader range of options with very few default choices built into the model. Other differences between the two models include the ability to specify the number of stream tubes at each cross section (up to five),

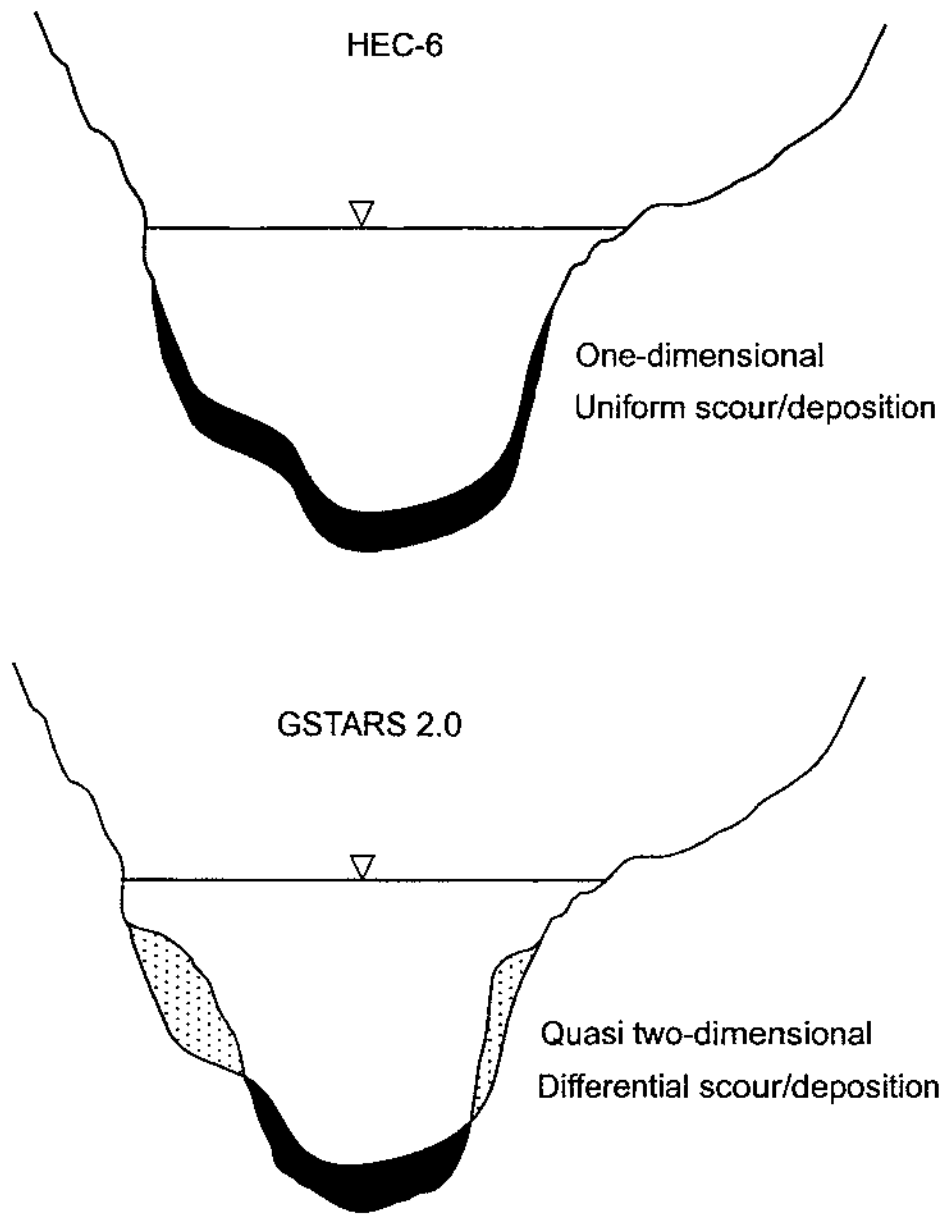


Figure 2.1. Schematic cross section showing differences in model characteristics between HEC-6 and GSTARS 2.0. The solid black pattern indicates scour along the bed of the channel, and the stippled pattern indicates deposition.

a different list of sediment transport equations from which to choose, and determining whether nonequilibrium sediment transport and stream power minimization procedures are appropriate for the application. Although both models include an option of choosing among a variety of sediment transport formulas, neither provides guidelines on selecting the appropriate formula. The most recent version of GSTARS can be downloaded from the internet at <http://www.usbr.gov/srhg/gstars/2.0/>.

2.3 Sediment Transport Model Applications

Numerous one-dimensional sediment transport models have been developed and tested in flumes and alluvial rivers of varied slopes, bed material, and grain sizes. Most often, engineering applications of one-dimensional sediment transport models test the resultant vertical scour and fill created by a proposed structure to assist general engineering design work and flood control implementation (Pickup, 1980; Gee, 1984; Copeland, 1986; Fischenich, 1990). Other applications of one-dimensional sediment transport modeling studies include assessing spawning habitat (Havis et al., 1996), especially downstream from dams (Wick, 1997), predicting degradation of the stream bed below dams (Krishnappan, 1985; Carriaga and Mays, 1995), and evaluating the effects of dam removal (Williams, 1977; Stoker and Williams, 1991).

GSTARS has been applied to alluvial rivers by Yang and Simoes (1998), and Yang et al. (1998b), to assess the quasi two-dimensional changes in a channel bed resulting from scour and fill. Applications of GSTARS to engineering problems include knickpoint migration that may undermine bridge piers and other structures, bed degradation and armoring resulting from installation of a dam, and reservoir sedimentation (Yang and Simoes, 1998). In the first two cases, GSTARS was tested

against flume data of other researchers, and against actual field data for the reservoir sedimentation study. The agreement between measurements and simulation was good, although the model tended to overpredict reservoir sedimentation in some areas.

2.4 Methodology

Fieldwork was conducted to monitor sediment movement within the North Fork Cache la Poudre River after the 1996 sediment release, and to establish a known condition for calibration of the models. Subsequent analyses were carried out to develop input files for both HEC-6 and GSTARS, calibrate the models, and verify the calibration on another pool within the North Fork system.

2.4.1 Calibration Data Set

Channel surveys were conducted along the study reaches (Figure 1.1) in October 1996, immediately following the sediment release; in March 1997 after the experimental discharge; and again in September 1997 after the snowmelt runoff had receded (Table 1.2; Figure 1.5). During all surveys, a total station with a prism mounted on top of a stadia rod was used to obtain x,y,z coordinates. Channel cross sections were surveyed and the thickness of reservoir sediment accumulation was determined by probing with a steel rod down to the original cobble and boulder channel bed. Pebble counts (Wolman, 1954) were conducted along the riffles within the study reaches to define the grain size distribution of the pre-reservoir-release bed material. Grab samples were collected from deposits along the margins of pools and from the bed of pools to quantify the grain size of reservoir sediment in the pools (Figure 2.2).

A sampling cross section was established in a riffle at Cross Section 1 and at Cross Section 17 at Reaches I and II, respectively (Figure 1.1). From February 22 to

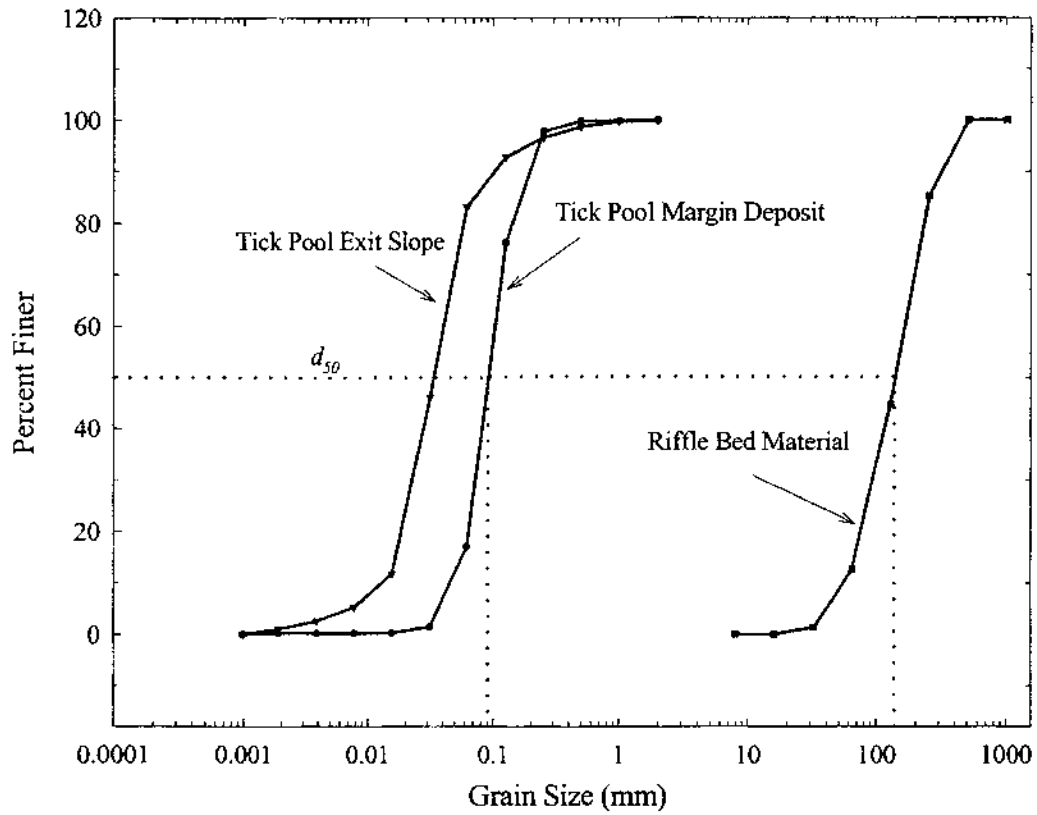


Figure 2.2. Grain size distribution of bed material from the Tick Pool and adjacent riffle during initial sampling in October 1996 immediately following the sediment release. The median diameter of bed material from the margin of the Tick Pool (0.092 mm) was used to evaluate various sediment transport equations prior to computer modeling.

September 3, 1997 the cross sections were sampled weekly. During the snowmelt peak (May to June) the sampling frequency was increased to twice a week. Flow depth and velocity at 0.4 and 0.6 the flow depth were measured at 1-m intervals, and bedload and suspended load samples were collected at four, 2-m intervals along the cross section (cross section widths varied from 12 to 15 m). The velocity measurements were collected with a Marsh-McBirney Model 2000, with each point measurement representing an average of five readings taken every 6 sec. These data were used to derive sediment and water rating curves, inflowing sediment loads, bed material gradation, and a starting water-surface elevation, which are required inputs for both sediment transport models. Details of the sampling methods and field procedures at the North Fork are presented more fully in Wohl and Cenderelli (2000).

A roughness coefficient for the sample Cross Section 17 (Figure 1.1) was determined using the Manning equation, as well as equations by Jarrett (1984, 1985), Limerinos (1970), and Hey (1979) and the field measurements of hydraulic and channel properties (Figure 2.3). Although none of the methods of estimating a flow resistance coefficient used in constructing Figure 2.3 is designed specifically for steep-gradient channels, the four selected are reasonable choices for the North Fork Poudre River. Jarrett's (1984, 1985) equation is based on empirical data from numerous channels, many of which are mountain rivers in Colorado, and incorporates the energy gradient and hydraulic radius to predict an n value. The equation developed by Limerinos (1970) relates n to hydraulic radius and particle size, and was derived from data on lower gradient rivers with bed material in the small gravel to medium-boulder size range. Hey (1979) developed an

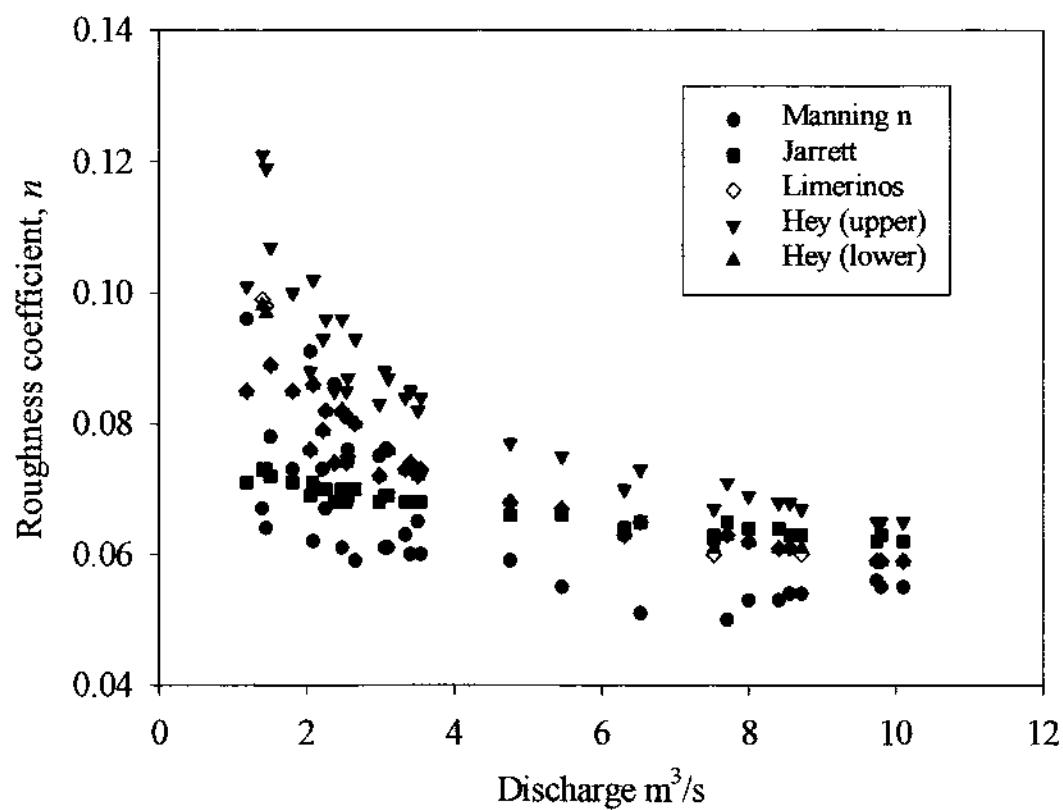


Figure 2.3. Comparison of flow resistance estimates at Cross Section 17 using various equations.

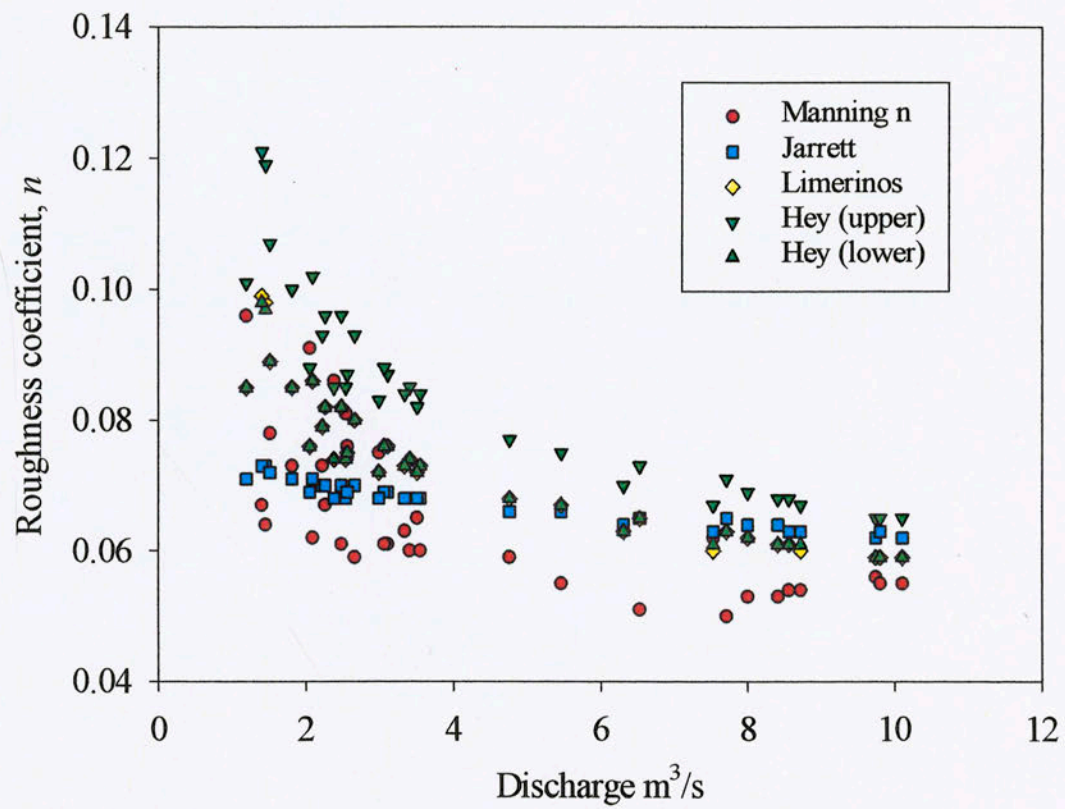


Figure 2.3. Comparison of flow resistance estimates at Cross Section 17 using various equations.

equation with an upper and lower estimate, based on data from gravel-bed rivers, which can be rearranged to solve for n .

For purposes of one- and semi-two dimensional modeling, a roughness coefficient of 0.07 was selected for the riffle portions of the modeling reach based on the comparison of estimates in Figure 2.3. A Manning's n value must be specified in both HEC-6 and GSTARS 2.0 for the discharge simulations conducted, and although there remains some uncertainty in the choice of appropriate roughness coefficients, the selection of Manning's equation as an estimate of n is considered reasonable for the current investigation. The Manning equation was developed to describe open-channel situations with fully turbulent flow where friction is controlled by surface drag from the bed sediments. Specification of pool roughness in the models is not based on calculations from hydraulic and channel conditions, because it was not possible to measure velocity in the pools over a range of flows because of pool depths that were greater than the length of the wading rod, and swift velocities at high flow. Rather, n in the pools was chosen as 0.04 based on knowledge of bed material and the boundary geometry. Sensitivity analyses on the effects of varied Manning's n were conducted using HEC-RAS, the U.S. Army Corps of Engineers Water Surface Profile program (U.S. Army Corps of Engineers, 1998b).

2.4.2 Sediment Transport Modeling

Two flow scenarios were simulated using HEC-6 and GSTARS: 1) a short-term, one-month experimental discharge, that represented the stepped-experimental release from Halligan Reservoir and, 2) a longer-term, six-month snowmelt discharge that represented runoff during the spring of 1997 (Table 2.1). Under both flow scenarios, two

end member simulations were conducted: default and robust simulations. Default simulations were used to determine the minimum input requirements to obtain reasonable results, and were constructed by selecting pertinent default options available in the model input. In many applications of sediment transport modeling, field-based measurements may be limited or unavailable, and the default values within the model would be selected by a user. During the robust simulations all available field data were utilized, thereby constraining the model through field quantification of input parameters. Table 2.1 lists the input parameters pertinent to the one-dimensional models HEC-6 and GSTARS as applied to the North Fork.

Table 2.1. Discharge scenarios modeled using HEC-6 and GSTARS 2.0 to evaluate pool recovery along the North Fork Cache la Poudre River.

| Flushing Flow | Magnitude | Duration |
|------------------------|---|----------|
| Experimental Discharge | 3.4 m ³ /sec (dam outlet capacity) | 1 month |
| Snowmelt Runoff | 10 m ³ /sec (snowmelt peak) | 6 months |

All model scenarios were simulated using the October 1996 cross sectional elevations to define the bed topography following the sediment release. Additionally, the actual hydrograph for both the experimental release and the snowmelt runoff were reproduced as a series of steady flows and input into HEC-6.

In HEC-6, the main default values substituted for field data that are difficult or time-intensive to obtain include: (1) elevation of the model bottom at each cross section, or the thickness of the sediment deposit from the reservoir, and (2) transport of cohesive silt and clay (<0.0625 mm). Standard simulations of HEC-6 compute only deposition of silt and clay, and if erosion of silt and clay is desired, then shear stress thresholds for fine-grained, cohesive sediments must be prescribed. Likewise, GSTARS requires

additional input if sediment size fractions less than 0.0625 mm are transported (recall that approximately 92% of the initial grain size distribution of pool sediment following the release was silt and clay). Theoretical data from Ariathurai and Arulanandan (1977) were used to specify the necessary values of shear stress for cohesive sediment transport in both models.

Initially, model calibration was conducted on the Ouzel and Tick Pools within Reach II (Figure 1.1). Model calibration is the process by which adjustments are made to coefficients and parameters used by the model with the objective, in this case, of minimizing differences between field-measured amounts of pool scour and fill and the model-computed values. Subsequent verification simulations were conducted on the Goose Pool (Reach I; Figure 1.1) to substantiate the credibility of the calibration runs. Model settings established on the Ouzel and Tick Pools were applied without modification to the Goose Pool for verification of the calibrated results. A model is not considered fully calibrated until the model coefficients and parameters are verified for other sites under similar conditions (Beck, 1991).

Sensitivity analyses were then performed to identify the most sensitive coefficients and parameters requiring the most attention in the calibration and validation process. A range of values analyzed for sensitivity is included in Table 2.2.

Table 2.2. Input parameters for one-dimensional models HEC-6 and GSTARS 2.0 for simulations along the North Fork Cache la Poudre River.

| HEC-6 | Sensitivity range tested | GSTARS 2.0 | Sensitivity range tested |
|---|---|---|---|
| Manning's n values | 0.02-0.06 pools* | Number cross sections | Not tested, see text |
| Cross section location | Not tested, see text | Cross section properties | N/A, known values |
| Cross section coordinates | N/A, known values | Number of subchannels | N/A, known values |
| Moveable bed limits | With and without | Cross section geometry | N/A, known values |
| Sediment properties | N/A, known values | Roughness coefficients | 0.02-0.06 pools* |
| Iterations of Exner Eq. | 0, 25, 50 | Number of iterations | 1-3 days |
| Cohesive sediment transport | Yes, no | Number of stream tubes | 3-5 |
| Sediment transport formulas for sand transport (14 available) | Ackers-White, Yang, DuBoys, Toffaletti and Schoklitsch, Meyer- Peter and Muller | Type of discharge input | N/A, known values |
| Parameters for clay, silt, sand transport | N/A, known values | Type of stage input | N/A, known values |
| Discharge-sediment load relationship | N/A, known values | Sediment transport equation (10 available) | Ackers-White, Yang, DuBoys, Toffaletti, Meyer- Peter and Muller |
| Total sediment load | N/A, known values | Nonequilibrium sediment transport | Yes, no |
| Grain size fractions of sediment load | N/A, known values | Sediment discharge | N/A, known values |
| Bed material gradation | N/A, known values | Water temperature | Not tested, see text |
| Water discharges | N/A, known values | Number of sediment size fractions | N/A, known values |
| Downstream boundary condition | N/A, known values | Sediment size groups | N/A, known values |
| Water temperature | Not tested, see text | Sediment size distribution | N/A, known values |
| Flow Duration | 1 month, 6 months | Transport parameters for cohesive sediments | Varied shear stress threshold, rates of erosion |

*Sensitivity analyses of Mannings n evaluated using HEC-RAS (U.S. Army Corps of Engineers, 1998b). N/A is not applicable

2.4.3 Step Backwater Computations

Both HEC-6 and GSTARS utilize the standard-step method for solving the energy equation to derive a water-surface profile for the modeled reach. As a means of isolating the hydraulic component of the models, the U.S. Army Corps of Engineers Water Surface Profile program, HEC-RAS, (U.S. Army Corps of Engineers, 1998b), was employed to test the effects of varied Manning's n . HEC-RAS estimates of the friction slope were also obtained for subsequent sediment transport calculations. The HEC-RAS model was released in 1996 as a replacement for HEC-2 with a superior user interface and extended capabilities for analysis of transcritical flow profiles. A modified form of the one-dimensional standard step method incorporates the momentum equation for use in situations where flow passes through critical depth. The model requires the assumption of a hydrostatic pressure distribution and is applicable to slopes less than 10 percent.

2.4.4 Sediment Transport Capacity

Sediment transport computations were completed for the Tick Pool using six sediment transport equations to determine the best fit between measured and calculated sediment transport rates, prior to selecting equations to be used in subsequent simulations within HEC-6 and GSTARS. In this way knowledge of the agreement between predicted and measured sediment transport rates could be acquired *a priori*. This knowledge is useful because the models give no indication of an over- or underprediction of sediment transport capacities through the reach of interest unless data exist for comparison.

Three bedload equations including DuBoys, Meyer-Peter and Muller (in Julien, 1995), and Schoklitsch (in Bathurst et al., 1987), and three total load equations, Ackers-White (in Julien, 1995), Yang's (1973) sand equation, and Engelund-Hansen (in Julien,

1995), were selected for the comparison (Appendix A). In addition, an equation presented by Julien (2001) was included in the comparison as a means of estimating unit bed sediment discharge as a function of grain size and dimensionless shear stress. The first six equations were selected based on similarity of conditions for which the equations were developed (i.e., slope, grain size) and the North Fork Poudre River, availability of the equation as an option in HEC-6 and GSTARS, and ease of spreadsheet manipulation. The equation of Julien (2001) was used to determine whether it substituted as a simplified version of Yang's (1973) formula. In a study of channel changes along the Rio Grande River (C. Leon, pers. comm., 2001), Julien's (2001) equation most closely approximated field-measured sediment transport rates, and nearly approximated transport rates predicted by the Yang (1973) equation.

The median diameter (d_{50}) of sediment moving through the Tick Pool, as collected from a depositional site within the pool, was used to apply the bedload and total load transport formulas. Bedload refers to the transport of sediment particles that frequently maintain contact with the bed, and bedload equations are empirical methods of estimating bedload transport in the absence of actual transport rates. The equations can be applied using either the median grain size (d_{50}) of the bed material or the size fractions of the bed material, where bed material refers to those size fractions that reside in the bed of the channel and which may or may not become entrained and transported as bedload. Because bedload from the pools could not be physically measured in the field, an estimate of bedload transport was obtained from the selected equations. It was assumed that the grain size distribution of sediment within a marginal channel bar of the Tick Pool (d_{50} of 0.0921 mm or very fine sand) represents what is moving in transport over the

immobile bed of the pool (bed material of the pools is in the cobble/boulder size range). Bedload was measured within the adjacent downstream riffle (Wohl and Cenderelli, 2000), at Cross Section 17 (Figure 1.1), providing a means of comparing the calculated and measured bedload transport rates for sediment moving through the Tick Pool.

Calculations using the bedload equations were compared to bedload quantities collected along sample Cross Section 17 (Figure 2.4). Figure 2.4 indicates that the methods of DuBoys, Meyer-Peter and Muller, and Schoklitsch overpredict the measured bedload transport of the North Fork by as much as three orders of magnitude for a d_{50} of very fine sand. The best agreement between measured and predicted quantities of bedload for the North Fork was obtained using the Schoklitsch equation (Figure 2.4), with the data converging with the 1:1 line at higher values of measured unit bedload discharge. Although the magnitude by which the equations overpredict is extreme, such an overprediction represents the state of the art in terms of current ability to quantify bedload transport within steep gradient, bedrock channels using the selected equations.

In a thorough analysis of twelve transport equations, Gomez and Church (1989) acknowledged that most of the formulas they tested overpredict bedload transport. Smart (1984) showed that the Schoklitsch equation overestimated transport for slopes greater than 3 percent, and Blizard (1994) found that the Schoklitsch formula overpredicted bedload discharge by three orders of magnitude on a snowmelt-dominated subalpine stream in the Rocky Mountains of Colorado. Bathurst et al. (1987) evaluated the applicability of several sediment transport equations to steep gradient rivers. Bedload discharge calculations using the Schoklitsch equation showed the lowest mean error for

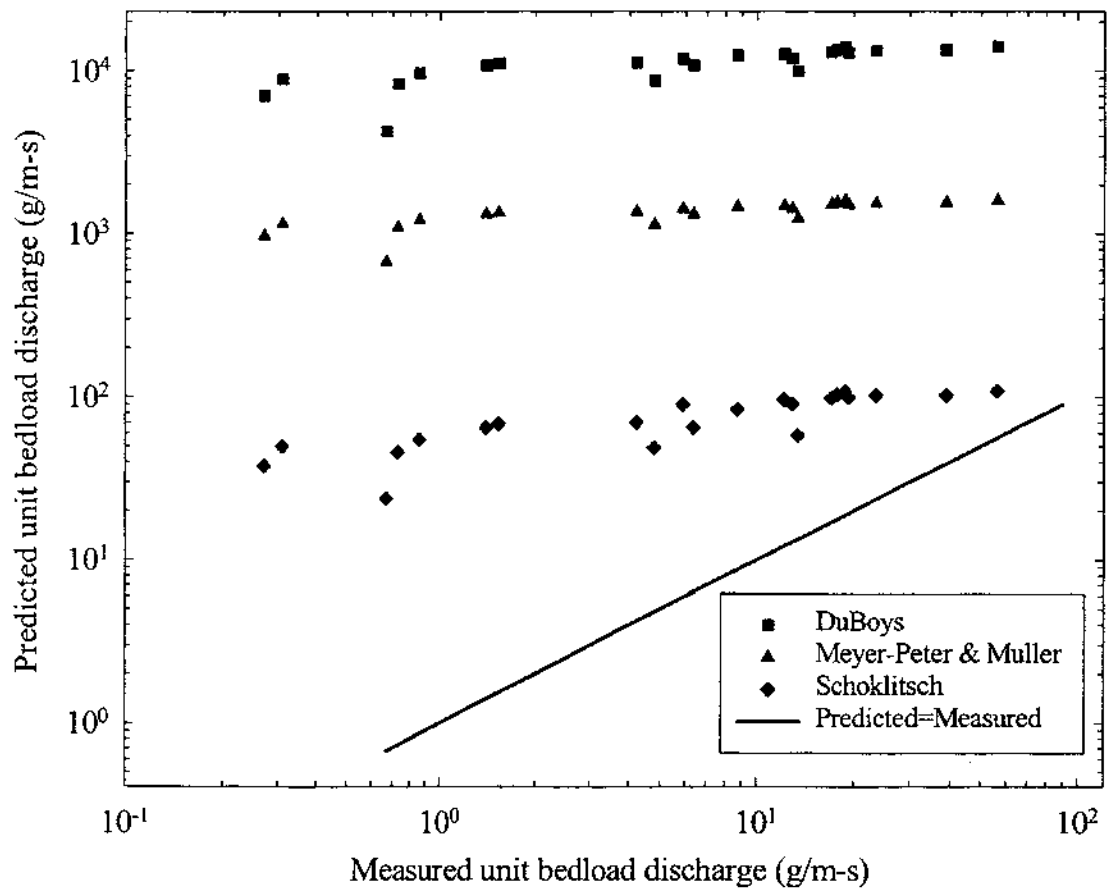


Figure 2.4. Predicted versus measured unit bedload discharge for the Tick Pool obtained from estimates using three bedload equations. The assumption that bedload discharge at Cross Section 17 (downstream riffle) equals the bedload discharge of the Tick Pool is applied.

flume data tested, and may be most applicable for small rivers with steep slopes (>1 percent) and relatively wide ranges of sediment size (1-1000 mm).

Because bedload quantities measured along the North Fork were a small percentage of the total measured load (between 0.68 to 32 percent), more accurate calculations of sediment transport capacity were anticipated from total load equations. Total load can be classified several ways (see Julien, 1995, p. 205). In this case, total load is distinguished by the type of sediment movement, moving either as bedload or suspended load. By calculating total sediment transport capacity using total load equations, the large proportions of suspended sediment released from Halligan Reservoir, that filled pools along the North Fork, would be accounted for in the formulas. The released reservoir sediment consisted of size fractions that were transported predominantly as suspended sediment, sizes that are not found in significant amounts in the pre-release bed material.

The total measured load of Figure 2.5 is the sum of bedload and suspended load quantities measured in the field. Yang's (1973) sand equation provided the closest agreement between measured and predicted rates of sediment discharge (Figure 2.5). Total load, using Yang's equation, is overpredicted by one order of magnitude, an improvement over the bedload equations, with Engelund-Hansen also providing slightly greater estimates. Julien's (2001) equation tended to overpredict total sediment discharge to the greatest degree at low discharges, but was within range of other selected equations at higher flows. For this investigation, Julien's (2001) approximation of unit bed sediment discharge is not considered a reasonable, simplified alternative to Yang's (1973) formula. The Ackers-White equation overpredicts sediment transport rate to the

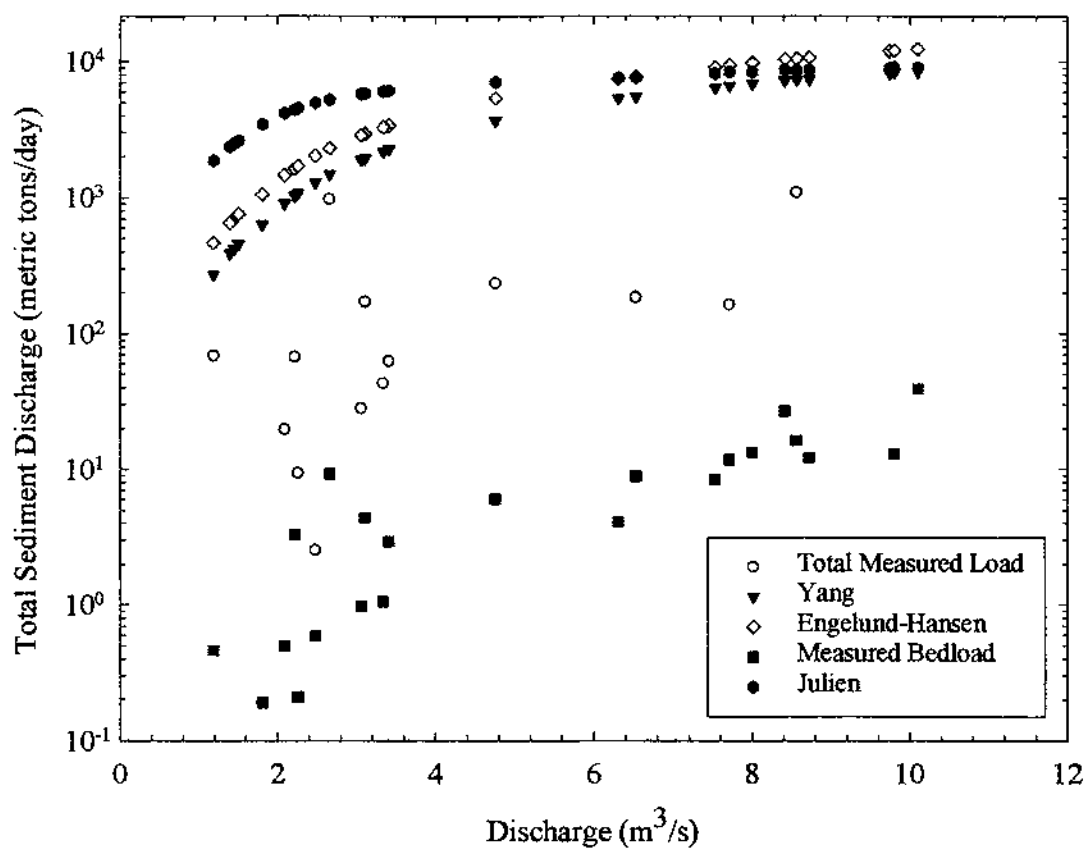


Figure 2.5. Comparison of measured and calculated sediment transport rates within the Tick Pool. The total measured load plot represents the sum of bedload and suspended load measured in the field. Total measured load was compared with estimates from different sediment transport equations to determine the most appropriate equation to select as input for the sediment transport models.

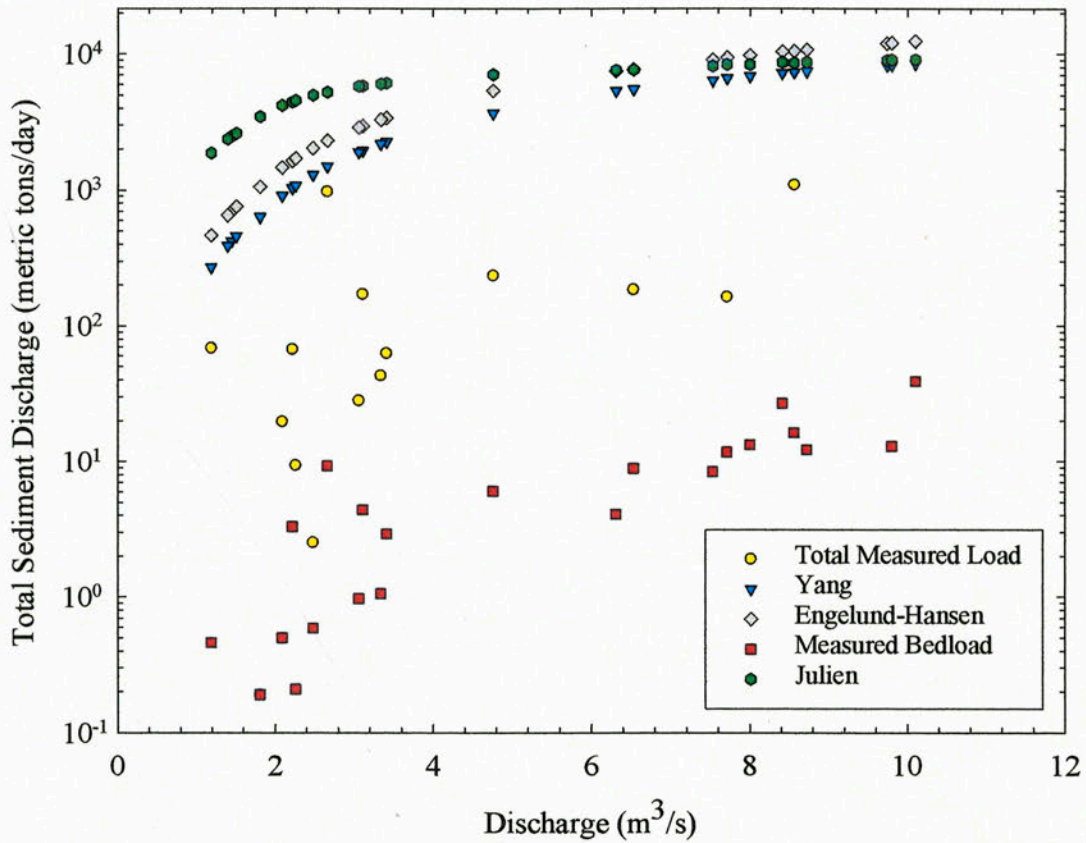


Figure 2.5. Comparison of measured and calculated sediment transport rates within the Tick Pool. The total measured load plot represents the sum of bedload and suspended load measured in the field. Total measured load was compared with estimates from different sediment transport equations to determine the most appropriate equation to select as input for the sediment transport models.

point of hyperconcentrated flow, and therefore, the data points were omitted from Figure 2.5. Although hyperconcentrated flows are possible within mountain channels, they are not very common under the snowmelt-dominated runoff regime of the Colorado Rocky Mountains. The overall disparity between actual transport rates along the North Fork and predictions of sediment transport capacity depicted in Figure 2.5 suggest that even following a clear water flush to remove sediment from the reservoir release supply-limited conditions existed along the study reaches. Whereas total sediment discharge measured along the North Fork ranged from less than 1 to 100 metric tons/day, the equations predict that the capacity to transport sediment was much greater, ranging from 270 to 12,000 metric tons/day. It is possible that the cohesive nature of the sediment filling pools and lining riffles along the North Fork influenced the sediment entrainment and transport processes such that the equations evaluated, which are for cohesionless sediment, are no longer valid. Wohl and Cenderelli (2000) report that portions of the bed sediment had a consistency of weak concrete, after the sediment became desiccated through subaerial exposure during winter low flows.

As a result of these preliminary computations, Yang's equation and a combination of the Toffaleti and Schoklitsch equations were selected for the initial model simulations in HEC-6. Unfortunately, the Schoklitsch equation was not an input option common to both HEC-6 and GSTARS and could not be evaluated via both models. The coupled Toffaleti-Schoklitsch was selected as an appropriate substitute. The only equation deemed applicable to the North Fork based on the preliminary sediment transport calculations, and common to the two models, was Yang's (1973) equation.

2.4.5 Scour and Fill

Modeled results in HEC-6 estimate average change in bed elevation over the duration of the hydrograph that was input into the model. As a one-dimensional model, HEC-6 calculates uniform bed change reported as average elevation change of the bed in a cross section. For comparison to the measured bed change in the pools obtained from field surveys, an estimate of the net bed change was obtained from a program called ‘Scour and Fill’ (U.S. Geological Survey, 1999), as was the maximum amount of bed change within the thalweg. The ‘Scour and Fill’ program overlays two cross sections, shows the area of scour and fill, and calculates the net areal change. This change in area was divided by the width of the channel to obtain the net vertical change along the cross section, or the average bed change, a quantity we considered to be more comparable to the average bed change estimated by HEC-6.

2.5 Modeling Results

2.5.1 HEC-6 Experimental Discharge

2.5.1.1 Default Simulations

All available HEC-6 default parameters for cross sections through the pools of the modeled reach were selected. Moveable bed limits, or the elevation of the model bottom below which no scour or deposition could occur, were set for the riffles. Only deposition of cohesive sediments is accounted for in the default simulations, and the sediment transport equations used were Yang’s and a Toffaleti-Schoklitsch combination.

During these default simulations, poor agreement was obtained between observed and modeled bed changes (Table 2.3). Columns 5 and 6 in Table 2.3 give estimates of

Table 2.3. HEC-6 results for experimental discharge simulations ($Q_{\text{peak}}=3.4 \text{ m}^3/\text{s}$) for default and robust data input within three pools along the North Fork Cache la Poudre River.

| | | DEFAULT SIMULATION | | | | | | ROBUST SIMULATION | | | | | |
|---------------------------|---------------|---------------------|--|---|---|--|--|---------------------|--|---|--|--|--|
| | | (1) Cross Sec | (2) Oct-Mar Thalweg Change (m) | (3) Average 'Scour and Fill' Bed Change (m) | (4) Average HEC-6 Bed Change (m) | (5) Model Accuracy (%) (4)/(2) | (6) Model Accuracy (%) (4)/(3) | (7) Cross Sec | (8) Oct-Mar Thalweg Change (m) | (9) Average 'Scour and Fill' Bed Change (m) | (10) Average HEC-6 Bed Change (m) | (11) Model Accuracy (%) (10)/(8) | (12) Model Accuracy (%) (10)/(9) |
| Yang | Tick Pool | 12 | -0.63 | 0.05 | -0.03 | 4.37 | -57.32 | 12 | -0.63 | 0.05 | -0.50 | 80.10 | -1050.96 |
| | | 13 | -0.22 | 0.24 | -0.04 | 16.44 | -15.23 | 13 | -0.22 | 0.24 | -0.17 | 76.71 | -71.07 |
| | | 14 | 0.50 | 0.15 | 0.00 | -0.61 | -2.09 | 14 | 0.50 | 0.15 | -0.23 | -46.01 | -156.90 |
| | Ouzel Pool | 2 | 1.20 | 0.36 | 0.45 | 37.66 | 124.37 | 2 | 1.20 | 0.36 | 0.03 | 2.80 | 9.24 |
| | | 3 | 0.49 | 0.02 | 0.04 | 8.70 | 254.55 | 3 | 0.49 | 0.02 | -0.02 | -4.97 | -145.45 |
| | | 4 | 0.75 | 0.15 | 0.00 | 0.00 | 0.00 | 4 | 0.75 | 0.15 | -0.09 | -11.38 | -57.73 |
| | Goose Pool | 4 | -0.46 | -0.22 | -0.35 | 76.16 | 156.89 | 4 | -0.46 | -0.22 | -0.42 | 91.39 | 188.27 |
| | | 5 | -0.57 | -0.16 | -0.24 | 42.25 | 148.78 | 5 | -0.57 | -0.16 | -0.74 | 129.95 | 457.63 |
| | | 6 | -0.74 | -0.18 | -0.16 | 21.40 | 86.24 | 6 | -0.74 | -0.18 | -2.69 | 362.96 | 1462.69 |
| Toffaleti- Schoklitsch | Tick Pool | 12 | -0.63 | 0.05 | -0.03 | 4.85 | -63.69 | 12 | -0.63 | 0.05 | -0.50 | 80.10 | -1050.96 |
| | | 13 | -0.22 | 0.24 | -0.02 | 6.85 | -6.35 | 13 | -0.22 | 0.24 | -0.17 | 76.71 | -71.07 |
| | | 14 | 0.50 | 0.15 | -0.02 | -4.29 | -14.64 | 14 | 0.50 | 0.15 | -0.23 | -46.01 | -156.90 |
| | Ouzel Pool | 2 | 1.20 | 0.36 | 0.58 | 48.60 | 160.50 | 2 | 1.20 | 0.36 | 0.17 | 14.50 | 47.90 |
| | | 3 | 0.49 | 0.02 | 0.14 | 27.95 | 818.18 | 3 | 0.49 | 0.02 | 0.00 | 0.62 | 18.18 |
| | | 4 | 0.75 | 0.15 | 0.00 | 0.00 | 0.00 | 4 | 0.75 | 0.15 | -0.09 | -11.38 | -57.73 |
| | Goose Pool | 4 | -0.46 | -0.22 | -0.31 | 67.55 | 139.15 | 4 | -0.46 | -0.22 | -0.49 | 106.62 | 219.65 |
| | | 5 | -0.57 | -0.16 | -0.05 | 9.63 | 33.90 | 5 | -0.57 | -0.16 | -0.50 | 88.24 | 310.73 |
| | | 6 | -0.74 | -0.18 | 0.00 | 0.00 | 0.00 | 6 | -0.74 | -0.18 | -2.74 | 370.37 | 1492.54 |

Columns 5 and 6 represent model accuracy from HEC-6 using maximum thalweg change and average 'Scour and Fill' bed change, respectively. Negative values indicate a model prediction of scour when aggradation occurred, or vice versa. Percentages greater than 100 indicate an over-prediction by HEC-6.

the percentage of the measured bed change that is predicted by the model, calculated by two methods, dividing column 4 by 2, and 4 by 3, respectively. The model accuracy for two of the three cross sections through the Ouzel and Tick Pools varied from 0 to 38 percent for Yang's equation, and 0 to 49 percent for the Toffaleti-Schoklitsch equation for the experimental discharge simulations with default settings (Table 2.3). In other words, HEC-6 predicted between 0 and 49 percent of the vertical bed change that was measured in the field within two pools, using two different sediment transport equations. Modeling accuracy results using the maximum thalweg change (Column 5) are greater than those using the net bed change from 'Scour and Fill' (Column 6, Table 2.3). The results of the average bed change calculated by 'Scour and Fill' consistently show over- and underpredictions of bed change, hence the negative values and values greater than 100 percent in Table 2.3. Because of this discrepancy, subsequent discussions of model accuracy refer to estimates that incorporate the actual thalweg change (Columns 5 and 11).

2.5.1.2 Robust Simulations

Increased data input for robust simulations includes allowing for both deposition and erosion of cohesive sediments, and setting the elevation of the model bottom to the depth of sediment accumulated above the bed in the pools. In essence, the robust simulations utilized the entire suite of field data that was collected over the course of one year.

Results of the robust simulations under the experimental discharge hydrograph for the Tick Pool show a noted improvement over the default simulations. The percentage of bed change predicted by HEC-6 that was measured in the field increased to between 77

and 80 percent for two of the three cross sections in the Tick Pool (Table 2.3; Figure 2.6). At Cross Section 14, scour was predicted by HEC-6 for both simulations over the experimental discharge when 0.5 m of aggradation actually occurred between October 1996 and March 1997. Cross Section 14 is located at the exit slope of the Tick Pool, where a combination of the reverse gradient and the low magnitude experimental discharge enhanced sediment deposition. Results of robust simulations within the Ouzel Pool showed no improvement over the default settings.

2.5.2 HEC-6 Snowmelt Runoff

2.5.2.1 Default Simulations

Snowmelt runoff simulations for the six month hydrograph, using default parameters, provided a more consistent match between the observed and predicted bed changes for the Tick Pool. Between 23 and 75 percent of the observed bed change in the Tick Pool was modeled by HEC-6 for both Yang's and the Toffaletti-Schoklitsch equations (Table 2.4; Figure 2.7). Predictions of bed change for the Ouzel Pool again were in poor agreement with field measurements.

2.5.2.2 Robust Simulations

When the full set of field data is used, HEC-6 was able to predict 53 to 100 percent of the actual bed change measured in both pools for the robust simulations over the longer, six-month time period (Table 2.4; Figure 2.7). This increased accuracy between observed and predicted values of bed change in the Tick and Ouzel Pools for both sediment transport equations was derived by increasing the length of the simulated

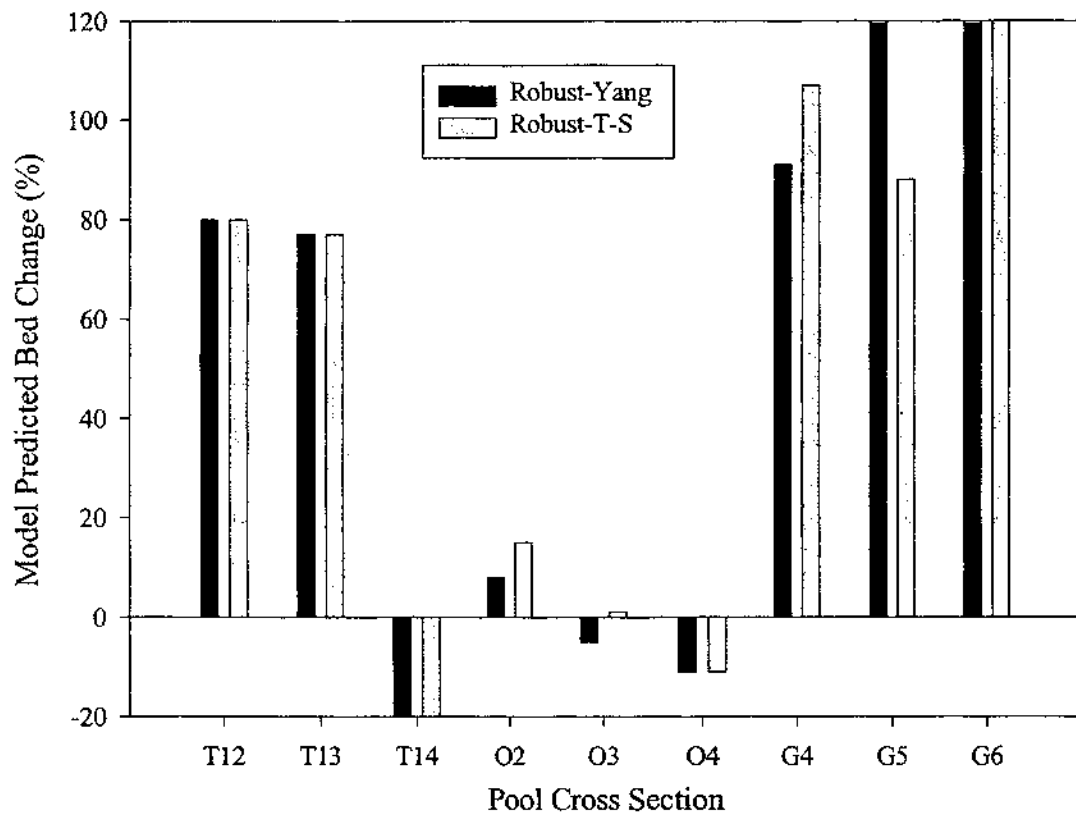


Figure 2.6. HEC-6 results for the experimental discharge ($Q_p=3.4 \text{ m}^3/\text{s}$) for robust data input within three pools along the North Fork for two sediment transport equations; the Yang equation and the Toffaleti-Schoklitsch equation. T12, T13, T14 indicate Cross Sections 12, 13, and 14 within the Tick Pool; O2, O3, O4 indicate Cross Sections 2, 3, and 4 within the Ouzel Pool; G4, G5, G6 indicate Goose Pool cross sections.

Table 2.4. HEC-6 results for snowmelt runoff discharge simulations ($Q_{peak}=10.1\text{m}^3/\text{s}$) for default and robust data input within three pools along the North Fork Cache la Poudre River.

| | | DEFAULT SIMULATION | | | | | | ROBUST SIMULATION | | | | | |
|-----------------------------|---------------|---------------------|---|---|---|--|--|---------------------|---|---|--|--|--|
| | | (1) Cross Sec | (2) Oct-Aug Thalweg Change (m) | (3) Average 'Scour and Fill' Bed Change (m) | (4) Average HEC-6 Bed Change (m) | (5) Model Accuracy (%) (4)/(2) | (6) Model Accuracy (%) (4)/(3) | (7) Cross Sec | (8) Oct-Aug Thalweg Change (m) | (9) Average 'Scour and Fill' Bed Change (m) | (10) Average HEC-6 Bed Change (m) | (11) Model Accuracy (%) (10)/(8) | (12) Model Accuracy (%) (10)/(9) |
| Yang | Tick Pool | 12 | -0.63 | -0.12 | -0.47 | 75.24 | 388.47 | 12 | -0.63 | -0.12 | -0.63 | 100.00 | 516.29 |
| | | 13 | -0.22 | -0.17 | -0.15 | 67.61 | 87.11 | 13 | -0.22 | -0.17 | -0.17 | 78.87 | 101.63 |
| | | 14 | -0.77 | -0.20 | -0.18 | 23.41 | 89.12 | 14 | -0.77 | -0.20 | -0.41 | 53.17 | 202.42 |
| | | | | | | | | | | | Aver = | 77.35 | |
| | Ouzel Pool | 2 | -0.61 | -0.11 | 0.04 | -6.03 | -32.43 | 2 | -0.61 | -0.11 | -0.44 | 72.86 | 391.89 |
| | | 3 | -0.80 | -0.06 | -0.01 | 1.53 | 20.30 | 3 | -0.80 | -0.06 | -0.32 | 40.61 | 538.07 |
| | | 4 | -0.30 | 0.02 | -0.01 | 4.08 | -66.67 | 4 | -0.30 | 0.02 | -0.16 | 55.10 | -900.00 |
| | | | | | | | | | | | Aver = | 56.19 | |
| | Goose Pool | 4 | -0.50 | N/A | -0.20 | 40.24 | N/A | 4 | -0.50 | N/A | -0.33 | 66.46 | N/A |
| | | 5 | -1.12 | -0.84 | -0.22 | 19.62 | 26.00 | 5 | -1.12 | -0.84 | -0.33 | 29.16 | 38.64 |
| | | 6 | -2.63 | -1.25 | -0.04 | 1.62 | 3.41 | 6 | -2.63 | -1.25 | -2.07 | 78.68 | 165.21 |
| | | | | | | | | | | | Aver = | 58.10 | |
| Toffaletti - Schoklitsch | Tick Pool | 12 | -0.63 | -0.12 | -0.47 | 74.76 | 385.96 | 12 | -0.63 | -0.12 | -0.63 | 100.00 | 516.29 |
| | | 13 | -0.22 | -0.17 | -0.15 | 67.61 | 87.11 | 13 | -0.22 | -0.17 | -0.17 | 78.87 | 101.63 |
| | | 14 | -0.77 | -0.20 | -0.20 | 25.40 | 96.68 | 14 | -0.77 | -0.20 | -0.41 | 53.17 | 202.42 |
| | | | | | | | | | | | Aver = | 77.35 | |
| | Ouzel Pool | 2 | -0.61 | -0.11 | 0.09 | -15.08 | -81.08 | 2 | -0.61 | -0.11 | -0.20 | 32.66 | 175.68 |
| | | 3 | -0.80 | -0.06 | -0.01 | 1.15 | 15.23 | 3 | -0.80 | -0.06 | -0.21 | 26.05 | 345.18 |
| | | 4 | -0.30 | 0.02 | -0.02 | 5.10 | -83.33 | 4 | -0.30 | 0.02 | -0.16 | 55.10 | -900.00 |
| | | | | | | | | | | | Aver = | 37.94 | |
| | Goose Pool | 4 | -0.50 | N/A | -0.17 | 34.15 | N/A | 4 | -0.50 | N/A | -0.48 | 95.73 | N/A |
| | | 5 | -1.12 | -0.84 | -0.04 | 3.27 | 4.33 | 5 | -1.12 | -0.84 | -0.57 | 51.23 | 67.89 |
| | | 6 | -2.63 | -1.25 | 0.05 | -1.74 | -3.65 | 6 | -2.63 | -1.25 | -1.97 | 74.74 | 156.93 |
| | | | | | | | | | | | Aver = | 73.90 | |

Columns 5 and 6 represent model accuracy from HEC-6 using maximum thalweg change and average 'Scour and Fill' bed change, respectively. Negative values indicate a model prediction of scour when aggradation occurred, or vice versa, and percentages greater than 100 indicate an overprediction by HEC-6.

flow duration and the discharge magnitude. These snowmelt simulations offer a vast improvement over the results for the default runs.

Using all available field data the model became insensitive to sediment transport formula selection, and the resultant scour and deposition were nearly identical for the two equations selected (Table 2.4, Column 11 for both Yang's and the combined Toffaleti-Schoklitsch). These findings were similar for other equations tested during the sensitivity analysis. Apparently, the HEC-6 model was sufficiently constrained by the known field data that the variations between the transport formulas produced negligible bed changes. At this point we considered the model robustly calibrated.

Interpretation of the modeling results is based on an expectation of accuracy that is relative to the ability of commercially available numerical models to represent sediment transport within steep gradient, immobile boundary channels; a greater than 50 percent agreement between measured and HEC-6 modeled bed change is reasonable, given the stochastic nature of the processes being modeled along the North Fork. Water resource managers need to make their own situation-dependent decisions regarding the reasonableness of their model output, as guided by the management decisions of interest. For example, the HEC-6 modeling results can be viewed in terms of pool depth recovery to better understand and predict fish reestablishment. For a given climate, water managers could use scenarios of fish populations (species, size, number of individuals) along a river reach to estimate minimum pool volume needed for overwinter habitat, setting guidelines for acceptable modeling results that fit with the objectives and uncertainties of the modeling effort. In addition, the models can be applied to a series of

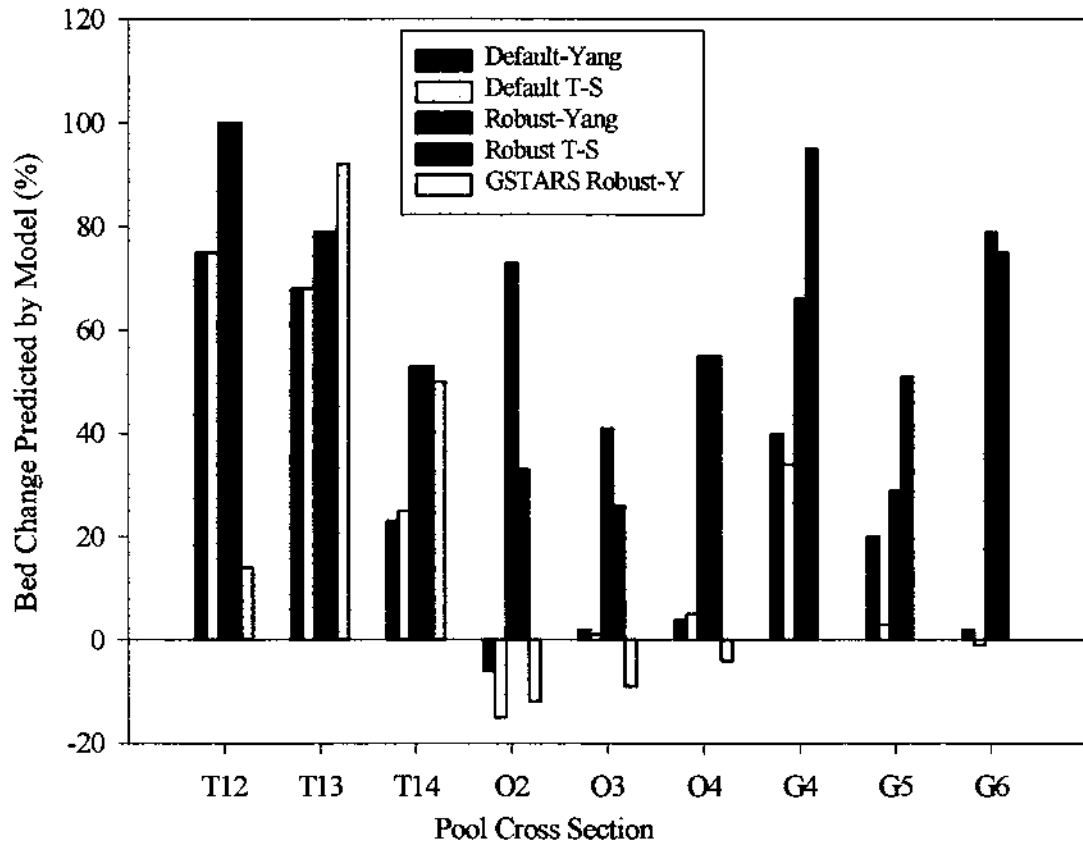


Figure 2.7. HEC-6 and GSTARS 2.0 results for the snowmelt runoff simulation for default and robust data input within three pools along the North Fork. Two sediment transport equations were evaluated; the Yang equation (indicated by Y) and Toffaleti-Schoklitsch (indicated by T-S). Letters along the x-axis denote cross sections within the Tick Pool (T), cross sections within the Ouzel Pool (O), and Goose Pool cross sections (G). Results in black, white, red and green are from HEC-6, whereas yellow bars indicate GSTARS results.

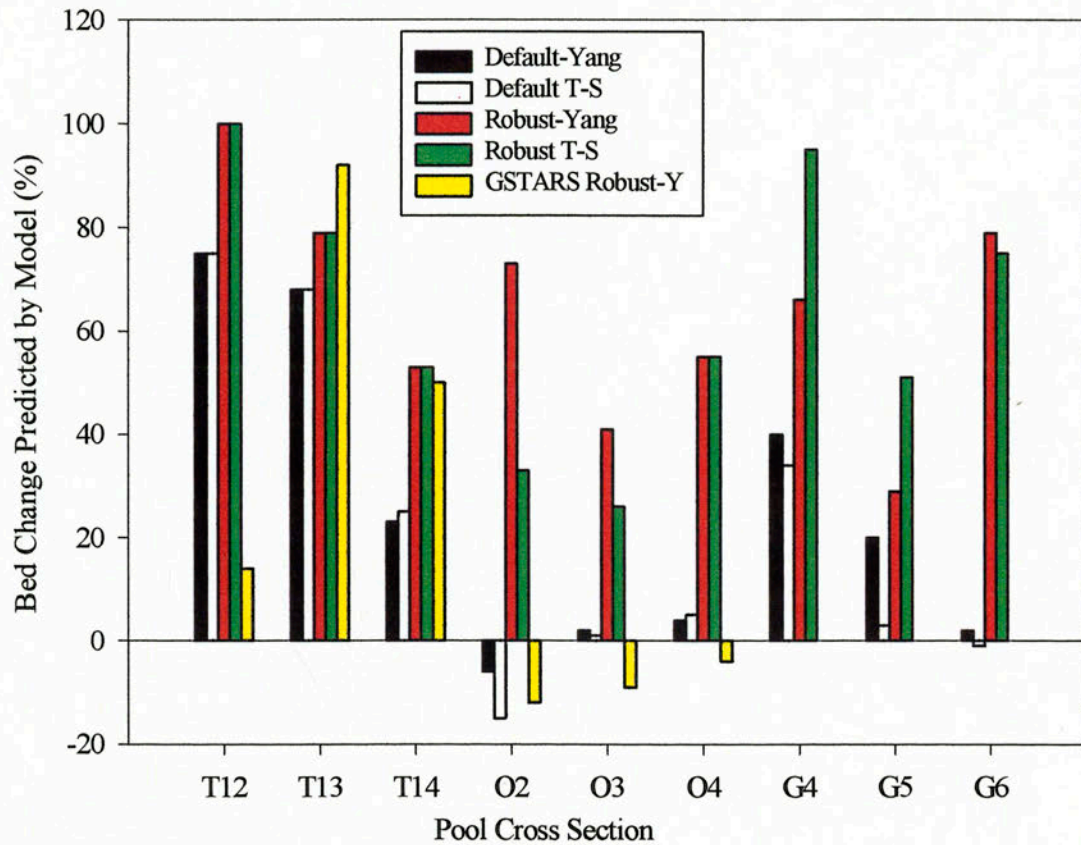


Figure 2.7. HEC-6 and GSTARS 2.0 results for the snowmelt runoff simulation for default and robust data input within three pools along the North Fork. Two sediment transport equations were evaluated; the Yang equation (indicated by Y) and Toffaleti-Schoklitsch (indicated by T-S). Letters along the x-axis denote cross sections within the Tick Pool (T), cross sections within the Ouzel Pool (O), and Goose Pool cross sections (G). Results in black, white, red and green are from HEC-6, whereas yellow bars indicate GSTARS results.

flows and range of time periods to test hypothetical situations that will answer questions regarding residence times of pool sediment.

2.6 Model Validation

Validation of the calibrated model settings in HEC-6 on the Goose Pool (Figure 1.1) yielded an accuracy of 21 to 76 and 0 to 68 percent of the measured bed change for the default simulation of the experimental discharge using the Yang and Toffaleti-Schoklitsch equations, respectively (Table 2.3). Robust simulations of the experimental discharge overpredicted the actual bed change within two of the three pool cross sections.

The default and robust simulations for the snowmelt hydrograph generated a more consistent match between field measurements and model predictions, with the strongest match for the robust simulations (Table 2.4; Figure 2.7). Between 58 and 74 percent, on average, of the actual field scour or deposition was predicted by the model, depending upon the sediment transport equation chosen. If HEC-6 calibrated model settings were applied to yet another pool along the North Fork, at least 58 percent of the observed vertical bed change would be predicted by the model, provided the requisite data for a robust simulation over the snowmelt runoff were available. Pool depth recovery of 58 percent may be sufficient sediment removal to support fish over a winter, and sediment transport modeling would then provide useful information to answer questions of channel recovery. Depending on the target recovery depth or volume for the pools of interest, the results of the HEC-6 simulations could be evaluated accordingly. However, the results and verification would be obtained only after a year of data collection, the time involved in the case of the North Fork to gather enough field data to calibrate and validate the models.

2.7 Sensitivity Analysis

Sensitivity analyses were conducted on Manning's n value to assess the effect on water-surface profiles calculated using HEC-RAS (U.S. Army Corps of Engineers, 1998b). Less than 10 cm change in the elevation of the water-surface profile resulted from increasing or decreasing n by ± 10 to ± 50 percent beyond beginning values (Appendix B). Contraction and expansion values were taken from recommendations in the HEC-6 User's Manual as 0.1 and 0.3, respectively (U.S. Army Corps of Engineers, 1998a). A 10 cm fluctuation in water-surface profile is acceptable for the North Fork because Manning's n was actually back-calculated (Section 2.4.1), and a reasonable range of n was established that is well within the sensitivity range tested, so the 10 cm fluctuation is probably a maximum estimate.

Sensitivity analyses by O'Connor and Webb (1988) for paleofloods have shown that the location and density of cross sections are the most important requirements for accurate water-surface profiles. Cross sections should be spaced to adequately represent any abrupt geometry changes within the channel, with closer spacing around bends and through expanded and contracted areas, and where bed slope changes. The choice of cross sections is considered adequate for the configuration of the North Fork (Figure 1.1), and sensitivity analyses were not completed on cross section number and placement. Likewise, water temperature was not tested for sensitivity. Water temperature was set at 5 degrees centigrade, a temperature known to be reasonable for snowmelt runoff-dominated rivers during the spring and summer months.

Three additional sediment transport equations were assessed in a sensitivity analysis within HEC-6 (Appendix C) to evaluate the effects of different sediment transport formulas within the model, in spite of the knowledge acquired during the

preliminary analyses intended to assist in formula selection (Section 2.4.4). The modeling results were found to be tremendously sensitive to selection of formula, producing changes in bed elevation that varied by as much as a 400 percent overprediction of field-quantified bed changes. Selection of Ackers-White, DuBoys, and Meyer-Peter and Muller sediment transport equations within the HEC-6 input consistently overpredicted the measured bed elevation changes within the North Fork study area. These results are consistent with those from the preliminary analysis of sediment transport, and underscore the need to evaluate transport equations prior to selecting one (or more) for the modeling.

2.8 GSTARS 2.0 Results

2.8.1 Experimental Discharge

Minimal default options are available for the user in GSTARS. As such, no default simulations comparable to the HEC-6 results were conducted.

2.8.1.1 Robust Simulations

Results of the GSTARS modeling for the Tick Pool indicate that between 13 and 90 percent of the measured bed scour at two of the three cross sections was predicted by GSTARS (Table 2.5). Similar to the HEC-6 results, bed scour rather than aggradation was predicted by GSTARS for Cross Section 14. Model accuracy for the Ouzel Pool was lower, with a 1 to 14 percent match between model predictions and field measurements of bed change over the three pool cross sections. This is consistent with the lower accuracy findings using HEC-6. The geometry of the Ouzel Pool, with its large eddy

Table 2.5. GSTARS 2.0 results for both the experimental and snowmelt discharge simulations using the robust data input within two pools along the North Fork Cache la Poudre River. Results are derived using Yang's (1973) sand transport equation.

| ROBUST SIMULATION, EXPERIMENTAL DISCHARGE | | | | | | | | ROBUST SIMULATION, SNOWMELT | | | | | | |
|---|---------------|---------------------|--|---|------------------------------------|---------------------------------|---------------------------------|-----------------------------|---------------------|--|---|-------------------------------------|----------------------------------|----------------------------------|
| | | (1) Cross Sec | (2) Oct-Mar Thalweg Change (m) | (3) Average 'Scour and Fill' Bed Change (m) | (4) GSTARS Bed Change (m) | (5) Model Accuracy (%) | (6) Model Accuracy (%) | | (7) Cross Sec | (8) Oct-Aug Thalweg Change (m) | (9) Average 'Scour and Fill' Bed Change (m) | (10) GSTARS Bed Change (m) | (11) Model Accuracy (%) | (12) Model Accuracy (%) |
| | | | | | | (4)/(2) | (4)/(3) | | | | | | (10)/(8) | (10)/(9) |
| Yang | Tick Pool | 12 | -0.63 | 0.05 | -0.08 | 13.50 | -177.07 | | 12 | -0.63 | 0.05 | -0.08 | 13.50 | -177.07 |
| | | 13 | -0.22 | 0.24 | -0.20 | 89.59 | -82.99 | | 13 | -0.22 | 0.24 | -0.20 | 92.11 | -82.99 |
| | | 14 | 0.50 | 0.15 | -0.39 | -77.67 | -264.85 | | 14 | -0.77 | 0.15 | -0.39 | 50.24 | -264.85 |
| | Ouzel Pool | 2 | 1.20 | 0.36 | 0.07 | 6.11 | 20.17 | | 2 | -0.61 | 0.36 | 0.07 | -12.06 | 20.17 |
| | | 3 | 0.49 | 0.02 | 0.07 | 14.47 | 423.64 | | 3 | -0.80 | 0.02 | 0.07 | -8.93 | 423.64 |
| | | 4 | 0.75 | 0.15 | 0.01 | 1.42 | 7.22 | | 4 | -0.30 | 0.15 | 0.01 | -3.57 | 7.22 |

pool of near-stagnant flow, sets up more complex hydraulics that are outside the range of even a quasi two-dimensional flow model.

2.8.2 Snowmelt Runoff

2.8.2.1 Robust Simulations

By increasing the length of flushing discharge from one month to six months to include the snowmelt runoff hydrograph, GSTARS predictions of bed scour and/or aggradation range between 13 and 92 percent of actual field measurements for the Tick Pool (Table 2.5; Figure 2.7). The model appears to be insensitive to increased time period over which a simulation is run because the GSTARS predictions of bed change are identical (Column 5 and 11 of Table 2.5).

Although other sediment transport equations were selected in subsequent simulations of GSTARS 2.0, the resultant differences in bed elevation were minimal (<5%), so only results using Yang's (1973) equation are presented in Table 2.5.

2.9 Discussion

Sediment transport equations appropriate to steep gradient rivers have not yet been developed and, by necessity, relationships designed for lowland rivers are typically employed. Sediment transport equations developed for alluvial rivers have limited applicability to the North Fork because of the effects of bed armoring, spatially limited sediment supply, and the bimodal distribution of sediment sizes comprising the bed compared to the sediment sizes in transport. The preliminary analyses to determine the appropriate sediment transport formula(s) for the steep gradient, bedrock-controlled North Fork indicate that the total load formulas gave more satisfactory results than the

bedload formulas tested. The success with total load equations is consistent with the flume experiment of Tingsanchali and Supharatid (1996) in which the performance of HEC-6 was investigated. These investigators found that the Toffaleti and Yang total load equations gave the most satisfactory prediction of actual bed profiles within the flume under various conditions of flow and sediment transport.

Once the appropriate equation was identified, further analysis indicated that the modeling results of HEC-6 and GSTARS are limited in ways specific to the conditions along the North Fork. The major limitation of HEC-6 is that it is a purely one-dimensional model, which leads, by necessity, to simplification of the complex, three-dimensional flow in rivers. HEC-6 cannot account for the following hydraulic conditions present in pools along the North Fork that include: (1) lateral flow separation, or eddies, where a majority of sediment was deposited during the sediment release from Halligan Reservoir, (2) bank erosion or lateral channel migration, which occurred as a thalweg was re-excavated through the pools after the release, (3) differential scour and deposition over the width of a cross section, which occurred as sediment was simultaneously eroded out of the central, high velocity thalweg and deposited along the channel margins in the pools, and (4) temporal changes in sediment supply and bed material grain size distribution. In spite of these limitations, HEC-6 is a model likely to be selected by water resource managers faced with assessing and mitigating the effects of a reservoir sediment release. As a result of testing the applicability of HEC-6 on a high gradient, bedrock fluvial system, it is determined that it can be used in such systems to answer questions regarding the percentage of pool recovery as a function of discharge for post-sediment release channel restoration.

A major limitation of GSTARS is the model's insensitivity to long-term simulations and varied sediment transport equations. The present configuration of the GSTARS code does not accommodate large differences in grain sizes of bed sediment over short distances, such as between riffles comprised of cobbles and boulders, and adjacent pools of silt and fine sand (F. Simoes, personal communication, 1999).

The Bureau of Reclamation developed GSTARS for internal use rather than to suit the needs of the general public (F. Simoes, personal communication, 1999). As such, GSTARS assumes a much higher level of user knowledge in hydraulics and sediment transport, and incorporates fewer default options. The capabilities of GSTARS were severely underutilized in the North Fork application, and the power of the model is best expressed in situations of sand transport where stream power minimization is important. Future releases of GSTARS that specifically address river sedimentation downstream from dams are currently under development (Simoes and Yang, 2000). The version of GSTARS used in this investigation (2.0) is not recommended as an applicable model for mountain rivers receiving large volumes of fine-grained sediment onto an originally coarse bed.

Realistic evaluation of the time investment is necessary to determine the suitability of modeling channel recovery scenarios. Once the field data are collected, a first time user of HEC-6 should expect to devote substantially more time than someone with prior modeling experience and knowledge of hydraulic and sediment transport processes. Although much of the input for GSTARS can be derived from HEC-6, with minor format changes, the time investment using GSTARS is considerably longer given

the greater number of built-in options which give the modeler as much control as possible.

2.10 Summary

Simulations using HEC-6 produced reasonable, first-order approximations of the pool bed changes resulting from scour and fill after the sediment release from Halligan Reservoir. Default simulations produced minimal accuracy for all three pools modeled and, therefore, limit the management capabilities of HEC-6 to situations with adequate field data. Average pool-wide trends of predicted versus observed aggradation and degradation for three pools along the North Fork were greater than 50 percent for the long-term, snowmelt runoff hydrograph using HEC-6 and Yang's (1973) sand transport equation. Average modeling accuracy was lower for the three pools when the combined Toffaleti-Schoklitsch equation was used, ranging from 38 to 77 percent for the Tick and Ouzel Pools. All of these results, however, were generated only after using an extensive, field-based data set collected during weekly or biweekly field outings over the course of a one-year period.

The calibration results were verified on the Goose Pool, with generally poor agreement for the experimental discharge, but at least 58 percent and as high as 74 percent for the robust modeling, depending on the sediment transport equation selected. In both calibrated and verification simulations, the longer-term snowmelt runoff scenarios produced the closest agreement between modeled and measured bed change. The HEC-6 User's Manual (U.S. Army Corps of Engineers, 1998a) recommends long-term simulations over single event hydrographs, because of the bed instabilities that arise.

A one-month simulation, such as the experimental discharge, was apparently insufficient to stabilize the bed elevation computations.

Overall, modeling results for the Ouzel Pool are in poor agreement with field measurements. The Ouzel Pool has a large eddy (on channel right) of nearly stagnant flow. HEC-6 cannot account for the upstream component of flow, and treats the entire cross section as the effective width. The increased width, for the same depth, reduces velocity, and lower velocity translates into lower shear stress and hence lower sediment transport at the bed. One option of handling the eddy was to decrease the effective pool width in HEC-6 and obtain greater amounts of scour. Pool width was not altered in this investigation. A two-dimensional finite element model would more effectively cope with transport through the eddy pools (refer to Chapter 3).

The stepped, experimental discharge released from Halligan Reservoir produced improved pool volume for fish habitat, much greater than was predicted by the models. It could be that after five months of $0.1 \text{ m}^3/\text{s}$ flow, the initial $3.4 \text{ m}^3/\text{s}$ release of water along the North Fork, over a bed of silt and fine sand in the pools, entrained sediment by mechanisms that are not reproduced by one-dimensional sediment transport models. Those five months of flow at $0.1 \text{ m}^3/\text{s}$ were not simulated, but rather the model was started at the beginning of the experimental release in February. The field data attest to the fact that pulsed experimental releases are effective at entraining and transporting sediment, as pulsed flow increases shear stresses beyond that of gradually increased flow (Wohl and Cenderelli, 2000).

Model calibration on two pools and validation on one pool of the North Fork indicate that at least 58 percent of observed bed changes after a sediment release would

be predicted by HEC-6. For model applications where predictions of pool recovery for fish habitat are concerned, such as the North Fork, 58 percent accuracy renders the model a useful predictive tool to answer many management questions. In order to use HEC-6, adequate data and extensive calibration are required. Two of the input parameters that must be defined for each river system are thickness of sediment accumulated above the bed, in order to specify the elevation of the model bottom, and allowance for deposition and erosion of cohesive sediments, if appropriate. Also, the selection of sediment transport formula has the most substantial effect on the computed results, and knowledge of the applicability of various equations to the system of interest is critical. One-dimensional sediment transport models can only be useful long-term predictors of channel bed elevation changes if adequate data are collected and calibration is performed.

Current releases of GSTARS are not constructed to reflect physical processes similar to those operating along the North Fork, and therefore, GSTARS is not well adapted to steep-gradient bedrock channels filled with fine-grained material from a reservoir release.

For water resource managers faced with a newly-filled channel reach resulting from a reservoir sediment release, HEC-6 simulations could be conducted to establish flushing flows. In the case of the North Fork, greater than 50 percent pool recovery was achieved at a discharge of $10.1 \text{ m}^3/\text{s}$. Simulations could be run, for example, until the desired pool recovery was achieved, and the associated flow could be requested as the minimum flushing discharge for sediment mobilization and transport. One constraint that must be recognized is the heavy data dependence of HEC-6; without good field control through a reliable, accurate, field-derived data set, the model predictions are subject to

extreme error. However, computer models are useful tools, and in situations with restrictions on available flow for transporting sediment associated with a reservoir release, one-dimensional sediment transport modeling is still preferable to uncalibrated estimates of flushing discharges.

CHAPTER 3 TWO-DIMENSIONAL HYDRAULIC MODELING

3.1 Introduction

Flow separation and recirculating eddies comprise a large portion of the stream flow within pools of the bedrock-controlled North Fork Cache la Poudre River. Secondary flow in eddy pools strongly influences sediment transport and deposition, and pools function as sediment-storage sites, the infilling of which can impair critical habitat for aquatic organisms. Because of the recognized limitations of a one- and semi-two dimensional model in coping with eddy flow, and the significant cross-stream variability of flow within pools, a multi-dimensional model was hypothesized to better represent the hydraulic conditions of eddy pools along the North Fork (*Hypothesis 3.1*). If the hydraulic conditions of the eddy pools can be accurately simulated with a numerical flow model, then inferences about sediment mobility and transport within pools that influence erosion and deposition could be made at a resolution more conducive to understanding pool sediment dynamics. To test this hypothesis, a two-dimensional hydraulic model, RMA2, was applied to the Tick Pool along the North Fork (Figure 1.1). The study reach for the two-dimensional modeling was reduced from 400 m in length to one pool, 70 m long, in order to obtain model results on a scale useful for management decisions regarding pool recovery and the habitat needs of fish.

3.2 Model Characteristics

The computer model RMA2 is a two-dimensional finite element model that computes water-surface elevations and depth-averaged horizontal velocity components for free-surface turbulent flow (Donnell et al., 1997). RMA2 is a numerical model that relies on dividing the flow domain into discrete but not necessarily uniform increments or elements, and on the use of iterative numerical approximation techniques to approach a convergent solution to the non-linear mathematical expressions that describe two-dimensional flow. Numerical models of this type are based on a vertically-integrated form of the full three-dimensional Reynolds-averaged Navier-Stokes equations for turbulent flow, known as the shallow-water equations (Donnell et al., 1997). The model was originally created by Norton et al. (1973) for the U.S. Army Corps of Engineers, subsequently modified by the U.S. Army Corps of Engineers (King, 1990), and more recently coupled with a pre- and post-processing interface called Surface-Water Modeling System (SMS). SMS was developed at Brigham Young University's Environmental Modeling Research Laboratory and is distributed through Environmental Modeling Systems, Inc., (EMS-I). SMS provides the user a set of graphical tools with which to build the setup files for RMA2 and to graphically display the model output. (Version 6.0 of SMS was used in this research, and version 4.3 of RMA2 was used.) SMS also interfaces with other computational fluid dynamic models such as FESWMS (Froehlich, 1989) and HIVEL2D (Berger and Stockstill, 1995). RMA2 is designed to model subcritical flow conditions under the assumption of a hydrostatic pressure distribution and is, therefore, incapable of handling substantial vertical accelerations in the flow. The computer program solves the depth-integrated equations for conservation

of mass (equation 3.1) and momentum in the x (equation 3.2) and y (equation 3.3) directions (from Donnell et al., 1997):

$$\frac{\partial h}{\partial t} + h \left(\frac{\partial u}{\partial x} + \frac{\partial v}{\partial y} \right) + u \frac{\partial h}{\partial x} + v \frac{\partial h}{\partial y} = 0 \quad (3.1)$$

$$\frac{\partial u}{\partial t} + u \frac{\partial u}{\partial x} + v \frac{\partial u}{\partial y} + g \left(\frac{\partial h}{\partial x} + \frac{\partial a}{\partial x} \right) - \frac{\varepsilon_{xx}}{\rho} \frac{\partial^2 u}{\partial x^2} - \frac{\varepsilon_{xy}}{\rho} \frac{\partial^2 u}{\partial y^2} + \frac{gu}{C^2 h} \sqrt{u^2 + v^2} = 0 \quad (3.2)$$

$$\frac{\partial v}{\partial t} + u \frac{\partial v}{\partial x} + v \frac{\partial v}{\partial y} + g \left(\frac{\partial h}{\partial y} + \frac{\partial a}{\partial y} \right) - \frac{\varepsilon_{yx}}{\rho} \frac{\partial^2 v}{\partial x^2} - \frac{\varepsilon_{yy}}{\rho} \frac{\partial^2 v}{\partial y^2} + \frac{gv}{C^2 h} \sqrt{u^2 + v^2} = 0 \quad (3.3)$$

where

x = distance in the x -direction (streamwise)

u = horizontal flow velocity in the x -direction

y = distance in the y -direction (cross-stream)

v = horizontal flow velocity in the y -direction

t = time

g = acceleration due to gravity

h = water depth

a = elevation of the profile bottom

ρ = fluid density

ε_{xx} = normal turbulent exchange coefficient in the x -direction

ε_{xy} = tangential turbulent exchange coefficient in the x -direction

ε_{yx} = tangential turbulent exchange coefficient in the y -direction

ε_{yy} = normal turbulent exchange coefficient in the y -direction

C = Chezy roughness coefficient (converted from Manning's n)

Numerical solutions to the flow equations yield water depth and x - and y -components of depth-averaged velocity for each node in the flow field. RMA2 assumes a slip condition (non-zero velocities) along the boundary such that the resistance coefficients are applied only along the bed. The model is designed to simulate both unsteady and

steady flow. Turbulent energy losses between elements are simulated in the model using the Boussinesq eddy viscosity concept (Le Mehaute, 1976), whereby the eddy viscosity coefficients are represented in equations 3.2 and 3.3 by the turbulent exchange coefficients ε_{mn} .

3.3 Applications of Two-Dimensional Hydraulic Models

Most studies involving two-dimensional hydraulic models require the improved representation of flow complexities, and hence the need for a model that incorporates not only the streamwise but also the cross-stream components of flow. Typically the limitations of a one-dimensional model drive the need for applications of a two-dimensional hydraulic model. For example, Miller (1994) cites limitations with one-dimensional models in predicting stage around constrictions (e.g. fans) where there are complex flow patterns and a general sensitivity of flood-flow patterns to changes in topographic features. As a result, Miller (1994) incorporated a two-dimensional hydraulic model to evaluate hydraulic patterns around debris fans.

Within the last decade, two-dimensional flow models have gained increasing use in geomorphologic studies. The applications include evaluating floodplain inundation (Bates et al., 1992), modeling flow processes in a multi-thread channel (Lane and Richards, 1998), investigating flow in bends (Hodkinson, 1996), or research investigating the interaction between the boundary conditions and the flow field in bedrock channels (Miller and Cluer, 1998). Often, the application of a two-dimensional flow model requires a sediment transport component and determinations of bottom shear stress, such as evaluating the stability of channel islands at various discharges (Nelson,

1996), or assessing variations in boundary shear stress and the effects on bedload transport and bed-surface particle size (Lisle et al., 2000).

Like applications of one-dimensional models, two-dimensional models are becoming increasingly important in engineering design. Two-dimensional depth-averaged flow models provide the basis for predicting the local mean velocity in the vicinity of structures such as bridge piers, vanes and dikes, which can be compared with an estimate of the local threshold velocity for bed material entrainment in order to assess channel stability following construction of these features.

Specific applications of RMA-2 to engineering design studies include using the model to simulate river restoration alternatives for riparian habitat improvement by providing more frequent overbank flooding, and improving aquatic habitat through preferred hydraulic conditions along a reach of the Rio Grande (Byars et al., 2000). Applications also include modeling extreme low flow conditions at a natural riffle for the design of an artificial riffle (Peterson et al., 1995). Also, RMA-2V was used to design dike extensions that limit sediment deposition at the confluence of the Platte and Missouri Rivers (Zevenbergen et al., 1995).

More recently, two-dimensional flow models have been applied to aquatic ecology studies to determine habitat metrics as a function of flow (Leclerc et al., 1995; Ghanem et al., 1996), and in establishing instream flow requirements and the associated fish habitat needs (Anderson and Stewart, 2000; Stewart, 2001). In the research by Anderson and Stewart (2000) and Stewart (2001), RMA-2 was used to obtain detailed hydraulic information over a range of discharges, especially low flows, which was then coupled with meso-habitat availability and fish abundance data for the species of interest. In this

way, hydraulic properties within a habitat unit could be related to habitat utilization and variability at the scale of a fish community (Stewart, 2001).

In this application of RMA-2, a low and high discharge were simulated along the North Fork Poudre River to obtain improved representation of the flow patterns in pools dominated by flow separation and recirculation. Model results were then used to calculate boundary shear stress and sediment transport rates for comparison with the dataset of scour and deposition along the North Fork following the sediment release from Halligan Dam for inferences of pool sediment dynamics for fish habitat recovery.

3.4 Methods

3.4.1 Field Data Collection

Topographic field surveying of the Tick Pool was conducted in the fall of 1998 with the specific intent of developing a detailed map of the pool geometry for the two-dimensional modeling. The surveying was completed with a total station and prism mounted on a stadia rod, and x,y,z coordinates were obtained for each point. Survey points were taken at breaks in slope rather than along channel transects. The closure of the survey was within 3 cm. At the time of the pool survey, nearly 80% of the deposition resulting from the original 1996 sediment release had been removed by two seasons of relatively high, sustained snowmelt discharge along the North Fork.

Also during the 1998-1999 field work, two staff plates were mounted to the bedrock wall forming the left bank of the Tick Pool, immediately up and downstream of Cross Section 13 (Figure 1.1). Staff plates were read ten times over the next eighteen months, with higher frequency during the spring, to develop a stage-discharge relationship for the

Tick Pool that included flows consistent with the low and high discharges modeled using HEC-6 and GSTARS 2.0 (Chapter 2). In May 1999, one staff plate was washed out when discharge exceeded $30 \text{ m}^3/\text{s}$ during a rain-on-snow precipitation event. This storm generated the highest discharges recorded on the North Fork over the four years of field observation conducted for this research.

Automatic cameras were installed to photograph a portion of the Spring 1998 snowmelt (May 9-May 23: Table 1.2) when access to the river was restricted because of deep, swift flow. During this period, development of the eddy pool was very pronounced, with an naturally occurring foam developing on the water surface, delineating the eddy fence, and standing waves in the thalweg. Mean daily discharge at this time varied from 7.5 to $9.2 \text{ m}^3/\text{s}$. The timed photos were useful in comparing the hydraulic results of the two-dimensional model to flow patterns observed in the field.

During Spring 2000, velocity measurements were collected at a discharge of $4.05 \text{ m}^3/\text{s}$ within the Tick Pool along Cross Sections 12, 13 and 14 (Figure 1.1: Table 1.2). The velocity measurements were needed to calibrate and validate the results of the two-dimensional model. Velocity readings were made using a belly boat that was anchored by ropes to individuals standing on the banks. An one-dimensional, electromagnetic Marsh McBirney portable current meter mounted on an extended wading rod was used to collect the velocity measurements at 0.6 of the flow depth. Eight velocity measurements over five-second readings were averaged for each recorded measurement. Distances along the cross sections were measured at each velocity reading to locate velocity measurements on a map of channel coordinates. Given the swift nature of the current, even at $4.05 \text{ m}^3/\text{s}$, it was difficult to collect accurate readings in the thalweg without

being swept downstream. As such, velocity measurements are considered reliable only within the lower velocity eddies for the $4.05 \text{ m}^3/\text{s}$ discharge. It is these low-velocity eddies, however, that are important to overwinter fish survival, and hence the focus of this investigation. No velocity measurements were collected at the high flow discharge of $10.1 \text{ m}^3/\text{s}$.

3.4.2 Data Reduction

Survey data were reduced in ArcView by constructing a Triangular Irregular Network (TIN) of the Tick Pool reach, and developing channel cross sections as a line coverage for HEC-RAS modeling. Although a stage-discharge relationship was developed for the Tick Pool based on the staff plate readings and gage-recorded discharges, a downstream water-surface elevation is needed as an initial boundary condition for RMA2. HEC-RAS (U.S. Army Corps of Engineers, 1998b) was used to develop this stage-discharge relationship for the downstream-most cross section for both the $4.05 \text{ m}^3/\text{s}$ and the $10.1 \text{ m}^3/\text{s}$ discharge. The modeling reach was extended up- and downstream by adding artificial entrance and exit reaches upstream and downstream of the surveyed reach. The channel extension was incorporated to help stabilize the model and ensure that the region of interest was sufficiently isolated to prevent boundary effects, following the suggestions of Miller (1994).

3.4.3 Mesh Construction and Parameterization

SMS was used to build the finite element mesh for preparation in running RMA2. The x,y,z coordinates from the topographic survey were imported into SMS and were then triangulated to generate a mesh with either triangular and/or quadrilateral elements.

Both element shapes are supported by RMA2 within a single mesh, as are elements with curved sides. Where flow boundaries are relatively uniform, rectangular elements reduce the total number of elements within the model. Triangular elements are necessary in areas where flow boundaries do not allow four-sided rectangular elements (Donnell et al., 1997). One goal of mesh generation for the Tick Pool was to scale the elements in the finite element mesh such that the resolution of flow hydraulics is proportional to the bed roughness, so localized turbulence created by wake forces around boulders within the bed would be represented in the model output, without drastically increasing computational time. Various tools are available in SMS that help refine the computer-generated mesh, but mesh generation is by far the most time-consuming and important component of two-dimensional modeling using RMA2 (Donnell et al., 1997; Miller, 1995; Miller and Cluer, 1998).

3.4.3.1 Roughness

Once the mesh was created, material properties and boundary conditions were specified for each element in the finite element mesh. RMA2 allows the user to assign eddy viscosity and roughness coefficients through material types. Material types indicate a user-defined area of similar channel properties and hydraulic characteristics for which output is desired. Roughness coefficients were assigned to take into account the boundary geometry which is built into the two-dimensional form of the governing equations. In one-dimensional models, the Manning and Chezy coefficients account not only for boundary roughness but also for energy losses associated with an irregular boundary geometry. Because the boundary geometry is already accounted for in the two-dimensional flow model RMA2, a lower value of roughness coefficient should suffice to

describe boundary resistance alone. Several authors report that the results from a two-dimensional model are typically much less sensitive to the choice of roughness coefficients than in a one-dimensional model (Molls and Chaudhry, 1995; Ghanem et al., 1996). In general, roughness-coefficient values between 20-30 percent lower than those used in a one-dimensional model are specified for use in two-dimensional models (L. Zevenbergen and R. Jarrett, pers. comm. 2000). For this study, roughness parameters for the two-dimensional modeling were given values approximately 20 percent lower than one-dimensional model values for the low flow simulation (Table 3.1). Values were dropped 30 percent from one-dimensional values for the high flow simulation (Table 3.1), in order to account for increased depth at high discharge decreasing the influence of grain roughness. Sensitivity analyses were conducted on a range of roughness-coefficient values (between ± 10 and ± 25 percent of original values) to determine how the flow field responds to roughness adjustments.

Table 3.1. Roughness values for the Tick Pool used in one- and two-dimensional modeling for a low and high discharge simulation.

| Discharge (m ³ /s) | One-Dimensional | | | Two-Dimensional | | |
|-------------------------------|-----------------|---------------|---------------|-----------------|---------------|---------------|
| | Riffle <i>n</i> | Pool <i>n</i> | Wall <i>n</i> | Riffle <i>n</i> | Pool <i>n</i> | Wall <i>n</i> |
| 4.05 | 0.07 | 0.04 | N/A | 0.055 | 0.03 | 0.05 |
| 10.1 | 0.07 | 0.04 | N/A | 0.048 | 0.028 | 0.055 |

Because there is no mechanism by which to incorporate wall roughness in RMA2, Donnell et al. (1997) recommended that the user exaggerate the bed roughness on the elements forming the edge of the waterway in order to approximate the wall roughness. As such, a row of elements with higher roughness was added along the vertical walls of the modeling reach to add frictional resistance to retard flow (Table 3.1). Wall roughness

was not adjusted downward for the higher discharge simulation because more surface area of the bedrock walls bounding the Tick Pool are exposed to the flow during higher discharge, increasing skin friction. Wall roughness was increased slightly for the 10.1 m³/s simulation. Similar use of roughness along rock wall faces was applied by Miller (1995) to account for variations in channel morphology and boundary conditions.

3.4.3.2 Turbulent Exchange Coefficients

The fluid momentum transfer associated with exchanges of fluid masses moving at different speeds is called turbulence exchange (Tritton, 1988). The turbulent exchange coefficient, or eddy viscosity, describes the energy losses caused by turbulence. A turbulent exchange coefficient is included in RMA2 to facilitate the transfer of momentum from element to element. Unlike molecular viscosity, eddy viscosity is not truly a property of the fluid but is instead a property of the flow field and of the grid scale and solution technique used in the numerical model. Eddy viscosity is assigned by the user of RMA2 on either an element-by-element basis, or through a global parameter known as the Peclet option. The Peclet option assigns eddy viscosity based on the unique size and calculated velocity within each element. Dynamic eddy viscosity (in Pa-sec) defines the relationship between the velocity, elemental length, fluid density, and the Peclet number, as follows:

$$\varepsilon = \frac{\rho u dx}{P} \quad (3.4)$$

where

$$\rho = 1000 \text{ kg/m}^3 \text{ (assumed)}$$

u = average elemental velocity (m/s)

dx = length of element streamwise direction (m)

P = Peclet number

From equation (3.4) it is evident that dynamic eddy viscosity and Peclet number are inversely proportional. Eddy viscosity values that are too high (Peclet numbers that are too low) tend to dampen velocity and restrict the size of recirculating areas, whereas values that are too low may lead to numerical instability within the model (Miller and Cluer, 1998; Cluer, 1997). One main advantage of using the automatic assignment of elemental turbulence coefficients by Peclet number is that this provides ‘real time’ adjustment of eddy viscosity based upon the computed velocity and individual size of each element (Donnell et al., 1997). Generally, larger elements and elements with higher velocities will have larger eddy viscosity values at a given Peclet number. A recommended range of Peclet values is between 15 and 40 (Donnell et al., 1997). For simulations of the Tick Pool, the Peclet option was selected, and a value of 30 was originally assigned to the entire mesh, following the guidance of Miller (1994) who recommends that the final value of eddy viscosity chosen is the smallest value allowing a stable, convergent solution. The recommended range of dynamic eddy viscosity in Donnell et al. (1997) is 10-100 Pa-sec, and although turbulent exchange is assigned through the Peclet number, if that option is chosen, the model output allows users to track eddy viscosity values to ensure they stay within recommended ranges.

3.4.3.3 Wetting and Drying

RMA2 has the capability of handling the wetting and drying of elements within the mesh via two mechanisms; elemental elimination or gradual wetting and drying through a property called marsh porosity. The elemental elimination approach removes an element from the computational domain whenever the water depth at any one of its nodes approaches zero. This has the potential of creating isolated areas that are no longer connected with the main body of flow, thereby causing problems with conservation of mass as well as oscillations in velocity and water level from one iteration to the next (Donnell et al., 1997). For the Tick Pool analysis, the marsh porosity option was selected because it allows for the gradual transition between wet and dry conditions by retaining partially wet elements in the mesh until all nodes in the model are dry. Although the marsh porosity algorithm was designed for use in wetlands with broad, flat areas that are subject to wetting and drying with modest changes in stage, the use of marsh porosity also promotes smoother approaches to convergent solutions when used in bedrock systems with steep sidewalls and irregular boundaries (Miller, 1994; Miller and Cluer, 1998).

3.4.4 Model Simulations Using RMA2

Two discharge simulations were carried out in RMA2 for the Tick Pool: a low flow discharge of $4.05 \text{ m}^3/\text{s}$, representing the discharge capacity of the outlet valves at the base of Halligan Dam; and a high flow simulation of $10.1 \text{ m}^3/\text{s}$, representing the peak snowmelt discharge during Summer 1997. Although attempts were made to simulate comparable discharges using the one-, semi-two, and two-dimensional models, control of the hydraulic gate that open the valves at the base of Halligan Dam is crude, releasing

flows ranging from 3.4 m³/s to 4.1 m³/s at maximum capacity. As a result, there is a small disparity between the low flow simulations of Chapter 2 (3.4 m³/s), which is the peak of the experimental discharge (and the maximum outlet capacity prior to spillover of Halligan Dam), and those reported here using RMA2 (4.05 m³/s). The two low-flow discharges are considered comparable enough, however, to be treated as the peak of the experimental discharge, or the maximum outlet capacity.

Simulations in RMA2 require specification of a downstream water-surface elevation that is above the highest node in the mesh, which typically requires a beginning stage greater than normal depth along the downstream boundary. Thus, model simulations start with a relatively flat longitudinal water-surface profile, and with each set of iterations in RMA2 the water level is gradually decreased, or ‘stepped’ down towards normal depth, until a final solution is obtained. The stepping down process in RMA2 can be very difficult and time consuming, especially when mesh boundaries change with wetting and drying of elements; when parts of the flow field have areas of steep lateral or longitudinal slope, and sharp changes in the direction of flow; or where large volumes of water flow into small elements (Bates et al., 1992). Because RMA2 uses results from the previous time step for initial guesses for water surface slope, depth, and velocity, it is critical to step the model down slowly, sometimes on the centimeter scale, to avoid numerical instability and failure to converge to a viable solution.

Additionally, model users must designate whether dynamic or steady state conditions will be simulated. In river settings where the morphology changes gradually and depth and velocity are not significantly affected by the river stage at a previous time, steady-

state conditions for modeling are most appropriate. For the present study, only steady-state conditions were simulated.

3.4.5 Bed Shear Stress and Particle Stability

Results of the modeling provide depth-averaged velocity and depth for each node in the simulated channel reach. Bed shear stress can be calculated from the RMA2 output in SMS using a formulation that assumes a logarithmic velocity profile (Richardson et al., 1990; Julien, 1995). Although the North Fork is a steep-gradient mountain river and velocity profiles might be expected to follow the S-shape that Jarrett (1991) found for many Front Range rivers, the logarithmic profile is more appropriate for the North Fork (Wohl and Cenderelli, 2000); hence, the equation is deemed reasonable. The following equation provides a measure of bed shear stress in Pa (after Richardson et al., 1990, and Julien, 1995):

$$\tau_o = \frac{\rho u^2}{\left[5.75 \log \left(12.27 \frac{y_o}{k_s} \right) \right]^2} \quad (3.5)$$

where

ρ = density of the fluid (kg/m³)

u = depth-averaged velocity from the RMA2 results (m/s)

y_o = flow depth from RMA2 results (m)

k_s = height of roughness elements, or the d_{50} of bed sediment (m)

Bed shear stress was then compared to the critical value of shear stress at incipient motion for very fine sand ($d_{50} = 0.092$ mm) sampled from the marginal bar of the Tick

Pool. The critical value of the Shields parameter τ_{*c} corresponds to the beginning of particle motion, and was determined from the van Rijn (1984) sediment transport relationship as follows:

$$\tau_{*c} \cong 0.14 D_*^{-0.64} \quad (3.6)$$

where

D_* = the dimensionless particle diameter, determined from

$$D_* = d_s \left[\frac{(G-1)g}{\nu^2} \right]^{\frac{1}{3}} \quad (3.7)$$

where

d_s = a selected sediment diameter, the d_{50} of bed material (m)

G = specific gravity of the particle

g = acceleration due to gravity (m/s^2)

ν = kinematic viscosity of the fluid (m^2/s)

Critical shear stress for the sand diameter sampled was then determined by

$$\tau_c \cong \tau_{*c} (G-1) \rho g d_{50} \quad (3.8)$$

where

τ_{*c} = critical Shields parameter (dimensionless)

G = specific gravity of the particle

ρ = density of the fluid (kg/m^3)

g = acceleration due to gravity (m/s^2)

d_{50} = median particle diameter (m)

The threshold of incipient motion was then determined for flow on a plane bed under turbulent flow over a hydraulically rough boundary by comparing the ratio of τ_o/τ_c . The ratio of bed shear stress to critical shear stress can be considered an index of particle stability, as in Cluer (1997), such that ratios greater than one indicate particle mobility, ratios equal to one represent incipient motion, and ratios less than one denote particle stability. This approach was used to map the spatial distribution of boundary shear stress within the modeled reach, and to identify probable areas where very fine sand would be stable or deposited, as well as areas where transport or scour would occur within the Tick Pool.

An assumption of the critical Shields parameter is that sediment particles for which incipient motion is to be determined rest on a plane bed with an overlying horizontal water surface. Boundary geometry of the North Fork consists of a well developed pool-riffle sequence, where water-surface elevation of the pool remains relatively flat, even at the highest discharge measured. Because the calculations of incipient motion do not include the effect of rotation of a particle resting on a slope, particle stability is probably overestimated in areas with steep slopes, such as the entrance to the Tick Pool. However, the depth-averaged two-dimensional modeling results used to calculate the available bed shear stress ignore vertical fluid motions directed upward from the steep pool slopes. This may result in an underestimation of shear stress that may tend to counteract the effect of overestimated shear. The assumption of a plane bed does not negate the utility of predicting areas of probable sediment transport and immobility, especially in areas of the channel where bed slope is shallow, such as the upstream eddy pool, along the banks, and in backwater areas, all of which are important habitat for fish.

A coupled three-dimensional hydraulic and sediment transport model would be required to more accurately address the three-dimensional hydrodynamic forces acting on particles within an undulating, pool-riffle bed. This level of numerical modeling is beyond the scope of my investigation.

3.4.6 Sediment Transport

Patterns of sediment mobility were further explored by calculating transport rates using the output from RMA2. This allowed a comparison between the transport rates derived from the two-dimensional modeling and the preliminary analyses of sediment transport at Cross Section 13 of the Tick Pool presented in Chapter 2. Two sediment transport equations were selected for input into SMS; the Schoklitsch equation for bedload transport, and Yang's (1973) sand transport equation. These were selected to maintain consistency between equations used in the one- and semi-two dimensional modeling and more detailed hydraulic information obtained from RMA2. (See Appendix A for both equations.) Inferences about the relative ability to transport sediment within the Tick Pool are used to further explain the mechanisms by which pools are excavated and fish habitat is restored following a sediment release.

3.5 Results

3.5.1 HEC-RAS

Water-surface elevations for the low ($4.05 \text{ m}^3/\text{s}$) and high discharge ($10.1 \text{ m}^3/\text{s}$) were calculated in HEC-RAS, and then input into RMA2 as initial boundary conditions. The water-surface elevations and corresponding pool depths from HEC-RAS were compared with the stage-discharge relationship (Figure 3.1) derived from the staff plate installed on

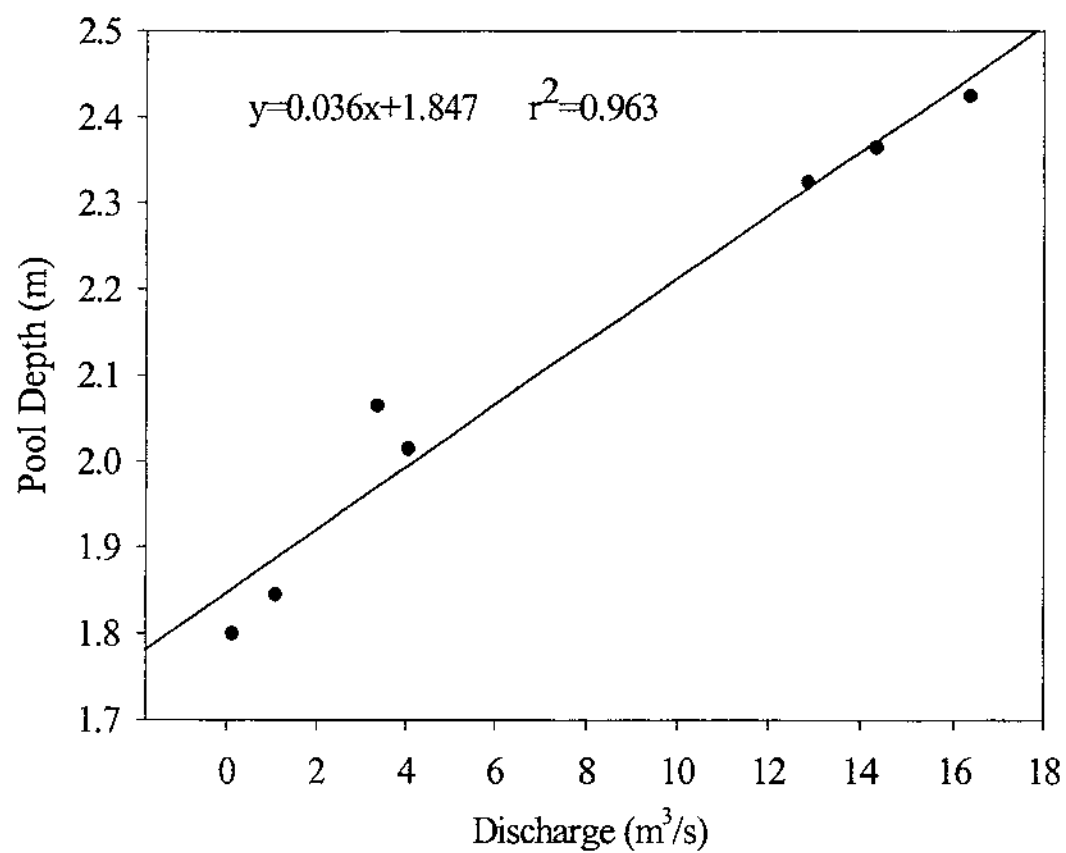


Figure 3.1. Stage-discharge relationship for the Tick Pool, North Fork River.

the bedrock wall forming the left bank of the Tick Pool. Pool water-surface elevation for a discharge of $4.05 \text{ m}^3/\text{s}$ is 100.74 m (Table 3.2), corresponding to a maximum pool depth of 2.03 m, which differed from the staff gage reading for the Tick Pool by 2 cm. At a discharge of $10.1 \text{ m}^3/\text{s}$, pool water-surface elevation from HEC-RAS is 101.02 m (Table 3.2), producing a pool depth of 2.29 m, which is 7 cm greater than the depth from the staff plate measurements. Pool depth differences of 2 and 7 cm between HEC-RAS modeled estimates and readings of the staff gage for the low and high discharge, respectively, are considered within a reasonable error range, and deemed useful for comparisons with the RMA2 results.

Table 3.2. HEC-RAS results for a low and high discharge, compared to stage-discharge relationship of pool depth for the Tick Pool.

| Discharge (m^3/s) | HEC-RAS WSEL (m) | Maximum HEC-RAS Pool Depth (m) | Maximum Gaged Pool Depth (m) | Maximum Cross Section Velocity (m/s) | HEC-RAS S_f |
|--|---------------------|---|------------------------------------|--|------------------|
| 4.05 | 100.74 | 2.03 | 2.01 | 0.4 | 0.000056 |
| 10.1 | 101.02 | 2.29 | 2.22* | 0.82 | 0.000152 |

Note: Maximum gaged depth for a discharge of $10.1 \text{ m}^3/\text{s}$ was determined from the linear regression equation of Figure 3.1. WSEL indicates water-surface elevation, and S_f is friction slope at the cross section nearest the staff gage.

3.5.2 Finite Element Mesh and Parameterization

The bathymetry of the Tick Pool (Figure 3.2) shows the compound nature of laterally-constricted pools along the North Fork. The deepest portion of the pool is immediately downstream from the bedrock constriction, in the lee of the outcrop forming the left bank, with a secondary topographic low upstream in the larger eddy. At the highest gaged discharge for which a pool depth was recorded ($16.3 \text{ m}^3/\text{s}$), pool depth in the downstream eddy was approximately 2.5 m.

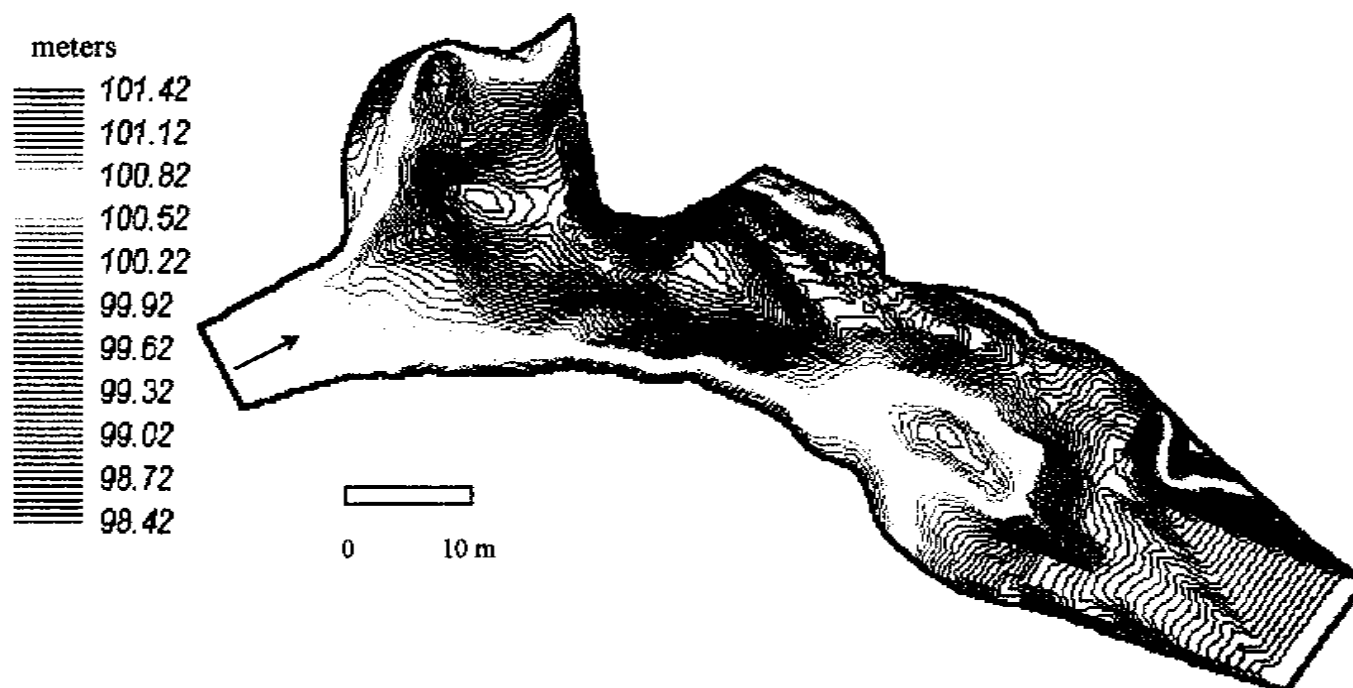
elevation

Figure 3.2. Topographic map of the Tick Pool for the two-dimensional hydraulic modeling. The irregularly shaped boundary is due to bedrock outcrops along the study reach. Brown line is model boundary.

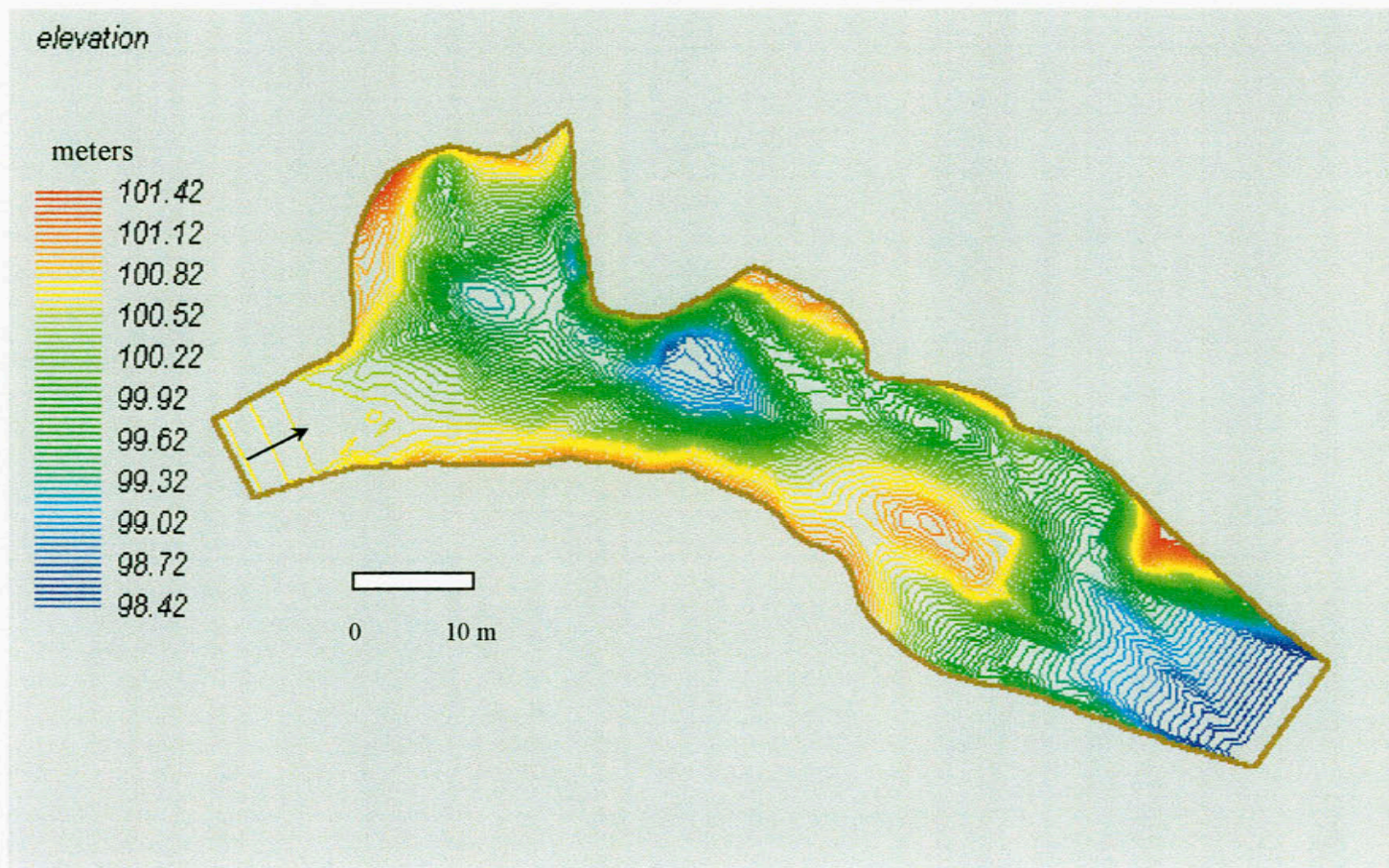


Figure 3.2. Topographic map of the Tick Pool for the two-dimensional hydraulic modeling. The irregularly shaped boundary is due to bedrock outcrops along the study reach. Brown line is model boundary.

The finite element mesh generated in SMS for the Tick Pool (Figures 3.3 and 3.4) is comprised predominantly of rectangular elements, each with an area of approximately 1 m² in the thalweg of the Tick Pool. The triangular elements within the large, upstream eddy pool have areas that are less than 1 m², and rectangular elements along the perimeter of the upstream eddy and in the downstream riffle are approximately 1.5 m². Donnell et al. (1997) report that rectangular elements are more stable numerically, having eight nodes versus the six nodes of triangular elements. In areas where the channel curves, triangular elements were used for better resolution within the eddy pools. The mesh quality indicators within SMS showed no major warnings regarding construction of the finite element mesh, except for a maximum slope violation, which is common for meshes constructed for rivers with steep gradients.

Manning's roughness coefficients for various material types are shown in Figures 3.3 and 3.4, for the low and high discharge simulations, respectively. The artificial channel extensions on the upper and lower ends of the reach were assigned higher roughness values in order to slow the flow into and out of the model reach, which improved the stability of the numerical solution. A roughness coefficient of 0.1 was assigned to the vegetated mid-channel bar downstream of the Tick Pool to significantly retard flow around and onto the bar edges at high discharges.

3.5.3 Experimental Discharge – RMA2

The spatial pattern of flow hydraulics for a discharge of 4.05 m³/s within the Tick Pool is illustrated by velocity vectors (Figure 3.5) and a contour plot of velocity magnitude (Figure 3.6). In general, the figures of velocity vector and magnitude show overall consistency with the expected hydraulic conditions in pools along mountain rivers

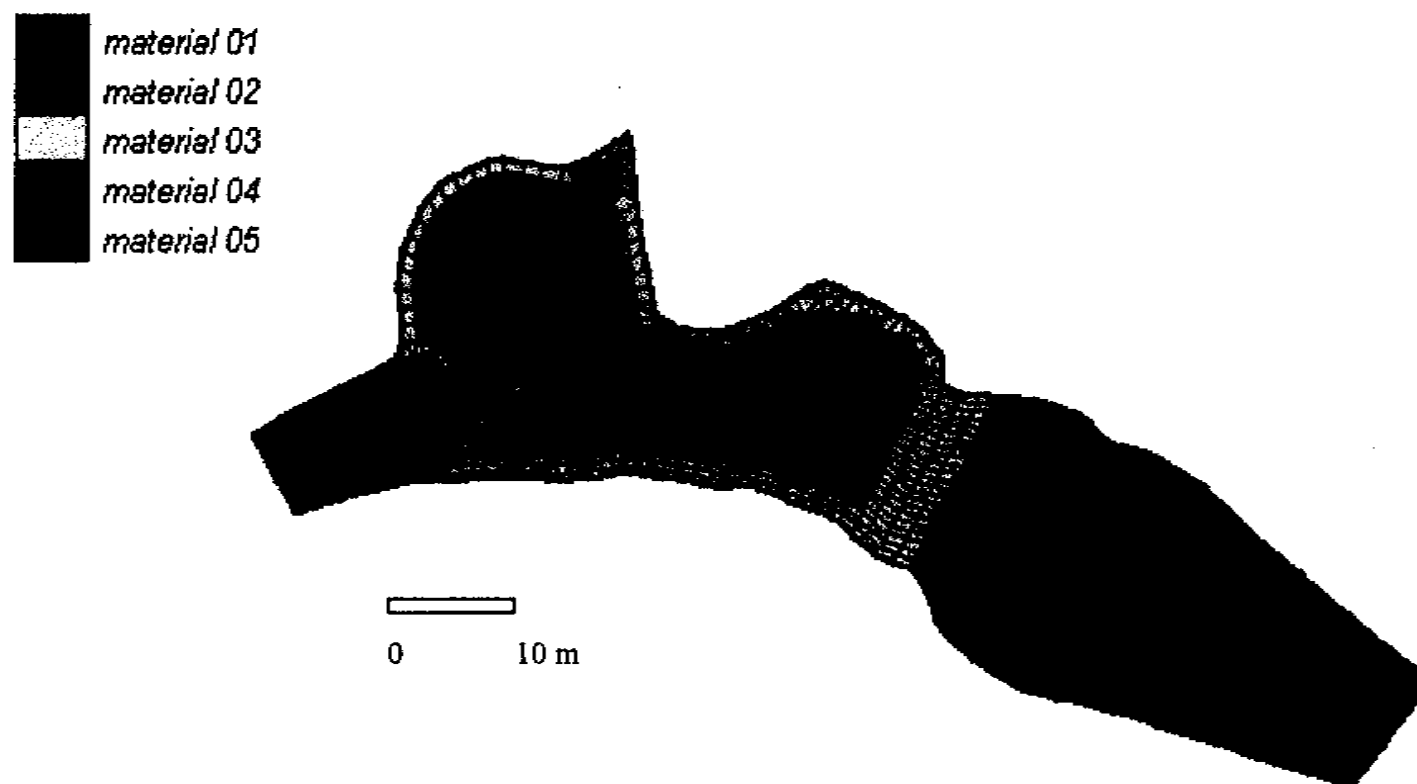


Figure 3.3. Finite element mesh and material properties for the low flow simulation in RMA2. Material 1 was assigned a roughness coefficient of 0.06; material 2 roughness coefficient = 0.055; material 3 roughness coefficient=0.05; material 4 roughness coefficient=0.03; material 5 roughness coefficient=0.1.

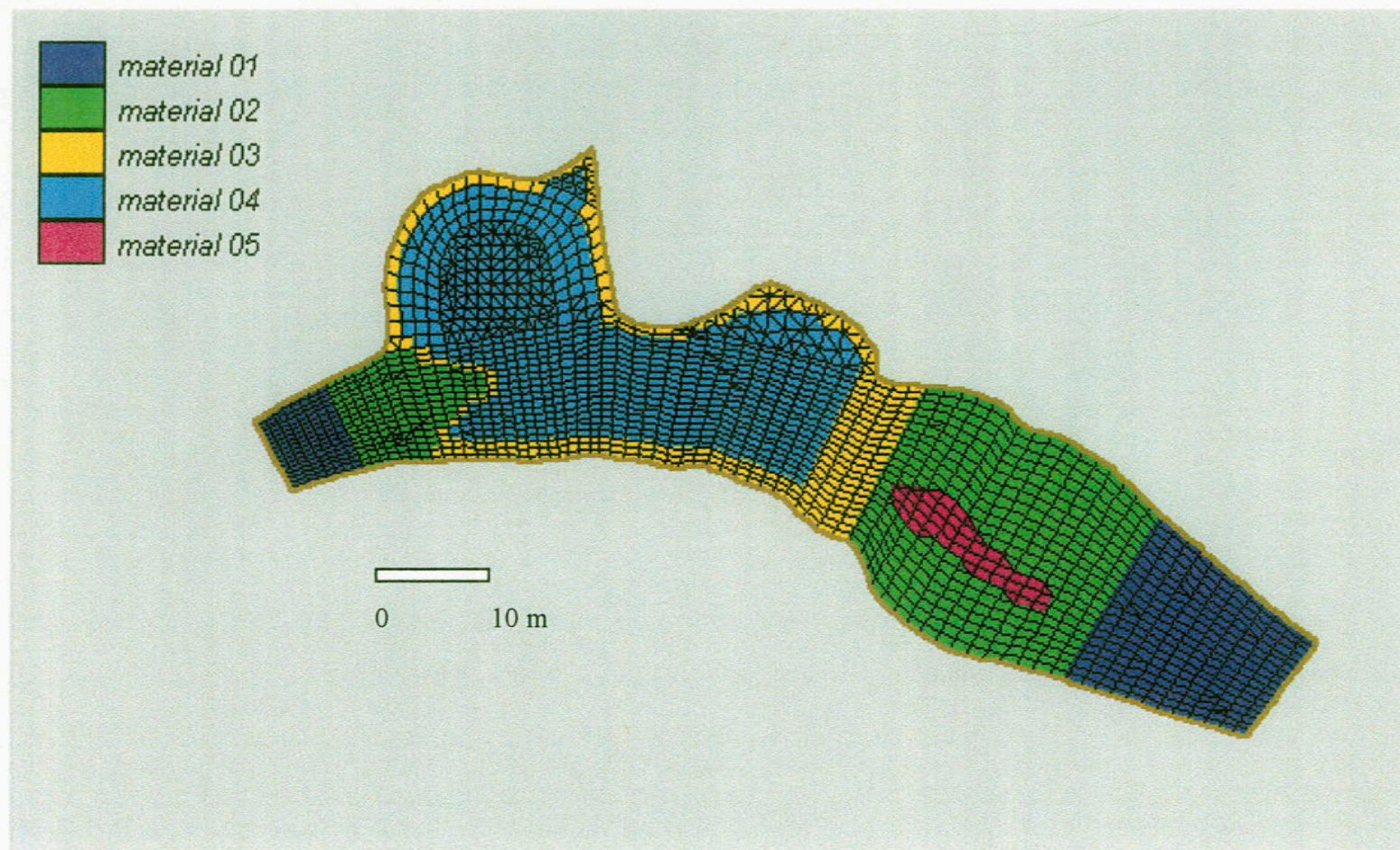


Figure 3.3. Finite element mesh and material properties for the low flow simulation in RMA2. Material 1 was assigned a roughness coefficient of 0.06; material 2 roughness coefficient = 0.055; material 3 roughness coefficient=0.05; material 4 roughness coefficient=0.03; material 5 roughness coefficient=0.1.

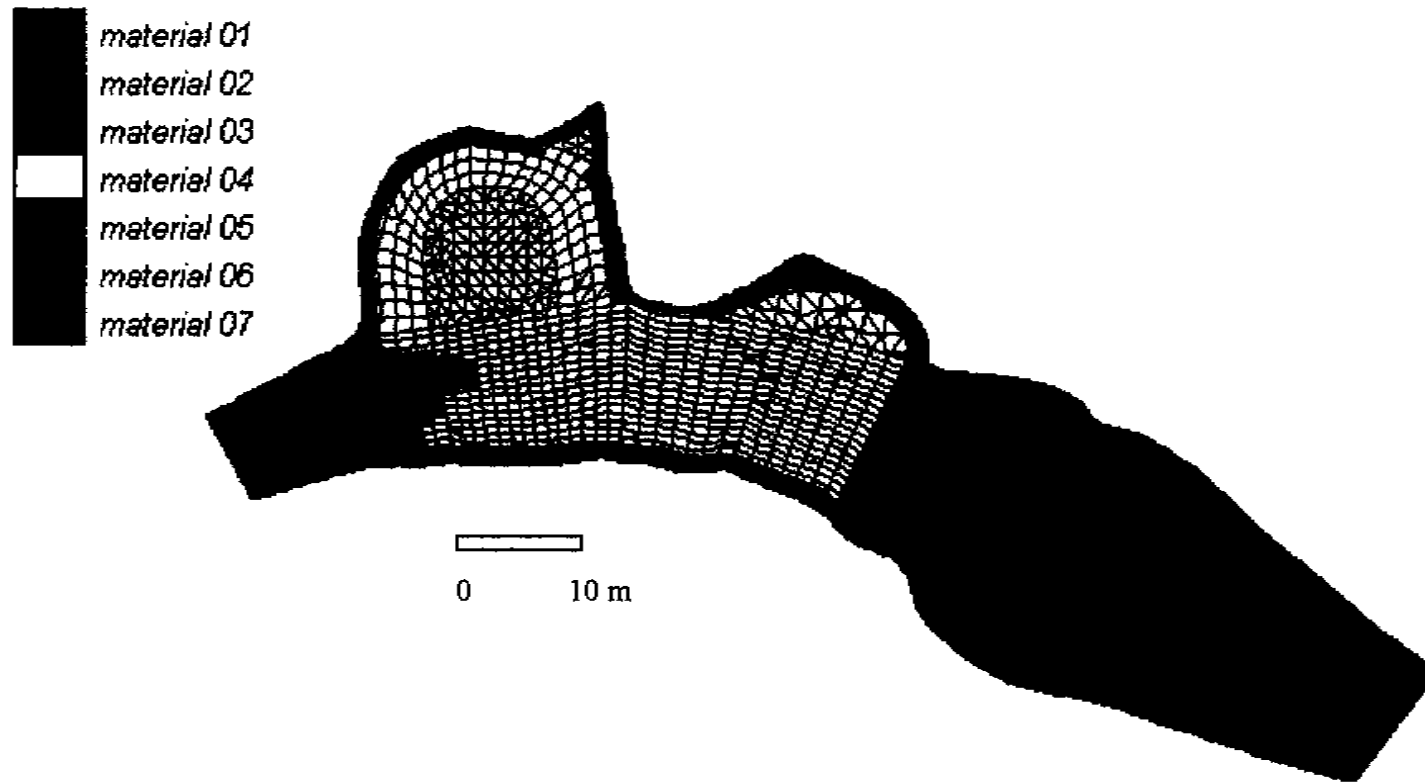


Figure 3.4. Finite element mesh and material properties for the high flow simulation in RMA2. Material 1 was assigned a roughness coefficient of 0.06; material 2 roughness coefficient = 0.048; material 3 roughness coefficient=0.045; material 4 roughness coefficient=0.028; material 5 roughness coefficient=0.1; material 6 roughness coefficient=0.055; material 7=0.08.

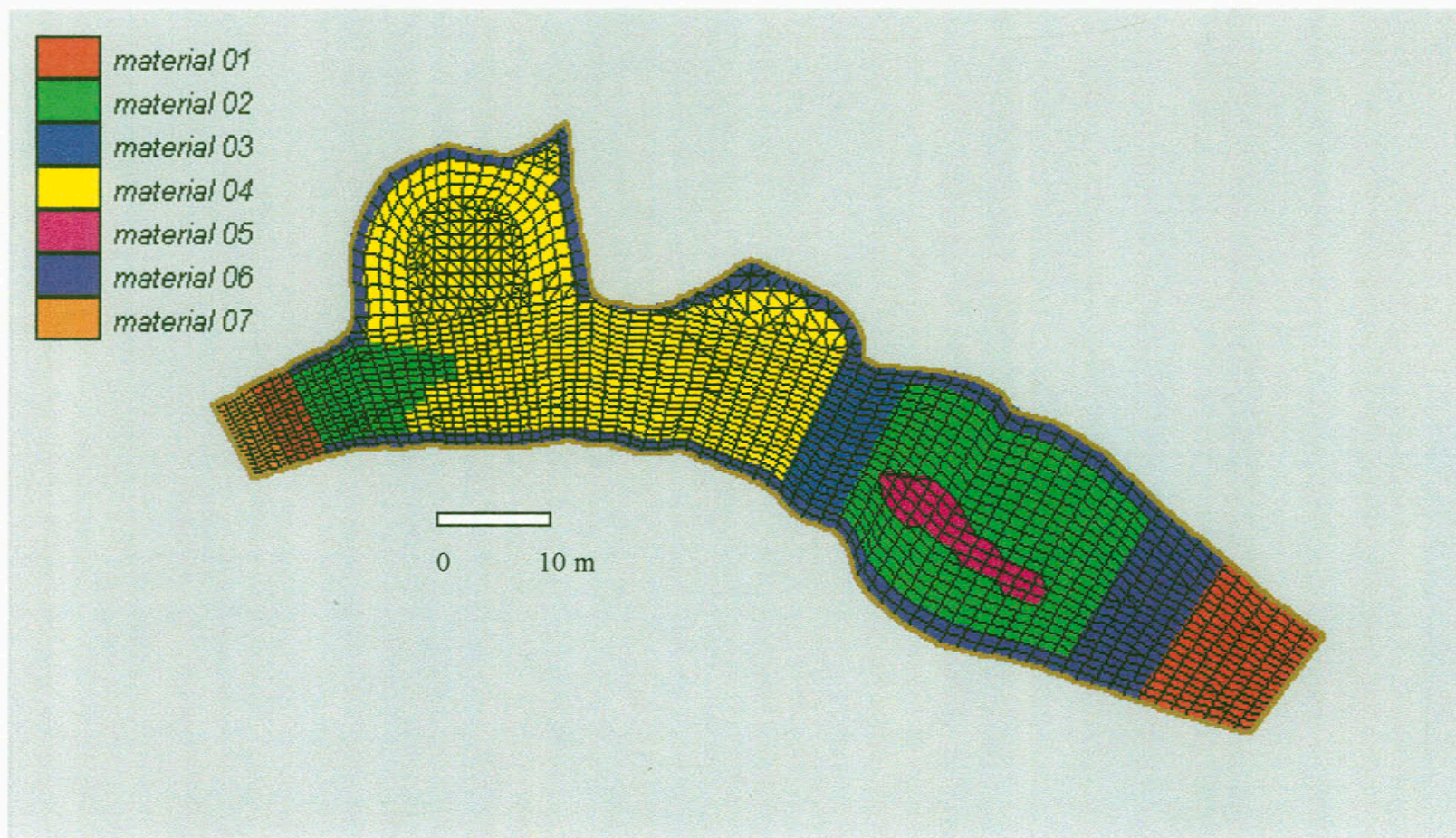


Figure 3.4. Finite element mesh and material properties for the high flow simulation in RMA2. Material 1 was assigned a roughness coefficient of 0.06; material 2 roughness coefficient = 0.048; material 3 roughness coefficient=0.045; material 4 roughness coefficient=0.028; material 5 roughness coefficient=0.1; material 6 roughness coefficient=0.055; material 7=0.08.

created by channel constrictions. The surface patterns of flow predicted by the model are representative of observed flow (Figure 3.7) for the Tick Pool. A thread of high velocity exists along the channel thalweg, with a maximum depth-averaged velocity of 1.02 m/s at the bedrock constriction. Findings by Thompson et al. (1998) relate similar high velocity flow at a constriction to the mechanics of pool formation, whereby the converging flow generates sufficient velocity and bed shear stress to scour out the bed material, creating a pool. Likewise, Miller (1994) found that the occurrence of velocity peaks, and associated shear stress, in and downstream from the narrowest part of the constrictions he was modeling, were also consistent with observations of scour holes tending to form at such locations.

Simulated velocity within the Tick Pool decreases in all areas on either side of the swift thalweg (Figure 3.5). These areas are characterized by flow separation and recirculation zones (Figure 3.7). The boundary layer separates away from the relatively confined upstream riffle, forming the upstream eddy, and reattaches at the constriction, forming the downstream eddy (both on the channel left). The well-developed recirculating zone in the upstream eddy is readily visible in the modeling results, showing strong, upstream flow lateral to the main channel (Figure 3.5). Maximum depth-averaged velocity in the upstream eddy, as predicted by RMA2, is 0.31 m/s, occurring at the apex of the recirculating cell, where surface flow becomes directed shoreward and loses all downstream component of flow. Interestingly, the location of maximum eddy velocity in the Tick Pool corresponds to sites of higher velocity documented within primary-eddy return currents, which bisect separation and reattachment bars, along the Colorado River in Grand Canyon (Schmidt, 1990). Flume experiments simulating recirculating flow

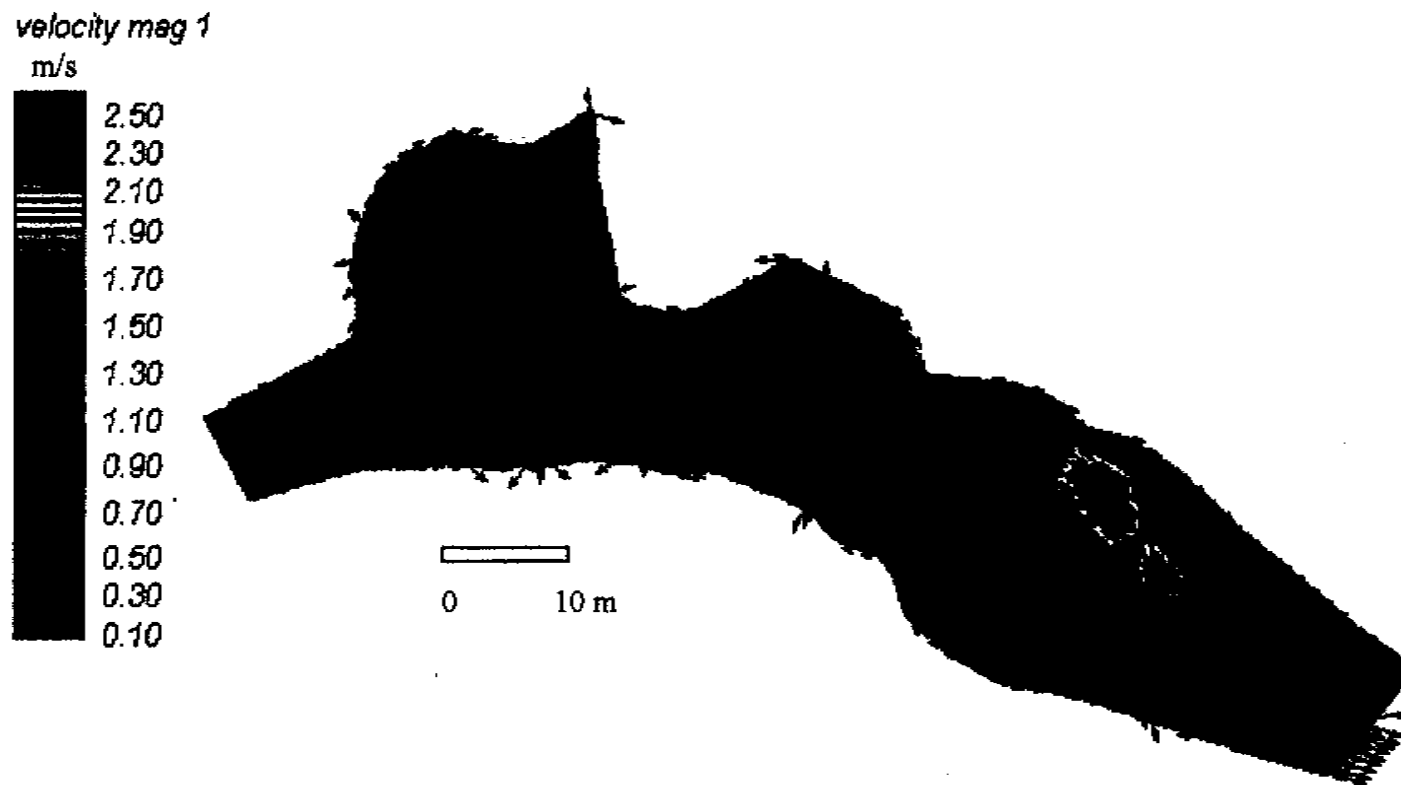


Figure 3.5. Velocity magnitude plot for low flow simulation in RMA2. Color contours are in m/s and arrows are a fixed length and are not scaled to the magnitude of the velocity.

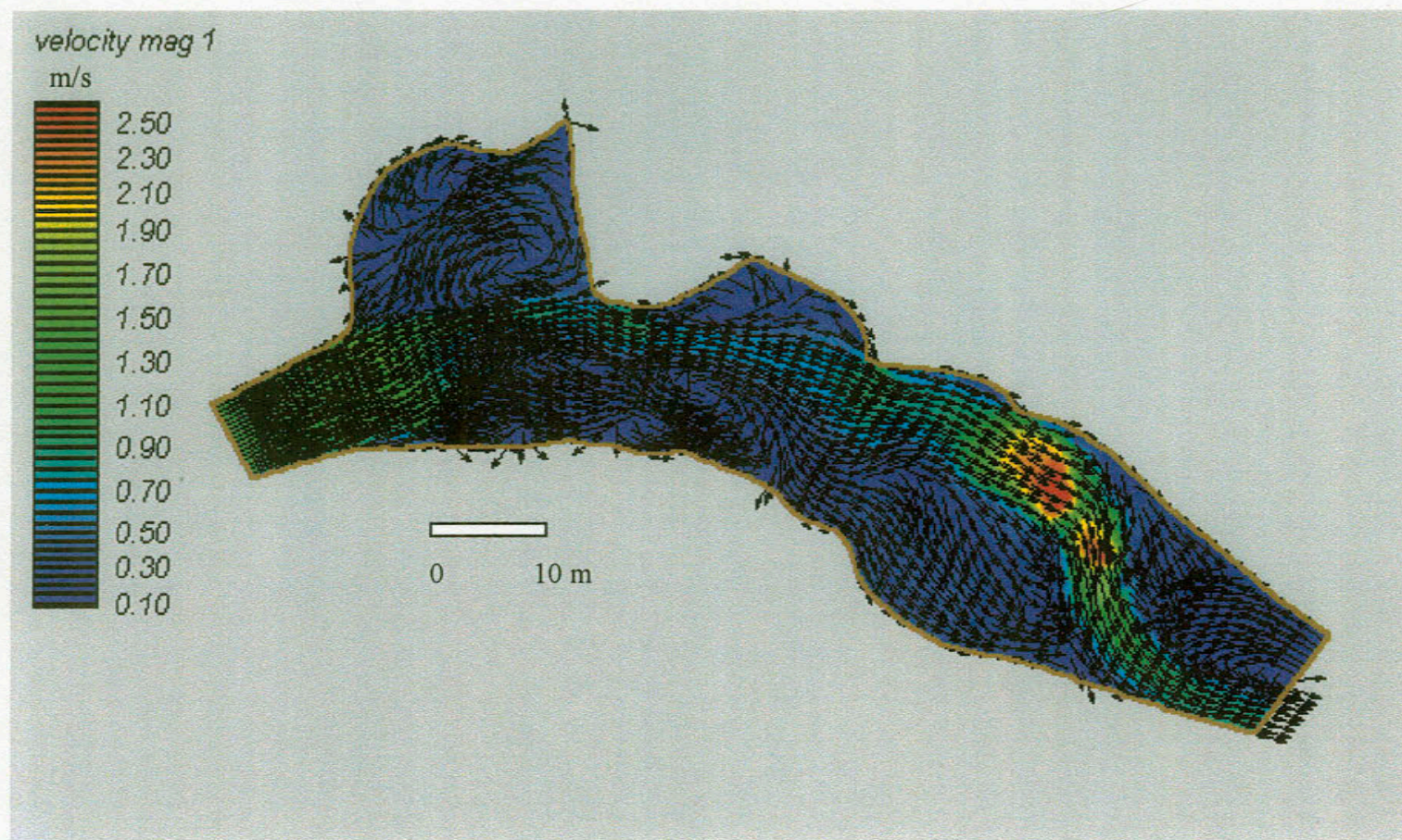


Figure 3.5. Velocity magnitude plot for low flow simulation in RMA2. Color contours are in m/s and arrows are a fixed length and are not scaled to the magnitude of the velocity.

velocity mag 1

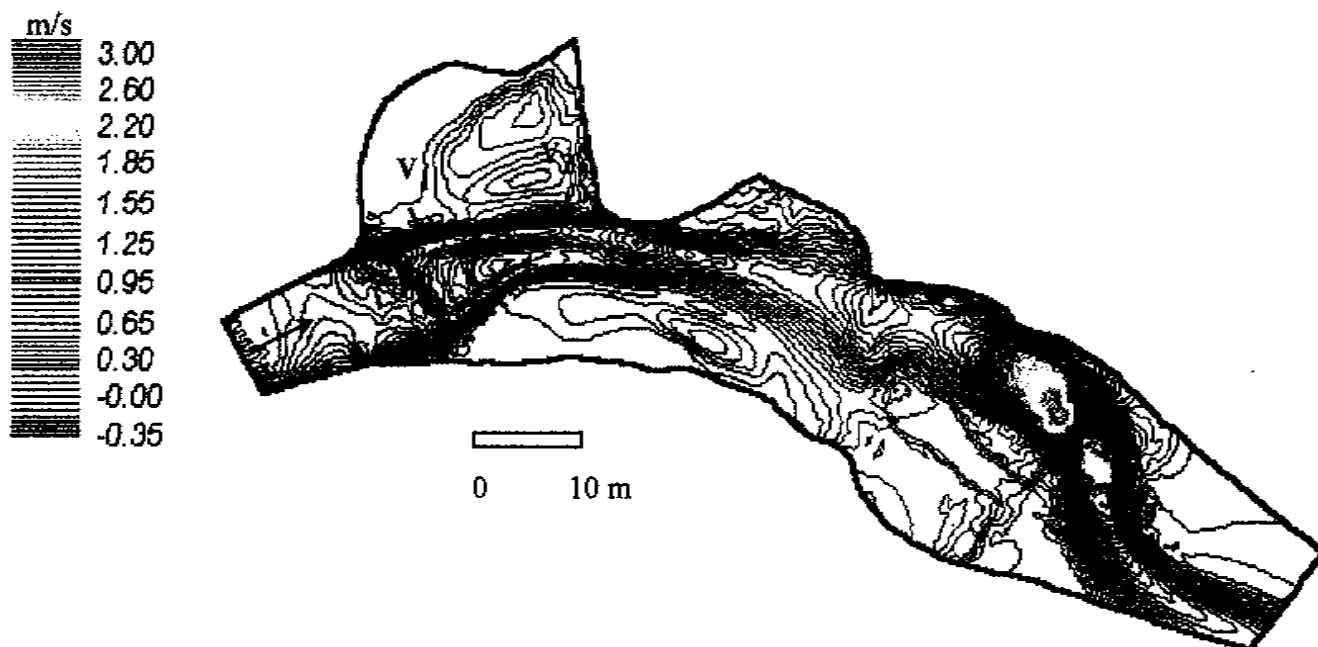


Figure 3.6. Contour plot of velocity magnitude for low flow simulation in RMA2. Velocity gradient was calculated between the upstream eddy and the main flow at lines labeled v_1 and v_2 .

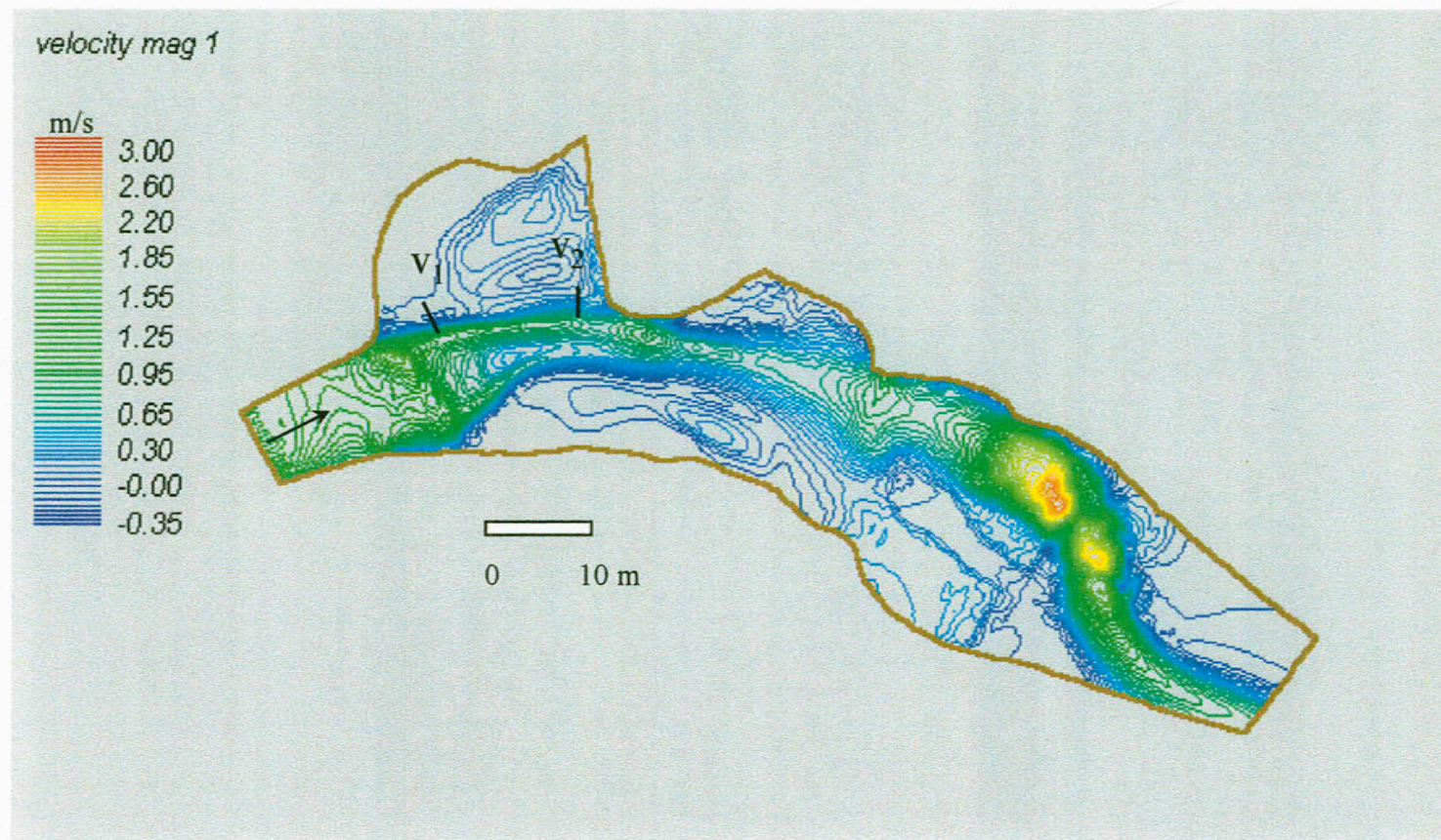


Figure 3.6. Contour plot of velocity magnitude for low flow simulation in RMA2. Velocity gradient was calculated between the upstream eddy and the main flow at lines labeled v_1 and v_2 .



Figure 3.7. View downstream of the Tick Pool at a discharge of $3.4 \text{ m}^3/\text{s}$, comparable to the experimental release from Halligan Dam during Spring 1997. Person (at arrow) is standing on upstream side of vegetated, mid-channel bar which demarcates the location of the adjacent riffle.



Figure 3.7. View downstream of the Tick Pool at a discharge of $3.4 \text{ m}^3/\text{s}$, comparable to the experimental release from Halligan Dam during Spring 1997. Person (at arrow) is standing on upstream side of vegetated, mid-channel bar which demarcates the location of the adjacent riffle.

measured maximum instantaneous velocities along the flume wall in the backflow region (Schmidt et al., 1993). The maximum backflow speeds approached the mean downstream velocity (Schmidt et al., 1993). In addition, initial work relating hydraulic parameters to scallop dimensions in caves indicates much higher velocities in those portions of recirculating eddies that direct flow back upstream (G. Springer, pers. comm., 2001).

The recirculation zone downstream from the constriction on the left bank of the Tick Pool is smaller and weaker, with less well-organized velocity vectors (Figure 3.5). An additional area of flow separation and recirculation occurs on the right side of the channel, opposite the bedrock constriction.

Within the entire modeled reach, the highest depth-averaged velocity, 2.74 m/s, occurs on the left side of the mid-channel bar (red zones on Figure 3.5), in an area where the local slope increases to nearly 0.04 m/m, and where turbulent flow over boulder-sized bed clasts appears to be creating supercritical flow. Plots of Froude number for the entire mesh (not shown) indicate isolated areas of supercritical flow in this downstream riffle which resulted in model instabilities and difficulties in converging to a numerically stable downstream water-surface elevation. Velocity estimates and associated calculations within the Tick Pool are far enough away from the riffle (10 m) and regions of supercritical flow to be considered reliable. No hydraulic and sediment transport interpretations were made for the downstream riffle because of the effects of transient supercritical flow, a condition that violates the basic assumption of the RMA2 model.

The velocity gradient of the shear zone in the upstream eddy was calculated across elements near the flow separation point on the left side of the channel, and was then

compared to the velocity gradient near the bedrock outcrop (Figure 3.6). The velocity gradient at the expansion point is 0.62 m/s-m, compared to 0.345 m/s-m at the bedrock outcrop on the channel-left. The abrupt expansion into the pool from the riffle at Cross Section 11 (Figure 1.1) sets up the steep velocity gradient in that area. At the bedrock constriction, flow enters the eddy pool where the velocity and corresponding pressure gradients are shallower, initiating the recirculating flow.

Centripetal acceleration of the eddy, or the magnitude of the acceleration of a particle of water moving in the eddy, is calculated in m/s^2 by:

$$a_c = \frac{v^2}{r} \quad (3.5)$$

where

v = maximum linear velocity on the outward edge of the eddy (m/s)

r = radius of the eddy (m)

Because centripetal acceleration is directed at the center of the eddy, it can also be an indicator of eddy strength, and centripetal acceleration should increase as eddy velocity increases with increasing discharge. Centripetal acceleration of the upstream eddy at $4.05 \text{ m}^3/\text{s}$ is 0.014 m/s^2 , with a maximum velocity of 0.31 m/s over an eddy radius of 6.90 m . For comparison, centripetal acceleration within the downstream eddy at the same discharge is 0.009 m/s^2 , calculated from a maximum velocity of 0.17 m/s over a radius of 3.38 m . Flow velocity in the downstream eddy is slightly more than half the magnitude of velocity in the upstream eddy, yet the smaller radial arm of the downstream eddy means that it attains 64 percent of the strength of the upstream eddy. If eddy strength translates directly into sediment entrainment and transport potential, then

sediment persistence within eddies following a sediment release becomes most effective at combinations of high velocity over a small eddy radius, which should correspond to an eddy geometry that minimizes the initial volume of sediment storage. At combinations of lower velocity and large eddy radius, the eddy strength will be lower, possibly indicating greater ease of sediment removal because of lower eddy strength via centripetal acceleration.

3.5.3.1 Model Calibration and Validation

Validation data were collected for the low discharge only, along Cross Sections 12, 13, and 14 of the Tick Pool (Figure 1.1). Figure 3.8 shows a plot of computed versus observed velocity measurements for initial model settings in RMA2. There is good agreement between computed and observed velocity for velocities less than about 0.15 m/s, or the low flow areas within the eddy pools. At higher discharges, there is considerable scatter of points, with no consistent over- or under-prediction of velocity by the model. The high degree of scatter is attributed to errors in measuring velocity in swifter portions of the Tick Pool, which are also the areas that get scoured of sediment more readily with any increase in discharge. It is the low velocity areas of the pools that are more important in terms of fish habitat. In these areas longer residence time of sediment in pools is a concern for reestablishing critical habitat areas, especially in winter.

Calibration and validation of the model occurred simultaneously, as recommended by Donnell et al. (1997), using eddy viscosity (Peclet number) (Table 3.3) and a comparison with measured velocity. A linear regression, forced through a zero intercept, was completed for each plot of computed versus observed velocity with varied eddy viscosity

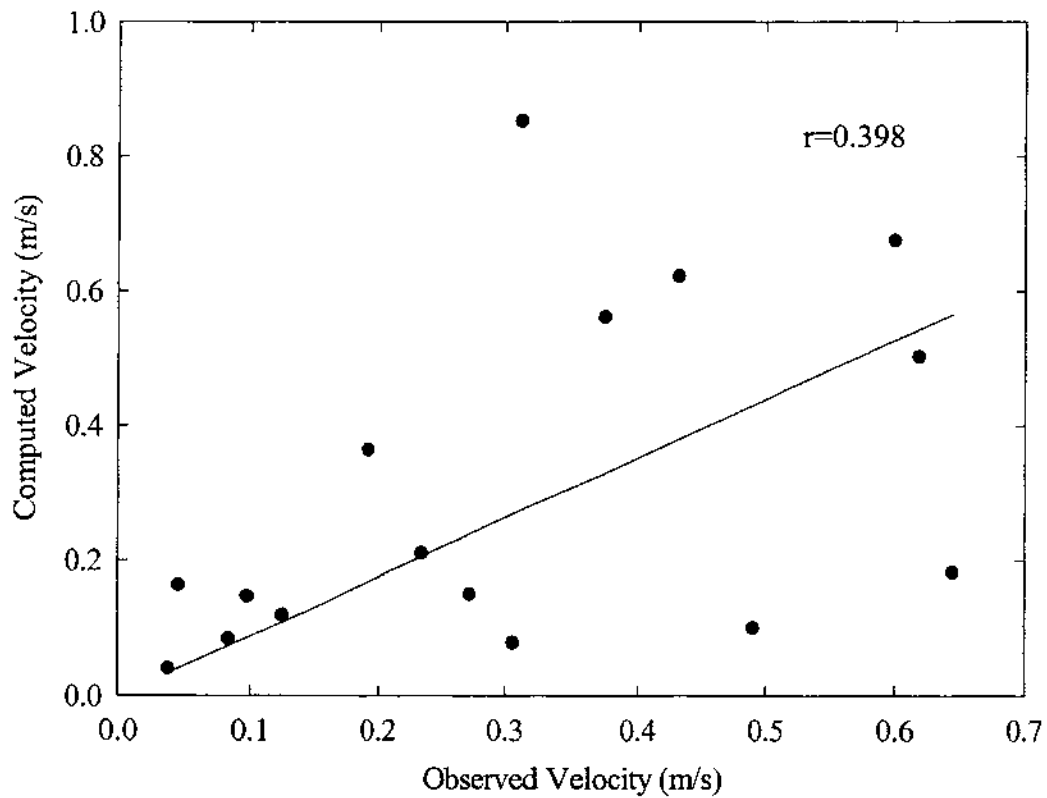


Figure 3.8. Computed versus observed velocity magnitude for low flow simulation in RMA2. Correlation coefficient, r , indicates the strength of the relationship between computed and observed values. The line is fitted line through the origin.

and roughness to provide a means of comparing the effects of parameter variations on the hydraulic results. The correlation coefficient (r) varies from +1 to -1, and was used to measure the strength of the relationship between model estimates and field measurements of velocity. A higher correlation coefficient indicates a stronger relationship between model predictions of velocity and field measurements (Table 3.3).

Initially, a Peclet number of 30, with original riffle and pool roughness of 0.055 and 0.03, respectively, produced a correlation coefficient of 0.398 (Figure 3.8). Water-surface elevation of the pool was estimated in RMA2 at 100.82 m (Table 3.3), as compared to the HEC-RAS estimate of 100.76 m. The maximum pool depth within the model domain was 2.07 m versus a staff plate measure of pool depth at 2.03 m. These results indicate that RMA2 modeling of the Tick Pool produced pool water-surface elevations and pool depths within 4-6 cm of field measurements. Velocity estimates from RMA2 for the slow-flowing eddy are in strong agreement with the field measurements of velocity as well (Figure 3.8). Subsequent simulations with variations in Peclet number, from 20-40 (Table 3.3), were used to calibrate the model, and indicate minimal effect on the resultant water-surface elevation and maximum pool depth (less than 1 cm). Moreover, maximum velocity in the eddy pool varied by only 0.002 m/s for a decrease in Peclet number from 30 to 20 (Table 3.3). Velocity at the constriction decreased with a decrease in Peclet number (increased eddy viscosity), but the change is not substantial (6 percent). These findings are consistent with those of Cluer (1997), who noted that lower Peclet numbers dampen velocity through greater turbulent exchange. A 66 percent drop in Peclet number (from 30 to 20) has an overall minimal effect on the Tick Pool hydraulics.

Table 3.3. Modeling results from RMA2 for varied Peclet number for the low flow discharge, 4.05 m³/s.

| Varied Peclet Number | Pool Location | Maximum Velocity (m/s) | Minimum Velocity (m/s) | WSEL (m) | Maximum Depth (m) | Correlation Coefficient, r |
|----------------------|---------------|------------------------|------------------------|----------|-------------------|----------------------------|
| 30 | Eddy | 0.312 | 0.0108 | 100.82 | 2.07 | 0.398 |
| | Constriction | 1.02 | | 100.80 | | |
| 20 | Eddy | 0.310 | 0.00932 | 100.82 | 2.08 | 0.367 |
| | Constriction | 0.962 | | 100.81 | | |
| 40 | Eddy | Diverged | Diverged | Diverged | Diverged | N/A |
| | Constriction | Diverged | Diverged | Diverged | Diverged | N/A |

Note: N/A indicates not applicable, and 'diverged' indicates the model diverged and a solution was not achieved.

A Peclet number of 40 resulted in model divergence. Apparently, a Peclet number of 40 is too great, resulting in dynamic eddy viscosity that is too low to transfer momentum sufficiently to generate a stable model solution. Eddy viscosity values obtained from RMA2 simulations for the Tick Pool, for which the best results were obtained (Peclet number of 30), varied between 7-112 Pa-sec. Guidelines in the documentation recommend keeping eddy viscosity values between 10-100 Pa-sec (Donnell et al., 1997).

3.5.3.1.1 Sensitivity Analyses

Evaluation of the effect of varied Manning n on the hydraulic results are provided in Table 3.4. Manning n was systematically altered in the RMA2 files to values that were between ± 10 and ± 25 percent in the riffle upstream from the Tick Pool, followed by similar changes for the pool. Decreasing roughness in the riffle within the specified range caused the model solution to diverge. Increasing roughness caused a variation in water-surface elevation of 1-2 cm higher than original values, and maximum depth varied by only 3 cm. Overall, the HEC-RAS-predicted water-surface elevation of 100.76 m was

overestimated by RMA2 by a maximum of 8 cm for the greatest change in n (+25 percent).

Adjusting roughness coefficients in the Tick Pool proper resulted in similar minor fluctuations in the maximum depth and water-surface elevation of the pool predicted by RMA2 (Table 3.4; lower half). There is no more than a 6 cm difference between the pool water-surface elevation estimate of 100.76 m from HEC-RAS and the water-surface elevation resulting from a +25 percent change in roughness for the Tick Pool. Also, maximum pool depth predicted by RMA2 was 2.08 m for a +25 percent increase in roughness, just 5 cm greater than the staff plate measurement of 2.03 m. Correlation coefficients for the various simulations (Table 3.4) indicate minimal improvement in the relationship between computed and observed velocity magnitudes as a consequence of adjusting roughness. Model-predicted velocity most closely agrees with field velocity measurements for n values +25 percent greater than the original 0.03 value selected for the Tick Pool (Table 3.4).

In comparing the results of Table 3.3 and 3.4, it appears that higher roughness suppresses maximum velocity slightly more than an increase in eddy viscosity over the range of values tested. Maximum depth-averaged velocity at the constriction was suppressed to the greatest degree by a Peclet number of 20 (Table 3.3). An even larger drop in maximum depth-averaged velocity occurred when adjacent riffle n values and pool n values were increased by 25 percent over original values. The difference, however, is relatively minor, never altering the predicted maximum depth-averaged velocity by more than 11 percent of the maximum 1.02 m/s figure predicted for the constriction under calibrated settings of Peclet number and roughness.

Table 3.4. Modeling results from RMA2 for varied roughness coefficient for adjacent riffles (upper half of table), and pool portions of the study reach (lower half) for the low flow discharge, 4.05 m³/s.

| Varied Riffle 'n' Value | Pool Location | Maximum Velocity (m/s) | Minimum Velocity (m/s) | WSEL (m) | Maximum Depth (m) | Correlation Coefficient, r |
|--|--------------------------|---------------------------------------|---------------------------------------|-----------------|------------------------------|---------------------------------------|
| Original (0.055) | Eddy | 0.312 | 0.0108 | 100.82 | 2.07 | 0.398 |
| | Constriction | 1.02 | | 100.80 | | |
| +10% (0.0605) | Eddy | 0.278 | 0.00766 | 100.83 | 2.09 | 0.314 |
| | Constriction | 0.968 | | 100.82 | | |
| -10% (0.0495) | Eddy | Diverged | Diverged | Diverged | Diverged | N/A |
| | Constriction | Diverged | Diverged | Diverged | Diverged | |
| +25% (0.0688) | Eddy | 0.248 | 0.0115 | 100.84 | 2.10 | 0.113 |
| | Constriction | 0.908 | | 100.83 | | |
| -25% (0.0413) | Eddy | Diverged | Diverged | Diverged | Diverged | N/A |
| | Constriction | Diverged | Diverged | Diverged | Diverged | |
| Varied Pool 'n' Value | Pool Location | Maximum Velocity (m/s) | Minimum Velocity (m/s) | WSEL (m) | Maximum Depth (m) | Correlation Coefficient, r |
| Original (0.03) | Eddy | 0.312 | 0.0108 | 100.82 | 2.07 | 0.398 |
| | Constriction | 1.02 | | 100.80 | | |
| +10% (0.033) | Eddy | 0.291 | 0.00732 | 100.82 | 2.07 | 0.399 |
| | Constriction | 0.991 | | 100.81 | | |
| -10% (0.027) | Eddy | 0.332 | 0.0146 | 100.81 | 2.07 | 0.396 |
| | Constriction | 1.03 | | 100.80 | | |
| +25% (0.0375) | Eddy | 0.262 | 0.00633 | 100.82 | 2.08 | 0.400 |
| | Constriction | 0.953 | | 100.81 | | |
| -25% (0.0225) | Eddy | 0.383 | 0.021 | 100.81 | 2.07 | 0.392 |
| | Constriction | 1.07 | | 100.80 | | |

Note: N/A indicates not applicable, and 'diverged' indicates the model diverged and a solution was not achieved.

This analysis indicates that RMA2 results are largely insensitive to adjustments in roughness coefficient, but more sensitive to selection of Peclet number and eddy viscosity. Miller and Cluer (1998) found that the importance of assigning roughness values is diminished for two-dimensional models, and is replaced by an overall model sensitivity to eddy viscosity. In a comparison of two- and three-dimensional hydraulic models, Lane et al. (1999) conclude that two-dimensional models required corrections for the effects of secondary circulation on the depth-averaged flow field to match the predictive abilities of the three-dimensional model, and that the two-dimensional model was much less sensitive to topographic variability and much more sensitive to friction parameterization. The original assignment of roughness coefficient by material type for the Tick Pool is considered representative of the grain roughness of the study reach. Also, the selection of a Peclet number of 30 minimized model sensitivity.

3.5.4 Snowmelt Runoff – RMA2

Simulations completed for the higher discharge of $10.1 \text{ m}^3/\text{s}$ used the same finite element mesh as that used for the low flow. The high flow required adjustments to the roughness coefficients to account for increased flow depth over the channel boundary (Figure 3.4). In general, roughness was decreased for all material types by 30 percent over one-dimensional model values (Table 3.1).

Velocity vectors for the high snowmelt runoff (Figure 3.9) and a contour plot of velocity magnitude (Figure 3.10) show patterns of velocity distribution similar to those for the low flow results. Maximum velocity within the Tick Pool occurs at the bedrock constriction (1.73 m/s), with recirculating flow developed in both the upstream and downstream eddies (Figure 3.9, Figure 3.11). The eddy cell size is larger at this higher

velocity mag 1

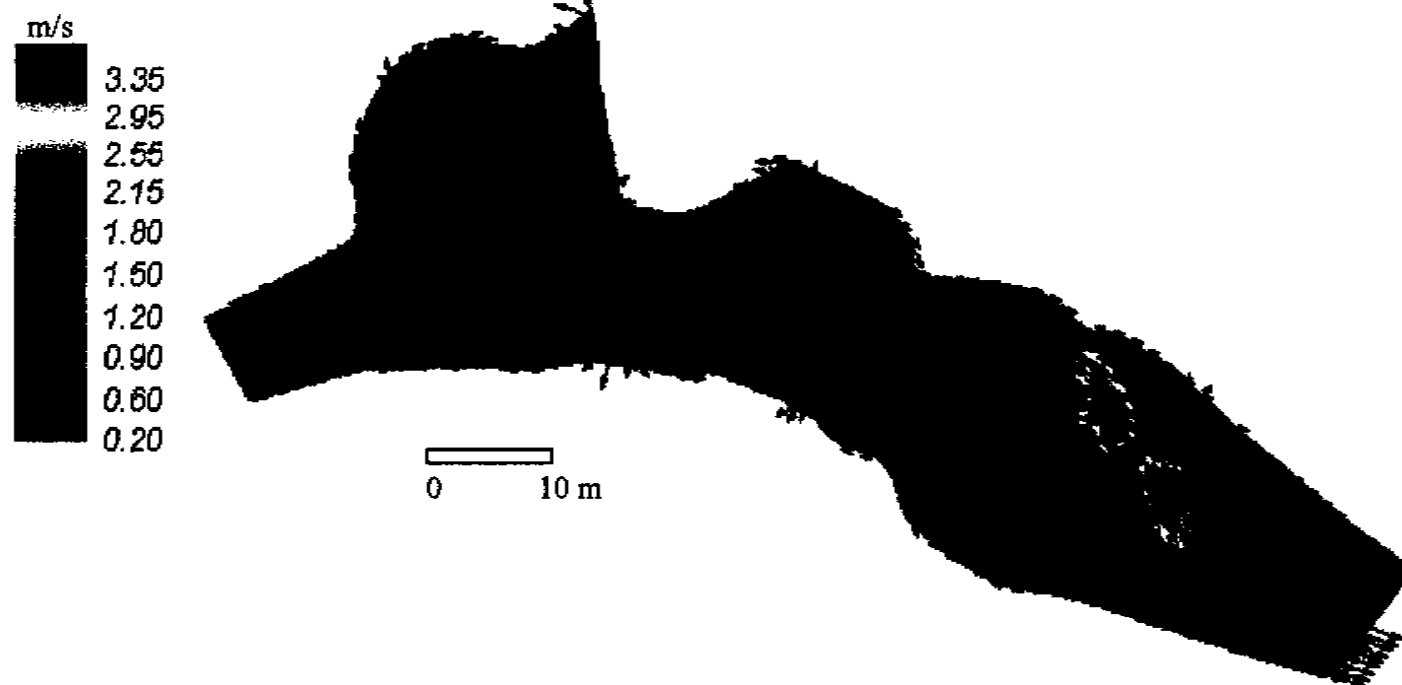


Figure 3.9. Velocity magnitude plot for high flow simulation in RMA2. Color contours are in m/s and arrows are a fixed length and are not scaled to the magnitude of the velocity

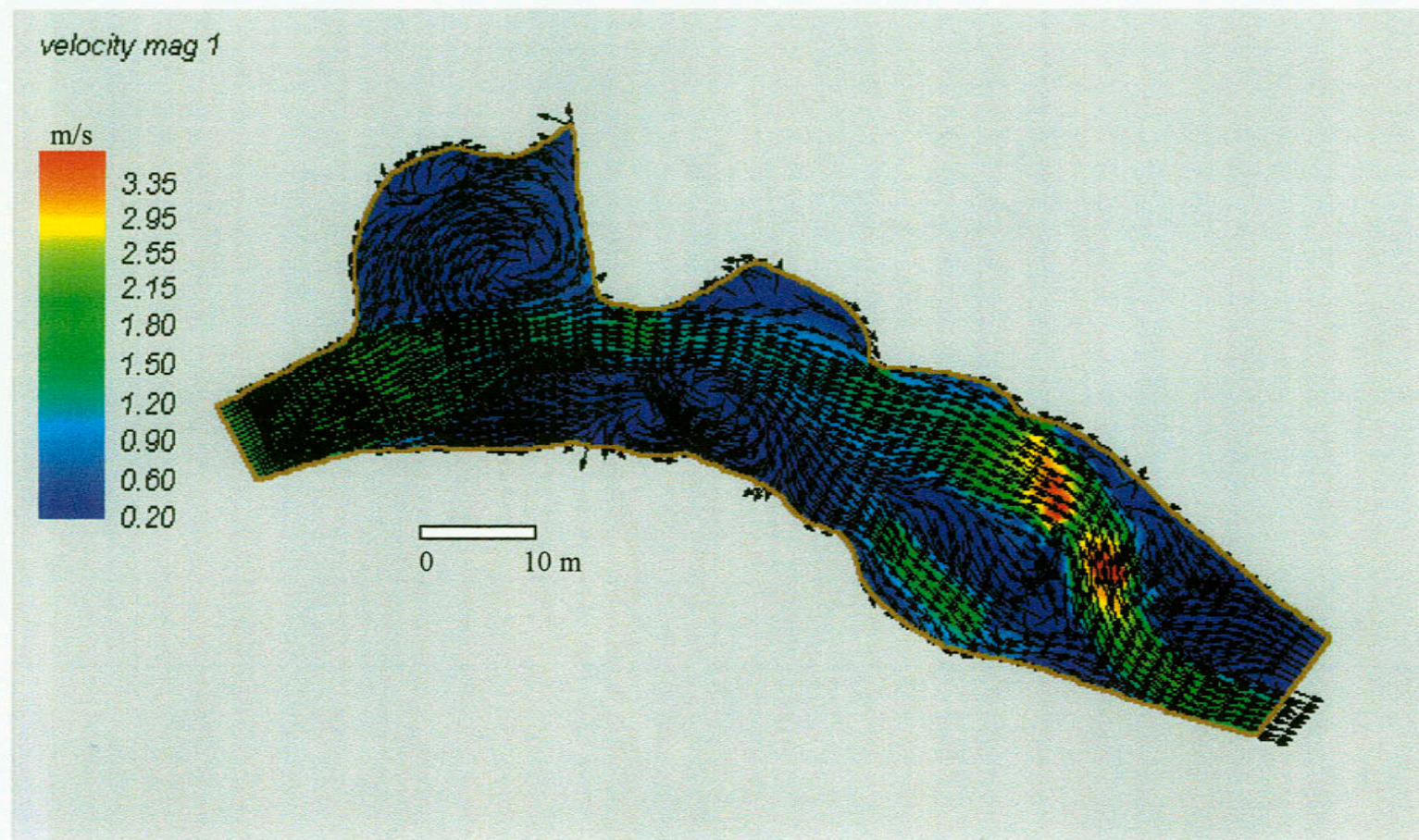


Figure 3.9. Velocity magnitude plot for high flow simulation in RMA2. Color contours are in m/s and arrows are a fixed length and are not scaled to the magnitude of the velocity

velocity mag'1

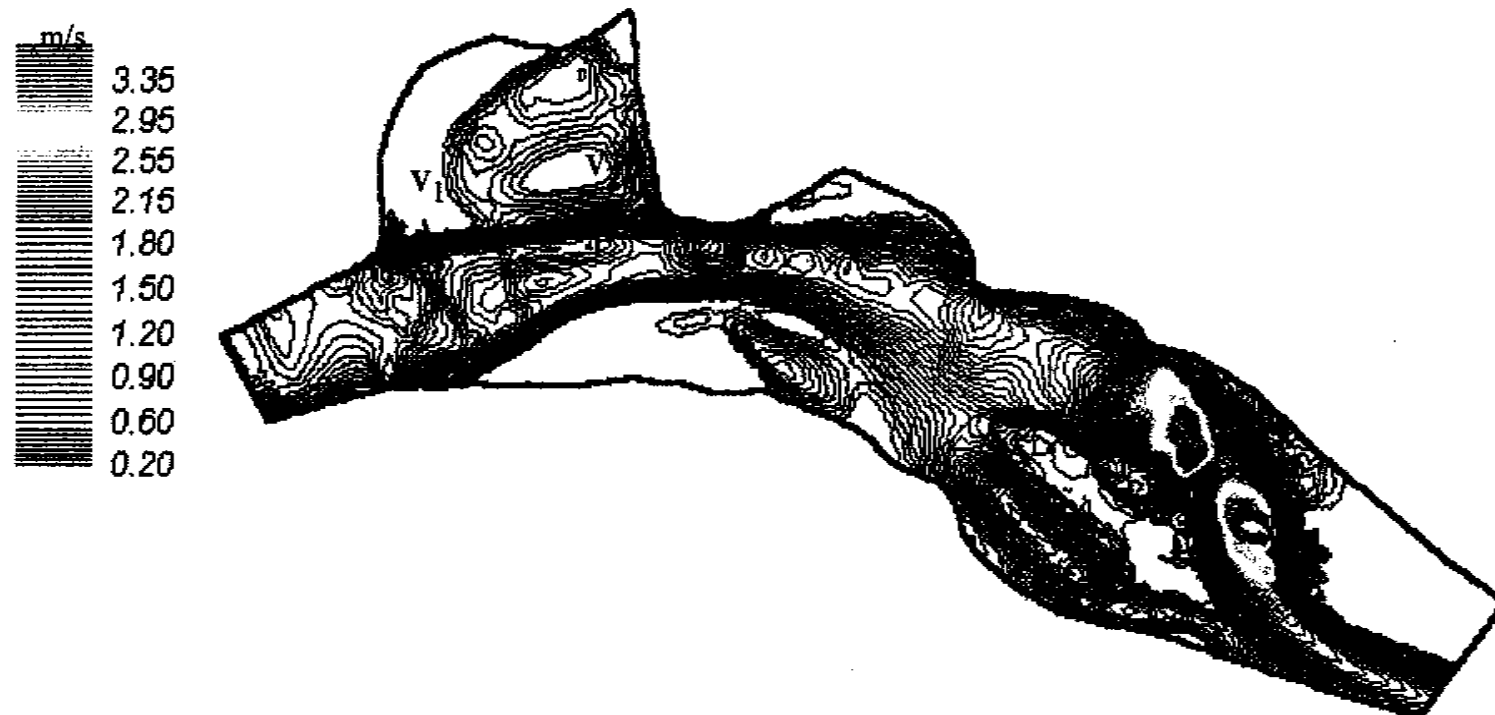


Figure 3.10. Contour plot of velocity magnitude for high flow simulation in RMA2. Velocity gradient was calculated between the upstream eddy and the main flow at lines labeled v_1 and v_2 .

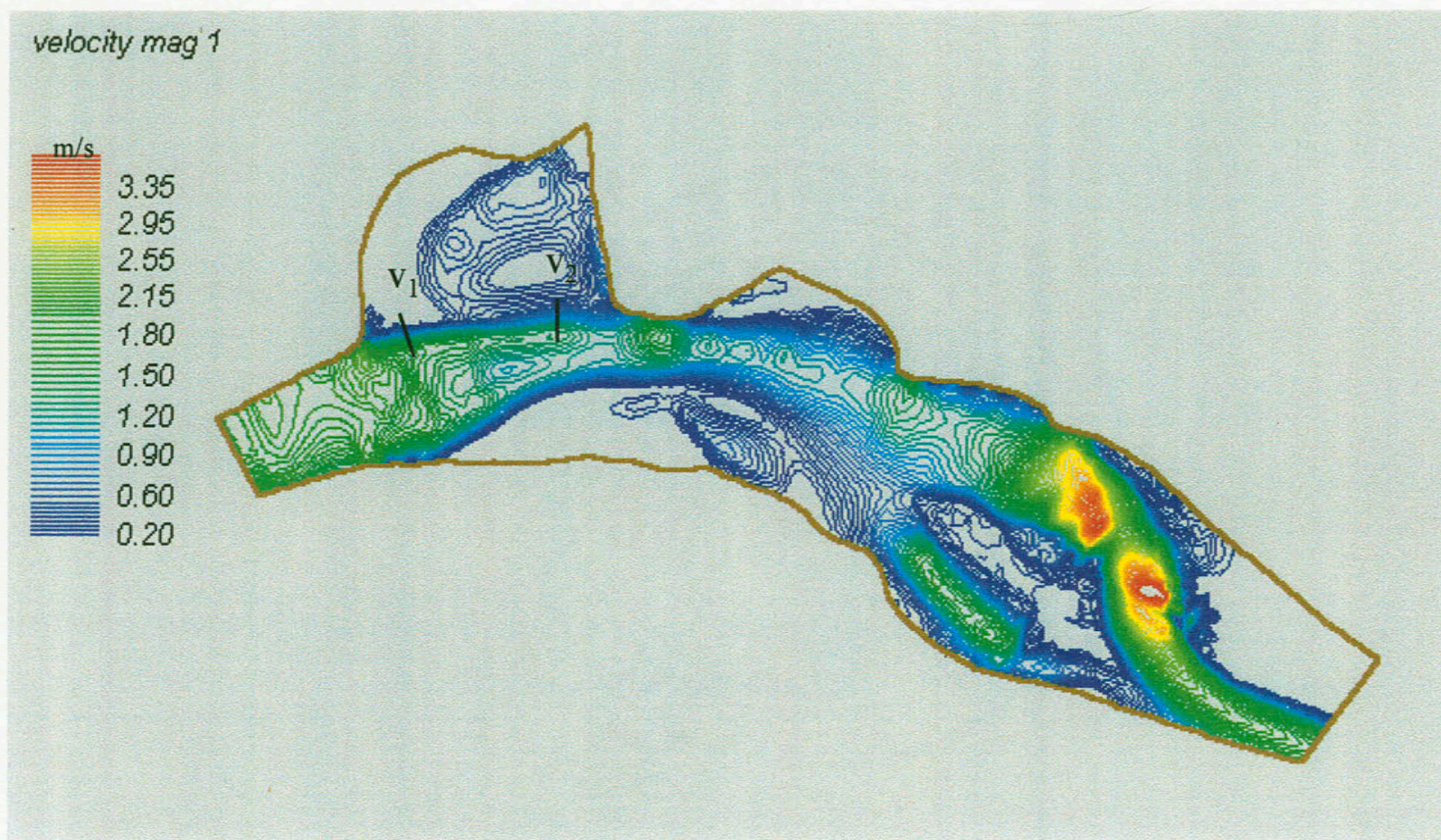


Figure 3.10. Contour plot of velocity magnitude for high flow simulation in RMA2. Velocity gradient was calculated between the upstream eddy and the main flow at lines labeled v_1 and v_2 .

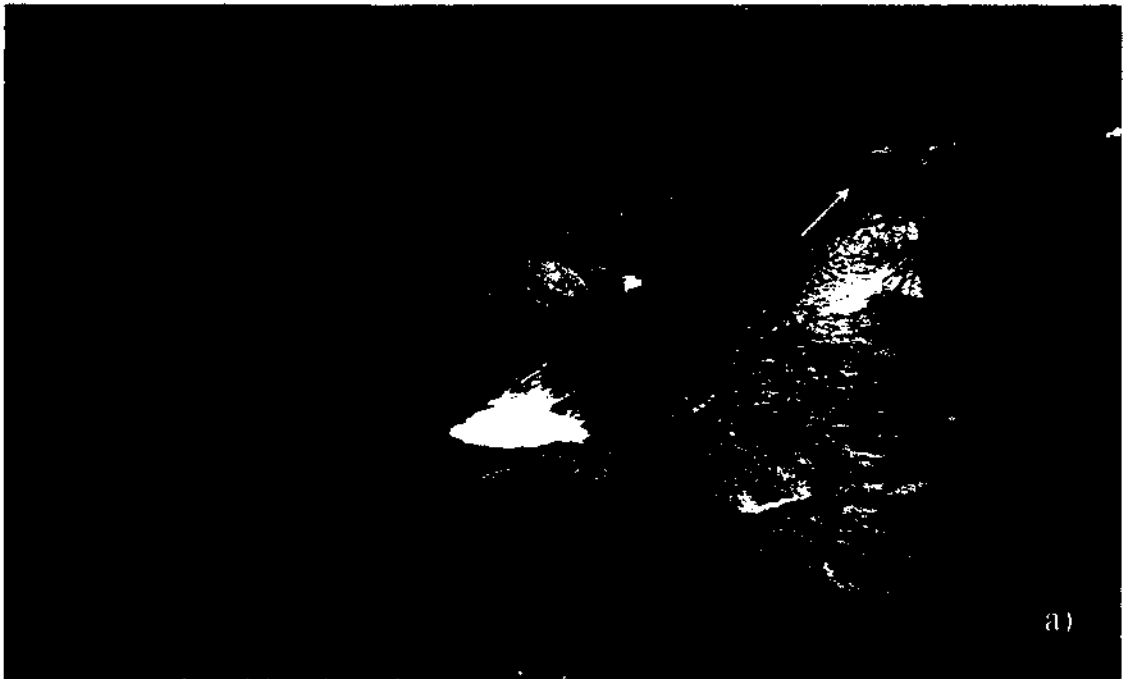


Figure 3.11. View of Tick Pool a) looking downstream, and b) looking upstream at a discharge of $8.41 \text{ m}^3/\text{s}$, comparable to the peak snowmelt runoff discharge during Summer 1997. Note the area of turbulent flow (arrow) adjacent to the left bank, upper right a), and submerged portion of the mid-channel bar, lower left b).



Figure 3.11. View of Tick Pool a) looking downstream, and b) looking upstream at a discharge of $8.41 \text{ m}^3/\text{s}$, comparable to the peak snowmelt runoff discharge during Summer 1997. Note the area of turbulent flow (arrow) adjacent to the left bank, upper right a), and submerged portion of the mid-channel bar, lower left b).

discharge for all recirculating zones within the Tick Pool, although the geometry of the pool is fixed by the immobile bedrock boundary. In rivers with more alluvial control along the banks, recirculating eddies are free to elongate with increasing discharge. Schmidt (1990) reports a three-fold increase in eddy length along the Colorado River in Grand Canyon with increasing discharge.

The velocity gradient across the shear zone of the upstream eddy, calculated over the same range of elements as shown in Figure 3.6, is 0.779 m/s-m at the expansion/flow separation point, versus 0.407 m/s-m for the downstream portion of the eddy fence at the contact with the bedrock outcrop. A steep velocity gradient at the point of expansion on the left side of the channel corresponds to rapidly increasing pressure in that area. The shallower velocity gradient near the bedrock outcrop allows transfer of mass into the eddy by a more gradual increase in pressure, and drives the strong recirculating flow within the eddy. As mentioned in Chapter 1, the adverse pressure gradient within the eddy sets up conditions for recirculating flow (Chang, 1970).

Maximum depth-averaged velocity for the entire model is 3.91 m/s, attained in the downstream riffle on the left side of the mid-channel bar (Figure 3.9), an area that is characterized by surface turbulence on the left side of the mid-channel bar in the photo (Figure 3.11a). Calculations of Froude number indicate small, isolated areas of supercritical flow in the downstream riffle at a discharge of 10.1 m³/s. A similar assumption is that the transcritical flow predicted by RMA2 is sufficiently far from the Tick Pool to allow for interpretation of the modeling results.

Centripetal acceleration within the upstream eddy at a discharge of 10.1 m³/s, calculated over a similar range of elements to those shown on Figure 3.6, is 0.049 m/s²

(maximum velocity of the eddy is 0.61 m/s over a radius of 7.5 m). This is 3.5 times larger than the acceleration in the upstream eddy at the low flow discharge. With a more than doubling of the discharge between the low and high flows, the upstream eddy expanded in size by over 0.5 m, with a concomitant doubling of the maximum velocity of the eddy. Assuming this measure of the acceleration of a water particle applies to sediment particles, the persistence of sediment within the eddy would likewise be greater at the higher discharge because of the stronger center-seeking acceleration which hinders the transfer of sediment back into the main flow. The size and strength of recirculating zones within the Tick Pool are discharge-dependent but to a lesser degree than other laterally confined rivers where bank material is comprised of alluvium and the length of the eddy can expand and contract accordingly (Schmidt, 1990). Other factors influencing the length of recirculating zones include the width-to-depth ratio of the constriction, and the unit discharge (Schmidt, 1990). The dimensions of the large upstream eddy within the Tick Pool are largely fixed, anchored by the bedrock outcrop at Cross Section 13.

For comparison, the centripetal acceleration for the downstream eddy in the lee of the bedrock constriction at a discharge of $10.1 \text{ m}^3/\text{s}$ is 0.046 m/s^2 , an acceleration that is nearly equal that for the upstream eddy (0.049 m/s^2). At the higher discharge, the combination of high flow velocity (0.265 m/s) and small eddy radius (1.51 m) in the downstream eddy results in similar eddy strength, or acceleration toward the center of the eddy. In spite of the greater depth-averaged velocity (0.61 m/s) in the upstream eddy, the large eddy radius in the upstream pool offsets somewhat the increased velocity. Whereas a small eddy radius enhances centripetal acceleration for a given discharge, the smaller radius can also serve to limit the volume of sediment deposition occurring in eddies in the

first place. Thus, a small eddy with high centripetal acceleration may not transfer sediment back to the main flow very efficiently, but the small volume of deposition causes less habitat loss than large, weakly accelerating eddies with ample sediment storage. If eddy strength can be used as an index of potential sediment persistence, then a trade-off exists between eddy size, maximum velocity, and proximity to the central thalweg. Large pools with ample storage, in off-channel locations where the thalweg does not comprise a large portion of the pool, are prime candidates for strong eddy circulation and long-term sediment storage.

3.5.4.1 Model Calibration and Validation

Velocity measurements were not collected for the high flow discharge of $10.1 \text{ m}^3/\text{s}$ because of the hazards associated with wading the river at higher flows. Calibration of the high flow simulations relied on pool depth measurements from the staff plate and automatic, repeat photographs of the pool depicting the location of the shear zone, size of the recirculating cell, and extent of water inundation. Results of the $10.1 \text{ m}^3/\text{s}$ RMA2 simulation are consistent with the timed photos that show a flat water surface in both the upstream and downstream eddy pools (Figure 3.11). This is corroborated by the two-dimensional modeling results, which predicted a consistent water-surface elevation of 101.12 m throughout the Tick Pool (Table 3.5). The location and extent of the eddy fence in the photos matches the location of the shear zone shown in the model results of Figure 3.9, where a layer of naturally occurring foam delineates the upstream eddy fence, and in the lee of the bedrock constriction (Figure 3.11).

A water depth of 2.22 m within the downstream eddy was determined from the linear regression equation of Figure 3.1 for a discharge of $10.1 \text{ m}^3/\text{s}$. The water depth of 2.38 m

was predicted by RMA2 for this area of the compound Tick Pool. At this discharge, the nose of the mid-channel bar was submerged (lower left, Figure 3.11b).

Table 3.5. Modeling results for the Tick Pool from RMA2 for the high flow discharge, 10.1 m³/s, with model settings similar to the low discharge simulation except for roughness coefficients.

| Pool Location | Maximum Depth-Averaged Velocity (m/s) | Predicted WSEL (m) | Predicted Maximum Pool Depth (m) | Observed Maximum Pool Depth (m) |
|---------------|---------------------------------------|--------------------|----------------------------------|---------------------------------|
| Constriction | 1.73 | 101.12 | 2.38 | 2.22 |

Water-surface elevation of the Tick Pool predicted from HEC-RAS for 10.1 m³/s is 101.02 m (Table 3.2). Depending on the comparison, whether water-surface elevation or pool depth, a difference of 10-16 cm exists between predicted and observed values (Table 3.5). The accuracy of reading the staff plate at high discharge, when standing waves were evident along the thalweg through the constriction, is estimated to be ± 5 cm. In the end, the range of error does not substantially impede the utility of the modeling results in predicting pool depth.

3.5.5 Hydraulic Properties and Sediment Deposition

A qualitative comparison of sedimentation patterns along the North Fork with model predictions of hydraulic parameters is a useful, first approach to linking modeled and observed results. Throughout the pools observed along the North Fork, deposition occurred beneath recirculating areas where velocity and associated shear stress are lower (compare Figures 3.5, 3.9, 3.12 and 3.13, with Figure 3.14). In the Tick Pool, for example, deposition was observed in the upstream and downstream eddy pools, as a marginal channel bar adjacent to the right bank (Figure 3.14), and beneath a recirculation zone opposite the channel constriction depicted in the modeling results. The most

4.0 Boundary Shear Stress

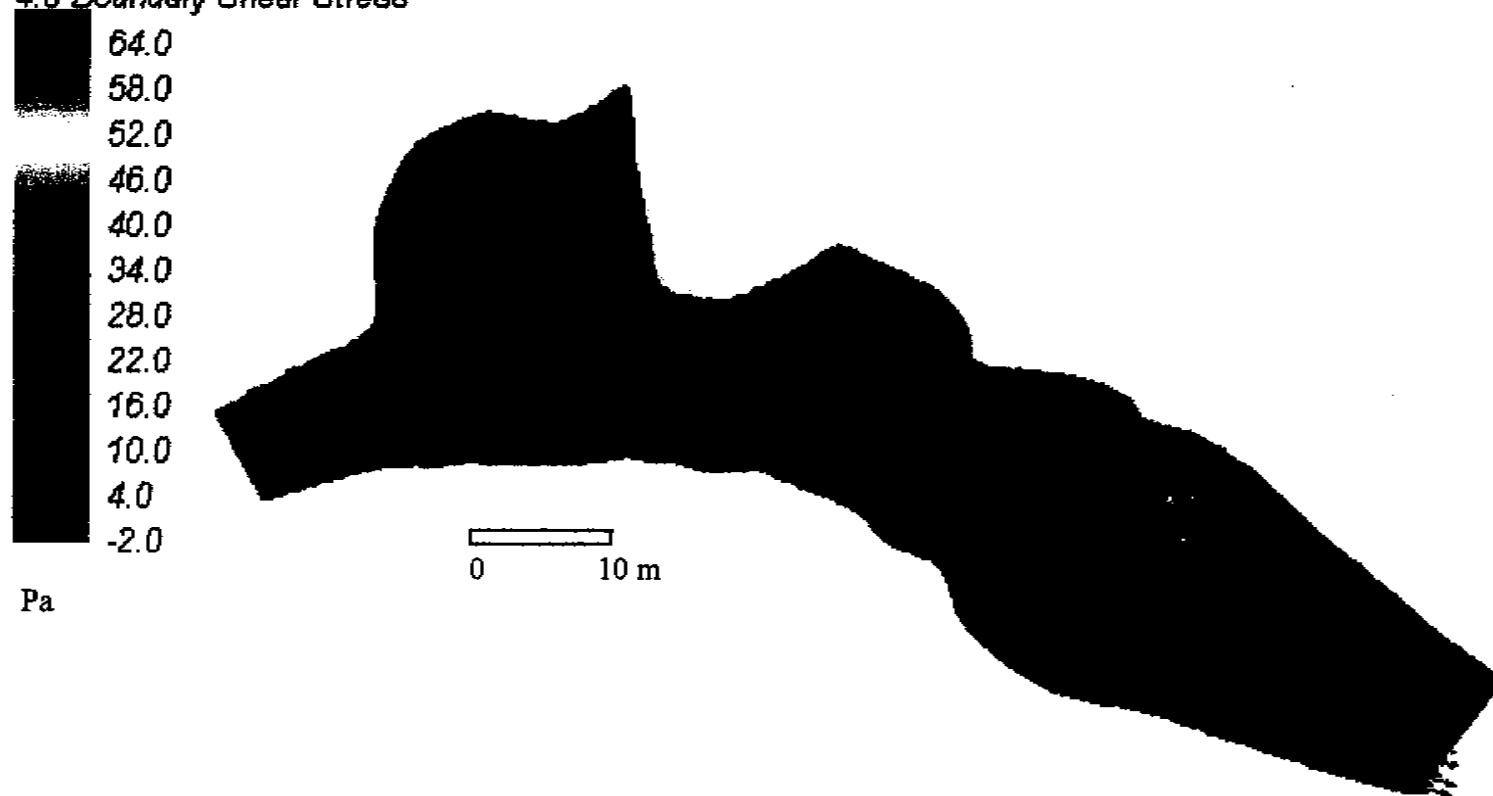


Figure 3.12. Boundary shear stress (Pa) for low flow simulation based on depth and depth-averaged velocity estimates from RMA2. Velocity vectors are superimposed on the color contour plot of boundary shear stress, and vectors are scaled to the magnitude of velocity. Vectors for areas of very low velocity are omitted.

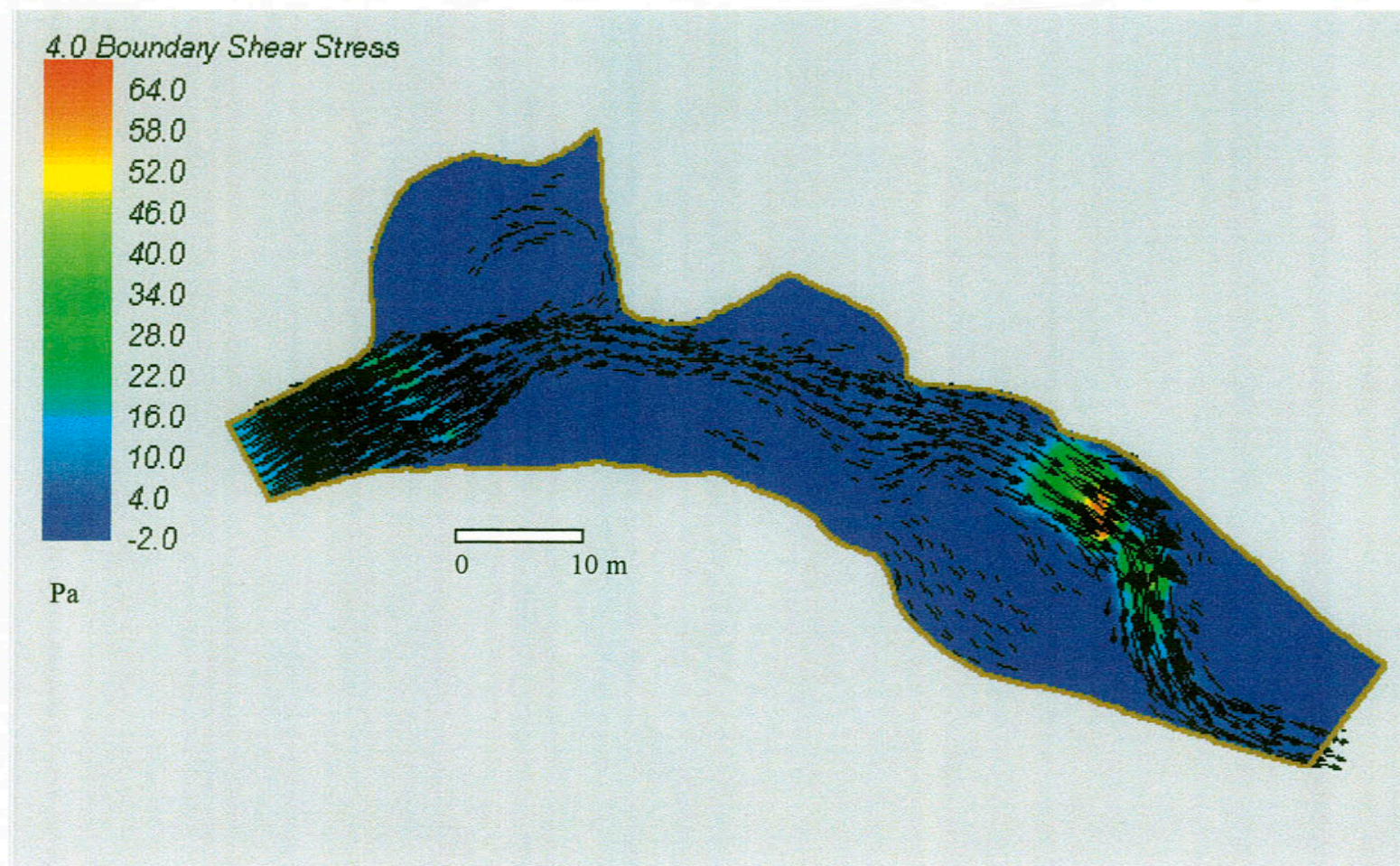


Figure 3.12. Boundary shear stress (Pa) for low flow simulation based on depth and depth-averaged velocity estimates from RMA2. Velocity vectors are superimposed on the color contour plot of boundary shear stress, and vectors are scaled to the magnitude of velocity. Vectors for areas of very low velocity are omitted.

10.1 Boundary Shear Stress

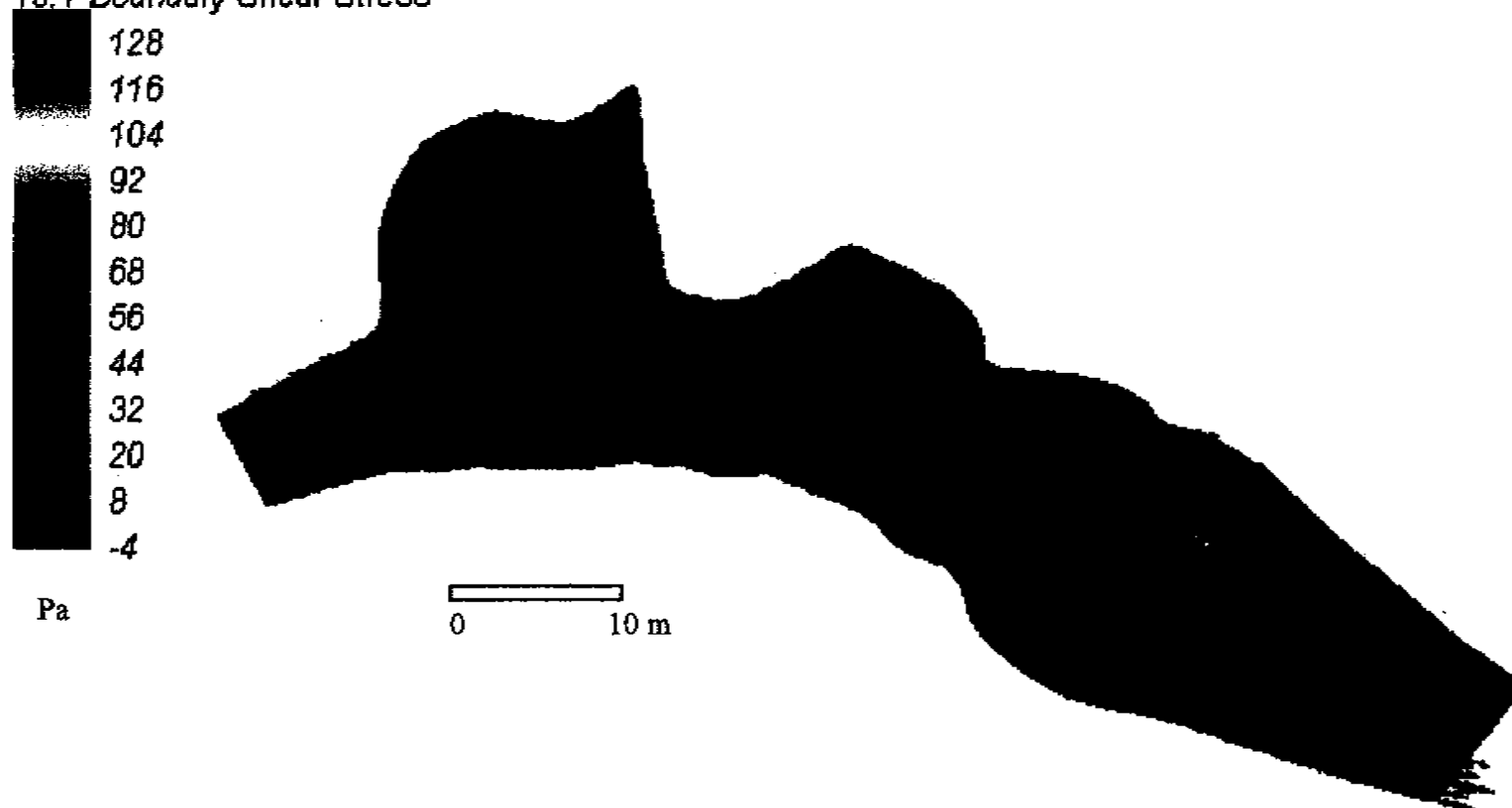


Figure 3.13. Boundary shear stress (Pa) for the high flow simulation based on depth and depth-averaged velocity estimates from RMA2. Velocity vectors are superimposed on the color contour plot of boundary shear stress, and vectors are scaled to the magnitude of velocity. Vectors for areas of very low velocity are omitted.

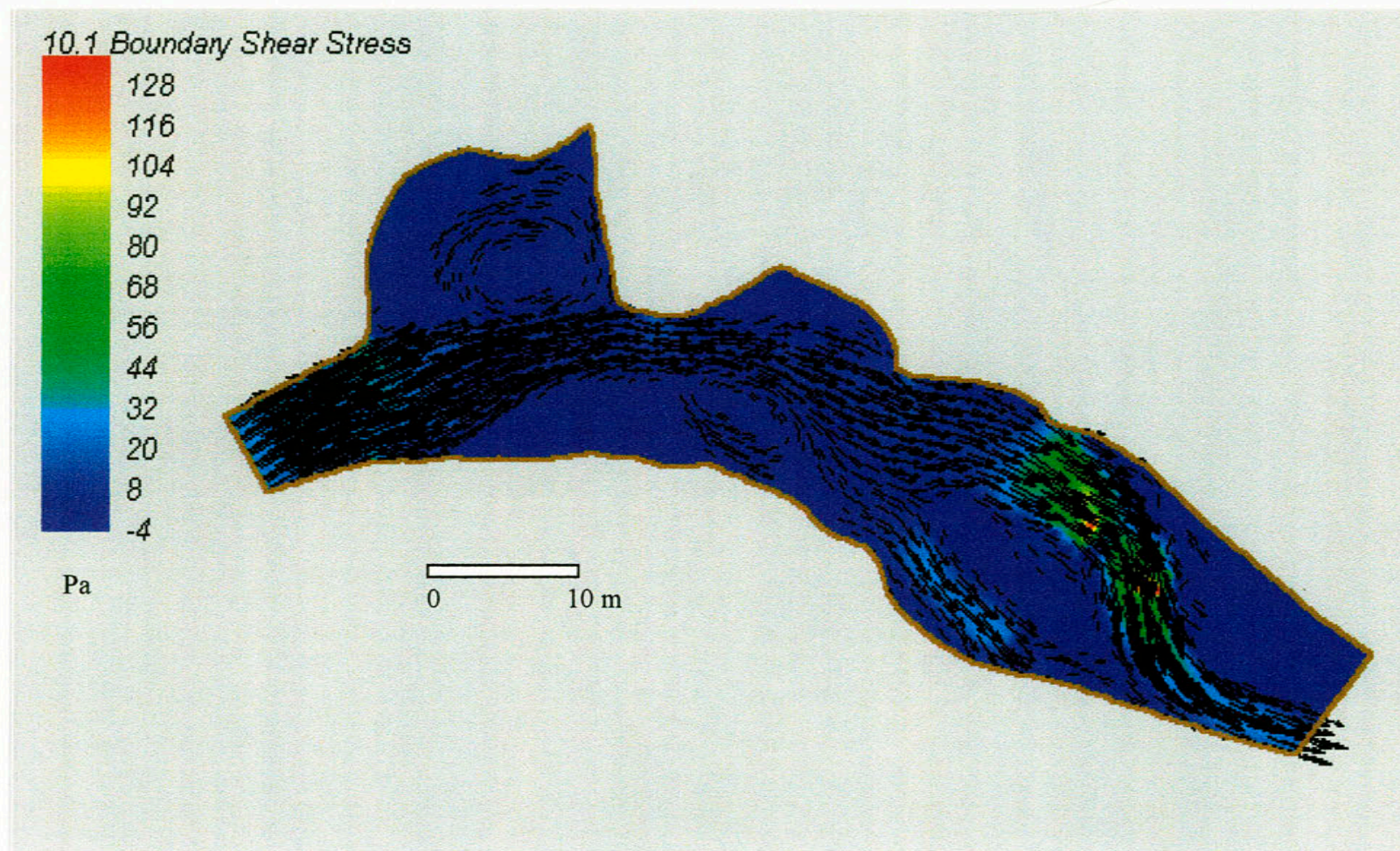


Figure 3.13. Boundary shear stress (Pa) for the high flow simulation based on depth and depth-averaged velocity estimates from RMA2. Velocity vectors are superimposed on the color contour plot of boundary shear stress, and vectors are scaled to the magnitude of velocity. Vectors for areas of very low velocity are omitted.

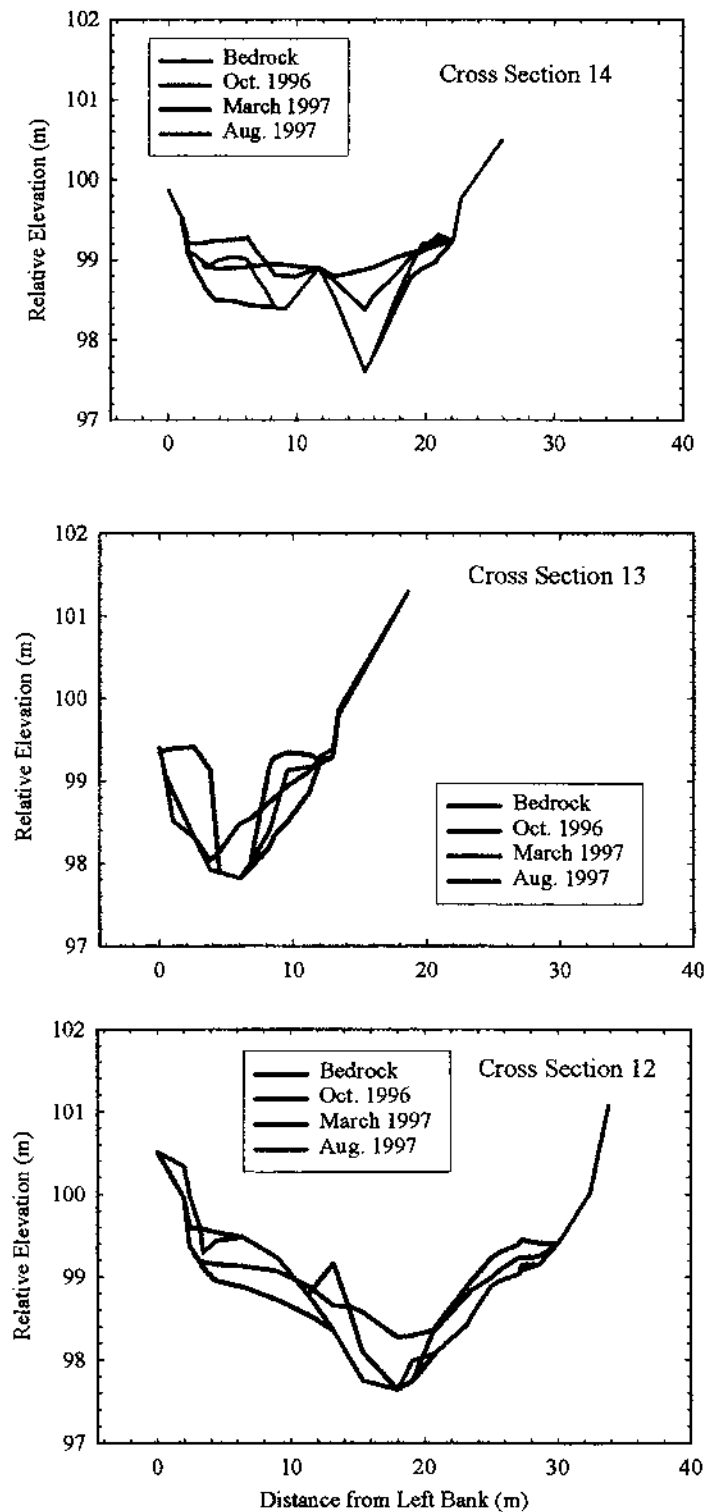


Figure 3.14. Cross sections through the Tick Pool, North Fork Poudre River following field surveys of bed changes due to scour and deposition of reservoir-released sediment. Cross Section 12 is upstream, Cross Section 14 is downstream.

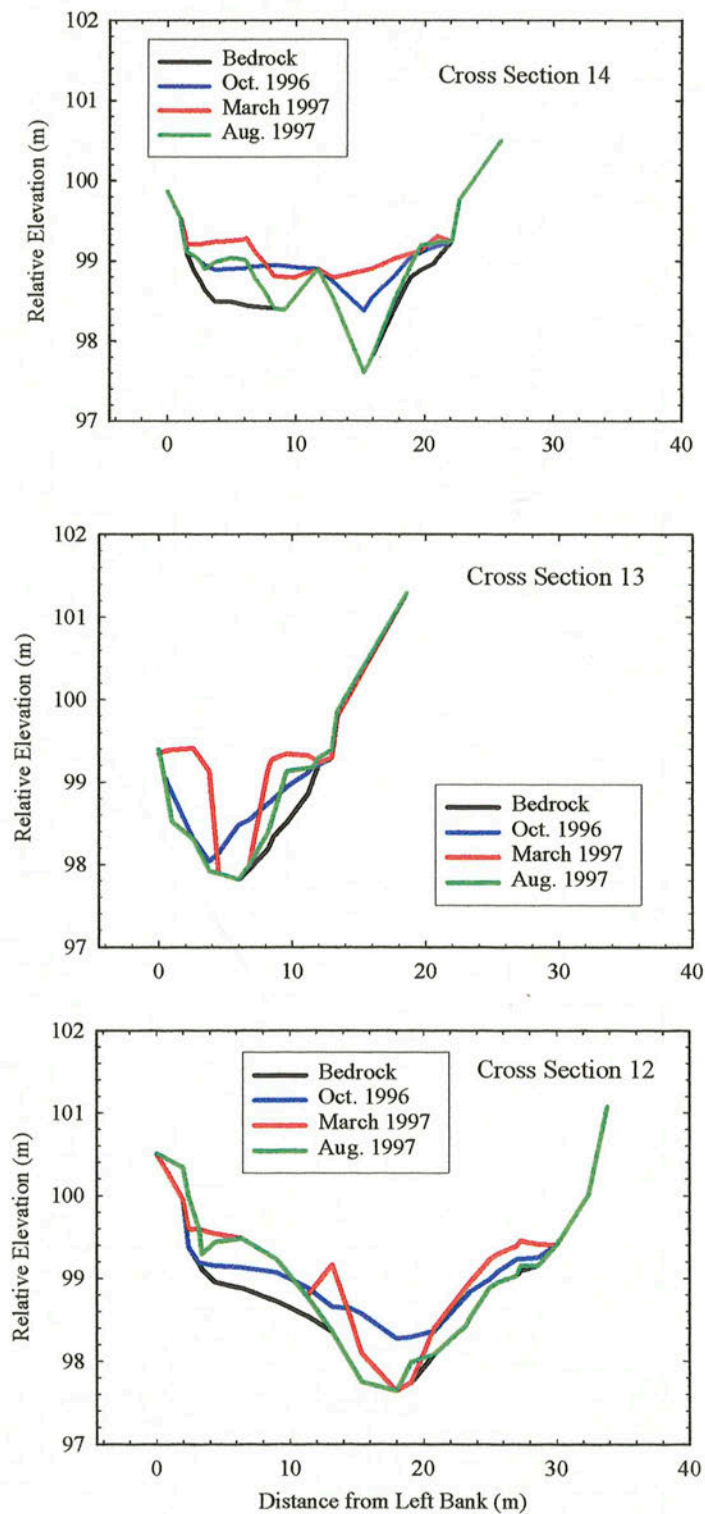


Figure 3.14. Cross sections through the Tick Pool, North Fork Poudre River following field surveys of bed changes due to scour and deposition of reservoir-released sediment. Cross Section 12 is upstream, Cross Section 14 is downstream.

persistent deposition in the eddy pools occurred as bars adjacent to the banks of the channel, at velocity and shear stress minima, enhancing sediment deposition. Also, mid-channel bars downstream from pools are common along the North Fork, as exemplified by the bar immediately downstream from the Tick Pool (Figure 3.7), which demarcates the head of the adjacent riffle. Miller (1994) found that the formation of bars, and in some cases gravel lobes, immediately downstream from scour holes is consistent with patterns of pool-riffle development. He found a rapid decrease in shear stress downstream from pools, which coincides with a decrease in local transport capacity, resulting in sediment deposition (Miller, 1994). Because of the regulated nature of flow from Halligan Dam, many of the bars are becoming densely vegetated, and are not overtopped and stripped of vegetation by high flows as would normally be the case. Qualitative observations of aerial photographs spanning the years 1938 to 1988 indicate that, on some of the bars, bar width is increasing with time, decreasing the effective width of the channel of the North Fork (TNC, 2001).

3.5.6 Bed Shear Stress and Incipient Motion

Although no direct sediment dynamics were modeled using RMA2, improved hydraulic information, particularly in the eddy pools, was provided from the modeling results to allow inferences about pool sediment transport and deposition. A corollary to *Hypothesis 3.1* is to evaluate whether inferences about sediment movement that can be derived from the two-dimensional modeling results are an improvement over estimates from the one- and semi two-dimensional sediment transport models.

Calculations of boundary shear stress for both the low and high discharge indicate high boundary shear along areas of the channel with high velocity, especially along the

thalweg of the Tick Pool, and at upstream and downstream riffles (Figures 3.12 and 3.13). Critical shear stress (τ_c) for the d_{50} of marginal pool sediment (0.092 mm) is 0.145 Pa. Maximum values of boundary shear stress for the upstream riffle and the pool thalweg are 27 Pa and 7 Pa, respectively. As long as there is a supply of erodible sediment along the central flow path, sediment up to very coarse gravel ($\tau_c=26$ Pa; after Julien, 1995) and medium gravel ($\tau_c=5.7$ Pa; after Julien, 1995) can be transported within riffles and the pool thalweg, respectively. Within the Tick Pool, boundary shear stress decreases by an order of magnitude from the pool thalweg to the recirculating eddy cell, limiting the transport potential in eddy areas to sediment in the sand size range.

An index of particle stability, obtained as the ratio of boundary shear stress to critical shear stress (τ_o/τ_c), provides a basis for identifying probable areas of particle mobility throughout the study reach. Particle stability plots for both the 4.05 m³/s and 10.1 m³/s discharge simulation are shown in Figures 3.15 and 3.16. Areas in red represent ratios of $\tau_o/\tau_c > 1$, where particles in the very fine sand range are expected to be in motion. At a discharge of 4.05 m³/s boundary shear stress in excess of critical shear dominates the central portion of the channel (Figure 3.15). Observations and field measurements (Figure 3.14) show that sediment was scoured from the central thalweg of Cross Sections 12 and 13, coincident with areas of predicted bed mobility on Figure 3.15. Sediment infilling occurred in the thalweg of Cross Section 14 (Figure 3.14) following the experimental release, however, which was predicted as an area of scour based on particle stability analysis. Other areas of predicted particle mobility (red zones, Figure 3.15) include a nearly circular pattern in the upstream eddy and a small isolated area in the

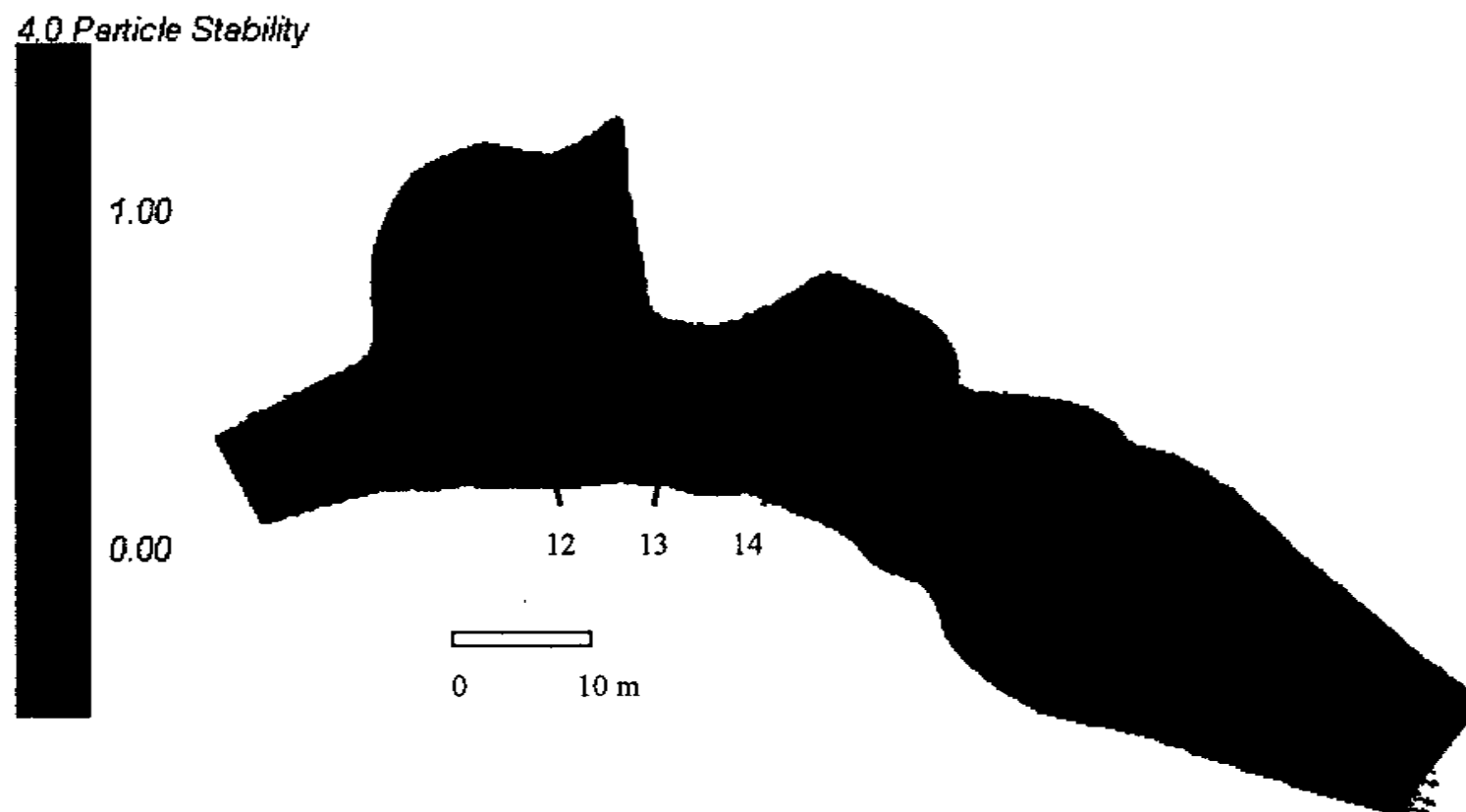


Figure 3.15. Dimensionless particle stability, τ_o/τ_c , for the low flow simulation. Values greater than 1 indicate particle mobility, values equal to 1 indicate incipient motion, and values less than one indicate particle stability. Lines across the channel denote Cross Sections 12, 13 and 14.

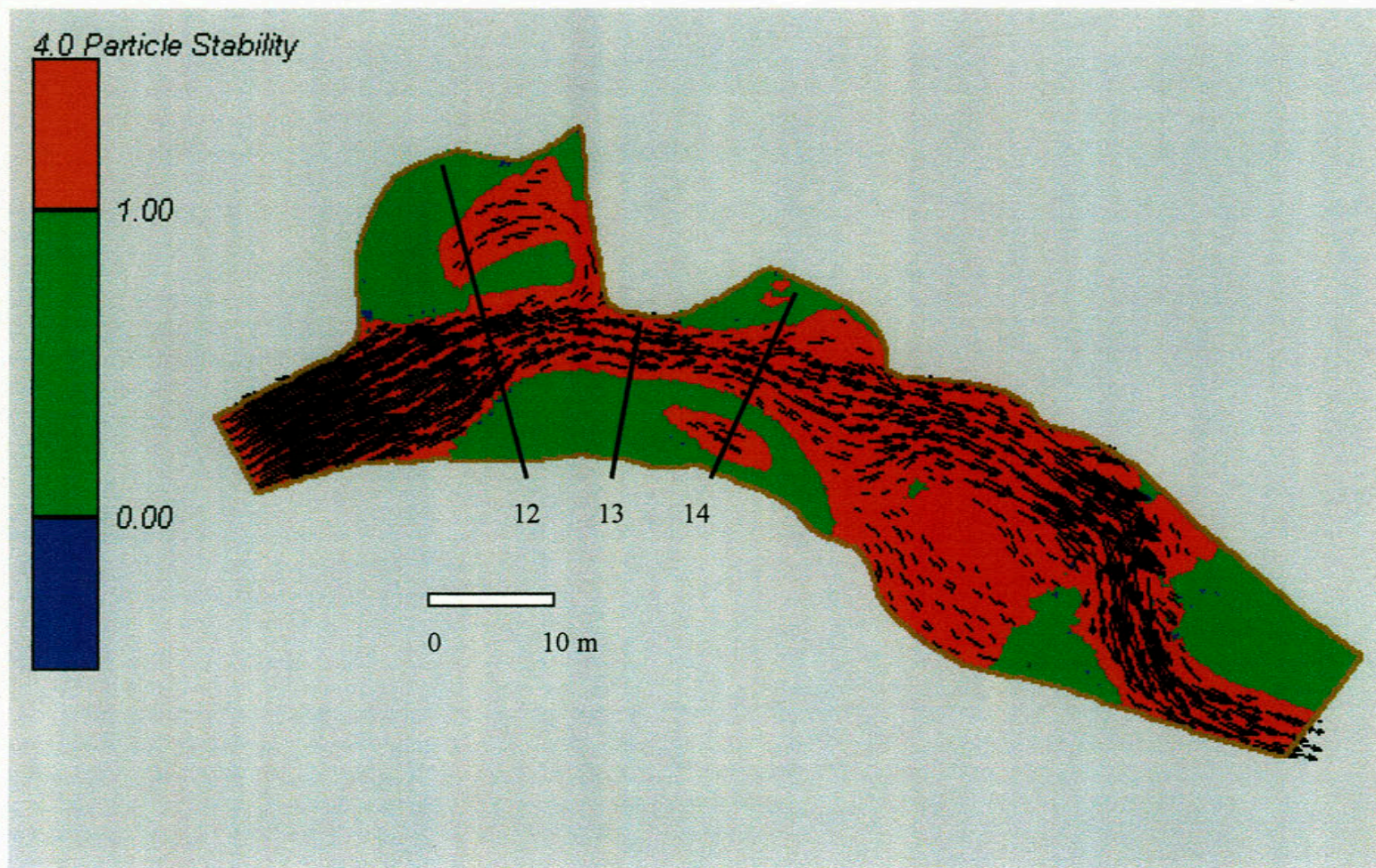


Figure 3.15. Dimensionless particle stability, τ_o/τ_c , for the low flow simulation. Values greater than 1 indicate particle mobility, values equal to 1 indicate incipient motion, and values less than one indicate particle stability. Lines across the channel denote Cross Sections 12, 13 and 14.

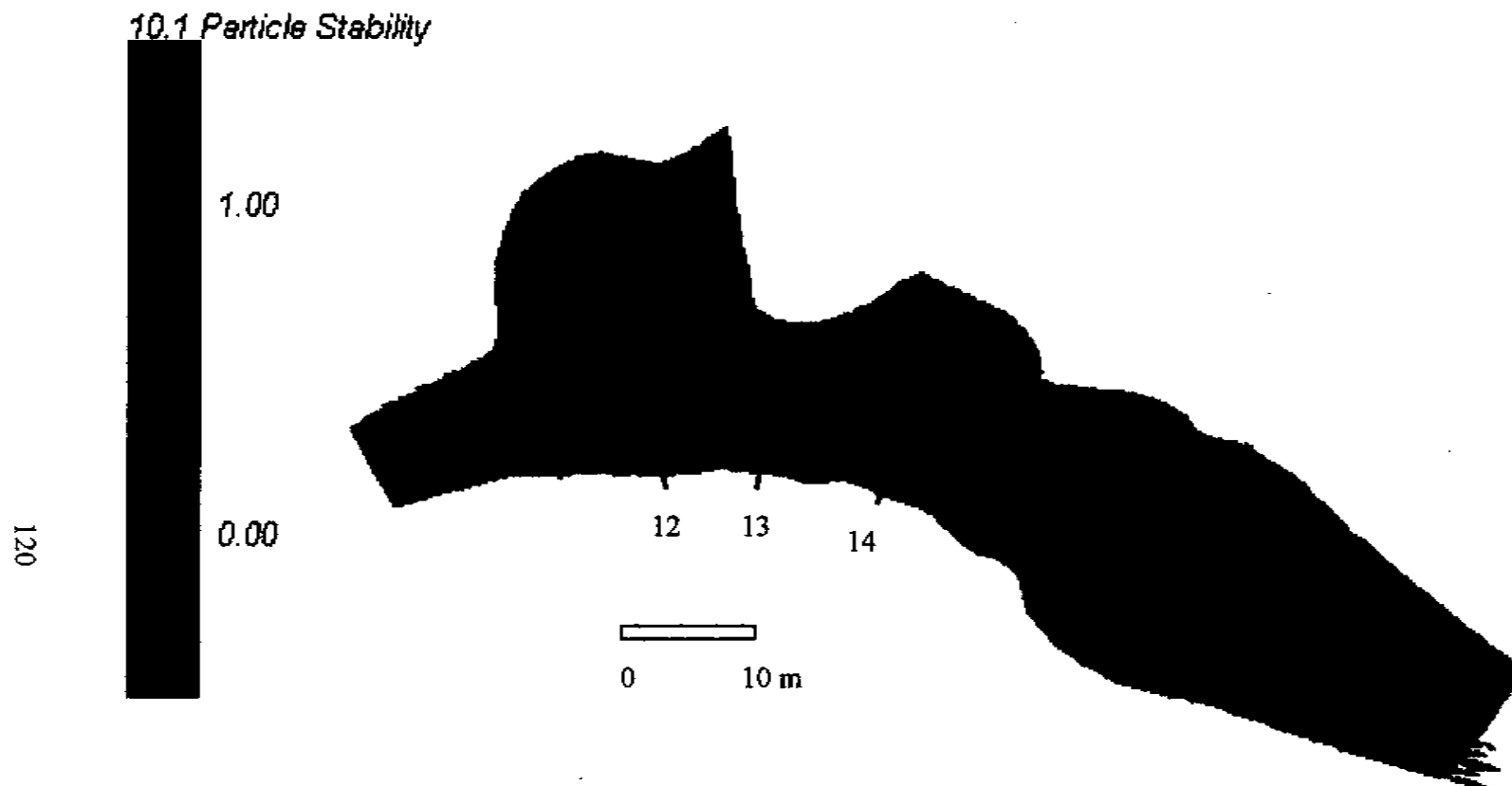


Figure 3.16. Dimensionless particle stability, τ_o/τ_c , for the high flow simulation. Values greater than 1 indicate particle mobility, values equal to 1 indicate incipient motion, and values less than 1 indicate particle stability. Lines across the channel denote Cross Sections 12, 13 and 14.

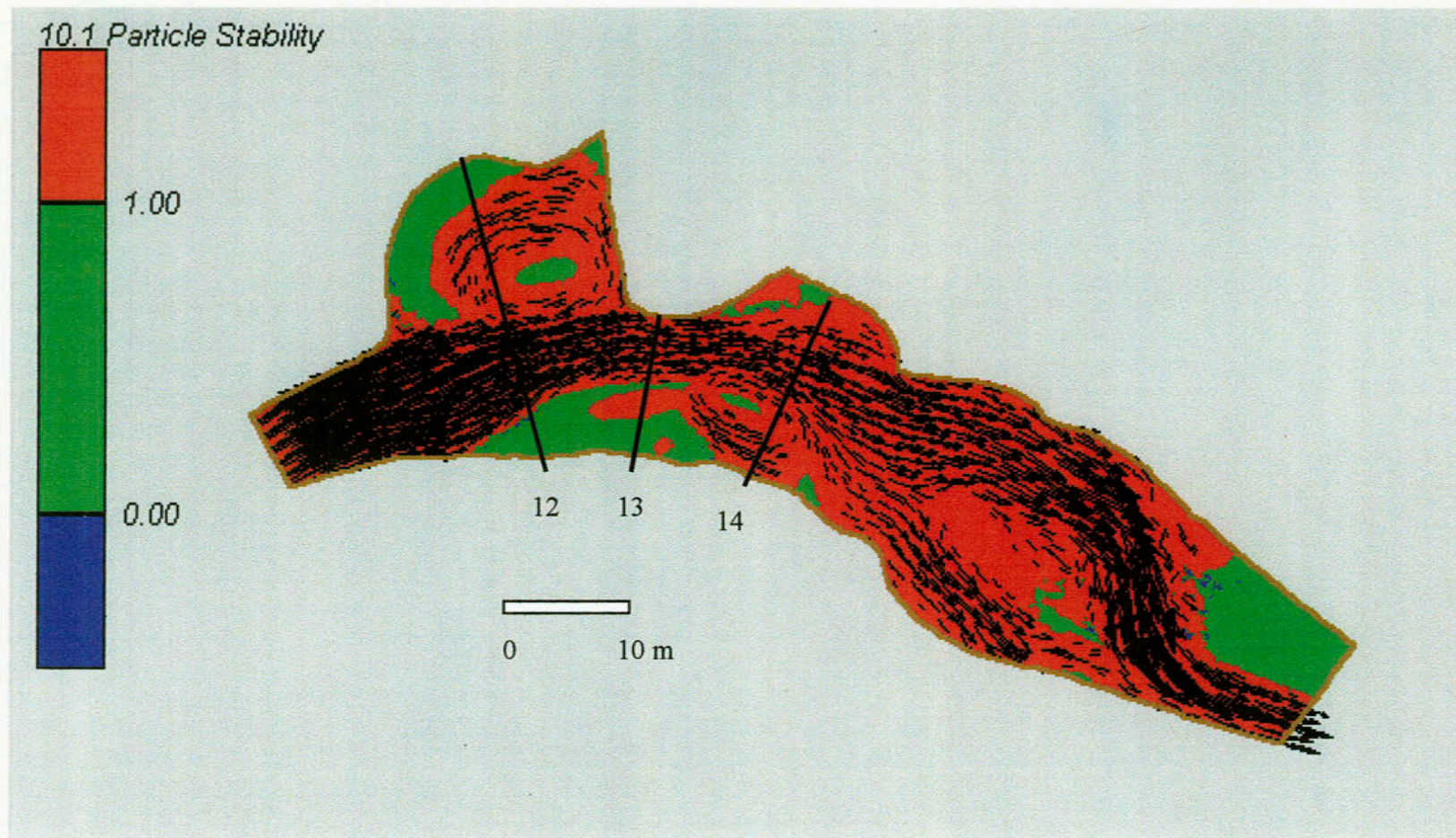


Figure 3.16. Dimensionless particle stability, τ_o/τ_c , for the high flow simulation. Values greater than 1 indicate particle mobility, values equal to 1 indicate incipient motion, and values less than 1 indicate particle stability. Lines across the channel denote Cross Sections 12, 13 and 14.

eddy on the right side of the channel immediately downstream of the constriction. Field measurements did not document substantial scouring of very fine sand at a discharge of $4.05 \text{ m}^3/\text{s}$ in the upstream eddy nor in the eddy adjacent to the right bank along Cross Section 14. Instead, aggradation was detected in the upstream eddy and within the marginal bar next to the right bank downstream from the constriction. Field measurements note overall aggradation of sediment on top of and higher than the original sediment release surface in both of these locations as a result of the experimental discharge in Spring 1997. The scouring of sand in the upstream eddy pool and along the right bank predicted through a particle stability index (Figure 3.15) is inconsistent with the buildup of a sizeable bar within the upstream eddy and as a marginal bar near the right bank over that time (Figure 3.14).

Regions of green (Figure 3.15) indicate areas of particle stability where boundary shear does not exceed critical values. At low discharges comparable to the outlet valve capacity of Halligan Dam, the particle stability index indicates that sediment is stable within low velocity, shoreward areas of the upstream and downstream eddy. The zone of predicted sediment stability on the right side of the channel at Cross Section 13 (Figure 3.15) is compatible with known deposition of the large, marginal bar adjacent to the right bank that was formed following the experimental discharge from Halligan Dam (Figure 3.14).

At the high discharge of $10.1 \text{ m}^3/\text{s}$, a similar pattern of predicted particle mobility is seen, with shear stress in excess of the critical value predicted for a majority of the model domain (Figure 3.16). Predicted particle mobility for the high flow discharge is substantially expanded within all eddies upstream and downstream from the bedrock

constriction relative to the low flow. The full circular pattern of sediment mobility within the upstream eddy (Figure 3.16) is compatible with the development of a larger eddy cell at high flows that was presented in Section 3.5.4. The minimal green areas within Figure 3.16 suggest that shear stresses were sufficient to scour bed sediments within the eddy pools and from marginal bars, and that sediment in the fine sand range is highly mobile at a discharge of $10.1 \text{ m}^3/\text{s}$. However, the scouring of sediment that did take place as a result of the snowmelt runoff occurred primarily within the thalweg of the upstream and downstream eddies of the Tick Pool, and through the constriction (Figure 3.14) where velocity is the highest. The lateral bars within the upstream portion of the pool were degraded more on the right side of the channel than on the left, despite predictions of bed stability against both the right and left bank in Figure 3.16. Hardly any additional scouring of sediment within the marginal bar along the left bank occurred in the upstream eddy following snowmelt discharge. Likewise, uniform scour along Cross Section 14 (Figure 3.16) is predicted. Uniform scour occurred between March 1997 and August 1997 up to a point, leaving residual bars adjacent to both banks that occupy areas important for fish habitat (Figure 3.14).

Although it is likely that very fine sand moving in suspension was transferred into the upstream eddy at these high flows, it was not possible to determine whether that transfer of sediment back across the shear zone into the main flow occurred. Sediment transport across eddy fences has been observed through boils rising from the bed and migrating across the shear zone (Schmidt, 1990), but similar macroturbulent upwellings were not observed along the North Fork study reach because of high turbidity.

Overall, modeling results and field observations confirm some of the observed patterns of sediment transport within this sediment supply-limited system, where nearly all of the fine-grained sediment supplied to the North Fork from the Halligan Reservoir release can be transported downstream. Sediment deposition within the low velocity eddies where sediment is more persistent may be more representative of a transport-limited condition, with the result that full recovery of eddy pool habitat along the North Fork may never be achieved. Complete scouring of sediment deposited in eddies within the study reach is hindered by several factors, including: 1) regulated flows from Halligan Dam that restrict discharge, velocity and hence turbulence in eddy pools, 2) fixed eddy geometry that cannot change beyond the confines of the bedrock walls, and 3) the cohesion of fine grained sediment from the release, which requires greater shear stress to entrain and transport.

In calculating various sediment transport parameters that rely on boundary shear stress, it is important to remember that the velocity of the bed may be much less than the depth-averaged velocity reported by RMA2, and hence particle mobility of bed sediments may be much less. Also, the actual grain size of sediment originally transported and deposited into the eddy was smaller than very fine sand. The sediment filling in pools in the vicinity of the modeling reach was primarily silt and clay. As a result, cohesive sediment properties of sediment entrainment and transport become a factor, but were not considered in-depth during this analysis. Channel bed sediment coarsened to a d_{50} of very fine sand following the experimental release from the dam. Hence, this research focused on sediment transport in the sand range.

3.5.7 Sediment Transport Calculations

Although the particle stability index delineates probable zones of sediment mobility and immobility, it does not adequately explain patterns of sedimentation and erosion observed and measured in the field. Most importantly, a particle stability index based on hydraulic modeling results of a particular peak discharge is too simplistic. It does not allow for spatial and temporal variability of sediment aggradation and degradation that accompany hydraulic conditions of a rising and falling hydrograph. Whereas the March 1997 experimental release completely scoured the thalweg of the Tick Pool to bedrock, lateral bars aggraded during the same discharge event, presumably during the falling limb when flow was less competent to transport the large supply of sediment delivered from upstream pools. As a final means of addressing the disparity between results of the calculated shear stress distribution and field evidence, rates of bedload were calculated from the modeling results. The relative transport capacities for areas of the Tick Pool may provide a more useful depiction of sedimentation patterns than the mobile versus stable modes of particle stability.

Using the Schoklitsch equation, unit bedload calculations by mass for the modeled reach predict a range of maximum bedload transport rates between 50-80 g/m-s at the constriction for a discharge of 4.05 m³/s (Figure 3.17; Table 3.6). (A range of bedload transport rates is provided in Table 3.6 (column 4) because transport capacity was calculated in SMS at all nodes within the finite element mesh, and to select one node of maximum bedload transport would misrepresent the results.) Unit discharge, a component of the Schoklitsch equation, is greatest at the constriction. It follows that bedload transport would also reach a maximum at this location. Minimum unit bedload

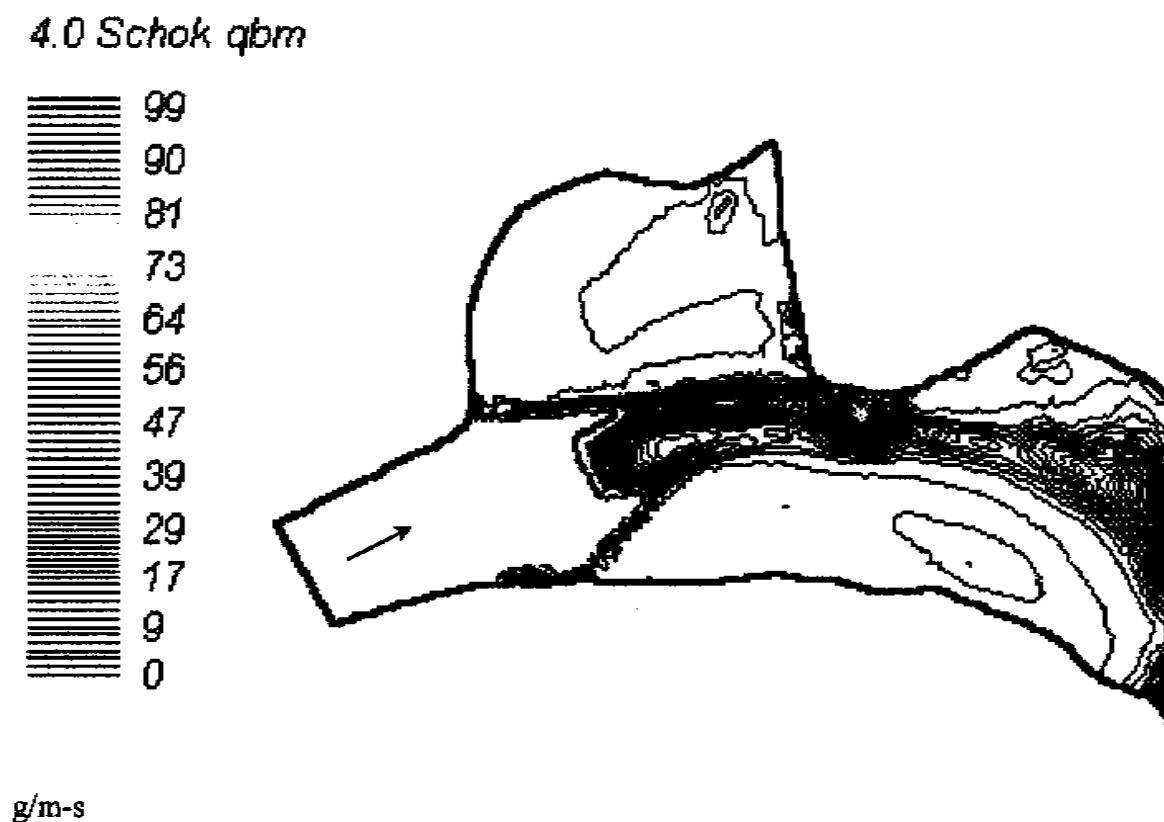


Figure 3.17. Bedload transport in g/m-s estimated from the Schoklitsch equation and results from the RMA2 modeling for a discharge of $4.01 \text{ m}^3/\text{s}$. The area shown is limited to the Tick Pool because estimated bedload transport is applicable only to regions with constant roughness coefficient. The roughness coefficient was used to derive friction slope, which was used in the calculations.

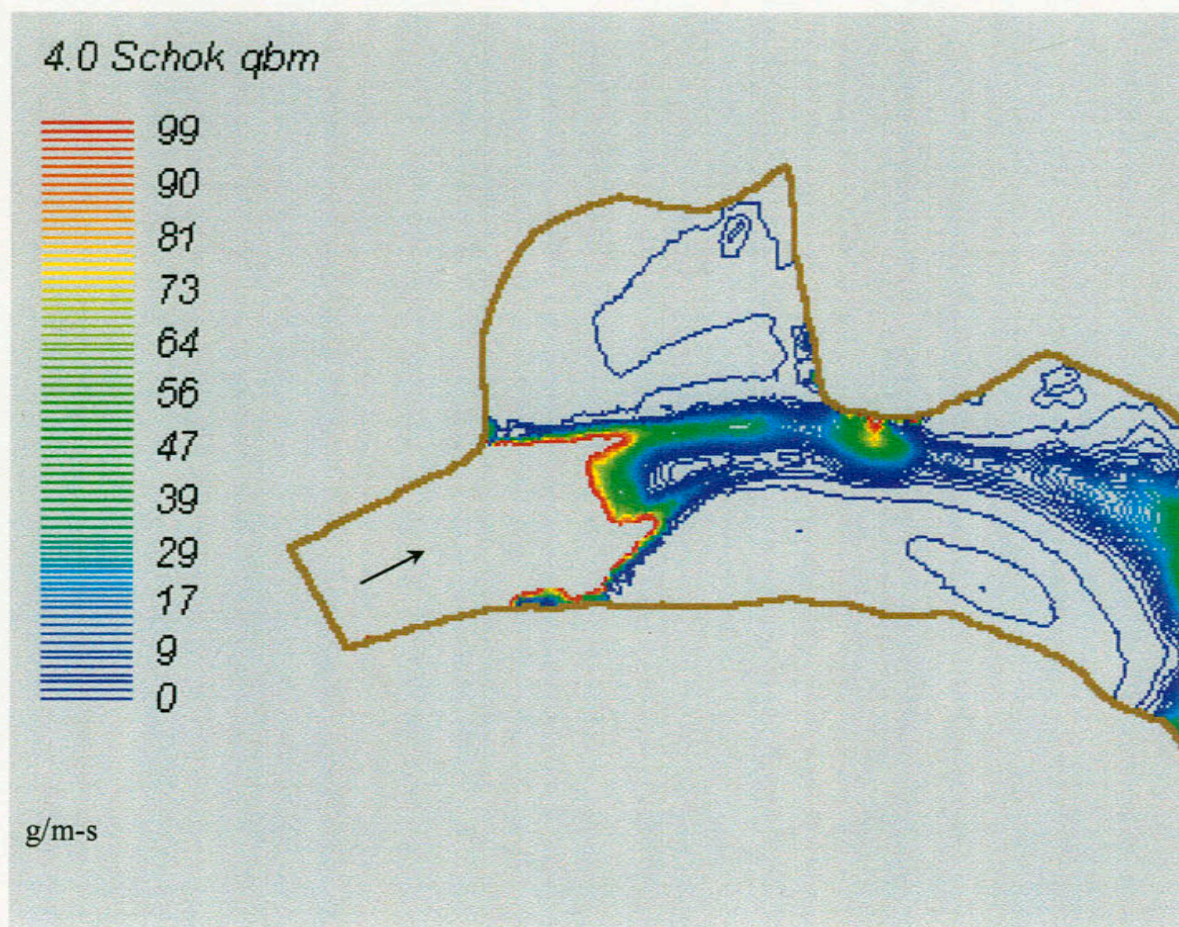


Figure 3.17. Bedload transport in g/m-s estimated from the Schoklitsch equation and results from the RMA2 modeling for a discharge of 4.01 m³/s. The area shown is limited to the Tick Pool because estimated bedload transport is applicable only to regions with constant roughness coefficient. The roughness coefficient was used to derive friction slope, which was used in the calculations.

transport occurred in the central portion of the upstream eddy, where negative transport capacities were predicted (Figure 3.17). Transport of sediment into the eddy is clearly a process that occurred along the North Fork, as exemplified along cross sections within the Tick Pool. One plausible interpretation of Figure 3.17 recognizes that transport rates in the eddy were sufficiently small relative to the central thalweg to allow transport out of the eddy, hence a sizeable bar developed in the upstream region of recirculating flow.

Calculations of bedload transport from the RMA2 results show small quantities of sediment in transit over the bar surface, which is not corroborated by the field evidence. The mid-channel bar is heavily vegetated and sediment transport on the bar surface is physically impossible at the simulated low flow. Because the marsh porosity option allows water to flow over the mid-channel bar even at the low discharge, to prevent wetting and drying of nodes, a shallow depth of water is predicted over the bar, with small quantities of bedload transport predicted (less than 5 g/m-s).

Even at the higher discharge, where maximum bedload transport at the constriction was between 300-400 g/m-s (Figure 3.18; Table 3.6), the relative difference between transport in the eddy and the main flow was insufficient to erode and transport sediment as bedload out of the eddy. In the composite cross sections of Figure 3.14, there was minimal erosion of sediment from the eddy bars as a result of the snowmelt discharge. Interestingly, calculations of bedload transport rate in SMS for a 4.05 m³/s and 10.1 m³/s discharge are on the same order of magnitude as the rates predicted by bedload transport formulas used to assist with transport formula selection presented in Chapter 1 (Table 3.6, column two versus four). The previous results in column two of Table 3.6 were developed for a cross section only, with rates of 75.96 g/m-s and 108.68 g/m-s predicted

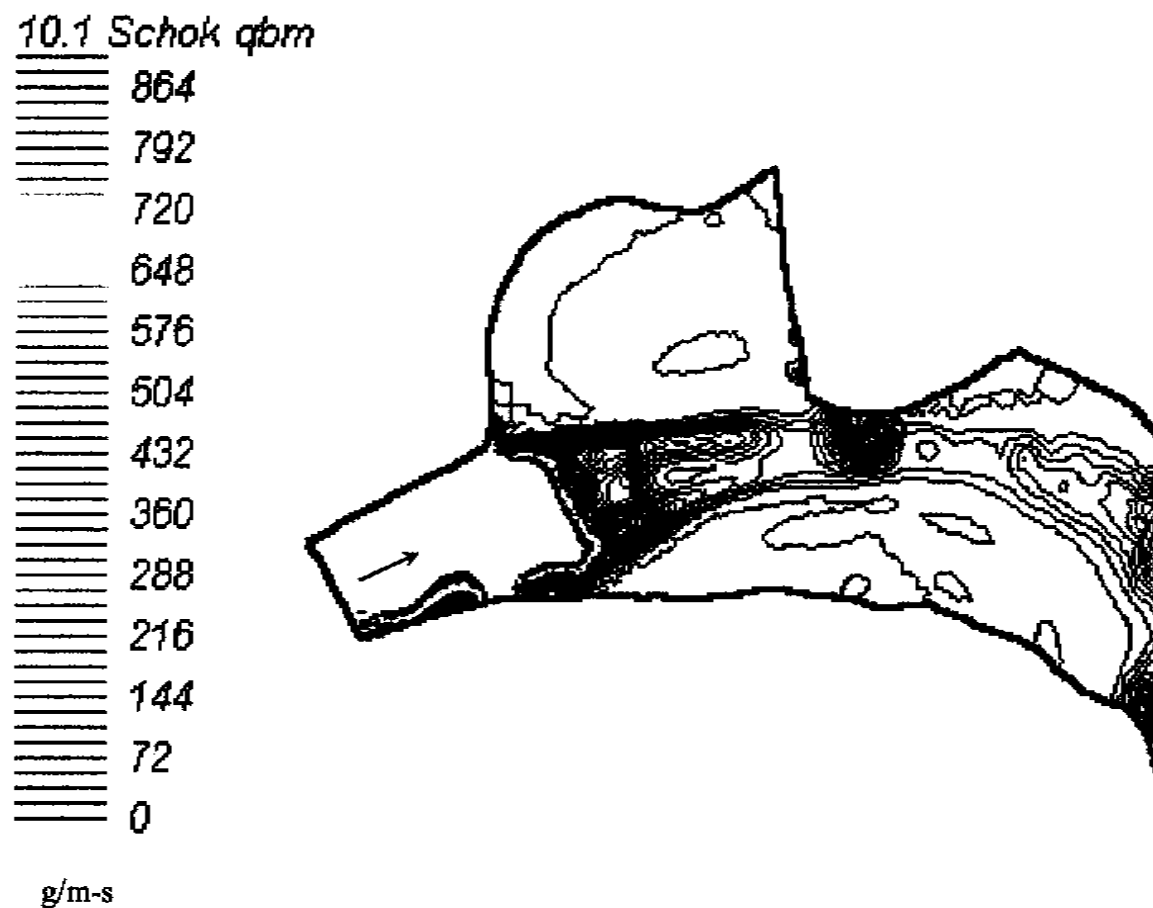


Figure 3.18. Bedload transport in $g/m-s$ estimated from the Schoklitsch equation and high flow results from RMA2 for a discharge of $10.1 \text{ m}^3/s$. The area shown is limited to the Tick Pool because estimated bedload transport is applicable only to regions with constant roughness coefficient. The roughness coefficient was used to derive friction slope, which was used in the calculations.

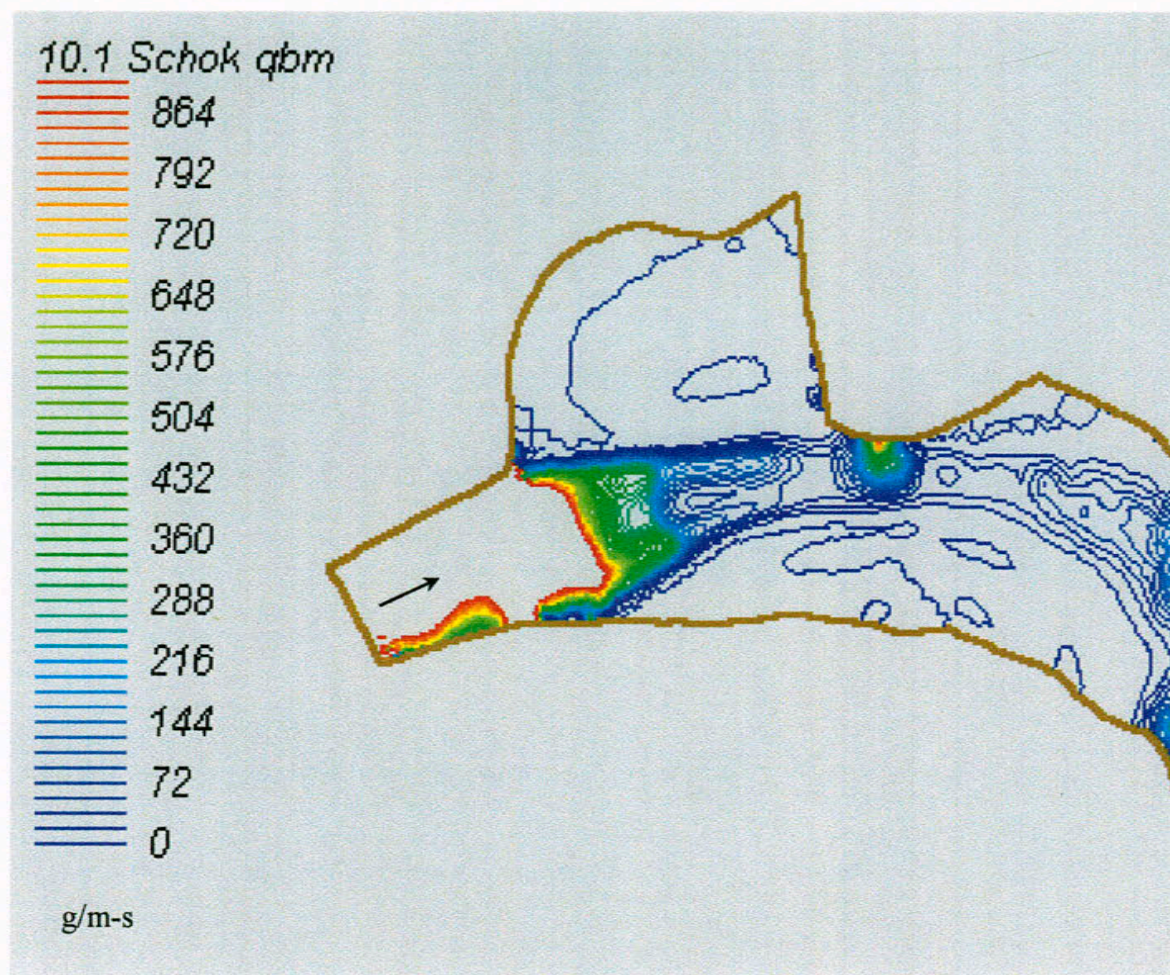


Figure 3.18. Bedload transport in g/m-s estimated from the Schoklitsch equation and high flow results from RMA2 for a discharge of $10.1 \text{ m}^3/\text{s}$. The area shown is limited to the Tick Pool because estimated bedload transport is applicable only to regions with constant roughness coefficient. The roughness coefficient was used to derive friction slope, which was used in the calculations.

from the Schoklitsch equation for the low flow and high flow, respectively (Table 3.6; Figure 2.4). The range of maximum bedload transport estimated by RMA2 for the Tick Pool (Table 3.6, column 4) is probably more accurate than the transport estimates at Cross Section 13 (Table 3.6, column 3) because of the improved estimate of friction slope in RMA2. Friction slope is calculated for each node using the RMA2 results, as is bedload transport rate. In contrast, a cross-sectional averaged friction slope derived from HEC-RAS was used in calculations of column 3. In any event, the estimated bedload transport rates calculated for a cross section and via RMA2 results are still one order of magnitude greater than the 5.14 g/m-s and 56.46 g/m-s measured in the field at the Cross Section 17 riffle in the months following the Halligan Dam sediment release. Based on these calculations, sediment transport capacity within the Tick Pool was supply limited, even following the reservoir sediment release. Estimates of bedload transport rates using the Schoklitsch equation indicate that bedload transport could have been an order of magnitude greater for the flows measured provided the supply of sediment was available

Table 3.6. Comparison of measured and predicted bedload transport rates. Estimates of bedload transport using the Schoklitsch equation for columns (3) and (4) were calculated for a single cross section and derived from the RMA2 results, respectively.

| Discharge (1) | Measured bedload at Cross Section 17 (2) | Estimated bedload transport at Cross Section 13 (3) | RMA2 estimate of maximum pool bedload transport (4) |
|------------------------|--|--|--|
| 4.05 m ³ /s | 5.14 g/m-s* | 75.96 g/m-s* | 50-80 g/m-s |
| 10.1 m ³ /s | 56.46 g/m-s | 108.68 g/m-s | 300-400 g/m-s |

Note: Values of measured and calculated bedload transport rates with an asterisk (*) were linearly interpolated from known rates for discharges of 3.34 m³/s and 4.76 m³/s.

Applications of bedload transport equations to areas where there are no direct measurements of bedload must rely on reasonable assumptions. First, because it was

physically impossible to measure bedload in any of the pools along the North Fork, the assumption was made that sediment moving through the riffle at Cross Section 17 (Figure 1.1) would be representative of quantities moving through the Tick Pool. Second, and probably more important in explaining the disparity between measured and predicted bedload transport rates, is the assumption of unlimited sediment supply. Calculations using the Schoklitsch equation (columns 2 and 3 Table 3.6) assume a constant supply of sediment with a certain d_{50} , in this case 0.092 mm. In reality, upstream pools acting as the sediment sources to downstream areas became depleted and eventually flushed of sediment, resulting in transport along the North Fork that was even more supply limited. Because transport of bedload following the sediment release was heavily influenced by upstream supply, it may be more instructive to view the RMA2 estimated bedload transport rates as representative of the full transport potential of the North Fork, should the supply be available.

Similar calculations of total load were attempted using Yang's (1973) equation in SMS, but limitations with the data calculator in SMS preclude accurate calculation. Although much of the sediment within the North Fork was transported in suspension during initial releases from the dam, bedload transport was sustained much longer over the snowmelt hydrograph, and the Schoklitsch equation is assumed to be an appropriate predictor of transport capacity along the North Fork. No other additional transport formulas were investigated because of the tendency for various transport capacity equations to overpredict transport rates relative to known values (see Chapter 2).

Bedload transport patterns depicted on Figures 3.17 and 3.18 may also be overly simplistic, offering an incomplete view of the dynamics of sediment movement within

pools such as the Tick Pool. There appear to be four additional factors that influence sediment transport and deposition along the North Fork: 1) sediment may be entering the eddy but is unable to cross back through the eddy fence, and hence gets trapped in the eddy; 2) velocity on the bed is probably less than depth-averaged velocity used in the calculations, so overall transport potential is less than indicated in the figures; 3) sediment in the eddy is probably finer than 0.092 mm so cohesive forces become important for sediment mobilization; and 4) one aspect of the transport potential of the eddy not accounted for in the two-dimensional model is the vertical upwellings, which are important to the recirculation in zones of flow separation. Because the RMA2 model, like the one-dimensional and semi two-dimensional models, was evaluated for its predictive ability, and compared to actual field measurements of sediment aggradation and degradation under changing discharge, the model limitations are informative for potential users without introducing error into projections of sediment clearing within pools of the North Fork.

3.6 Discussion

Bedrock channels provide particular challenges to numerical modeling efforts, and test the capabilities of many of the available models such as RMA2. Most often the field data needed for verification of multi-dimensional models are not available. Even with the capabilities of present-day high speed data collection equipment, it is difficult and often impossible to obtain field data for the critical conditions of highest flow within bedrock rivers. One advantage of using computer simulation modeling techniques, however, is to fill gaps between temporally and spatially widespread field data in order to develop a more comprehensive understanding of high flow hydraulics. The collection of detailed

information on the spatial pattern of water-surface profiles, velocities, sediment transport rates, roughness parameters, and time-varying boundary conditions may not be feasible, and often is equipment, time, and labor intensive. Under these circumstances the use of a numerical model may provide insights that might not otherwise be available.

The chief uncertainty of the two-dimensional modeling along the North Fork involves the depth-averaged velocity predictions in the swifter portions of the channel where calibration data were not collected at the high discharge of $10.5 \text{ m}^3/\text{s}$. Thus, the results reported here for the Tick Pool are most useful for understanding hydraulic conditions at low flow, and for predicting very general spatial patterns of scour and deposition at low discharge. Whether or not the results are sufficient for other applications is in large part a question of the objectives of the modeling project. For example, if the model results are to be used for calculating local sediment transport rates and simulating bed scour and deposition over time, it is important to note that most bedload transport equations are proportional to velocity raised to an exponent between three and four (Graf, 1971). Thus the predicted local bedload transport rates, based on model results for the upstream eddy pool, might be much more accurate than that predicted for the central thalweg where velocity is much higher and has not been thoroughly calibrated, at either the low or high discharge. This could lead to an overprediction of transport rates in the thalweg. However, because the low-velocity recirculating eddies within the Tick Pool provide important fish habitat, the estimates of bedload transport using the results from RMA2 are probably reasonable. The model RMA2, in conjunction with parameters and settings derived for the Tick Pool, could be applied to other pools along the North Fork with the

expectation of achieving comparable accuracy of reproducing low velocity hydraulic conditions.

Although the general hydraulic patterns of flow are considered reasonable for the Tick Pool, more uncertainty is introduced when interpreting the sediment transport characteristics predicted by RMA2. The main reason for this is that the complexities of higher order models such as RMA2 outstrips the available data and the ability to collect data. For example, the spatial and temporal sedimentation patterns along the North Fork are based on cross sectional surveys that were repeated three times. Inferences of sedimentation from the two-dimensional modeling results are based on depth-averaged velocity and depth for every node in the finite element mesh. The detail of the mesh vastly exceeds the spatial control on sediment aggradation and degradation collected along cross sections, which limits the extent of the interpretations that can be made. Even though the application of two-dimensional models provides improved insight into rivers, the primary difficulty is in collecting validation data that are sufficiently detailed to approach that of the modeling results. Given the increased sophistication of field tools such as the Acoustic Doppler Velocimeter (ADV) for acquiring two- and even three-dimensional velocity readings, and the use of GPS (Global Positioning Satellites) and sonar for surveying and collecting bathymetry data in rivers, it may not be long before the data match the resolution needs of the model.

One of the most important lessons learned from the two-dimensional modeling effort is the tendency to misuse and exaggerate the results. As Miller and Chuer (1998, p. 100) warn:

“It is inevitable that, as flow models of increasing complexity become more popular and easier to use, it will also become easier to confuse simulation with reality. In some cases the models will actually be good enough to provide accurate answers, but the increasing sophistication of visualization tools will ensure that even inaccurate results can be made to look convincing.”

3.7 Summary

The major features of the velocity field in the Tick Pool for a low and high discharge were reproduced by the two-dimensional model RMA2. Areas of high velocity occupy the central thalweg, with lower velocities predicted for the recirculation zones upstream and downstream from the bedrock constriction. Automatic photographs and field observations over a range of discharges were useful for evaluating the predictive ability of the model. Modeling results of depth-averaged velocity agree with validation data of velocity for low velocity areas only. Difficulty in acquiring accurate velocity readings in the swifter portions of the flow limits the certainty of the results to areas with velocity of 0.15 m/s and less. The maximum gaged pool depth for the upstream eddy differed from the maximum depth predicted by RMA2 for the low and high discharge by 6 and 16 cm, respectively. Water-surface elevations of the pool predicted by RMA2 for both simulation discharges vary from those calculated by HEC-RAS by no more than 10 cm. Extrapolation of the hydraulic properties of the pools, based on RMA2 output, is reasonable for other compound pools along the North Fork. Apparently, flow scenarios simulated in RMA2 are representing the hydraulic processes involved in flow separation and recirculation of eddy pools fairly well. However, the utility of the model, as applied to making predictions of sediment removal from pools, is low relative to the one-dimensional results. Model validation utilized varied roughness coefficients, which indicated that RMA2 was largely insensitive to adjustments in roughness coefficient.

The main limitation of the model for the purposes of this study is the inability to directly predict pool bed changes as a result of scouring reservoir sediment from pools. Inferences of sediment mobility through a particle stability index indicate that areas of scour coincide with areas of high velocity and high boundary shear stress, and that deposition occurs in low velocity, low boundary shear stress areas. The particle stability index is overly simplified, predicting either particle motion or stability, and does not allow for the simultaneous transport, aggradation, and degradation that accompany flow. Bedload transport capacities, as predicted by the Schoklitsch equation, are on the same order of magnitude as the rates predicted by bedload transport formulas used in earlier formula selection, but are probably more accurate because nodal friction slope values from the modeling results are used in the transport calculations.

The modeling results from RMA2 are of limited validity, for most applications, without adequate field data for calibration. Abundant field-based measurements of velocity over a range of flows would ensure the most robust modeling results for purposes of investigating hydraulic conditions in a channel of interest. The use of RMA2 to assess issues regarding sediment releases is hampered by the uncertainties of inferring sediment transport processes using results from a hydraulic flow model. If delineation of general patterns of sediment aggradation and degradation suffice for a particular project then RMA 2 is suitable. However, the use of a two-dimensional sediment transport model, such as SED2D, is recommended to more thoroughly address sediment transport into and out of eddy pools. This investigation modeled one pool to determine sediment-release pool aggradation and degradation. Future users may include reaches spanning two pools and one riffle, such that the transfer of sediment from one pool to the next

would be represented in the process. The trade-off between the utility of the modeling results, and mesh simplicity, computational time, and effort to collect adequate validation data must be considered.

CHAPTER 4 CONCEPTUAL MODEL OF POOL SEDIMENTATION PATTERNS

4.1 Introduction

Numerical modeling of pool sediment dynamics can replicate various patterns of erosion and deposition observed along the study reach of the North Fork Poudre River. The one-, semi-two, and two-dimensional modeling also provide long-term simulations and a means of evaluating the sediment flushing effectiveness of low and high discharges, and estimates of bedload transport rates based on more accurate hydraulic conditions at those discharges. The main limitation of the numerical models evaluated for this research, however, is that mathematical representations of the physical system are limited with respect to providing insight into the simultaneous sediment deposition, storage, and transport that are relevant to habitat management for fish and other aquatic organisms. Also, the level of expertise required to master the models, and the time and cost required to calibrate and validate the results, become a limiting factor in acquiring useful results for water-resource specialists charged with managing lands that have undergone or are subject to periodic sedimentation hazards. As such, numerical models may have restricted management and predictive capabilities in certain situations. The current state of numerical models applied to fluvial science is that, for the foreseeable future, input data requirements will remain high and labor intensive. In addition, training

in hydraulics and sediment transport is necessary to interpret the reasonableness of the model output in the context of the study objectives.

Conceptual models offer a powerful alternative to the more rigorous, time- and labor-intensive modeling efforts required of one- and two-dimensional numerical models. A conceptual model offers general guidelines to assist in understanding and predicting physical processes operating within a system that affect such responses as channel sedimentation patterns. A conceptual model of channel sedimentation relies on a qualitative understanding of the processes that govern sediment erosion and deposition within pools along mountain rivers. Rather than numerically routing water and/or sediment through a reach of interest via a computer model, water managers could use field-based characteristics of a channel, along with information about the sediment contained in the release, to understand and predict recovery processes and rates for a particular river. A conceptual model can also provide insight into the interaction of processes operating at various length and time scales, and the importance of scale in assessing sedimentation patterns following a sediment release. In the end, all applications of flow models are strengthened by a process-level, conceptual understanding by the modeler for the geomorphic environment of interest.

Relatively few studies are available for which conceptual models of sediment movement in mountain rivers have been developed. Conceptual models are more common for lowland alluvial rivers (Wohl, 2000), where the understanding of river behavior has progressed to the point of predicting such aspects as: downstream increases in width, depth, and velocity as a function of discharge (Leopold and Maddock, 1953); graded longitudinal profiles that reflect a balance between slope and the prevailing water

and sediment discharges (Mackin, 1948; Leopold and Bull, 1979); the concave shape of river profiles (Hack, 1957); vertical velocity profiles in which velocity varies with the logarithm of distance from the bed (Leopold et al., 1964); and downstream variation in flow energy expenditure (Knighton, 1999). Now that relationships are beginning to emerge for the controls on channel gradient, velocity profiles, and energy expenditure along steep-gradient streams, the next step will be greater development of conceptual models that incorporate the unique properties of mountain rivers. To this end, as a final objective (*Hypothesis 4.1*), a conceptual model of sediment movement along the North Fork Poudre River is developed to determine the utility of such a model relative to the previously discussed numerical models for predicting channel recovery for habitat needs following a reservoir sediment release.

Wohl and Cenderelli (2000) found that the main factors governing complete pool volume restoration along the North Fork are the storage of sediment in upstream pools which function as sediment delivery sites to downstream pools, pool geometry, and flow hydraulics. As a consequence of bedrock control, large portions of the pools are characterized by flow separation and recirculating zones of flow within eddies. The role of these eddies in storing and releasing sediment at different discharges is critical to an understanding of channel recovery for fish habitat. It follows then that the goal of a conceptual model for the North Fork is to identify when eddies function as sources and sinks of sediment, and to understand the changing source/sink linkages within eddies over time. Ultimately, the long-term storage and persistence of sediment within eddy pools may have the largest bearing on channel restoration efforts for the reestablishment of fish habitat. Lastly, a conceptual model can also facilitate development of sediment

release strategies for the management of sediment within reservoirs, and can help identify important background data needs prior to a release, in order to mitigate the downstream effects of a reservoir sediment release.

4.2 Sediment Supply to Mountain Rivers

Study of the response of rivers to the delivery of a large volume of sediment provides insight into the processes and rates by which channels adjust and compensate for the increased sediment load. Mountain rivers in particular are prone to sediment input in the form of pulses rather than a more continuous supply, largely because a strongly seasonal discharge and limited sediment supply produce episodic sediment movement (Wohl, 2000). Also, mountain rivers are more susceptible to disturbances that generate and deliver large quantities of sediment such as landslides and debris flows from steep, surrounding hillsides, and because anthropogenically-induced activities such as mining and timber harvesting are more prevalent in mountainous regions. These large sediment disturbances offer opportunities to evaluate and identify the thresholds for channel change, and the associated recovery from a given disturbance. Despite the seemingly site-specific understanding of sedimentation patterns derived in this study, there are some underlying predictable sedimentation patterns that have been identified and that should hold in general for other systems. Examples of these sedimentation patterns are provided in Section 4.2.2.

4.2.1 Previous Research on Sediment Influxes to Mountain Rivers

In a review of published data sets and observations derived from mountain channels, a general observation is that the delivery of large quantities of sediment to channels can

result from multiple sources (Table 4.1). A common outcome of many natural and anthropogenic phenomena occurring within a drainage basin is increased sediment production such that sediment loads to rivers are rapidly increased beyond normal ranges. These releases of sediment have been referred to as sediment pulses and sediment slugs, which are discrete inputs of large amounts of sediment producing a transient topographic high on the bed of the river. A decline or cessation in sediment supply over time is the most characteristic feature of sediment slugs and pulses (Rutherford, 2001). Once a sediment pulse is delivered to a mountain river, the deposit may travel downstream as a wave of deposition such as that proposed by Gilbert (1917) for the Sacramento River tributaries receiving sediment from hydraulic gold mining. Repeat measurements of peak aggradation have documented translation of the wave-form downstream over time (Lisle, 1982; Pickup et al., 1983; Madej and Ozaki, 1996). In these cases, the streambed did not aggrade uniformly; rather, aggradation lagged both in time and space as the sediment wave moved downstream. Alternatively, the sediment pulse can generate a long, flat deposit creating a plane bed along the river profile, translating downstream over time as sediment is moved from pool to pool (Wohl and Cenderelli, 2000). In another example, Sutherland et al. (1998) monitored channel aggradation resulting from a landslide, and noted that the sediment pulse dispersed in place. Therefore, there are multiple responses to rapid channel aggradation and multiple mechanisms by which sediment is transported out of a channel system.

Table 4.1. Examples of published datasets on sediment influxes to mountain rivers using either reach- or width-scale resolution.

| Sediment Source and Result | Location | Reference |
|--|--|---|
| Deposition from 1976 flood | Big Thompson River Basin, CO | Shroba et al. (1979) |
| Pool infilling resulting from 1955, 1964 floods and logging | Various Rivers, NW CA Redwood Creek, CA | Lisle (1982); Wohl et al. (1993) Madej and Ozaki (1996) |
| Dam break deposition | Fall River, CO | Jarrett and Costa (1986); Anthony (1987); Pitlick (1993) |
| Channel aggradation following dam removal | Clearwater River, ID | Williams (1977) |
| Aggradation from reservoir releases of water and/or sediment | Colorado River, Grand Canyon, AZ | Schmidt (1990); Rubin et al. (1990); Cluer (1997) |
| | North Fork Poudre River, CO | Wohl and Cenderelli (2000); Rathburn and Wohl (2001) |
| Pool sedimentation | Trinity River and tributaries, CA | Lisle and Hilton (1992) |
| Aggradation from mining activity | Yuba River, CA | Gilbert (1917) |
| | Kawerong River, Papua New Guinea | Pickup et al. (1979) |
| | Ringarooma River, Tasmania | Knighton (1989) |
| | Bear River, CA | James (1991, 1993) |
| | Middle Fork South Platte River | Hilmes and Wohl (1995) |
| | Ok Tedi River, Papua New Guinea | Pickup et al. (1983); Higgins et al. (1987); Parker et al. (1996) |
| Glacial outburst coarse sediment deposition | Mt. Everest Region, Nepal | Cenderelli and Wohl (1998) |
| Channel aggradation resulting from volcanic eruptions | Toutle River, Mt. St. Helens, WA | Simon (1999) |
| | Mt. Pinatubo, Philippines | Montgomery et al. (1999) |
| Channel sedimentation from mass movement | Navarro Creek, CA | Hansler et al. (1998) |
| Floodplain accretion from deforestation | New Zealand | Gomez et al. (1998) |
| Channel sedimentation resulting from fire | Buffalo Creek, CO | Jarrett and Browning (1999) |

Studies of waste disposal from mining operations have generated a majority of the data on episodic delivery of sediment pulses to rivers (Table 4.1). The research efforts have been focused on understanding overall channel aggradation, channel planform

changes, meander migration, and the rates of channel recovery following an intense mining-induced sediment disturbance (e.g., Knighton, 1989; James, 1991, 1993; Pickup et al., 1983; Higgins et al., 1987; Hilmes and Wohl, 1995; Parker et al., 1996, among others). Typically, many of the natural or human-caused events that deliver increased sediment loads to downstream rivers disturb sizeable areas of the landscape, and impact tens to hundreds of river kilometers as the introduced sediment is transported downstream. Out of necessity, many of the initial studies, therefore, emphasized the reach-scale perspective, assessing large stretches of river that underwent extreme channel aggradation and degradation as a result of the sediment pulse.

4.2.2 Reach Scale Response to a Sediment Pulse – A Review

On the largest scale of observation pertinent to this study, the sedimentation patterns can be broken out at the reach scale, where reaches represent a segment of uniform channel morphology that is at least several channel widths in length. In this case, the appropriate reach-scale channel morphologic unit for the North Fork is a pool-riffle sequence, where regularly spaced pools and riffles represent the characteristic bedform.

Rivers exhibit three dominant reach-scale responses to an increase in sediment load, either 1) transporting the introduced load, 2) aggrading portions of the channel, or 3) degrading or incising the deposited sediment (Figure 4.1). For each sediment pathway there is a hierarchy by which sediment is partitioned into various channel components, depending on sediment supply or the order of events (Figure 4.1). In order to use Figure 4.1, channel reaches subject to sediment loading must first be delineated. The primary criteria by which channel reaches are distinguished, for purposes of evaluating channel response to a sediment release, are channel gradient, followed by channel complexity, or

Reach-Scale Response to a Sediment Release

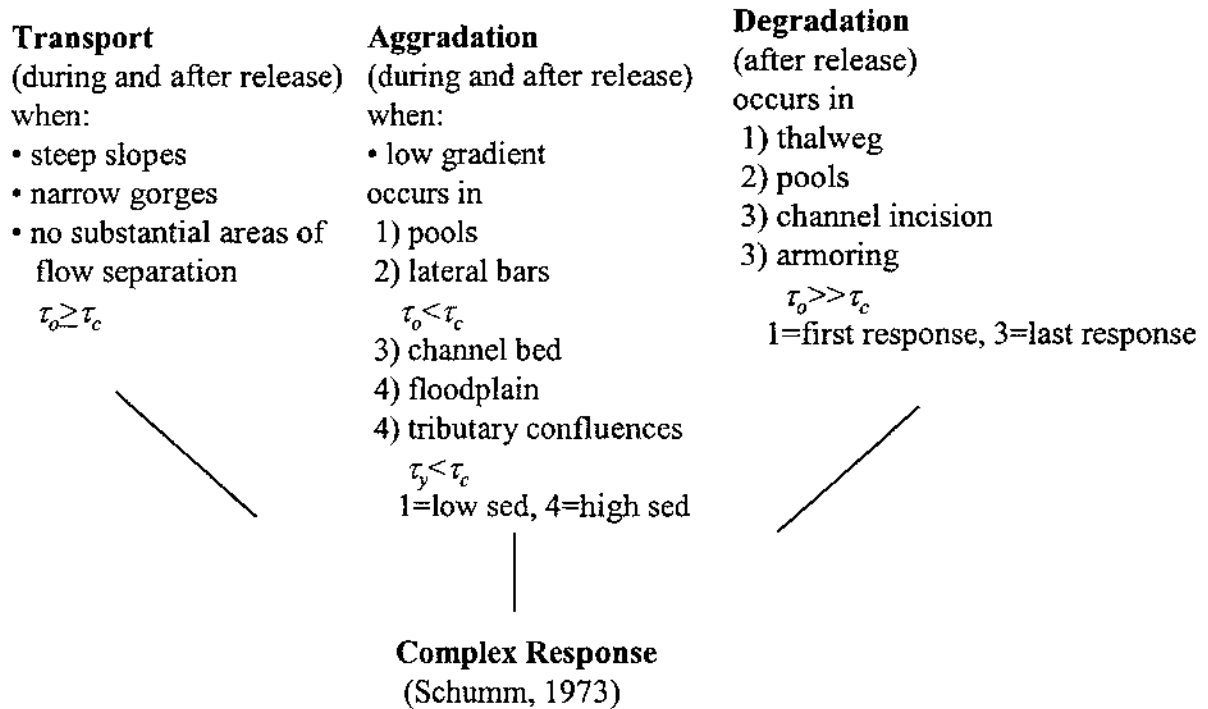


Figure 4.1 Reach-scale conceptual model of channel response to a sediment release.

the amount of flow separation and recirculation. Rivers with bed gradients greater than or equal to 0.02 m/m are considered steep-gradient (Jarrett, 1992), and will respond to sediment influxes by transporting the majority of the imposed load. However, steep-gradient channels may possess large, low-velocity areas lateral to the channel where flow separation and recirculation change the sediment transport patterns. In these cases, it is important to quantify the degree to which the recirculating zones off-set the overall transport tendency of a steep-gradient reach.

The first pathway of response to a sediment pulse is the transport of sediment, which occurs in reaches with steep slopes, such as in headwater areas, or where the channel is laterally confined through narrow gorges, or where there are no substantial areas of flow separation (Figure 4.1). Transport of sediment occurs in these reaches because effective boundary shear stress, τ_o , is greater than the critical shear stress, τ_c , required to initiate transport for a specified grain size. Actual quantification of τ_o at the reach scale will require approximation of mean conditions. Boundary shear stress, for example, is a function of bed-gradient and flow depth. These must be averaged across space (either at the cross-sectional or reach level) and potentially across a range of discharges. Critical shear stress can only be applied to a single grain size, which is assumed to be representative of the entire grain-size distribution.

In the second pathway of response (Figure 4.1) aggradation occurs where the channel gradient shallows, or where abrupt channel expansions create flow separation and zones of reduced flow velocity and deposition. In general, the patterns of aggradation are controlled by: characteristics of the sediment release; water discharge accompanying the release; and channel geometry, such that boundary shear, τ_o , is less than critical shear

stress, τ_c , needed for the initiation of particle motion. Initial channel aggradation occurs in pools, with numerous studies documenting preferential infilling of pools resulting from large increases in sediment load (Lisle, 1982; Madej and Ozaki, 1996; Wohl and Cenderelli, 2000). Pool deposition can effectively create a more uniform reach gradient and flow depth, and enhance bed mobility because the finer-grained sediment delivered to the channel decreases bed roughness. Simultaneous with pool deposition, if sediment supply remains high, can be the development of lateral bars, often in low-velocity areas adjacent to the banks of the channel. Aggradation of marginal bars along the North Fork occurred adjacent to pools, where channel expansions created recirculating eddies.

At some point under conditions of sustained sediment supply, it is hypothesized that hyperconcentrated flow is established when the concentration of sediment becomes so great as to affect the fluid and sediment transport properties. The volumetric sediment concentrations of hyperconcentration range from 5 to 60 percent (Julien, 1995). In the case of the North Fork, one interpretation of the aggradational sequence includes the establishment of hyperconcentrated flow to explain why, when shear stresses were sufficient to transport sand, deposition of sand occurred. It is plausible that the onset of hyperconcentrated conditions resulted in a sufficient volume of sand to overwhelm the transport capacity of the channel. At this point, deposition within the channel bed occurred, causing a loss of channel capacity, elevated channel bed, and floodplain accretion. The volume of deposition on the channel bed necessary to cause overbank flooding and floodplain aggradation would depend on subsequent flow magnitudes. For example, a ten percent loss of channel conveyance through sedimentation might not create overbank flow during a two-year recurrence interval flood, whereas the

sedimentation could cause overbank flow during a five-year flood that would normally be contained within the channel.

In rivers with tributaries, deposition within tributary confluences would result during overbank flooding and backwater effects at the confluence. Because hyperconcentrations deform differently than clear-water flows (Julien, 1995), the conditions of sediment transport include a yield stress, τ_y , such that aggradation results when the yield stress is less than critical shear, τ_c , for the final phases of aggradation (Figure 4.1).

In general, channel aggradation tends to oversteepen channel slopes. With a reduction or cessation in the sediment supply and with the release of clear water, existing deposits become scoured and degradation occurs (Figure 4.1). During degradation, bed shear stress, τ_o , exceeds the critical shear stress, τ_c , required to move sediment.

The first response during the degradational phase is incision of the channel thalweg, followed by pool excavation, and overall channel bed incision (Figure 4.1). The degradation phase along the North Fork occurred mainly as selective transport, in that sediment was entrained as a function of grain-size. Smaller clasts were more readily mobilized from the bed surface and were preferentially mobile at low flow (Wohl and Cenderelli, 2000). Sustained selective transport without a constant supply of sediment leads to the development of a stable armor layer (Sutherland, 1987) through progressive winnowing of fine material from the bed. Armoring of the bed along the North Fork, as the final phase of degradation (Figure 4.1), indicates re-exposure of the original cobble-boulder bed resulting from the flushing of reservoir sediments.

Other aspects of the sediment pulse figure prominently in the reach-scale response model to a large influx of sediment. These include the grain size distribution of the sediment comprising the pulse, and the sediment release volume. In general, sediment moving as bedload is deposited closer to the release source, whereas suspended sediment is transported farther downstream. In addition, the overall sediment volume decreases in the downstream direction.

It is important to recognize the complex nature of the sediment pathways, and the concurrence of the responses in time and space. Schumm's (1973) complex response model for the stages of channel adjustment following channel incision also applies as a model of channel aggradation and degradation on the North Fork system following the reservoir sediment release. Transport, aggradation and degradation can occur concurrently within a reach, depending on the characteristics of the channel, the flow regime, and the properties of the released sediment. This is demonstrated along the North Fork where channel behavior alternated between aggradation and degradation both downstream, cross stream, and with time, as sediment from upstream pools was mobilized and transported into downstream, more distal pools.

4.2.3 Width-Scale Response to a Sediment Pulse – A Review

Of the list presented in Table 4.1, only four sites were investigated for sediment aggradation and degradation on the scale of a single channel width. At these sites, sediment movement was monitored on a scale that discerns the differential sedimentation patterns along a cross section, or on the scale of an individual deposit. The studies with width-scale resolution include: 1) aggradation of separation and reattachment bars in Grand Canyon (Schmidt, 1990; Rubin et al., 1990), 2) channel morphologic changes

associated with mining along the Bear River (James, 1991), 3) an overall measure of pool sedimentation along tributaries of the Trinity River (Lisle and Hilton, 1992), and 3) channel aggradation and degradation within the North Fork Poudre River (Wohl and Cenderelli, 2000; Rathburn and Wohl, 2001). The emphasis on the width-scale in these previous studies stems from research hypotheses that require details of sediment movement that would be missed on a larger scale of analysis. Likewise, along the North Fork, the simultaneous marginal aggradation and thalweg degradation that occurred within pools following the original sediment release, necessitates a conceptual model that captures, even qualitatively, the transport of sediment into and out of eddy pools. Only in this way can the processes that govern sediment movement within eddies be incorporated into management decisions that are relevant to reestablishing fish habitat.

A majority of the examples of sediment influxes in Table 4.1 originate from research on mountain channels with a pool-riffle bed configuration. However, few of the studies discuss the detailed physical characteristics of the pools, such as whether or not the pools exhibit a compound (i.e. two-part) nature. Previous researchers may not have recognized the importance of the upstream, or compound portion of pools, or the link between upstream and downstream eddies within one pool in governing pool hydraulics and sediment distribution. The upstream eddy is created because of backwater ponding upstream from a constriction, serving to elevate the water surface in a manner that drives the central flow of water through the constriction. Pools along the Cache la Poudre River, North Saint Vrain Creek, Boulder Creek, and Clear Creek in Colorado, and possibly many others, also show a compound characteristic (D. Thompson, E. Wohl, pers. comm., 2001). It is likely that many pools in mountainous regions may show

compound traits, such that the sediment dynamics described herein are pertinent to regions beyond the Front Range of Colorado. Also, the lack of information about compound pools in the literature may be the result of studies conducted at a scale too coarse to resolve the details of pools that influence sediment delivery and storage. Such details would be more readily detected on the width scale. Like reach-scale perspectives of rivers, predictable patterns of transport, aggradation, and degradation may emerge from the width-scale consideration of a sediment release in laterally-confined rivers. At a minimum, a width-scale conceptual model bridges the gap in knowledge that prevents the development of general predictive models that successfully link sediment supply to changes in habitats of aquatic organisms.

Two of the studies cited in Table 4.1 have developed conceptual models specific to the rivers of interest. For example, Schmidt (1990) presents a model of sand movement into and out of recirculating zones along the Colorado River in Grand Canyon. At high discharge, sand from separation and reattachment bars is entrained by turbulent boils, and is either redistributed within the recirculation zone, exchanged with the main current, or deposited in the vicinity of stagnation points associated with separation and reattachment points (Schmidt, 1990). As discharge in the Colorado River recedes, the size of the recirculation zone decreases as the separation point and reattachment point migrate closer together, additional deposition occurs, and the previously-deposited sediment may be reworked. This results in a constant flux of sediment into and around eddy zones, with some high-discharge sand deposits temporarily isolated from low-discharge erosive capabilities, depending on the sequence of flows. Lisle and Hilton (1992) developed a model of deposition within pools, based on the available pool volume, the sediment

supply, and hence the supply of mobile sediment in a stream channel. In situations with abundant sediment, pools may be 'volume-limited' because pool volume is small and sediment storage limited, or because the discharge or constriction ratio is low and the central scouring jet of flow through the thalweg is weak. In channels with a limited sediment supply, pools are termed 'jet limited' if a high discharge and/or high constriction ratio maintains a strong central jet, limiting the volume of fine sediment deposited. The most notable aspect of these conceptual models is the focus on width-scale resolution, describing the sediment dynamics to allow resolution of individual deposits or areas of scouring.

4.3 Conceptual Model of Pool Sedimentation for the North Fork

A width-scale conceptual model for laterally-constricted pools has been developed based on observations of sediment movement over time in four pools along the North Fork Poudre River. Figure 4.2 is a composite of three cross sections through one compound pool, the Tick Pool, and illustrates the scour and deposition measured in the field following the 1996 sediment release. In the upstream, constricted, and downstream portions of the pool (Figure 4.2), aggradation from the experimental discharge occurred on top of and higher than the original depositional surface. Original deposition within the pools elevated the channel bottom causing a loss of channel capacity. As a result, sediment mobilized from upstream, more proximal pools during the experimental discharge in Spring 1997 was transported and deposited into lateral pool areas that were otherwise not available under normal discharges. These areas are important low velocity areas for fish and other aquatic organisms. It is important to note that there are nineteen

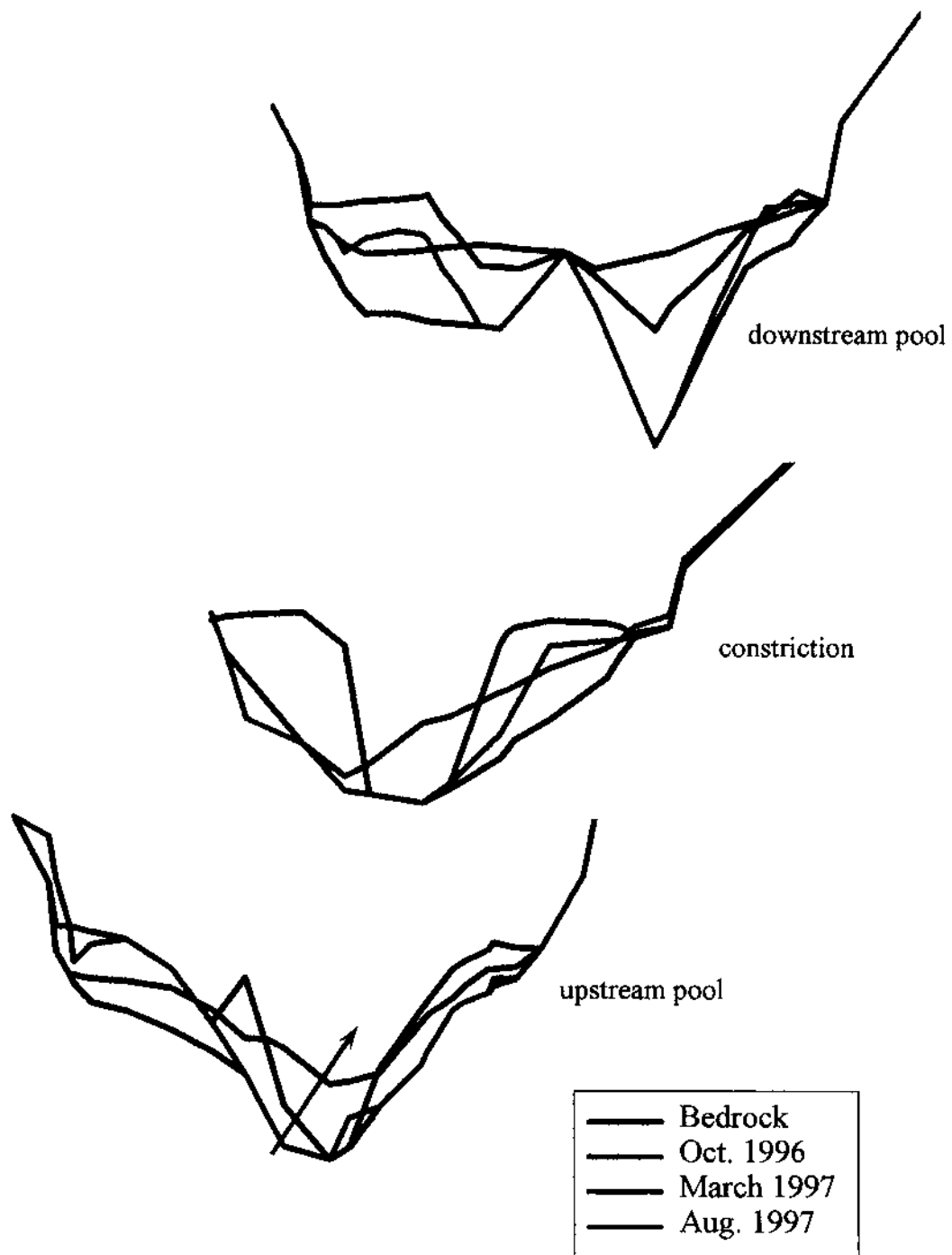


Figure 4.2. Composite cross sections through the Tick Pool showing aggradation and degradation of reservoir sediments over the 1996- 1997 hydrograph. Perspective is looking from upstream to downstream through the compound pool.

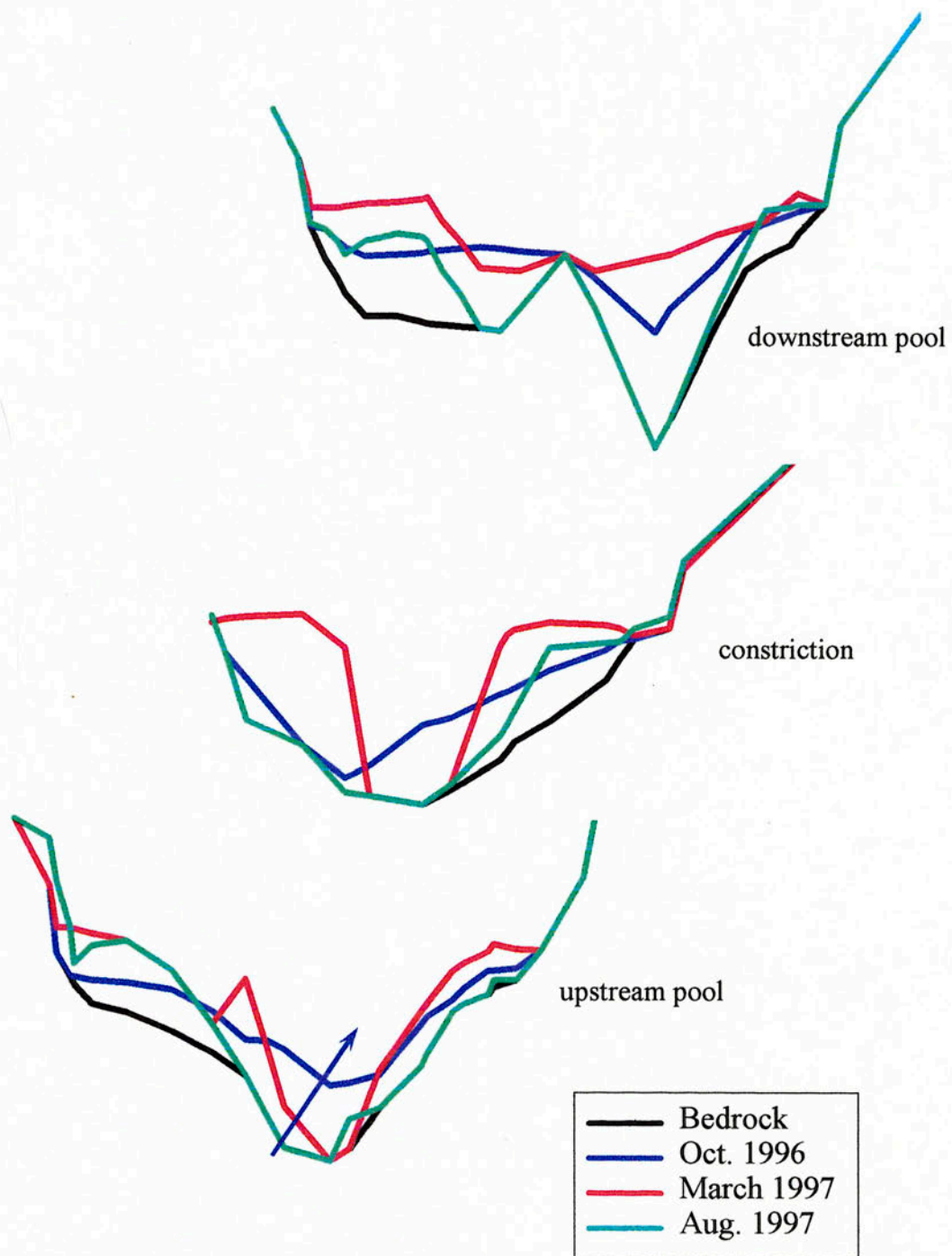


Figure 4.2. Composite cross sections through the Tick Pool showing aggradation and degradation of reservoir sediments over the 1996- 1997 hydrograph. Perspective is looking from upstream to downstream through the compound pool.

pools upstream from the Tick Pool, all of which were filled between 60 to 100 percent with fine sediment from the reservoir release (Wohl and Cenderelli, 2000). Interestingly, pools more proximal to the dam did not exhibit this extreme, additional aggradation of bars within eddies. Instead, proximal pools such as the Goose Pool became sequentially scoured with each discharge event (Figure 4.3), except for minimal sediment deposition on marginal bars adjacent to both banks. The disparity in channel response within proximal and distal pools results from the sediment supply from upstream pools becoming rapidly depleted. Although the North Fork uniformly lost pool capacity during the initial aggradation from the reservoir release, the lack of a sufficient sediment source in proximal pools prevented further aggradation in lateral portions of pools during subsequent flows. Only two pools exist between the Goose Pool and Halligan Dam.

One potential mechanism for describing sediment dynamics in more distal pools is illustrated in Figure 4.4, using the Tick Pool as an example. The conceptual model is designed to recognize the importance of simultaneous scour and deposition in improving or degrading aquatic habitat quality, and in identifying whether areas of long-term storage may be influenced by subsequent flows of water and sediment. At low flows (Figure 4.4a), sediment deposition is limited to small recirculating areas on the shoreward side of the eddy because the angle of inflowing water into the upstream pool keeps most of the fine sediment in transport. As discharge increases (Figure 4.4b), the reattachment point begins to migrate downstream, eventually becoming anchored on the bedrock constriction, thereby increasing the size of the recirculation zone. The upper limit in size of the recirculation zone is attained when the reattachment point becomes fixed on the bedrock outcrop. At moderate discharges (Figure 4.4b), a strong, prominent eddy fence

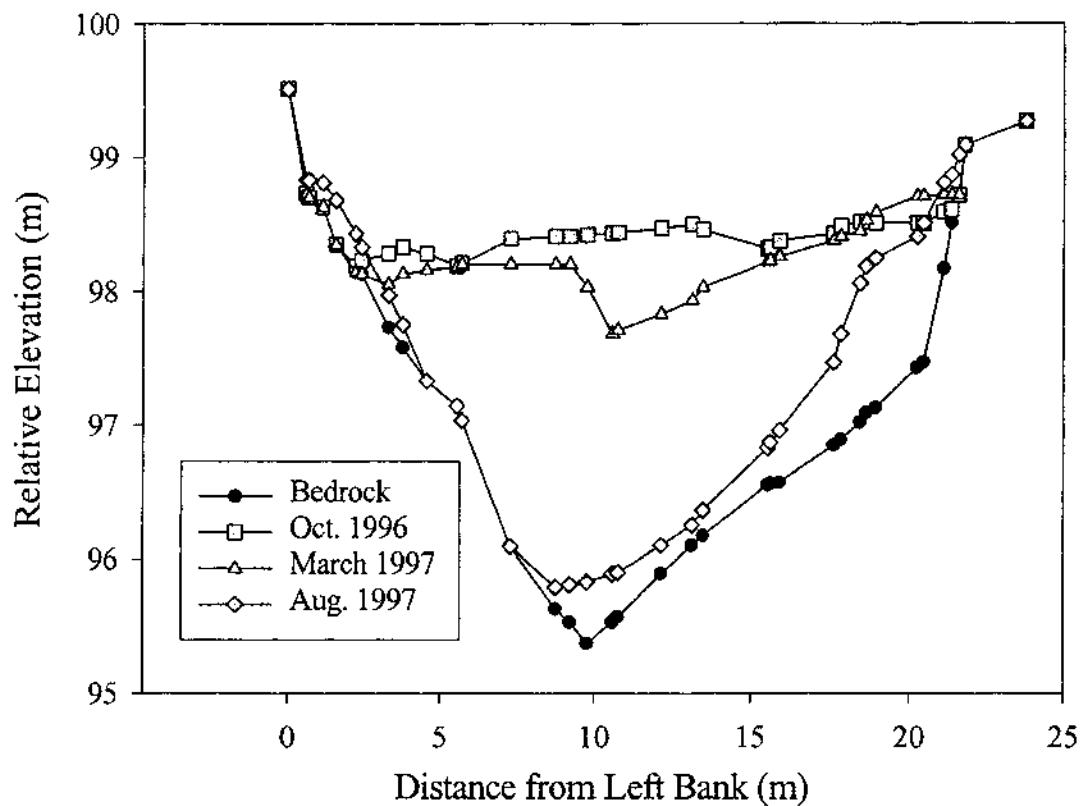


Figure 4.3. Cross section within the Goose Pool, 0.5 km downstream from Halligan Dam showing sequential scour of reservoir sediment over the sediment monitoring period, October 1996-August 1997.

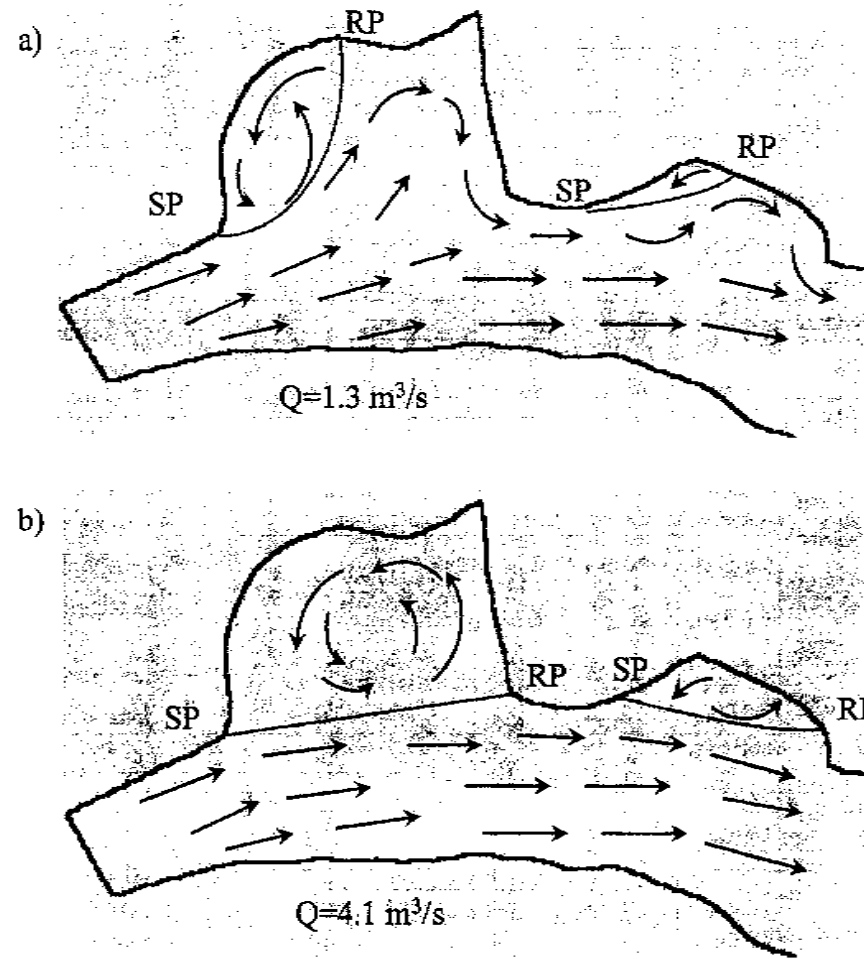


Figure 4.4. Conceptual model for laterally-confined compound pools using the Tick Pool as an example. At low discharge shown in a) deposition is restricted to small recirculation zones in upstream and downstream eddies. As discharge increases in b) the reattachment point (RP) moves downstream and becomes fixed on the bedrock outcrop. The separation point (SP) does not migrate with higher discharges, preventing low flow deposits from being eroded. Arrows indicating velocity are highly schematic and not to scale.

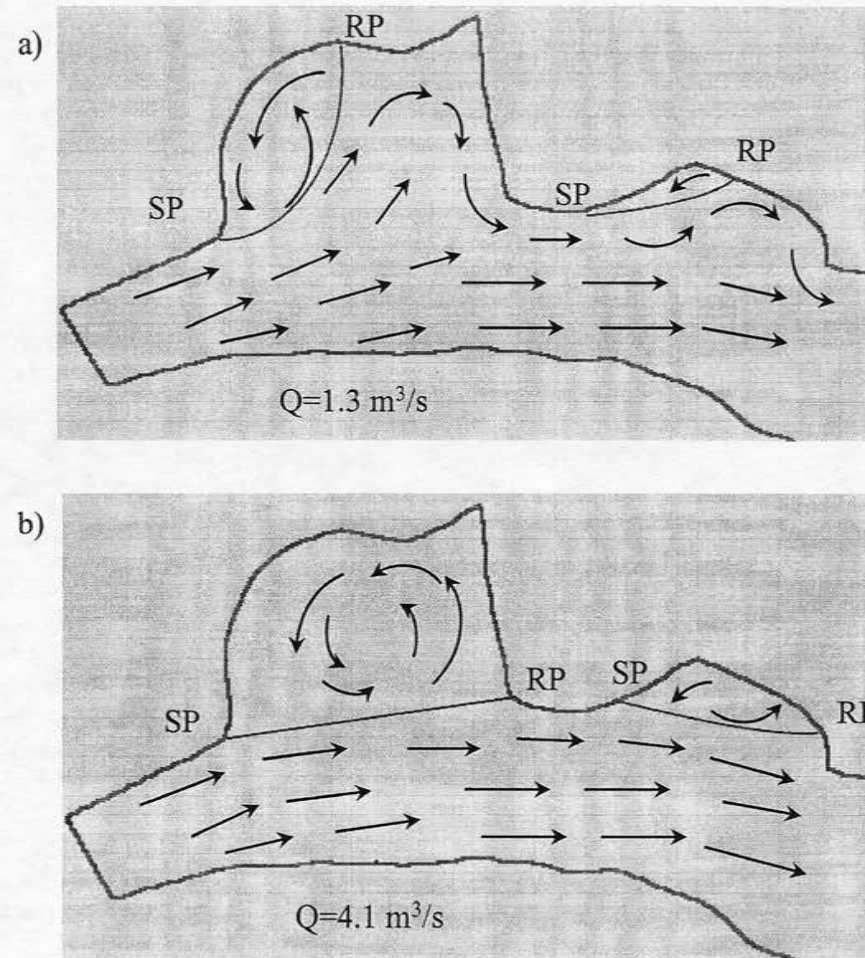


Figure 4.4. Conceptual model for laterally-confined compound pools using the Tick Pool as an example. At low discharge shown in a) deposition is restricted to small recirculation zones in upstream and downstream eddies. As discharge increases in b) the reattachment point (RP) moves downstream and becomes fixed on the bedrock outcrop. The separation point (SP) does not migrate with higher discharges, preventing low flow deposits from being eroded. Arrows indicating velocity are highly schematic and not to scale.

or shear zone develops, and the trajectory of inflowing water becomes oriented directly downstream rather than into the upstream eddy. Sediment that was deposited at lower discharges is not flushed out of the eddy at higher flows because of the strong recirculating flow and pronounced eddy fence. The separation point within the upstream eddy of the Tick Pool remains fixed on the downstream bank of the riffle, and the vertical bedrock walls that form the left bank of the Tick Pool dictate the permanent position of the separation and reattachment points at high flows. At discharges greater than $10 \text{ m}^3/\text{s}$, because of the fixed nature of the eddy fence and the limited size of the upstream and downstream recirculation zones, the only notable changes in the Tick Pool were an increase in flow depth and increased flow velocity.

Similar patterns of deposition and erosion have been observed in Grand Canyon by Schmidt (1990), and were described briefly in the previous section. The main difference between the North Fork and the Colorado River is that separation points within eddies of the Colorado River also move upstream at higher discharges, eventually inundating the debris fans that form the famous rapids of Grand Canyon, as the reattachment point migrates downstream. These high discharges scour the finer-grained separation deposits on the backside of the eddy, often down to the coarse material that mantles the debris fans, because the effect of the constriction is essentially eliminated once the debris fan becomes overtopped. Because of the compound nature of pools within the North Fork, the separation point within the upstream eddy does not result from a channel constriction, but rather a channel expansion at the downstream end of a relatively narrow riffle. Hence, the separation point is fixed at the downstream end of the riffle, resulting in more persistent fine-sediment deposition (Figure 4.2), and possibly long-term storage within

the upstream or compound portion of the eddy. As a result, once a large volume of sediment is delivered to a confined channel such as the North Fork, the width-scale characteristics of the pools, the proximity to the sediment source, and the post-sediment release flows dictate where the sediment is stored and for how long.

Once sediment from the release is partitioned into storage sites, mechanisms by which that sediment might be removed from sensitive habitat areas can be identified. Sediment removal from the constricted portion of the pool (Figure 4.2, middle cross section) can be explained by Thompson's (1997) model of pool flushing. Sediment deposited in steep-sided marginal bars within pools may slump into the pool thalweg during waning stages of flow. With an increase in discharge, the slumped sediment will be scoured out of the pool by a central jet of high velocity flow. In this way, central portions of pools may have a mechanism for self-clearing, given the proximity to the constriction, whereas the recirculating zones have the potential for persistent sediment deposition.

Sedimentation within compound pools of mountain rivers occurs as transient sediment storage and transfer such that proximal pools are sources of sediment for more distal pools, and distal pools may be long-term sinks of sediment depending on pool geometry. The deposits from a sediment pulse can be viewed as sediment in transit, although the movement is intermittent. All of the sediment released from Halligan Dam can be considered as a slowly moving system, which is especially true of supply-limited systems, where sediment transport will occur provided the hydraulic conditions are satisfied. There may be some permanent deposits, however, where sediment gets captured in recirculating flow of eddy pools and is not released under current discharge

regimes. In these cases, channel storage through aggradation can buffer the sediment load delivered to the mouths of rivers, and have the greatest consequences for restoration of fish habitat.

4.4 Channel Recovery

Channel recovery is an important issue given recent concerns over habitat loss. The persistence of sediment storage in channels can be an important contributor to the loss of aquatic habitat. This needs to be understood in terms of the duration of the sediment impact with respect to the research objectives. Throughout this document, reference to channel recovery has implied restoring pool volume to original pre-sediment release quantities by comparing cross section channel-bed elevations within a pool to pre-release channel levels. Using these criteria, Wohl and Cenderelli (2000) were able to conclude that nearly 80 percent of pools along the North Fork were cleared of sediment following the sustained, high magnitude 1997 snowmelt runoff. Pool volume recovery is only one measure of channel recovery, however. Another measure of channel recovery is the re-establishment of a previous channel morphology, such as well-developed pool-riffle sequences. Pitlick (1993) describes channel recovery as “the re-establishment of a quasi-equilibrium channel in response to changes in discharge and sediment load” (Pitlick, 1993, p. 657). He found that channel morphology within upstream portions of the Fall River recovered rapidly (within 5 years) after a catastrophic flood and its associated sediment input. Downstream reaches of Fall River took longer to recover because of the continued supply of sediment, and because the sediment was mobile less of the time. Madej and Ozaki (1996) used the return to a former channel-bed elevation as their measure of channel recovery. Their recurrent monitoring of channel bed elevation

documented that the persistence of the sediment impact on Redwood Creek was at least 20 years. This is a much longer recovery time (>20 years) following a less catastrophic event than that studied by Pitlick (1993). Channel width, yet another indicator of channel recovery, had not yet returned to pre-sediment pulse widths at Redwood Creek by 1996. The sediment release along the North Fork appears to be the only example in the literature of channel recovery efforts directed at pool recovery specifically for the reestablishment of fish habitat.

4.5 Recommended Sediment Monitoring Background Data

As the multiple uses and social values for rivers continue to include enhanced restoration efforts, adjusted operating regimes for dams, dam removal, endangered species protection, and flood protection (Graf, 2001), the issues and uncertainties surrounding sediment releases into mountain rivers will often revolve around sedimentation hazards within the downstream channel. Conceptual models of channel sedimentation, such as that developed for the North Fork Poudre River, are additionally relevant for identifying data needs prior to releasing sediment to minimize impacts to the downstream channel.

Access to certain pre-sediment release data is key to predicting, with any level of certainty, the complex interactions between sediment transport and deposition, and ultimately the response of the aquatic ecosystem. These pre-release data can be categorized under four main headings: 1) channel geometry data, 2) hydrologic data, 3) sediment characteristics, and 4) ecological characteristics. Necessary channel geometry data include detailed, accurate surveys of the channel to delineate the channel morphology both across a channel and along the longitudinal profile, and fieldwork that

delineates the dominant bedforms, number of pools, pool geometry, and eddy size.

Hydrologic data entail gaining an understanding of the annual hydrograph via gaging data or field-derived discharge measurements, release options from the upstream dam, if present and, ideally, the response of width-scale channel features to variations in discharge. Characteristics of the sediment include the volume and size distribution of the released sediment, whether or not contaminants are present within the sediment, bed material and mobility, and sediment discharge curves. Finally, ecological considerations depend on the primary management questions surrounding a particular sediment release, specific to the river of interest. These considerations might include questions such as: is the primary ecological concern spawning or overwinter habitat, nursery issues, or substrate stability for macroinvertebrates?; does the timing of the sediment release need to consider fish and insect life cycles, or exotic plant life cycles?

If the concern over a sediment release focuses on pools and riffles, as at the North Fork, more coordinated field data can be collected to resolve key uncertainties within the pool-riffle complex. The following aspects of a mountain channel with pool-riffle systems should be addressed:

Pools and pool infilling

- Pool geometry (size, simple or complex, size of recirculating zone, and proximity to thalweg)
- Distance from sediment source (closer pools lose greater volume but flush first)
- Grain size of released sediment (closer pools receive coarser grain size distribution, is the sediment cohesive?)
- Bed material (bed typically coarser in mountain rivers, helps investigator infer thickness of release sediment)
- Hydrologic regime (snowmelt-dominated rivers have a single spring peak)

Riffles

- Bed material grain size (indicates shielding potential, aquatic habitat needs)
- Bars at heads of riffles
- Lateral bars
- Bed mobility (shear stress/grain size)

4.6 Sediment Release Recommendations

Planning for a sediment release must include consideration of the timing and magnitude of the release in conjunction with all of the above data needs in order to properly mitigate the impacts to the downstream channel. In the case of the North Fork, where water and sediment releases are regulated by Halligan Dam, options are available to manipulate the timing and magnitude of a sediment release. If the goal of sediment management practices for Halligan Reservoir and the North Fork is to minimize deposition within pools for maximum fish habitat, then sediment partitioning within pools must be addressed. For sediment management within low velocity, recirculating eddy pools, a sediment release coincident with a low discharge would minimize loss of backwater habitat within compound pools in the canyon. Based on the available information, the most effective transmission of sediment through the compound pools in the North Fork is achieved by a continuous slurry of sediment at a discharge sufficiently low to prevent the establishment of a strong eddy shear zone, mimicking the transport depicted in Figure 4.4a. Observations of flow between 1.3 and 3.4 m³/s, and two-dimensional hydraulic modeling at 4.01 m³/s, show that at low discharges the angle of flow into the eddy creates minimal area for deposition, and a minimal hydraulic barrier to sediment transport. In this way, sustained sluicing of reservoir sediment would transport the sediment as far downstream as possible, before subsequent releases of clear water

mobilize upstream sediment, causing aggradation within sensitive habitat. The stepped, experimental release in February and March 1997 (peak discharge of $3.4 \text{ m}^3/\text{s}$) was effective at mobilizing large volumes of sediment, but contributed to additional deposition within eddy pools because of the elevated channel bed and a loss of channel capacity.

If sediment management within the deepest portions of pools is of primary concern, then release recommendations need to focus on maximizing flushing flow discharges from Halligan Dam. As noted previously, the snowmelt runoff discharge during the spring and summer of 1997, which peaked at $10.1 \text{ m}^3/\text{s}$, was responsible for scouring sediment from pools, and restoring approximately 80 percent of the original pool volume. A study assessing riparian restoration of the North Fork within The Nature Conservancy's Phantom Canyon Preserve recommends that optimal sediment management in Halligan Reservoir should include the release of sediment in spring prior to the snowmelt peak flow, such that a high magnitude flow is available as a follow-up to the initial sediment release (TNC, 2001). A flow of $10.1 \text{ m}^3/\text{s}$ was recommended during years of sufficient snowmelt. During years of spring snowmelt insufficient to achieve the higher recommended flushing discharge, a short-term release with a rapid rate of increase in discharge is recommended. Rapidly increasing flows (i.e., steep ascending limb of hydrograph) are highly effective at scouring and transporting material. During the stepped, pre-snowmelt discharge in spring 1997, discharge was increased by $0.03 \text{ m}^3/\text{s}$ per hour for two days. As a result, scouring of a narrow, deep thalweg occurred in every pool surveyed within the Phantom Canyon study reach (Wohl and Cenderelli, 2000). The trade-off was the simultaneous, additional aggradation which occurred as marginal bars

in the lower velocity compound portions of the pool. Also, the gradual stepping-down of discharge on the descending limb of the hydrograph was important for minimal deposition from a clear water release after the initial sediment pulse.

One additional aspect of a sediment release pertains to the aquatic community. For the species of fish and macroinvertebrates present within the North Fork system, Zuellig and Kondratieff (pers. comm., 2000) suggest that summer and fall releases may have a greater impact on these aquatic communities than do releases in the spring (TNC, 2001). One final recommendation included in TNC (2001) provides for the release of sediment from Halligan Dam during the spring, if necessary, given that the release be conducted at more frequent intervals and consist of lower total sediment volume than has occurred over the past seventy years of management. Based on historical and oral accounts, it appears that past sediment releases consisted of a large volume of sediment per release, occurring at an interval of about once every ten years (TNC, 2001).

4.7 Summary

Large injections of sediment into mountain channels are the by-product of many natural and anthropogenic activities. These sediment inputs have been referred to as sediment slugs and pulses, and are known to attenuate downstream over time. Numerous examples of sediment pulses to mountain rivers are available in the literature, although most of the research focuses on the reach-scale response to the sediment influx. A reach-scale perspective is useful for identifying major pathways of sediment transport, or modes of sediment behavior. Transport, aggradation, and degradation of the sediment within a sediment pulse occur in a predictable hierarchy, often coincident in time in a complex response. Resolution of processes on a reach scale is too coarse to capture the

details of sediment delivery, storage and transfer that are key to understanding the impacts of sediment releases on aquatic ecosystems.

A width-scale conceptual model of sediment movement into and out of laterally-confined eddy pools is based on the pool geometry, distance from the dam (a surrogate measure of the upstream sediment supply), and the hydraulics associated with varying discharges. Low to moderate discharges limit deposition into small, backwater areas of eddy pools, and with increasing discharge, migration of the reattachment point causes persistent sediment deposition with the development of a strong shear zone. The conceptual model of sediment movement into and out of eddies provides a basis for understanding and predicting the effects of a reservoir sediment release on a mountain river.

Release recommendations for Halligan Dam are developed that allow for prioritization of pool habitat. Low, continuous releases of water and sediment that conduct the reservoir sediment well into the North Fork system will serve to maintain eddy pool habitat. In contrast, high flushing flows following a sediment release are directed at moving sediment out of the central thalweg portions of pools, to maximize pool depth. Stepped or pulsed releases of clear water following a sediment release may be useful for evacuating marginal deposits provided channel capacity loss is minimal. Otherwise, initial releases of clear water may induce sedimentation into areas not otherwise available if the channel bed is elevated. Therefore, consideration should be given to the nature and timing of reservoir sediment releases with regard to the most sensitive component of the aquatic habitat system.

A conceptual model for laterally-confined pools is a useful means of predicting channel response to a sediment release relative to numerical models. The conceptual model evolved, however, only after completing the one-, semi-two, and two-dimensional numerical modeling and after recognizing the deficiencies of those models in predicting sediment transport and storage in pools. In situations where numerical modeling is infeasible, conceptual models are a useful first-approach to understanding sedimentation patterns. Based on the results of this investigation, the most relevant insight into pool sediment storage and delivery arises through dual use of numerical and conceptual models. Whereas the numerical models provided estimates of scour and fill for low and high magnitude discharges as potential continuous or stepped releases, the conceptual model provides a relevant scale of investigation for water resource specialists faced with habitat management following sediment releases.

CHAPTER 5 CONCLUSIONS

5.1 Introduction

Predicting the response of a river channel to alteration in flow hydrology or sediment supply is one of the most difficult and important tasks carried out by engineers and geomorphologists providing information to resource managers (Nelson, 1996). A huge volume of literature has been developed to address all the issues associated with increased sediment supply, only a portion of which has been referenced in this document. Elevated sediment loads can affect channels in multiple and dramatic ways. It takes an integrated, multidisciplinary approach to understand the erosional and depositional processes resulting from a large influx of sediment into a mountain channel, and predict the lasting impacts to the aquatic ecosystem. The emphasis of this research is on evaluating the predictive ability of various hydraulic and sediment transport models, and the utility of the models in meeting specific objectives of predicting pool volume recovery following a reservoir sediment release along a mountain river.

5.2 One- and Semi-Two-Dimensional Numerical Modeling

The results of Chapter 2 partially support *Hypothesis 2.1*, that one- and semi-two dimensional sediment transport models are useful predictive tools for determining pool recovery following a reservoir sediment release. Of the two models evaluated, HEC-6 model predictions of pool bed change agree with field measurements of pool scour and

deposition to a much greater degree than GSTARS2.0 (Table 5.1). Average pool-wide trends of predicted versus observed aggradation and degradation for three pools along the North Fork were 58 percent (on average) for the long-term, snowmelt runoff simulation using HEC-6 and Yang's (1973) sand transport equation. These results indicate that at least 58 percent of observed bed changes after a sediment release would be predicted by HEC-6. The predictive utility of HEC-6 as applied to the North Fork is moderate to high (Table 5.1), in that estimates of fish survival by water resource managers following a reservoir sediment release would be based on knowledge of pool depth recovery of greater than 50 percent. In addition, HEC-6 simulations have utility for predicting flushing flows directed at pool recovery. Model simulations could be run until the desired pool recovery was achieved, and the associated flow could be requested as the minimum flushing discharge for sediment mobilization and transport.

Table 5.1. Comparison of numerical models based on certain criteria by which potential users might evaluate the models for applicability to a given sediment release situation.

| | HEC-6 | GSTARS 2.0 | RMA2 |
|--|--|---|---|
| Data Requirements | moderate-high | moderate-high | high |
| Expertise | moderate | moderate-high | very high |
| Results | >50% accuracy, pool-wide trend | 13-90% accuracy, no pool-wide trends | replicated low-velocity areas well, general flow field for low and high discharge |
| Advantages | cross section based, default options, sediment transport model | cross section based, semi two-dimensional, sediment transport model | nodal hydraulic parameters, visual display of output |
| Limitations | purely one-dimensional, limited transport formulas | few default options, not suited for stratified beds | hydraulic model only, outstrips calibration data, calibration data difficult to collect |
| Predictive Ability for North Fork Application | moderate-good | low | moderate |
| Predictive Utility for Pool Habitat Restoration | moderate-good | low | low |

5.3 Two-Dimensional Hydraulic Modeling

Lateral variations in velocity are important to an understanding of channel dynamics, especially where flow separation and recirculating eddies are significant components of the flow field, particularly in bedrock channels with irregular boundaries. The two-dimensional hydraulic modeling was designed to overcome the limitations of a purely one- and semi-two dimensional model.

The results of the two-dimensional hydraulic modeling (Chapter 3) partially support *Hypothesis 3.1*, in that the delineation of eddy pool flow recirculation is improved using a two-dimensional model. By the very construct of RMA2, the cross-stream component of flow is accounted for, and modeling simulations of low and high discharge for the North

Fork show well-developed recirculating zones of flow that are in broad agreement with timed photographs and field measurements of depth and velocity within low velocity pools. The second half of *Hypothesis 3.1* was not well supported by the modeling; inferred sediment transport did not correspond well to field-measured patterns of erosion and deposition within eddy pools.

The main limitation in using RMA2 to infer sedimentation patterns is the inability to accurately represent the processes of sediment transport using a hydraulic model. Disparities between the resolution of the field data on sedimentation patterns, and the results of the sediment transport rates predicted using hydraulic modeling output, severely limit the extent to which field and modeling results can be compared. If broad hydraulic features, such as low velocity areas, are used to make predictions of sediment deposition and erosion, then the agreement between field and modeling data is greatly improved. In the end, the predictive ability of the two-dimensional model is moderate for low velocity areas of the pools. However, the predictive utility of RMA2 for this application along the North Fork is low (Table 5.1).

5.4 Conceptual Model for Laterally-Confined Pools

A conceptual model for mountain rivers responding to releases of sediment that drastically increase the sediment load of the river has great utility in helping to predict downstream trends in flow hydraulics and sediment transport, deposition, and erosion. Transport, aggradation, and degradation of the sediment from a sediment release occur in a predictable hierarchy on the reach scale, and may show a complex response to the large influx of sediment.

A width-scale conceptual model of sediment movement into and out of laterally-confined eddy pools is based on the pool geometry, distance from the dam, and the hydraulics associated with varying discharges. Low to moderate discharges limit deposition into small areas of flow recirculation in eddies. With increasing discharge, migration of the reattachment point downstream causes persistent sediment deposition with the development of a strong shear zone. The utility of the conceptual model relative to numerical models supports *Hypothesis 4.1*. A qualitative understanding of the processes associated with sediment scour and deposition within laterally-constricted pools helps fill in deficiencies in the predictions of the numerical models. Based on the results of this investigation, the combination of numerical and conceptual models provides the most robust understanding of sediment issues surrounding eddy pools.

Although the conceptual model emphasized width-scale sediment dynamics, it is imprudent to ignore the reach scale. Most important is recognizing the interrelationship between the scales, where the reach-scale sediment transport drives the main sediment delivery system, and the width-scale processes drive the pool-specific redistribution of sediment.

Many problems of river management arise from the inadequate prediction of sediment behavior during flood flows, and the effects of extreme increases in sediment supply on the downstream channel. Much of this uncertainty arises because of limits placed on our ability to observe the processes that lead to sediment movement in rivers. To this end, predictive instruments, such as models, are needed for long-term perspectives and hypothetical scenarios of flow releases or flushing discharges. Only through an understanding of the processes by which sediment moves in mountain rivers

can those interested in riverine health begin to develop ways of mitigating or limiting the occurrences of downstream hazards associated with sediment releases.

5.5 Recommendations for Future Work

Additional research pertaining to sediment releases into mountain rivers would benefit from numerical models that are specifically designed for systems with steep-gradients, complicated flow structures created by irregular bed topography and geometries, and fine sediment transport in an originally coarse-grained system. The main challenge of modeling is an accurate representation of transport processes of fine bed material in a steep-gradient, cobble-boulder channel. Any future modeling would also benefit from an increased spatial domain to include a treatment of sediment routing of a translating and dispersing slug. Additionally, improved accuracy of flow and sediment transport modeling requires more detailed field data on a scale commensurate with the model results. Although the field-data acquisition poses logistical problems at high flow, flume experiments may serve as an adequate analog provided that the conditions at the field site can be replicated. Given the recent interest in dam removal and the associated uncertainties of the sedimentation hazards, a successful solution to the problem of routing sediment released from a reservoir has important practical and scientific value. When and how sediment that accumulates behind a dam can be released so as to limit impacts to downstream aquatic ecosystems is highly useful, especially as reservoirs age and demand for water increases.

LITERATURE CITED

- American Rivers, 1999. Dam removal success stories: restoring rivers through selective removal of dams that don't make sense, accessed March 2000, <http://www.amriver.org/successstories.html>.
- Anderson, R.A., and Stewart, G.S., 2000. Riverine fish flow investigations, unpublished Federal Aid in Fish and Wildlife Restoration Job Progress Report. F-289.
- Anthony, D.J., 1987. Stage dependent channel adjustments in a meandering river, Fall River, CO, Unpublished MS thesis, Colorado State University, Ft. Collins, 180 p.
- Ariathurai, R. and Arulanandan, K., 1977. Erosion rates of cohesive soils, *Journal of Hydraulic Engineering*, vol. 104, p. 279-283.
- Baker, V.R., 1984. Recent paleoflood hydrology studies in arid and semi-arid environments, *EOS, Transactions, American Geophysical Union*, vol. 64, p. 893.
- Bates, P.D., Anderson, M.G., Baird, L., Walling, D.E., and Simm, D., 1992. Modelling floodplain flows using a two-dimensional finite element model, *Earth Surface Processes and Landforms*, vol. 17, p. 575-588.
- Bathurst, J. C., Graf, W.H., and Cao, H.H., 1987. Bed load discharge equations for steep mountain rivers, *in* Thorne, C.R., Bathurst, J.C., and Hey, R.D., eds., *Sediment transport in gravel-bed rivers*, John Wiley and Sons, p. 453-491.
- Beck, M.B., 1991. Principles of modelling, *Water Science and Technology*, vol. 24, no. 6, p. 1-8.
- Berger, R.C. and Stockstill, R.L., 1995. Finite-element model for high-velocity channels, *Journal of Hydraulic Engineering*, vol. 121, no. 10, p. 710-716.
- Blizard, C.R., 1994. Hydraulic variables and bedload transport in East St. Louis Creek, Rocky Mountains, Colorado, Unpublished MS thesis, Colorado State University, Ft. Collins, 175 p.
- Byars, M.S., Zevenbergen, L.W, and Lagasse, P.F., 2000. Hydraulic design for channel restoration on the Santa Ana of the Rio Grande, ASCE Water Resources Conference, Minneapolis, MN.

- Carling, P.A., 1995. Flow-separation berms downstream of a hydraulic jump in a bedrock channel, *Geomorphology*, vol. 11, p. 245-253.
- Carriaga, C.C., and Mays, L.W., 1995. Optimal control approach for sedimentation control in alluvial rivers, *Journal of Water Resources Planning and Management*, vol. 121, no. 6, p. 408-417.
- Cenderelli, D.A., and Wohl, E.E., 1998. Sedimentology and clast orientation of deposits produced by glacial-lake outburst floods in the Mount Everest region, Nepal, *in* Kalvoda, J., and Rosenfield, C.L., eds., *Geomorphological hazards in high mountain areas*, Kluwer Academic Publishers, Netherlands, p. 1-26.
- Chang, P.K., 1970, *Separation of flow*, Pergamon Press, London, 777 p.
- Clifford, N.J., 1993. Formation of riffle-pool sequences: field evidence for an autogenetic process, *Sedimentary Geology*, vol. 85, p. 39-51.
- Chuer, B.L., 1997. Eddy bar responses to the sediment dynamics of pool-riffle environments, Unpublished PhD dissertation, Colorado State University, Ft. Collins, 128 p.
- Collier, M., P., Webb, R.H., and Schmidt, J.C., 1996. Dams and rivers: a primer on the downstream effects of dams, U.S. Geological Survey Circular 1126, 94 p.
- Copeland, R.R., 1986. San Lorenzo River sedimentation study: numerical model investigation, Army Corps of Engineers, Waterways Experiment Station Technical Report HL-86-10, 75 p.
- Donnell, B.D., Finnie, J.L., Letter, J.V. Jr., McAnally, W.H. Jr., Roig, L.C., and Thomas, W.A., 1997. Users Guide to RMA2 WES Version 4.3, U.S. Army Corps of Engineers, Waterways Experiment Station Hydraulics Laboratory, 227 p.
- Fan, S., and Springer, F.E., 1990. Major sedimentation issues and ongoing investigations at the Federal Energy Regulatory Commission, *in* Chang, H.H., and Hill, J.C., eds., *Hydraulic engineering*, vol. 2, Proceedings of the 1990 National Conference, San Diego, CA, p. 1014-1020.
- Farnworth, E.G., et al., 1979. Impacts of sediment and nutrients on biota in surface waters of the United States, EPA-600/3-79-105, U.S. Environmental Protection Agency Report, Athens, GA.
- Fischenich, J.C., 1990. Cumulative impacts analysis on a midwest fluvial system, *in* Hydraulic Engineering, Proceedings of the 1990 National Conference, American Society of Civil Engineers, New York, p.802-807.

- Froehlich, D.C., 1989. Finite element surface water modeling system: two-dimensional flow in a horizontal plane – Users Manual, Federal Highway Administration Publication No. FHWA-RD-88-177, 285 p.
- Gee, D.M., 1984. Predictions of the effects of a flood control project on a meandering stream, Hydrologic Engineering Center Technical Paper 97, U.S. Army Corps of Engineers, Davis CA.
- Ghanem, A., Steffler, P., and Hicks, F., 1996. Two-dimensional hydraulic simulation of physical habitat conditions in flowing streams, Regulated Rivers Research and Management, vol. 12, p. 185-200.
- Gilbert, G.K., 1914. Transportation of debris by running water, U.S. Geological Survey Professional Paper 86, 221 p.
- Gilbert, G.K., 1917. Hydraulic-mining debris in the Sierra Nevada, U.S. Geological Survey Professional Paper 105.
- Gipple, C.J., 1995. Environmental hydraulics of large woody debris in streams and rivers, Journal of Environmental Engineering, vol. 121, p. 388-395.
- Gomez, B., and Church, M., 1989. An assessment of bed load sediment transport formulae for gravel bed rivers, Water Resources Research, vol. 25, no. 6, p. 1161-1186.
- Gomez, B., Eden, D.N., Peacock, D.H., and Pinkney, E.J., 1998. Floodplain construction by recent rapid vertical accretion: Waipaop River, New Zealand, Earth Surface Processes and Landforms, vol. 23, no. 5., p. 405-413.
- Graf, W.H., 1971. Hydraulics of sediment transport, McGraw-Hill, New York.
- Graf, W.L., 2001. Damage control: restoring the physical integrity of America's rivers. Annals of the Association of American Geographers, vol. 91, no. 1, p. 1-27.
- Gray, L.J., and Ward, J.V., 1982. Effects of sediment releases from a reservoir on stream macroinvertebrates, Hydrobiologia, vol. 96, no. 2, p. 177-184.
- Hack, J.T., 1957. Studies of longitudinal stream profiles in Virginia and Maryland, U.S. Geological Survey Professional Paper 294-B, p. 45-97.
- Hansler, M.E., Sutherland, D.G., Hilton, S.J., and Lisle, T.E., 1998. Sediment wave dispersion and the analysis of a one-dimensional bedload transport model, Navarro River, California, Geological Society of America Abstracts with Programs, vol. 29, no. 6, A-360.

- Havis, R.N., Alonso, C.V., and King, J.G., 1996. Modeling sediment in gravel-bedded streams using HEC-6, *Journal of Hydraulic Engineering*, vol. 122, no. 10, p. 559-564.
- Hey, R.D., 1979. Flow resistance in gravel-bed rivers, *Journal of the Hydraulics Division, Proceedings of the American Society of Civil Engineers*, vol. 105, p. 365-379.
- Higgins, R.J., Pickup, G., and Cloke, P.S., 1987. Estimating the transport and deposition of mining waste at Ok Tedi, *in* Thorne, C.R., Bathurst, J.C., and Hey, R.D., eds., *Sediment transport in gravel-bed rivers*, Wiley, Chichester, p. 949-976.
- Hilmes, M.M., and Wohl, E.E., 1995. Changes in channel morphology associated with placer mining, *Physical Geography*, vol. 16, no. 3, p. 223-242.
- Hodkinson, A., 1996. Computational fluid dynamics as a tool for investigating separated flow in river bends, *Earth Surface Processes and Landforms*, vol. 21, p. 993-1000.
- Howard, A.D., and Dolan, R., 1981. Geomorphology of the Colorado River, *Journal of Geology*, v. 89, p. 269-298.
- James, L.A., 1991. Incision and morphologic evolution of an alluvial channel recovering from hydraulic mining sediment, *Geological Society of America Bulletin*, no. 103, p. 723-736.
- James, L.A., 1993. Sustained reworking of hydraulic mining sediment in California: G.K. Gilbert's sediment wave model reconsidered, *Z. Geomorph. N.F.*, vol. 88, p. 49-66.
- Jarrett, R.D., 1984. Hydraulics of high-gradient streams, *Journal of Hydraulics Division, American Society of Civil Engineers*, vol. 110, p. 1519-1539.
- Jarrett, R.D., 1985. Determination of roughness coefficients for stream in Colorado, U.S. Geological Survey Water-Resources Investigations Report 85-4004, 54 p.
- Jarrett, R.D., 1991. Wading measurements of vertical velocity profiles, *Geomorphology*, vol. 4, p. 243-247.
- Jarrett, R.D., 1992. Hydraulics of mountain rivers, *in* Yen, B.C., ed., *Channel flow resistance: centennial of Manning's formula*, Water resource Publications, Littleton, CO, p. 287-298.
- Jarrett, R.D. and Costa, J.E., 1986. Hydrology, geomorphology, and dam-break modeling of the July 15, 1982, Lawn lake Dam and cascade dam failures, Larimer county, Colorado, U.S. Geological Survey Professional Paper 1369.

- Jarrett, R.D., and Browning, T.W., 1999. Geomorphic estimates of rainfall, floods, and sediment runoff; applied to the 1996 wildfire, Buffalo Creek, Colorado, Geological Society of America Abstracts with Program, vol.31, no.7, p.313.
- Julien, P. Y., 1995. Erosion and sedimentation, Cambridge University Press, New York, NY, 280 p.
- Julien, P.Y., 2001. River mechanics, unpublished course notes for CE 717, 469 p.
- Keller, E.A., 1971. Areal sorting of bedload material, the hypothesis of velocity reversal, Geological Society of American Bulletin, vol. 82, p. 279-280.
- Keller, E.A., and Melhorn, W.N., 1978. Rhythmic spacing and origin of pools and riffles, Geological Society of America Bulletin, vol. 89, p. 723-730.
- King, I.P., 1990. Program documentation: RMA2- a two dimensional finite element model for flow in estuaries and streams, version 4.3, Resource Management Associates, Lafayette, California.
- Knighton, A.D., 1989. River adjustment to changes in sediment load: the effects of tin mining on the Ringarooma River, Tasmania, 1875-1984, Earth Surface Processes and Landforms, vol. 14, p. 333-359.
- Knighton, A.D., 1998. Fluvial forms and processes: a new perspective, Arnold, London, 383 p.
- Knighton, A.D, 1999. Downstream variation in stream power, Geomorphology, vol. 29, p. 293-306.
- Kondolf, G.M., and Matthews, W.V.G., 1993. Management of coarse sediment on regulated rivers. Report 80 Water Resources Center, University of CA, Davis.
- Krishnappan, B.G., 1985. Comparison of MOBED and HEC-6 river flow models, Canadian Journal of Civil Engineering, vol. 12, p. 464-471.
- Lane, S.N., and Richards, K.S., 1998. Two-dimensional modelling of flow processes in a multi-thread channel, Hydrological Processes, vol. 12, p. 1279-1298.
- Lane, S.N., Bradbrook, K.F., Richards, K.S., Biron, P.A., and Roy, A.G., 1999. The application of computational fluid dynamics to natural river channels: three-dimensional versus two-dimensional approaches, Geomorphology, vol. 29, p. 1-20.
- Leclerc, M., Boudreault, A., Bechara, J.A., and Corfa, G., 1995. Two-dimensional hydrodynamic modeling: a neglected tool in the instream flow incremental methodology, Transactions American Fisheries Society, vol. 124, no. 5, p. 645-662.

- LeMehaute, B., 1976. An introduction to hydrodynamics and water waves, Springer-Verlag, New York.
- Leopold, L.B., and Maddock, T., 1953. The hydraulic geometry of stream channels and some physiographic implications, U.S. Geological Survey Professional Paper 252-G, 57 p.
- Leopold, L.B., and Bull, W.B., 1979. Base level, aggradation, and grade, Proceedings of American Philosophical Society, vol. 123, p. 168-202.
- Leopold, L.B., Wolman, M.G., and Miller, J.P., 1964, Fluvial processes in geomorphology, W.H. Freeman and Company, San Francisco, California, 522 p.
- Limerinos, J.T., 1970. Determination of the Manning coefficient from measured bed roughness in natural channels, U.S. Geological Survey Water Supply Paper 1898-B, 47 p.
- Lisle, T.E., 1979. A sorting mechanism for a riffle-pool sequence: summary, Geological Society of America Bulletin, vol. 90, p. 616-617.
- Lisle, T.E., 1982. Effects of aggradation and degradation on riffle-pool morphology in natural gravel channels, northwestern California, Water Resources Research, vol. 18, no. 6, p. 1643-1651.
- Lisle, T.E., 1986. Stabilization of a gravel channel by large streamside obstructions and bedrock bends, Jacoby Creek, northwestern California, Geological Society of America Bulletin, vol. 97, p. 999-1011.
- Lisle, T.E., and Hilton, S., 1992. The volume of fine sediment in pools: and index of sediment supply in gravel-bed streams, Water Resources Bulletin vol. 28, no.20, American Water Resources Association, p. 371-383.
- Lisle, T.E., Nelson, J.M., Pitlick, J. Madej, M.A., and Barkett, B.L., 2000. Variability of bed mobility in natural, gravel-bed channels and adjustments to sediment load at local and reach scales, Water Resources Research, vol. 36, no. 12, p. 3743-3755.
- Mackin, J.H., 1948. Concept of a graded river, Geological Society of America Bulletin, vol., 59, p. 463-512.
- Madej, M.A., and Ozaki, V., 1996. Channel response to sediment wave propagation and movement, Redwood Creek, California, USA, Earth Surface Processes and Landforms, vol. 21, p. 911-927.
- Middleton, G.V., and Southard, J.B., 1984. Mechanics of sediment movement, S.E.P.M. Short Course Number 3, Providence, Rhode Island, 401 p.

- Milhous, R., T., 1982. Effect of sediment transport and flow regulation on the ecology of gravel-bed rivers, *in* Hey, R.D., Thorne, C.R., and Bathurst, J.C., eds., Gravel-bed rivers, John Wiley and Sons, Chichester, p. 819-842.
- Miller, A.J., 1994. Debris-fan effects and flood hydraulics in river canyons: some implications from two-dimensional flow modeling, *Earth Surface Processes and Landforms*, vol. 19, p. 681-697.
- Miller, A.J., 1995. Valley morphology and boundary conditions influencing spatial patterns of flood flow, *in* Costa, J.E., Miller, A.J., Potter, K.W., and Wilcock, P.R., eds., Natural and anthropogenic influences in fluvial geomorphology, *Geophysical Monograph 89*, American Geophysical Union, p. 57-81.
- Miller, A.J., and Cluer, B.L., 1998. Modeling considerations for simulation of flow in bedrock channels, *in* Tinkler, K.J., and Wohl, E.E., eds., Rivers over rock: fluvial processes in bedrock channels, *Geophysical Monograph 107*, American Geophysical Union, p. 61-104.
- Molls, T., and Chaudhry, M.H., 1995. Depth-averaged open-channel flow model, *Journal of Hydraulic Engineering*, vol. 121, no. 6, p. 453-465.
- Montgomery, D.R., Panfil, M.S., Hayes, S.K., 1999. Channel-bed mobility response to extreme sediment loading at Mount Pinatubo, *Geology*, no. 27, vol. 3, p. 271-274.
- Nelson, J.M., 1996. Predictive techniques for river channel evolution and maintenance, *Water, Soil, and Air Pollution*, vol. 90, p. 321-333.
- Norton, W.R., King, I.P., and Orlob, G.T., 1973. A finite element model for lower Granite Reservoir, Water Resources Engineers, Inc., Walnut Creek, California.
- O'Connor, J.E., 1993. Hydrology, hydraulics, and geomorphology of the Bonneville Flood, *Geological Society of America Special Paper 274*, 83 p.
- O'Connor, J.E., and Webb, R.H., 1988. Hydraulic modeling for paleoflood analysis, *in* Baker, V.R., Kochel, R.C., and Patton, P.C., eds., *Flood Geomorphology*, John Wiley and Sons, Inc., New York, NY, p. 393-402.
- Parker, G., Cui, Y., Imran, J., and Dietrich, W., 1996. Flooding in the Lower Ok Tedi, Papua New Guinea due to disposal of mine tailing and its amelioration, *in* International seminar on recent trends of floods and their preventive measures, Post-seminar proceedings, Hokkaido River Disaster Prevention Research Center, Japan, p. 21-48.
- Patton, P.C., Baker, V.R., and Kochel, R.C., 1979. Slackwater deposits: a geomorphic technique for the interpretation of fluvial paleohydrology, *in* Rhodes, D.D., and Williams, G.P., eds., *Adjustments of the fluvial system*, Kendall/Hunt Publishing Co., Dubuque, Iowa.

- Peterson, M.R., Zevenbergen, L.W., and Blevins, J., 1995. Design of artificial riffles using RMA-2V two-dimensional hydraulic model, Proceedings of the First International Conference of Water Resources Engineering, San Antonio, Texas, August 14-18.
- Pickup, G., 1980. Hydrologic and sediment modelling studies in the environmental impact assessment of a major tropical dam project, *Earth Surface Processes and Landforms*, vol. 5, p. 61-75.
- Pickup, G. Higgins, R.J., and Warner, R.F., 1979. Erosion and sediment yield in Fly River drainage basins, Papua New Guinea, *International Association of Hydrological Science*, Publication No. 132, p. 438-456.
- Pickup, G., Higgins, R.J., and Grant, I., 1983. Modelling sediment transport as a moving wave – the transfer and deposition of mining waste, *Journal of Hydrology*, vol. 60, p. 281-301.
- Pitlick, J.C., 1993. Response and recovery of a subalpine stream following a catastrophic flood, *Geological Society of America Bulletin*, vol. 105, p. 657-670.
- Rathburn, S.L., 1993. Pleistocene cataclysmic flooding along the Big Lost River, east central Idaho, *Geomorphology*, vol. 8, p. 305-319.
- Rathburn, S.L., and Wohl, E.E., 2001. One-dimensional sediment transport modeling of pool recovery along a mountain channel after a reservoir sediment release, *Regulated Rivers Research and Management*, vol. 17, p. 251-273.
- Richardson, E.V., Simons, D.B., and Julien, P.Y., 1990. Highways in the river environment, U.S. Dept. of Transportation, Federal Highways Administration.
- Rubin, D.M. and McDonald, R.R., 1995. Nonperiodic eddy pulsations, *Water Resources Research*, vol. 31, no. 6, p. 1595-1605.
- Rubin, D.M., Schmidt, J.C., and Moore, J.N., 1990. Origin, structure, and evolution of a reattachment bar, Colorado River, Grand Canyon, Arizona, *Journal of Sedimentary Petrology*, vol. 60, no. 6, p. 982-991.
- Rutherford, I., 2001. Storage and movement of slugs of sand in a large catchment: developing a plan to rehabilitate the Glenelg River, SE Australia, *in* Anthony, D.J., Harvey, M.D., Laronne, J.B. and Mosely, M.P., eds., *Applying geomorphology to environmental management*, p. 309-333.
- Schlichting, H., 1979. *Boundary-layer theory*, McGraw-Hill, New York, 814 p.
- Schmidt, J.C., 1990. Recirculating flow and sedimentation in the Colorado River in Grand Canyon, Arizona, *Journal of Geology*, vol. 98, p. 709-724.

- Schmidt, J.C., and Rubin, D.M., 1995. Regulated streamflow, fine-grained deposits, and effective discharge in canyons with abundant debris fans, *in* Costa, J.E., Miller, A.J., Potter, K.W., and Wilcock, P.R., eds., *Natural and anthropogenic influences in fluvial geomorphology*, Geophysical Monograph 89, American Geophysical Union, p. 177-195.
- Schmidt, J.C., Rubin, D.M., and Ikeda, H., 1993. Flume simulation of recirculating flow and sedimentation, *Water Resources Research*, vol. 29, no. 8, p. 2925-2939.
- Schumm, S.A., 1965. Quaternary paleohydrology, *in* Wright, H.E., Jr. and Frey, D.G., eds., *The Quaternary of the United States*, Princeton University Press, Princeton, p. 783-794.
- Schumm, S.A., 1973. Geomorphic thresholds and the complex response of drainage systems, *in* Morisawa, M., ed., *Fluvial geomorphology*, Publications in Geomorphology, State University of New York, Binghamton, p. 299-310.
- Shields, F.D., Jr., Knight, S.S., and Cooper, C.M., 1994. Effects of channel incision on baseflow stream habitats and fishes, *Environmental Management*, vol. 18, p. 43-57.
- Shroba, R.R., Schmidt, P.W., Crosby, E.J., Hansen, W.R., and Soule, J.M., 1979. Geologic and geomorphic effects in the Big Thompson Canyon area, Larimer county, U.S. geological survey Professional Paper 1115B, p. 87-152.
- Simoes, F.J., and Yang, C.T., 2000. GSTARS3.0- A model for reservoir sedimentation, AGU Abstracts with Programs, American Geophysical Union Annual Meeting, San Francisco, CA.
- Simon, A. 1999. Channel and drainage-basin response of the Toutle River system in the aftermath of the 1980 eruption of Mount St. Helens, Washington, U.S., Geological Survey Open-File Report 96-633.
- Smart, G.M., 1984. Sediment transport formula for steep channels, *Journal of Hydraulic Engineering*, vol. 110, p. 267-276.
- Statzner, B., Gore, J.A., and Resh, V.H., 1988. Hydraulic stream ecology: observed patterns and potential applications, *Journal of North American Benthological Society*, vol. 7, no. 4, p. 307-360.
- Stewart, G.S., 2001. Two-dimensional hydraulic modeling for making instream-flow recommendations, Unpublished MS thesis, Colorado State University, Ft. Collins, CO, 80 p.

- Stoker, B.A., and Williams, D.T., 1991. Sediment modeling of dam removal alternatives, Elwha River, Washington, *in* Shane, R.M., ed., *Hydraulic Engineering: Proceedings of the National Conference on Hydraulic Engineering*, American Society of Civil Engineers, New York, p. 674-679.
- Sullivan, K., Lisle, T.E., Dolloff, C.A., Grant, G.E., and Reid, L.M., 1987. Stream channels: the link between forest and fishes, *in* Salo, E.O., and Cundy, T.W., eds., *Streamside management, forestry and fishery interactions*, College of Forest Resources, Univ. of Washington, Seattle, WA, p. 39-97.
- Sutherland, D.G., 1987. Static armour layers by selective erosion, *in* Thorne, C.R., Bathurst, J.C., and Hey, R.D., eds., *Sediment transport in gravel-bed rivers*, Chichester, UK, John Wiley and Sons, p. 243-267.
- Sutherland, D.G., Hansler, M.E., Hilton, S.J., and Lisle, T.E., 1998. Sediment wave evolution and channel morphologic changes resulting from a landslide, Navarro River, northwestern California, *Geological Society of America Abstracts with Programs*, vol. 29, no. 6, A-360.
- The Nature Conservancy, 2001. North Fork Cache la Poudre River: Phantom Canyon Preserve restoration recommendations, The Nature Conservancy unpublished report, 5 p.
- Thompson, D.M., 1994. Hydraulics and sediment transport processes in a pool-riffle Rocky Mountain stream, Unpublished MS thesis, Colorado State University, ft. Collins, CO, 288 p.
- Thompson, D.M., 1997. Hydraulics and pool geometry, Unpublished PhD dissertation, Colorado State University, Ft. Collins, CO, 260 p.
- Thompson, D. M., Nelson, J.M., and Wohl, E.E., 1998. Interactions between pool geometry and hydraulics, *Water Resources Research*, vol. 34, no. 12, p. 3673-3681.
- Thompson, D.M., Wohl, E.E., and Jarrett, R.D., 1996. A revised velocity-reversal and sediment-sorting model for a high-gradient, pool-riffle stream, *Physical Geography*, vol. 17, p. 142-156.
- Tingsanchali, T., and Supharatid, S., 1996. Experimental investigation and analysis of HEC-6 river morphological model, *Hydrological Processes*, vol. 10, p. 747-761.
- Tritton, D.J., 1988. *Physical Fluid Dynamics*, Clarendon Press, Oxford, 519 p.
- Tweto, O., 1979. *Geologic Map of Colorado*. U.S. Geological Survey, Denver, CO.
- U.S. Army Corps of Engineers, Hydrologic Engineering Center, 1998a. HEC-6 Scour and Deposition in Rivers and Reservoirs User's Manual, version 4.1, 164 p.

- U.S. Army Corps of Engineers, Hydrologic Engineering Center, 1998b. HEC-RAS River Analysis System User's Manual, version 2.2, 230 p.
- U.S. Geological Survey, 1999. Scour and Fill for Windows, version 2.0, Redwood National Park, Arcata, CA.
- van Rijn, L.C., 1984. Sediment Transport, Part III: Bedforms and alluvial roughness. *Journal Hydraulic Division, ASCE*, vol. 10, no. 12.
- Wick, E.J., 1997. Physical processes and habitat critical to the endangered razorback sucker on the Green River, Utah, Unpublished Doctoral Dissertation, Colorado State University, Ft. Collins, CO., 145 p.
- Wilcock, P.R., Kondolf, G.M., Matthews, W.V.G., Barta, A.F., 1996. Specification of sediment maintenance flows for a large gravel-bed river, *Water Resources Research*, vol., 32, no. 9, p. 2911-2921.
- Williams, D.T., 1977. Effects of dam removal: an approach to sedimentation, Hydrologic Engineering Center Technical Paper 50, U.S. Army Corps of Engineers, Davis, CA, 31 p.
- Williams, G.P., and Wolman, M.G., 1984. Downstream effect of dams on alluvial rivers, U.S. Geological Survey Professional Paper 1286, Government Printing Office, Washington, DC, 83 p.
- Wohl, E.E., 1992. Bedrock benches and boulder bars: floods in the Burdekin Gorge of Australia, *Geological Society of America Bulletin*, vol. 104, p. 770-778.
- Wohl, E.E., 1999. Inheriting our past: river sediment sources and sediment hazards in Colorado, *Colorado Water Resources Research Institute Water in the Balance*, no. 7, 26 p.
- Wohl, E.E., 2000. Mountain Rivers, *Water Resources Monograph 14*, American Geophysical Union, Washington, DC, 320 p.
- Wohl, E.E., and Cenderelli, D., 2000. Sediment deposition and transport patterns following a reservoir sediment release, *Water Resources Research*, vol. 36, no. 1, p. 319-333.
- Wohl, E.E., Vincent, K.R., and Merritts, D.J., 1993. Pool and riffle characteristics in relation to channel gradient, *Geomorphology*, vol. 6, p. 99-110.
- Wolman, M.G., 1954. A method of sampling coarse river-bed material, *EOS Transactions 35*, American Geophysical Union, no. 6, p. 951-956.

- Yang, C.T., 1973. Incipient motion and sediment transport, *Journal of Hydraulics Division*, 99 (HY10), p. 1679-1703.
- Yang, C.T., and Simoes, F.J., 1998. Simulation and prediction of river morphologic changes using GSTARS 2.0, *Proceedings of Third International Conference on Hydro-Science and Engineering*, Cottbus/Berlin, Germany, Aug. 31-Sept. 3.
- Yang, C.T., Trevino, M.A., and Simoes, F.J., 1998a. User's Manual for Generalized Stream Tube model for Alluvial River Simulation version 2.0 (GSTARS 2.0), U.S. Bureau of Reclamation Technical Service Group, Sedimentation and River Hydraulics Group, Denver, CO, 170 p.
- Yang, C.T., Trevino, M.A., and Simoes, F.J., 1998b. An enhanced generalized stream tube model for alluvial river simulation. *Proceedings of First Federal Interagency Hydrologic Modeling Conference*, Las Vegas, NV, April 19-23, p. 8.143-8.150.
- Zevenbergen, L.W., Peterson, M.R., and Remus, J.I., 1995. Two-dimensional sediment transport model of the Missouri-Platte River confluence, *Proceedings of the First International Conference of Water Resources Engineering*, San Antonio, Texas, August 14-18.
- Zuellig, R.E., Kondratieff, B.C., and Rhodes, H.A., in press. Benthos recovery after an episodic sediment release into a Colorado Rocky Mountain river, *Western North American Naturalist*.

APPENDIX A
SEDIMENT TRANSPORT EQUATIONS

Bedload Equations:

1) DuBoys Formula:
$$q_{bv} = \frac{0.173}{d_s^{3/4}} \tau_o (\tau_o - 0.0125 - 0.019d_s)$$

2) Meyer-Peter and Muller:
$$q_{bv} = 8(\tau_* - \tau_{*c})^{3/2} \sqrt{(G-1)gd_s^3}$$

3) Schoklitsch:
$$q_{bv} = \frac{2.5}{\rho_s/\rho} S^{3/2} (q - q_c)$$

$$\text{where } q_c = 0.26 \left(\frac{\rho_s}{\rho} - 1 \right)^{5/3} \frac{d_{40}^{3/2}}{S^{7/6}}$$

Total Load Equations:

4) Ackers and White:
$$C_W = c_{AW2} G \frac{d_s}{h} \left(\frac{V}{u_*} \right)^{c_{AW1}} \left[\frac{c_{AW5}}{c_{AW3}} - 1 \right]^{c_{AW4}}$$

$$c_{AW5} = \frac{u_*^{c_{AW1}}}{\sqrt{(G-1)gd_s}} \left[\frac{V}{\sqrt{32 \log(10h/d_s)}} \right]^{1-c_{AW1}}$$

for $1.0 < d_* < 60.0$ ($d_* = 6.8$, in this case),

$$c_{AW1} = 1.0 - 0.56 \log d_*$$

$$\log c_{AW2} = 2.8c6 \log d_* - (\log d_*)^2 - 3.53$$

$$c_{AW3} = \frac{0.23}{d_*^{1/2}} + 1.34$$

$$c_{AW4} = \frac{9.66}{d_*} + 1.34$$

5) Yang (1973) for sand:

$$\log C_{ppm} = 5.435 - 0.286 \log \frac{\omega d_s}{\nu} - 0.457 \log \frac{u_*}{\omega} + (1.799 - 0.409 \log \frac{\omega d_s}{\nu} - 0.314 \log \frac{u_*}{\omega}) \times \log \left(\frac{VS}{\omega} - \frac{V_c S}{\omega} \right)$$

$$\frac{V_c}{\omega} = \frac{2.5}{\log(u_* d_s / \nu) - 0.06} + 0.66 \text{ for } 1.2 < \frac{u_* d_s}{\nu} < 70$$

6) Engelund and Hansen:
$$C_w = 0.05 \left(\frac{G}{G-1} \right) \frac{VS_f}{[(G-1)gd_s]^{1/2}} \left[\frac{R_h S_f}{(G-1)d_s} \right]^{1/2}$$

7) Julien
$$Q_s = wq_s$$

where $q_s \cong 18\sqrt{gd_s^3\tau_*^2}$

Notation

| | |
|--------------|--|
| C_{ppm} | total sediment concentration by weight |
| d_s | particle size, d_{50} of the bed material used, unless otherwise specified |
| d_* | dimensionless particle diameter |
| g | gravitational acceleration |
| G | specific gravity |
| h | flow depth |
| q | water discharge per unit width of flow |
| q_c | critical value of q for initiation of sediment transport |
| q_{bv} | unit bedload discharge measured by volume (converted to mass for plotting on Figure 6) |
| w | channel width |
| R_h | hydraulic radius |
| S | channel slope |
| S_f | friction slope |
| u_* | shear velocity |
| V | depth-averaged flow velocity |
| V_c | average flow velocity at incipient motion |
| V_c/ω | dimensionless critical velocity at incipient motion |
| VS | unit stream power |
| ν | kinematic viscosity |
| ρ | density of water |
| ρ_s | density of sediment |
| ω | fall velocity |
| τ_0 | boundary shear stress |
| τ_* | dimensionless shear stress (Shields parameter) |
| τ_{*c} | critical bed shear stress (critical values of Shields parameter) |

APPENDIX B

HEC-RAS SENSITIVITY ANALYSIS

Q=3.4 m³/s; pool n=0.04; no change to riffle Manning value

| Cross Sec | Min Channel Elev (m) | <i>n</i> = +10% | <i>n</i> = -10% | <i>n</i> = +25% | <i>n</i> = -25% | <i>n</i> = +50% | <i>n</i> = -50% |
|-----------|-------------------------|-----------------|-----------------|-----------------|-----------------|-----------------|-----------------|
| | | WS Elev (m) | WS Elev (m) | WS Elev (m) | WS Elev (m) | WS Elev (m) | WS Elev (m) |
| 1 | 101.37 | 102.13 | 102.12 | 102.14 | 102.11 | 102.16 | 102.09 |
| 2 | 100.85 | 102.13 | 102.12 | 102.14 | 102.12 | 102.15 | 102.10 |
| 3 | 100.82 | 102.12 | 102.12 | 102.13 | 102.11 | 102.15 | 102.10 |
| 4 | 101.24 | 102.12 | 102.11 | 102.13 | 102.10 | 102.14 | 102.09 |
| 5 | 101.43 | 101.94 | 101.94 | 101.94 | 101.94 | 101.94 | 101.94 |
| 6 | 100.68 | 101.66 | 101.66 | 101.66 | 101.66 | 101.66 | 101.66 |
| 7 | 100.57 | 101.19 | 101.19 | 101.19 | 101.19 | 101.19 | 101.19 |
| 8 | 100.18 | 100.94 | 100.94 | 100.94 | 100.94 | 100.94 | 100.94 |
| 9 | 99.97 | 100.52 | 100.52 | 100.52 | 100.52 | 100.52 | 100.52 |
| 10 | 99.25 | 100.04 | 100.04 | 100.04 | 100.04 | 100.04 | 100.04 |
| 11 | 98.86 | 99.35 | 99.35 | 99.35 | 99.35 | 99.35 | 99.35 |
| 12 | 98.27 | 99.17 | 99.15 | 99.19 | 99.13 | 99.22 | 99.10 |
| 13 | 98.04 | 99.16 | 99.13 | 99.17 | 99.12 | 99.19 | 99.09 |
| 14 | 98.38 | 99.12 | 99.10 | 99.13 | 99.09 | 99.14 | 99.06 |
| 15 | 98.09 | 98.95 | 98.95 | 98.95 | 98.95 | 98.95 | 98.95 |
| 16 | 98.03 | 98.60 | 98.60 | 98.60 | 98.60 | 98.60 | 98.60 |
| 17 | 97.77 | 98.30 | 98.30 | 98.30 | 98.30 | 98.30 | 98.30 |
| 18 | 97.56 | 98.28 | 98.28 | 98.28 | 98.28 | 98.28 | 98.28 |
| 19 | 97.33 | 98.27 | 98.27 | 98.27 | 98.27 | 98.27 | 98.27 |

Q = 10.1 m³/s; pool n=0.04; no change to riffle Manning value

| Cross Sec | Min Channel Elev (m) | <i>n</i> = +10% | <i>n</i> = -10% | <i>n</i> = +25% | <i>n</i> = -25% | <i>n</i> = +50% | <i>n</i> = -50% |
|-----------|-------------------------|-----------------|-----------------|-----------------|-----------------|-----------------|-----------------|
| | | WS Elev (m) | WS Elev (m) | WS Elev (m) | WS Elev (m) | WS Elev (m) | WS Elev (m) |
| 1 | 101.37 | 102.48 | 102.46 | 102.50 | 102.45 | 102.53 | 102.43 |
| 2 | 100.85 | 102.50 | 102.48 | 102.51 | 102.47 | 102.53 | 102.46 |
| 3 | 100.82 | 102.48 | 102.46 | 102.48 | 102.45 | 102.50 | 102.44 |
| 4 | 101.24 | 102.47 | 102.46 | 102.48 | 102.45 | 102.49 | 102.44 |
| 5 | 101.43 | 102.36 | 102.36 | 102.36 | 102.36 | 102.36 | 102.36 |
| 6 | 100.68 | 102.06 | 102.06 | 102.06 | 102.06 | 102.06 | 102.06 |
| 7 | 100.57 | 101.61 | 101.61 | 101.61 | 101.61 | 101.61 | 101.61 |
| 8 | 100.18 | 101.32 | 101.32 | 101.32 | 101.32 | 101.32 | 101.32 |
| 9 | 99.97 | 100.82 | 100.82 | 100.82 | 100.82 | 100.82 | 100.82 |
| 10 | 99.25 | 100.39 | 100.39 | 100.39 | 100.39 | 100.39 | 100.39 |
| 11 | 98.86 | 99.60 | 99.60 | 99.60 | 99.60 | 99.60 | 99.60 |
| 12 | 98.27 | 99.61 | 99.59 | 99.63 | 99.57 | 99.66 | 99.55 |
| 13 | 98.04 | 99.57 | 99.55 | 99.59 | 99.53 | 99.61 | 99.50 |
| 14 | 98.38 | 99.55 | 99.54 | 99.57 | 99.53 | 99.59 | 99.51 |
| 15 | 98.09 | 99.24 | 99.24 | 99.24 | 99.24 | 99.24 | 99.24 |
| 16 | 98.03 | 98.80 | 98.80 | 98.80 | 98.80 | 98.80 | 98.80 |
| 17 | 97.77 | 98.62 | 98.62 | 98.62 | 98.62 | 98.62 | 98.62 |
| 18 | 97.56 | 98.56 | 98.56 | 98.56 | 98.56 | 98.56 | 98.56 |
| 19 | 97.33 | 98.54 | 98.54 | 98.54 | 98.54 | 98.54 | 98.54 |

Note: Cross Sections 1-4 are located within the Ouzel Pool; Stations 12-15 are within the Tick Pool.

APPENDIX C

HEC-6 SENSITIVITY ANALYSIS

| Sensitivity Analysis # | σ_{10} | σ_{20} | c | s | Movable Bed Limits | Iterations | Cohesive Seds | Sed. Transport Eq | Sed. Inflow | Bed Gradation | Starting WSEL (ft) | Time step (days) | Water Temp (deg F) | Simulation length (days) | Cross section | Qualitative Oct-Mar Thalgw Change | Oct-Mar Thalgw Change (ft) | Oct Thalgw Elevation (ft) | March Thalgw Elevation (ft) | Average HEC-6 Bed Change (ft) | HEC-6 Thalgw Elevation (ft) | HEC-6 WSEL (ft) | Modeling Accuracy (%) |
|------------------------|---------------|---------------|-----|-----|--------------------|------------|---------------|-------------------|-------------|-----------------------|--------------------|------------------|--------------------|--------------------------|---------------|-----------------------------------|----------------------------|---------------------------|-----------------------------|-------------------------------|-----------------------------|-----------------|-----------------------|
| 1 | | | 0.1 | 0.3 | default | default | default | Ackers-White | 3 Q and Qs | Xsec 1, 5, 13, 12, 17 | 320.58 | 2-8 | 40 | 37 | | | | | | | | | |
| (Oct-Mar) | 0.04 | 0.04 | | | | | | | | | | | | | 1 | None | 0.00 | 332.59 | 332.59 | -0.13 | 332.46 | 334.33 | |
| | 0.04 | 0.04 | | | | | | | | | | | | | 2 | Agradded | 3.93 | 330.86 | 334.79 | 0.29 | 331.15 | 334.33 | 7.4 |
| | 0.04 | 0.04 | | | | | | | | | | | | | 3 | Agradded | 1.61 | 330.76 | 332.37 | 0.01 | 330.77 | 334.32 | 0.6 |
| | 0.04 | 0.04 | | | | | | | | | | | | | 4 | Agradded | 2.46 | 332.14 | 334.63 | 0.02 | 332.16 | 334.33 | 0.6 |
| | 0.07 | 0.07 | | | | | | | | | | | | | 5 | None - r/fle | 0.00 | 332.76 | 332.76 | 0 | 332.76 | 333.81 | |
| | 0.07 | 0.07 | | | | | | | | | | | | | 6 | None - r/fle | 0.00 | 330.31 | 330.31 | 0 | 330.31 | 332.89 | |
| | 0.07 | 0.07 | | | | | | | | | | | | | 7 | None - r/fle | 0.00 | 329.96 | 329.96 | 0 | 329.96 | 331.32 | |
| | 0.07 | 0.07 | | | | | | | | | | | | | 8 | None - r/fle | 0.00 | 328.66 | 328.66 | 0 | 328.66 | 330.48 | |
| | 0.07 | 0.07 | | | | | | | | | | | | | 9 | None - r/fle | 0.00 | 327.98 | 327.98 | 0 | 327.98 | 329.49 | |
| | 0.07 | 0.07 | | | | | | | | | | | | | 10 | None - r/fle | 0.00 | 325.62 | 325.62 | 0 | 325.62 | 327.58 | |
| | 0.07 | 0.07 | | | | | | | | | | | | | 11 | None - r/fle | 0.00 | 324.33 | 324.33 | -0.98 | 323.35 | 324.58 | |
| | 0.04 | 0.04 | | | | | | | | | | | | | 12 | Scoured | -2.06 | 322.4 | 320.34 | -0.09 | 322.31 | 324.58 | 4.4 |
| | 0.04 | 0.04 | | | | | | | | | | | | | 13 | Scoured | -0.73 | 321.64 | 320.91 | -0.11 | 321.53 | 324.56 | 15.2 |
| | 0.04 | 0.04 | | | | | | | | | | | | | 14 | Agradded | 1.63 | 322.76 | 324.39 | -0.12 | 322.64 | 324.07 | -7.4 |
| | 0.04 | 0.04 | | | | | | | | | | | | | 15 | None | 0.00 | 321.81 | 321.81 | 0 | 321.81 | 323.47 | |
| | 0.07 | 0.07 | | | | | | | | | | | | | 16 | None - r/fle | 0.00 | 321.63 | 321.63 | -0.93 | 321.6 | 323.06 | |
| | 0.07 | 0.07 | | | | | | | | | | | | | 17 | None - r/fle | 0.00 | 320.78 | 320.78 | 0 | 320.78 | 321.83 | |
| | 0.07 | 0.07 | | | | | | | | | | | | | 18 | None - r/fle | 0.00 | 320.07 | 320.07 | 0 | 320.08 | 321 | 0.0 |
| | 0.07 | 0.07 | | | | | | | | | | | | | 19 | None - r/fle | 0.00 | 319.32 | 319.32 | 0 | 319.32 | 320.63 | 0.0 |
| 1a | | | 0.1 | 0.3 | default | 25 | default | Ackers-White | 3 Q and Qs | Xsec 1, 5, 10, 12, 17 | 320.58 | 2-8 | 40 | 37 | | | | | | | | | |
| | 0.04 | 0.04 | | | | | | | | | | | | | 1 | None | 0.00 | 332.59 | 332.59 | -0.15 | 332.44 | 334.33 | |
| | 0.04 | 0.04 | | | | | | | | | | | | | 2 | Agradded | 3.93 | 330.86 | 334.79 | 1.48 | 332.34 | 334.33 | 37.6 |
| | 0.04 | 0.04 | | | | | | | | | | | | | 3 | Agradded | 1.61 | 330.76 | 332.37 | 0 | 330.76 | 334.32 | 0.0 |
| | 0.04 | 0.04 | | | | | | | | | | | | | 4 | Agradded | 2.46 | 332.14 | 334.60 | 0.01 | 332.15 | 334.29 | 0.4 |
| | 0.07 | 0.07 | | | | | | | | | | | | | 5 | None - r/fle | 0.00 | 332.76 | 332.76 | 0.02 | 332.78 | 333.8 | |
| | 0.07 | 0.07 | | | | | | | | | | | | | 6 | None - r/fle | 0.00 | 330.31 | 330.31 | 0.01 | 330.32 | 332.8 | |
| | 0.07 | 0.07 | | | | | | | | | | | | | 7 | None - r/fle | 0.00 | 329.96 | 329.96 | 0.01 | 329.97 | 331.31 | |
| | 0.07 | 0.07 | | | | | | | | | | | | | 8 | None - r/fle | 0.00 | 328.66 | 328.66 | 0.03 | 328.69 | 330.48 | |
| | 0.07 | 0.07 | | | | | | | | | | | | | 9 | None - r/fle | 0.00 | 327.98 | 327.98 | 0.01 | 327.99 | 329.44 | |
| | 0.07 | 0.07 | | | | | | | | | | | | | 10 | None - r/fle | 0.00 | 325.62 | 325.62 | 0.02 | 325.64 | 327.58 | |
| | 0.07 | 0.07 | | | | | | | | | | | | | 11 | None - r/fle | 0.00 | 324.33 | 324.33 | -0.4 | 323.93 | 325.23 | |
| | 0.04 | 0.04 | | | | | | | | | | | | | 12 | Scoured | -2.06 | 322.4 | 320.34 | -0.07 | 322.33 | 324.54 | 3.4 |
| | 0.04 | 0.04 | | | | | | | | | | | | | 13 | Scoured | -0.73 | 321.64 | 320.91 | -0.03 | 321.61 | 324.5 | 4.1 |
| | 0.04 | 0.04 | | | | | | | | | | | | | 14 | Agradded | 1.63 | 322.76 | 324.39 | -0.08 | 322.66 | 324.05 | -4.9 |
| | 0.04 | 0.04 | | | | | | | | | | | | | 15 | None | 0.00 | 321.81 | 321.81 | -0.03 | 321.78 | 323.5 | |
| | 0.07 | 0.07 | | | | | | | | | | | | | 16 | None - r/fle | 0.00 | 321.63 | 321.63 | 0 | 321.63 | 323.06 | |
| | 0.07 | 0.07 | | | | | | | | | | | | | 17 | None - r/fle | 0.00 | 320.78 | 320.78 | 0 | 320.78 | 321.83 | |
| | 0.07 | 0.07 | | | | | | | | | | | | | 18 | None - r/fle | 0.00 | 320.07 | 320.07 | 0 | 320.08 | 320.85 | |
| | 0.07 | 0.07 | | | | | | | | | | | | | 19 | None - r/fle | 0.00 | 319.32 | 319.32 | 0 | 319.32 | 320.63 | |

| 16 | | 0.1 | 0.3 | 50 | default | Ackers-Whyte | 3 Q and Os | Xsec 1, 5, 10, 12, 17 | 320.58 | 2-8 | 40 | 37 | | | | | | | | | |
|----|------|------|--------|----|---------|--------------|------------|-----------------------|--------|-----|----|----|----|--------------|-------|--------|--------|-------|--------|--------|------|
| | 0.04 | 0.04 | | | | | | | | | | | 1 | None | 0.00 | 332.59 | 332.59 | -0.12 | 332.47 | 334.32 | |
| | 0.04 | 0.04 | | | | | | | | | | | 2 | Agradded | 3.93 | 330.86 | 334.79 | 1.46 | 332.32 | 334.32 | 37.1 |
| | 0.04 | 0.04 | | | | | | | | | | | 3 | Agradded | 1.61 | 330.76 | 332.37 | 0.01 | 330.77 | 334.31 | 0.6 |
| | 0.04 | 0.04 | | | | | | | | | | | 4 | Agradded | 2.46 | 332.14 | 334.60 | 0 | 332.14 | 334.28 | 0.0 |
| | 0.07 | 0.07 | 332.76 | | | | | | | | | | 5 | None - rifle | 0.00 | 332.76 | 332.76 | 0 | 332.76 | 333.81 | |
| | 0.07 | 0.07 | 330.31 | | | | | | | | | | 6 | None - rifle | 0.00 | 330.31 | 330.31 | 0 | 330.31 | 332.89 | |
| | 0.07 | 0.07 | 329.96 | | | | | | | | | | 7 | None - rifle | 0.00 | 329.96 | 329.96 | 0 | 329.96 | 331.32 | |
| | 0.07 | 0.07 | 328.66 | | | | | | | | | | 8 | None - rifle | 0.00 | 328.66 | 328.66 | 0 | 328.66 | 330.51 | |
| | 0.07 | 0.07 | 327.88 | | | | | | | | | | 9 | None - rifle | 0.00 | 327.88 | 327.88 | 0 | 327.88 | 329.31 | |
| | 0.07 | 0.07 | 325.62 | | | | | | | | | | 10 | None - rifle | 0.00 | 325.62 | 325.62 | 0 | 325.62 | 327.87 | |
| | 0.07 | 0.07 | 324.33 | | | | | | | | | | 11 | None - rifle | 0.00 | 324.33 | 324.33 | 0 | 324.33 | 325.62 | |
| | 0.04 | 0.04 | | | | | | | | | | | 12 | Scoured | -2.06 | 322.4 | 320.34 | -0.09 | 322.31 | 324.59 | 4.4 |
| | 0.04 | 0.04 | | | | | | | | | | | 13 | Scoured | -0.73 | 321.64 | 320.91 | -0.12 | 321.52 | 324.56 | 16.5 |
| | 0.04 | 0.04 | | | | | | | | | | | 14 | Agradded | 1.63 | 322.76 | 324.38 | -0.03 | 322.73 | 324.08 | -1.8 |
| | 0.04 | 0.04 | | | | | | | | | | | 15 | None | 0.00 | 321.81 | 321.81 | 0 | 321.81 | 323.5 | |
| | 0.07 | 0.07 | 321.63 | | | | | | | | | | 16 | None - rifle | 0.00 | 321.63 | 321.63 | 0 | 321.63 | 323.08 | |
| | 0.07 | 0.07 | 320.78 | | | | | | | | | | 17 | None - rifle | 0.00 | 320.78 | 320.78 | 0 | 320.78 | 321.83 | |
| | 0.07 | 0.07 | 320.08 | | | | | | | | | | 18 | None - rifle | 0.00 | 320.07 | 320.07 | 0 | 320.08 | 320.95 | |
| | 0.07 | 0.07 | 319.32 | | | | | | | | | | 19 | None - rifle | 0.00 | 319.32 | 319.32 | 0 | 319.32 | 320.63 | |
| 2 | | 0.1 | 0.3 | 50 | default | DuBoys's | 3 Q and Os | Xsec 1, 5, 10, 12, 17 | 320.58 | 2-8 | 40 | 37 | | | | | | | | | |
| | 0.04 | 0.04 | | | | | | | | | | | 1 | None | 0.00 | 332.59 | 332.59 | -0.34 | 332.25 | 334.32 | |
| | 0.04 | 0.04 | | | | | | | | | | | 2 | Agradded | 3.93 | 330.86 | 334.79 | 0 | 330.86 | 334.32 | 0.0 |
| | 0.04 | 0.04 | | | | | | | | | | | 3 | Agradded | 1.61 | 330.76 | 332.37 | 0.01 | 330.77 | 334.31 | 0.6 |
| | 0.04 | 0.04 | | | | | | | | | | | 4 | Agradded | 2.46 | 332.14 | 334.60 | 0.01 | 332.15 | 334.28 | 0.4 |
| | 0.07 | 0.07 | 332.76 | | | | | | | | | | 5 | None - rifle | 0.00 | 332.76 | 332.76 | 0 | 332.76 | 333.81 | |
| | 0.07 | 0.07 | 330.31 | | | | | | | | | | 6 | None - rifle | 0.00 | 330.31 | 330.31 | 0 | 330.31 | 332.89 | |
| | 0.07 | 0.07 | 329.96 | | | | | | | | | | 7 | None - rifle | 0.00 | 329.96 | 329.96 | 0 | 329.96 | 331.32 | |
| | 0.07 | 0.07 | 328.66 | | | | | | | | | | 8 | None - rifle | 0.00 | 328.66 | 328.66 | 0 | 328.66 | 330.51 | |
| | 0.07 | 0.07 | 327.88 | | | | | | | | | | 9 | None - rifle | 0.00 | 327.88 | 327.88 | 0 | 327.88 | 329.32 | |
| | 0.07 | 0.07 | 325.62 | | | | | | | | | | 10 | None - rifle | 0.00 | 325.62 | 325.62 | 0 | 325.62 | 327.87 | |
| | 0.07 | 0.07 | 324.33 | | | | | | | | | | 11 | None - rifle | 0.00 | 324.33 | 324.33 | 0 | 324.33 | 325.63 | |
| | 0.04 | 0.04 | | | | | | | | | | | 12 | Scoured | -2.06 | 322.4 | 320.34 | -0.09 | 322.31 | 324.58 | 4.4 |
| | 0.04 | 0.04 | | | | | | | | | | | 13 | Scoured | -0.73 | 321.64 | 320.91 | -0.16 | 321.48 | 324.55 | 22.1 |
| | 0.04 | 0.04 | | | | | | | | | | | 14 | Agradded | 1.63 | 322.76 | 324.39 | 0 | 322.76 | 324.08 | 0.0 |
| | 0.04 | 0.04 | | | | | | | | | | | 15 | None | 0.00 | 321.81 | 321.81 | 0.01 | 321.82 | 323.5 | |
| | 0.07 | 0.07 | 321.63 | | | | | | | | | | 16 | None - rifle | 0.00 | 321.63 | 321.63 | 0 | 321.63 | 323.08 | |
| | 0.07 | 0.07 | 320.78 | | | | | | | | | | 17 | None - rifle | 0.00 | 320.78 | 320.78 | 0 | 320.78 | 321.83 | |
| | 0.07 | 0.07 | 320.08 | | | | | | | | | | 18 | None - rifle | 0.00 | 320.07 | 320.07 | 0 | 320.08 | 320.95 | |
| | 0.07 | 0.07 | 319.32 | | | | | | | | | | 19 | None - rifle | 0.00 | 319.32 | 319.32 | 0 | 319.32 | 320.63 | |

192

[illegible]

[illegible]

| S | | 0.1 | 0.3 | 50 | deposition and erosion | Ackers- White | 3 Q and Qs | Xsec 1, 5, 10, 12, 17 | 320.58 | 2-8 | 40 | 37 | | | | | | | | |
|----|------|------|-----|--------|---------------------------|------------------|------------|--------------------------|--------|-----|----|----|----|--------------|-------|--------|--------|-------|--------|--------|
| | 0.04 | 0.04 | | 332.56 | | | | | | | | | 1 | None | 0.00 | 332.59 | 332.59 | 0 | 332.59 | 334.25 |
| | 0.04 | 0.04 | | 328.38 | | | | | | | | | 2 | Agradded | 3.93 | 330.96 | 334.79 | -0.13 | 330.99 | 334.26 |
| | 0.04 | 0.04 | | 327.58 | | | | | | | | | 3 | Agradded | 1.61 | 330.76 | 332.37 | -0.27 | 330.49 | 334.25 |
| | 0.04 | 0.04 | | 329.68 | | | | | | | | | 4 | Agradded | 2.46 | 332.14 | 334.60 | -0.28 | 331.86 | 334.24 |
| | 0.07 | 0.07 | | 332.76 | | | | | | | | | 5 | None - rifle | 0.00 | 332.76 | 332.76 | 0 | 332.76 | 333.81 |
| | 0.07 | 0.07 | | 330.31 | | | | | | | | | 6 | None - rifle | 0.00 | 330.31 | 330.31 | 0 | 330.31 | 332.89 |
| | 0.07 | 0.07 | | 329.96 | | | | | | | | | 7 | None - rifle | 0.00 | 329.96 | 329.96 | 0 | 329.96 | 331.32 |
| | 0.07 | 0.07 | | 328.66 | | | | | | | | | 8 | None - rifle | 0.00 | 328.66 | 328.66 | 0 | 328.66 | 330.53 |
| | 0.07 | 0.07 | | 327.98 | | | | | | | | | 9 | None - rifle | 0.00 | 327.98 | 327.98 | 0 | 327.98 | 329.34 |
| | 0.07 | 0.07 | | 325.62 | | | | | | | | | 10 | None - rifle | 0.00 | 325.62 | 325.62 | 0 | 325.62 | 327.67 |
| | 0.07 | 0.07 | | 324.33 | | | | | | | | | 11 | None - rifle | 0.00 | 324.33 | 324.33 | 0 | 324.33 | 325.62 |
| | 0.04 | 0.04 | | 320.34 | | | | | | | | | 12 | Scoured | -2.06 | 322.4 | 320.34 | -1.85 | 320.75 | 324.15 |
| | 0.04 | 0.04 | | 320.91 | | | | | | | | | 13 | Scoured | -0.73 | 321.64 | 320.91 | -0.56 | 321.08 | 324.13 |
| | 0.04 | 0.04 | | 320.24 | | | | | | | | | 14 | Agradded | 1.63 | 322.78 | 324.39 | -0.75 | 322.01 | 323.97 |
| | 0.04 | 0.04 | | 321.7 | | | | | | | | | 15 | None | 0.00 | 321.81 | 321.81 | -0.03 | 321.78 | 323.5 |
| | 0.07 | 0.07 | | 321.63 | | | | | | | | | 16 | None - rifle | 0.00 | 321.63 | 321.63 | 0 | 321.63 | 323.08 |
| | 0.07 | 0.07 | | 320.78 | | | | | | | | | 17 | None - rifle | 0.00 | 320.78 | 320.78 | 0 | 320.78 | 321.83 |
| | 0.07 | 0.07 | | 320.08 | | | | | | | | | 18 | None - rifle | 0.00 | 320.07 | 320.07 | 0 | 320.08 | 320.95 |
| | 0.07 | 0.07 | | 319.32 | | | | | | | | | 19 | None - rifle | 0.00 | 319.32 | 319.32 | 0 | 319.32 | 320.63 |
| 5a | | 0.1 | 0.3 | 50 | deposition and erosion | DuBoys's | 3 Q and Qs | Xsec 1, 5, 10, 12, 17 | 320.58 | 2-8 | 40 | 37 | | | | | | | | |
| | 0.04 | 0.04 | | 332.56 | | | | | | | | | 1 | None | 0.00 | 332.59 | 332.59 | 0 | 332.59 | 334.24 |
| | 0.04 | 0.04 | | 328.38 | | | | | | | | | 2 | Agradded | 3.93 | 330.96 | 334.79 | -0.47 | 330.39 | 334.26 |
| | 0.04 | 0.04 | | 327.58 | | | | | | | | | 3 | Agradded | 1.61 | 330.76 | 332.37 | -0.38 | 330.38 | 334.25 |
| | 0.04 | 0.04 | | 329.68 | | | | | | | | | 4 | Agradded | 2.46 | 332.14 | 334.60 | -0.28 | 331.86 | 334.24 |
| | 0.07 | 0.07 | | 332.76 | | | | | | | | | 5 | None - rifle | 0.00 | 332.76 | 332.76 | 0 | 332.76 | 333.81 |
| | 0.07 | 0.07 | | 330.31 | | | | | | | | | 6 | None - rifle | 0.00 | 330.31 | 330.31 | 0 | 330.31 | 332.89 |
| | 0.07 | 0.07 | | 329.96 | | | | | | | | | 7 | None - rifle | 0.00 | 329.96 | 329.96 | 0 | 329.96 | 331.32 |
| | 0.07 | 0.07 | | 328.66 | | | | | | | | | 8 | None - rifle | 0.00 | 328.66 | 328.66 | 0 | 328.66 | 330.53 |
| | 0.07 | 0.07 | | 327.98 | | | | | | | | | 9 | None - rifle | 0.00 | 327.98 | 327.98 | 0 | 327.99 | 329.34 |
| | 0.07 | 0.07 | | 325.62 | | | | | | | | | 10 | None - rifle | 0.00 | 325.62 | 325.62 | 0 | 325.62 | 327.67 |
| | 0.07 | 0.07 | | 324.33 | | | | | | | | | 11 | None - rifle | 0.00 | 324.33 | 324.33 | 0 | 324.33 | 325.62 |
| | 0.04 | 0.04 | | 320.34 | | | | | | | | | 12 | Scoured | -2.06 | 322.4 | 320.34 | -1.65 | 320.75 | 324.15 |
| | 0.04 | 0.04 | | 320.91 | | | | | | | | | 13 | Scoured | -0.73 | 321.64 | 320.91 | -0.56 | 321.08 | 324.13 |
| | 0.04 | 0.04 | | 320.24 | | | | | | | | | 14 | Agradded | 1.63 | 322.78 | 324.39 | -0.75 | 322.01 | 323.97 |
| | 0.04 | 0.04 | | 321.7 | | | | | | | | | 15 | None | 0.00 | 321.81 | 321.81 | -0.02 | 321.79 | 323.5 |
| | 0.07 | 0.07 | | 321.63 | | | | | | | | | 16 | None - rifle | 0.00 | 321.63 | 321.63 | 0 | 321.63 | 323.08 |
| | 0.07 | 0.07 | | 320.78 | | | | | | | | | 17 | None - rifle | 0.00 | 320.78 | 320.78 | 0 | 320.78 | 321.83 |
| | 0.07 | 0.07 | | 320.08 | | | | | | | | | 18 | None - rifle | 0.00 | 320.07 | 320.07 | 0 | 320.08 | 320.95 |
| | 0.07 | 0.07 | | 319.32 | | | | | | | | | 19 | None - rifle | 0.00 | 319.32 | 319.32 | 0 | 319.32 | 320.63 |

[illegible]

| 5d | 0.1 | 0.3 | 50 | deposition and erosion | Yang | 3 G and Qs | Xsec 1,5,10,12,17 | 320.58 | 2-8 | 40 | 37 | | | | | | | | |
|------|------|-----|--------|---------------------------|------|------------|----------------------|--------|-----|----|----|----|--------------|-------|--------|--------|-------|--------|--------|
| 0.04 | 0.04 | | 332.56 | | | | | | | | | 1 | None | 0.00 | 332.59 | 332.59 | 0.00 | 332.59 | 334.25 |
| 0.04 | 0.04 | | 328.39 | | | | | | | | | 2 | Agradded | 3.93 | 330.86 | 334.79 | 0.11 | 330.97 | 334.26 |
| 0.04 | 0.04 | | 327.59 | | | | | | | | | 3 | Agradded | 1.61 | 330.76 | 332.37 | -0.08 | 330.68 | 334.25 |
| 0.04 | 0.04 | | 328.68 | | | | | | | | | 4 | Agradded | 2.46 | 332.14 | 334.60 | -0.28 | 331.86 | 334.24 |
| 0.07 | 0.07 | | 332.76 | | | | | | | | | 5 | None - rille | 0.00 | 332.76 | 332.76 | 0.00 | 332.76 | 333.81 |
| 0.07 | 0.07 | | 330.31 | | | | | | | | | 6 | None - rille | 0.00 | 330.31 | 330.31 | 0.00 | 330.31 | 332.89 |
| 0.07 | 0.07 | | 329.96 | | | | | | | | | 7 | None - rille | 0.00 | 329.96 | 329.96 | 0.00 | 329.96 | 331.32 |
| 0.07 | 0.07 | | 328.66 | | | | | | | | | 8 | None - rille | 0.00 | 328.66 | 328.66 | 0.00 | 328.66 | 330.53 |
| 0.07 | 0.07 | | 327.88 | | | | | | | | | 9 | None - rille | 0.00 | 327.88 | 327.88 | 0.00 | 327.88 | 329.34 |
| 0.07 | 0.07 | | 325.62 | | | | | | | | | 10 | None - rille | 0.00 | 325.62 | 325.62 | 0.00 | 325.62 | 327.67 |
| 0.07 | 0.07 | | 324.33 | | | | | | | | | 11 | None - rille | 0.00 | 324.33 | 324.33 | 0.00 | 324.33 | 325.62 |
| 0.04 | 0.04 | | 320.34 | | | | | | | | | 12 | Scoured | -2.06 | 322.4 | 320.34 | -1.65 | 320.75 | 324.15 |
| 0.04 | 0.04 | | 320.91 | | | | | | | | | 13 | Scoured | -3.73 | 321.64 | 320.91 | -0.56 | 321.08 | 324.13 |
| 0.04 | 0.04 | | 320.24 | | | | | | | | | 14 | Agradded | 1.63 | 322.76 | 324.39 | -0.75 | 322.01 | 323.87 |
| 0.04 | 0.04 | | 321.7 | | | | | | | | | 15 | None | 0.00 | 321.61 | 321.61 | -0.03 | 321.78 | 323.50 |
| 0.07 | 0.07 | | 321.63 | | | | | | | | | 16 | None - rille | 0.00 | 321.63 | 321.63 | 0.00 | 321.63 | 323.08 |
| 0.07 | 0.07 | | 320.78 | | | | | | | | | 17 | None - rille | 0.00 | 320.78 | 320.78 | 0.00 | 320.78 | 321.83 |
| 0.07 | 0.07 | | 320.08 | | | | | | | | | 18 | None - rille | 0.00 | 320.07 | 320.07 | 0.00 | 320.08 | 320.85 |
| 0.07 | 0.07 | | 319.32 | | | | | | | | | 19 | None - rille | 0.00 | 319.32 | 319.32 | 0.00 | 319.32 | 320.63 |

| Sensitivity Analysis # | ρ_{20} | ρ_{40} | ρ | σ | Movable Bed Limits | Iterations | Cohesive Bed | Bed Transport Eq | Bed Inflow | Bed Gradation | Starting WSEL (ft) | Time step (days) | Water Temp (deg F) | Simulation length (days) | Cross section | Oct-Aug Thawing Change | Oct-Aug Thawing Change (ft) | Oct Thawing Elevation (ft) | August Thawing Elevation (ft) | Average HEC-4 Bed Change (ft) | HEC-4 Thawing Elevation (ft) | HEC-4 WSEL (ft) | Modeling Accuracy (%) |
|------------------------|-------------|-------------|--------|----------|--------------------|------------|------------------------|-------------------------|------------|-----------------------|--------------------|------------------|--------------------|--------------------------|---------------|------------------------|-----------------------------|----------------------------|-------------------------------|-------------------------------|------------------------------|-----------------|-----------------------|
| 1 | | | 0.1 | 0.3 | | 50 | deposition and erosion | Asker's White | 6 Q and Co | Xsec 1, 5, 10, 12, 17 | 320.58 | 2-8 | 40 | 137 | | | | | | | | | |
| (Oct-Aug) | 0.04 | 0.04 | | | 332.56 | | | | | | | | | | 1 | None | 0.00 | 332.59 | 332.59 | -0.03 | 332.56 | 334.64 | |
| | 0.04 | 0.04 | | | 328.39 | | | | | | | | | | 2 | Scoured | -1.99 | 330.66 | 328.87 | -0.46 | 330.4 | 334.66 | 23.09 |
| | 0.04 | 0.04 | | | 327.58 | | | | | | | | | | 3 | Scoured | -2.81 | 330.78 | 328.15 | -1.04 | 329.72 | 334.65 | 39.78 |
| | 0.04 | 0.04 | | | 329.68 | | | | | | | | | | 4 | Scoured | -0.98 | 332.14 | 331.16 | -0.54 | 331.6 | 334.65 | 65.33 |
| | 0.07 | 0.07 | | | 332.78 | | | | | | | | | | 5 | None - rfile | 0.00 | 332.78 | 332.78 | 0 | 332.78 | 334.44 | |
| | 0.07 | 0.07 | | | 330.31 | | | | | | | | | | 6 | None - rfile | 0.00 | 330.31 | 330.31 | 0 | 330.31 | 333.34 | |
| | 0.07 | 0.07 | | | 329.96 | | | | | | | | | | 7 | None - rfile | 0.00 | 329.96 | 329.96 | 0 | 329.96 | 332.01 | |
| | 0.07 | 0.07 | | | 328.66 | | | | | | | | | | 8 | None - rfile | 0.00 | 328.66 | 328.66 | 0 | 328.66 | 331.16 | |
| | 0.07 | 0.07 | | | 327.98 | | | | | | | | | | 9 | None - rfile | 0.00 | 327.98 | 327.98 | 0 | 327.98 | 329.86 | |
| | 0.07 | 0.07 | | | 325.62 | | | | | | | | | | 10 | None - rfile | 0.00 | 325.62 | 325.62 | 0 | 325.62 | 328.23 | |
| | 0.07 | 0.07 | | | 324.33 | | | | | | | | | | 11 | None - rfile | 0.00 | 324.33 | 324.33 | 0 | 324.33 | 325.82 | |
| | 0.04 | 0.04 | | | 320.34 | | | | | | | | | | 12 | Scoured | -2.06 | 322.4 | 320.34 | -2.06 | 320.34 | 324.32 | 99.87 |
| | 0.04 | 0.04 | | | 320.91 | | | | | | | | | | 13 | Scoured | -0.71 | 321.64 | 320.93 | -0.56 | 321.08 | 324.27 | 78.64 |
| | 0.04 | 0.04 | | | 320.24 | | | | | | | | | | 14 | Scoured | -2.52 | 322.76 | 320.24 | -1.34 | 321.42 | 324.24 | 53.15 |
| | 0.04 | 0.04 | | | 321.7 | | | | | | | | | | 15 | None | 0.00 | 321.81 | 321.81 | -0.03 | 321.78 | 323.76 | |
| | 0.07 | 0.07 | | | 321.63 | | | | | | | | | | 16 | None - rfile | 0.00 | 321.63 | 321.63 | 0 | 321.63 | 323.28 | |
| | 0.07 | 0.07 | | | 320.78 | | | | | | | | | | 17 | None - rfile | 0.00 | 320.78 | 320.78 | 0 | 320.78 | 321.98 | |
| | 0.07 | 0.07 | | | 320.08 | | | | | | | | | | 18 | None - rfile | 0.00 | 320.07 | 320.07 | 0 | 320.08 | 321.21 | |
| | 0.07 | 0.07 | | | 319.32 | | | | | | | | | | 19 | None - rfile | 0.00 | 319.32 | 319.32 | 0 | 319.32 | 320.8 | |
| 1a | | | 0.1 | 0.3 | | 50 | deposition and erosion | DuBois's | 6 Q and Co | Xsec 1, 5, 10, 12, 17 | 320.58 | 2-8 | 40 | 137 | | | | | | | | | |
| | 0.04 | 0.04 | | | 332.56 | | | | | | | | | | 1 | None | 0.00 | 332.59 | 332.59 | -0.03 | 332.56 | 334.63 | |
| | 0.04 | 0.04 | | | 328.39 | | | | | | | | | | 2 | Scoured | -1.99 | 330.66 | 328.87 | -1.69 | 329.17 | 334.68 | 84.81 |
| | 0.04 | 0.04 | | | 327.58 | | | | | | | | | | 3 | Scoured | -2.81 | 330.78 | 328.15 | -1.22 | 329.54 | 334.65 | 48.66 |
| | 0.04 | 0.04 | | | 329.68 | | | | | | | | | | 4 | Scoured | -0.98 | 332.14 | 331.16 | -0.54 | 331.6 | 334.65 | 55.33 |
| | 0.07 | 0.07 | | | 332.78 | | | | | | | | | | 5 | None - rfile | 0.00 | 332.78 | 332.78 | 0 | 332.78 | 334.43 | |
| | 0.07 | 0.07 | | | 330.31 | | | | | | | | | | 6 | None - rfile | 0.00 | 330.31 | 330.31 | 0 | 330.31 | 333.34 | |
| | 0.07 | 0.07 | | | 329.96 | | | | | | | | | | 7 | None - rfile | 0.00 | 329.96 | 329.96 | 0 | 329.96 | 332.01 | |
| | 0.07 | 0.07 | | | 328.66 | | | | | | | | | | 8 | None - rfile | 0.00 | 328.66 | 328.66 | 0 | 328.66 | 331.16 | |
| | 0.07 | 0.07 | | | 327.98 | | | | | | | | | | 9 | None - rfile | 0.00 | 327.98 | 327.98 | 0 | 327.98 | 329.86 | |
| | 0.07 | 0.07 | | | 325.62 | | | | | | | | | | 10 | None - rfile | 0.00 | 325.62 | 325.62 | 0 | 325.62 | 328.24 | |
| | 0.07 | 0.07 | | | 324.33 | | | | | | | | | | 11 | None - rfile | 0.00 | 324.33 | 324.33 | 0 | 324.33 | 325.8 | |
| | 0.04 | 0.04 | | | 320.34 | | | | | | | | | | 12 | Scoured | -2.06 | 322.4 | 320.34 | -2.06 | 320.34 | 324.33 | 99.87 |
| | 0.04 | 0.04 | | | 320.91 | | | | | | | | | | 13 | Scoured | -0.71 | 321.64 | 320.93 | -0.56 | 321.08 | 324.27 | 78.64 |
| | 0.04 | 0.04 | | | 320.24 | | | | | | | | | | 14 | Scoured | -2.52 | 322.76 | 320.24 | -1.34 | 321.42 | 324.24 | 53.15 |
| | 0.04 | 0.04 | | | 321.7 | | | | | | | | | | 15 | None | 0.00 | 321.81 | 321.81 | -0.03 | 321.78 | 323.76 | |
| | 0.07 | 0.07 | | | 321.63 | | | | | | | | | | 16 | None - rfile | 0.00 | 321.63 | 321.63 | 0 | 321.63 | 323.28 | |
| | 0.07 | 0.07 | | | 320.78 | | | | | | | | | | 17 | None - rfile | 0.00 | 320.78 | 320.78 | 0 | 320.78 | 321.98 | |
| | 0.07 | 0.07 | | | 320.08 | | | | | | | | | | 18 | None - rfile | 0.00 | 320.07 | 320.07 | 0 | 320.08 | 321.21 | |
| | 0.07 | 0.07 | | | 319.32 | | | | | | | | | | 19 | None - rfile | 0.00 | 319.32 | 319.32 | 0 | 319.32 | 320.8 | |
| 1b | | | 0.1 | 0.3 | | 50 | deposition and erosion | Mayer-Peter and Mueller | 6 Q and Co | Xsec 1, 5, 10, 12, 17 | 320.58 | 2-8 | 40 | 137 | | | | | | | | | |
| | 0.04 | 0.04 | | | 332.56 | | | | | | | | | | 1 | None | 0.00 | 332.59 | 332.59 | -0.03 | 332.56 | 334.68 | |
| | 0.04 | 0.04 | | | 328.39 | | | | | | | | | | 2 | Scoured | -1.99 | 330.66 | 328.87 | 0.45 | 331.31 | 334.87 | -22.58 |
| | 0.04 | 0.04 | | | 327.58 | | | | | | | | | | 3 | Scoured | -2.81 | 330.78 | 328.15 | 0.14 | 330.9 | 334.65 | -5.35 |
| | 0.04 | 0.04 | | | 329.68 | | | | | | | | | | 4 | Scoured | -0.98 | 332.14 | 331.16 | -0.53 | 331.61 | 334.65 | 54.36 |
| | 0.07 | 0.07 | | | 332.78 | | | | | | | | | | 5 | None - rfile | 0.00 | 332.78 | 332.78 | 0 | 332.78 | 334.46 | |
| | 0.07 | 0.07 | | | 330.31 | | | | | | | | | | 6 | None - rfile | 0.00 | 330.31 | 330.31 | 0 | 330.31 | 333.35 | |
| | 0.07 | 0.07 | | | 329.96 | | | | | | | | | | 7 | None - rfile | 0.00 | 329.98 | 329.96 | 0 | 329.96 | 332.01 | |
| | 0.07 | 0.07 | | | 328.66 | | | | | | | | | | 8 | None - rfile | 0.00 | 328.66 | 328.66 | 0 | 328.66 | 331.16 | |
| | 0.07 | 0.07 | | | 327.98 | | | | | | | | | | 9 | None - rfile | 0.00 | 327.98 | 327.98 | 0 | 327.98 | 329.87 | |
| | 0.07 | 0.07 | | | 325.62 | | | | | | | | | | 10 | None - rfile | 0.00 | 325.62 | 325.62 | 0 | 325.62 | 328.23 | |
| | 0.07 | 0.07 | | | 324.33 | | | | | | | | | | 11 | None - rfile | 0.00 | 324.33 | 324.33 | 0 | 324.33 | 325.82 | |
| | 0.04 | 0.04 | | | 320.34 | | | | | | | | | | 12 | Scoured | -2.06 | 322.4 | 320.34 | -2.06 | 320.34 | 324.32 | 99.87 |
| | 0.04 | 0.04 | | | 320.91 | | | | | | | | | | 13 | Scoured | -0.71 | 321.64 | 320.93 | -0.56 | 321.08 | 324.27 | 78.64 |
| | 0.04 | 0.04 | | | 320.24 | | | | | | | | | | 14 | Scoured | -2.52 | 322.76 | 320.24 | -1.34 | 321.42 | 324.24 | 53.15 |
| | 0.04 | 0.04 | | | 321.7 | | | | | | | | | | 15 | None | 0.00 | 321.81 | 321.81 | -0.03 | 321.78 | 323.76 | |
| | 0.07 | 0.07 | | | 321.63 | | | | | | | | | | 16 | None - rfile | 0.00 | 321.63 | 321.63 | 0 | 321.63 | 323.28 | |
| | 0.07 | 0.07 | | | 320.78 | | | | | | | | | | 17 | None - rfile | 0.00 | 320.78 | 320.78 | 0 | 320.78 | 321.98 | |
| | 0.07 | 0.07 | | | 320.08 | | | | | | | | | | 18 | None - rfile | 0.00 | 320.07 | 320.07 | 0 | 320.08 | 321.21 | |
| | 0.07 | 0.07 | | | 319.32 | | | | | | | | | | 19 | None - rfile | 0.00 | 319.32 | 319.32 | 0 | 319.32 | 320.8 | |

[illegible]

